

ABSTRACT

Title of Dissertation: BIOGEOGRAPHIC, GEOCHEMICAL, AND PALEOCEANOGRAPHIC INVESTIGATIONS OF OSTRACODES IN THE BERING, CHUKCHI, AND BEAUFORT SEAS

Laura Gemery, Doctor of Philosophy, 2022

Dissertation directed by: Dr. Lee Cooper, Professor, University Maryland Center for Environmental Science

In this study, I investigated the continental shelf environments of the Bering, Chukchi, and Beaufort Seas using species of Ostracoda and their shell chemistry as indicators of oceanographic conditions and change. Ostracodes are bivalved Crustacea that secrete a calcareous shell commonly preserved in sediments in the Arctic. Because ostracode species have survival limits controlled by temperature, salinity, oxygen, sea ice, food, and other habitat-related factors, they are useful ecological indicators. A primary objective of my dissertation research was to establish how their ecology, biogeography, and shell geochemistry is related to ocean variability in water mass properties and productivity at high latitudes. First, I examined community assemblages of ostracodes over several decades (1970-2018) in the northern Bering, Chukchi, and Beaufort Seas, and the main environmental factors that affect their biogeography. Results showed that large-scale south-to-north and small-scale nearshore-offshore gradients in ostracode community structure were tied to changes in water mass properties in combination with food sources and sediment substrate. Although the dominant species did not significantly

change over the investigated period, the frequency of two cold-temperate species that are primarily and previously restricted to shallow North Pacific sediments off Asia has increased during the last decade. This suggests that these species are responding to recent increases in coastal and mid-shelf bottom water temperatures and/or carbon flux to the benthos. A second goal was to assess the feasibility of using stable oxygen isotopes ($\delta^{18}\text{O}$) of carbonate from ostracode shells as paleoceanographic proxies for water mass identification on Arctic and subarctic continental shelves. Through the use of regression analyses, I established that the $\delta^{18}\text{O}$ values of carbonates from two species (of five investigated) can be reliable recorders of summer water mass changes in temperature and seawater $\delta^{18}\text{O}$ content. The third part of the study was to use results from these prior two goals in combination with data on biogenic silica, foraminifera assemblages and stable isotope composition of biogenic carbonates, to reconstruct 2,000 years of paleoceanography from a radiocarbon-dated sediment core on the Mackenzie Shelf of the Beaufort Sea. This high-resolution (sub-centennial) record identified shifts in multiple proxies that are related to climate oscillations such as the Medieval Climate Anomaly, the Little Ice Age, and the modern period of anthropogenic change. The overall findings of my dissertation research support the premise that on complex and dynamic continental shelves, paleoceanographic uncertainties can be addressed by documenting microfossil faunal assemblages, measuring stable isotope variability in microfossil carbonates, as well as relating the distribution of species in time with an understanding of species ecology.

BIOGEOGRAPHIC, GEOCHEMICAL AND PALEOCEANOGRAPHIC
INVESTIGATIONS OF OSTRACODES
IN THE BERING, CHUKCHI, AND BEAUFORT SEAS

by

Laura Gemery

Dissertation submitted to the Faculty of the Graduate School of the
University of Maryland, College Park, in partial fulfillment
of the requirements for the degree of
Doctor of Philosophy
2022

Advisory Committee:

Professor Lee W. Cooper, Chair, University Maryland Center for Environmental Science

Dr. Thomas M. Cronin, U.S. Geological Survey

Dr. Harry J. Dowsett, U.S. Geological Survey

Professor Jacqueline M. Grebmeier, University Maryland Center for Environmental Science

Associate Professor Laura Lapham, University Maryland Center for Environmental Science

© Copyright by
Laura Gemery
2022

Acknowledgements

I have benefited greatly from so many supportive and positive mentors and colleagues at the U.S. Geological Survey (USGS), the University of Maryland Center for Environmental Science (UMCES), and Stockholm University.

While my career path has been somewhat unconventional, two people were instrumental in fostering and building my interest and skills in science: my supervisor at USGS, Thomas Cronin, and my Advisory Committee Chair, Lee Cooper. Each took a chance on me with an opportunity to do science and mentored me along the way. I could not be more grateful for their dedication to me and their influence in my life's direction. Tom initially hired me to work in his lab "just for the summer" to see if I liked it. This morphed into several years getting my feet wet with training in micropaleontology (lots of bug picking and subtle shell-feature identification), lab processes (lots of mud washing) and learning about how very little things preserved in sediments are used for insights into past environments. All the while reading and re-reading papers to grasp the fundamentals of paleo reconstructions and attending seminars to try to absorb aspects of the interesting research buzzing around me at USGS.

Doing field work and research in high latitudes was a far-off aspiration, although I had been inspired by it during earlier jobs at National Science Teachers Association and National Wildlife Federation. In late 2008, I cold-called Lee and asked about his and Jackie Grebmeier's Arctic research and graduate studies at UMCES. By the end of our conversation, he invited me on a March 2009 cruise to the Bering Sea. What an amazing, albeit bleary-eyed experience on a ship literally coated in icicles in the middle of an icy, dark Sea. Our hoses and seafloor mud collections immediately froze on deck, so we brought them just inside the fantail and used hair dryers to thaw sediments in order to wash them! Despite this and other challenging conditions that followed on other cruises, Jackie has directing and executing science operations down to a fine and even creative art. The job gets done, and this is the lesson.

I've learned the most while at sea, and want to thank everyone involved with expeditions HLY0901, OCE2010, HLY1201, HLY1301, SWERUS-L2, HLY1702, HLY1801, Ryder 2019. Each has been a unique and irreplaceable learning experience. It has been a privilege to sail with some incredible scientists contributing new insights into the understanding of current and past Arctic processes and environments, and with whom I hope to continue working: Lloyd Keigwin, Martin Jakobsson, Matt O'Regan, Volker Brüchert, Leonid Polyak. Larry Mayer, Alan Mix. They share their knowledge freely, and I have learned so much from them during expeditions and core sampling visits. One constant on the HLY cruises has been working with Jackie, and admiring her level of enthusiasm, energy, grit, leadership and expertise that I will try to aspire to.

I could not be more fortunate that she, Tom and Lee served on my Masters committee and later continued to support me via my PhD committee. Walter Boynton was key in my academics during my Masters program, and on my Masters committee. He co-taught one of the best classes (Land Margin Interactions) at University of Maryland that helped my understanding of some fundamental science concepts. He is probably unaware how his funny stories about his early career and his wonderful demeanor and teaching style impacted me and helped my confidence. I also appreciate the example that Laura Lapham set for me about the process of science. In 2012, we sailed the Chesapeake Bay on R/V Rachel Carson and I felt right away that she was a person I would love to work more with and learn from. And I have benefitted from her on my PhD committee, especially with a deeper dive into sedimentary and diagenetic processes. Last but not least, USGS paleoclimate scientist Harry Dowsett rounds out my top-notch committee. Harry pushed me to consider my data and analyses much more critically. I am so grateful for the time and effort each of my committee members has invested in me. I also want to acknowledge Ning Zeng, who graciously served as the Dean's representative at my defense.

Cédric Magen ran all the ostracode isotope samples, and I appreciate his patience, long (and repeated) explanations about how stable isotope mass spectrometry works, and his careful contributions to my studies.

Having an office next to USGS Scientist Emeritus John Keith has been another lucky situation, and we have forged a friendship over the years that I cherish. I value his advice, stories, encouragement, conversations, knowledge and life-long learning interest in so many topics. I soon hope to read the many books that he has bequeathed to me!

The road to achieving my PhD has been comprised of more enlightening interactions, assistance and relationships for which I am grateful. Those included in this group are: Carina Johansson, Ruby Chiu, Moriaki Yasuhara, Christina Goethel, Chelsea Wegner-Koch, Miriam Jones, Robert Poirier, Lucy Roberts, Illaria Mazzini, Jesse Farmer, Ryan McAleer, Aaron Jubb, Marci Robinson, Chris Sweezy, Michael Toomey, Julia Seidenstein, Katherine Keller, Lynn Wingard, Peigen Lin, May Huang Huai-Hsuan, Steven Watson, Nick Vaka, Anna Ruefer.

I wish my dad was still here to have followed this journey. Growing up, we didn't have the means to travel, so he would tune-in to all the nature documentaries on TV with the likes of Marlin Perkins and Jacques Cousteau. Together we would sit--amazed and inspired by the natural world and its mysteries. I am deeply grateful for his quiet presence and profound influence. And my mom who always told me I could do whatever I put my mind to.

Finally, to top the list is my husband, Ronnie Lindsay, who was absolutely the best and most fun person to spend nearly 2 years in semi-COVID confinement with as I wrote my dissertation chapters and navigated work from home. He couldn't have been more thoughtful or considerate, and he adopted my goals and made them his priorities. I don't really think he likes reconciling and formatting all the references in my papers, but you'd never know it by his eagerness to help me in any way he can. Over the days he became really good at observing and anticipating what I might need-- a lot of this involved healthy food or time to workout or hike a trail with our dog. He would facilitate this for me on more days than I can count. He also made efforts to celebrate my small successes -- like finishing a chapter draft, or addressing Lee's always-constructive and extensive edits/comments of a chapter draft, and so forth -- down the process to journal publication. He has attentively listened to so many presentations, asked good questions and provided feedback to help me to continue to improve. His outlook is always positive and he

imparts that to me on the days I need it most. “Thank you” does not seem apt enough. But I thank him for his for inspiration, wit and laughter every day, easy-going nature, for sacrificing things he has wanted to do due to my schedule, and for walking this winding road with me.

Table of Contents

Acknowledgements	ii
Table of Contents	vi
List of Tables	ix
List of Supplementary Tables	xi
List of Figures	xii
List of Supplementary Figures	xviii
Chapter 1: Introduction and Background	1
1.1 General aspects of ostracode life history	1
1.2 Reference literature on ostracode taxa	2
1.3 Applications of ostracodes as indicators of benthic environments and change	3
1.4 Study motivation: Recent physical and biological changes in the Pacific Arctic	6
1.5 Environmental data collection in the Pacific Arctic	7
1.6 The Arctic Ostracode Database	7
1.7 Dissertation objectives and outline	8
Figures	12
Chapter 2: Biogeography and Ecology of Ostracoda in the U.S. northern Bering, Chukchi, and Beaufort Seas	13
2.1 Abstract	13
2.2 Introduction	14
2.2.1 Ostracodes as indicators of environmental change	15
2.2.2 Controls on marine ecosystems and benthic ostracode species	16
2.2.3 Environmental Setting	16
2.3 Materials and Methods	18
2.3.1 Sample collection and processing	18
2.3.2 Surface sediment characteristics	19
2.3.3 Statistical analyses	19
2.4 Results	20
2.4.1 Large-scale biogeography of ostracodes in the Bering, Chukchi, Beaufort Seas	22
2.4.2 Ecoregions and transects: ecological-scale ostracode assemblages	24
2.4.3 Time-series analysis	25
2.5 Discussion	26
2.5.1 Distribution and ecology of dominant and indicator taxa	26
2.5.2. Ecoregion transects: spatial relationships among ostracode biofacies	29
2.5.2.1 Chirikov Basin – DBO2	30
2.5.2.2 Southeast Chukchi Sea – DBO3	31
2.5.2.3 Central Chukchi Sea – Ledyard Bay	32
2.5.2.4 Northeast Chukchi Sea – Icy Cape 2018	34

2.5.2.5 Offshore Hanna Shoal, Northeast Chukchi Sea	34
2.5.2.6 Barrow Canyon/DBO5	35
2.5.2.7 Alaskan Beaufort Sea	36
2.5.3 Temporal trends in BCB Sea indicator species	38
2.6 Conclusions	39
2.7 Acknowledgements	41
Figures	42
Supplementary Figures	57
Tables	60
Supplementary Table	65
Chapter 3: Stable oxygen isotopes in shallow marine ostracodes from the northern Bering and Chukchi Seas	66
3.1 Abstract	66
3.2 Introduction	67
3.2.1 Goals of the study	68
3.2.2 Previous work	69
3.2.3 Cryophilic ostracode life history	70
3.2.4 Assumptions to address life history uncertainties	72
3.2.5 Regional setting	72
3.3 Materials and Methods	74
3.3.1 Ostracode surface sediment samples	74
3.3.2 Ostracode selection and preparation for isotope analysis	75
3.3.3 Collection and analysis of $\delta^{18}\text{O}_{\text{water}}$ and $\delta^{18}\text{O}_{\text{ost}}$	76
3.3.4 Ostracode $\delta^{18}\text{O}$, notation, and analyses	77
3.4 Results and Discussion	78
3.4.1 The relationships among $\delta^{18}\text{O}_{\text{water}}$ and water mass characteristics	79
3.4.2 Distribution and ecology of investigated ostracode species	82
3.4.3 Stable oxygen isotopes of Arctic ostracodes	83
3.4.4 Species-specific vital effect fractionations	84
3.4.5 Comparison of juvenile vs. adult $\delta^{18}\text{O}_{\text{ost}}$ and vital offsets	88
3.4.6 Intra-sample replicate measurements	88
3.4.7 The relationship of species $\delta^{18}\text{O}_{\text{ost}}$ to temperature, salinity and $\delta^{18}\text{O}_{\text{water}}$	90
3.4.7.1 <i>Normanicythere leioderma</i>	90
3.4.7.2 <i>Paracyprideis pseudopunctillata</i>	92
3.4.7.3 <i>Sarsicytheridea bradii</i>	92
3.4.7.4 <i>Heterocyprideis</i> spp.	93
3.5 Conclusions	93
3.6 Acknowledgements	95
Figures	96
Supplementary Figures	103
Tables	112
Chapter 4: Multi-proxy record of ocean-climate variability during the last two millennia on the Mackenzie Shelf, Beaufort Sea	123

4.1 Abstract	123
4.2 Introduction	124
4.2.1 Arctic climate variability during the last 2,000 years	126
4.2.2 Environmental significance of microfossil species	127
4.2.2.1 Atlantic water species	129
4.2.2.2 Eurytopic Arctic shelf species	130
4.2.2.3 Low-salinity tolerant species	131
4.2.3 Note on <i>Cassidulina teretis</i> taxonomy	132
4.3 Regional setting	133
4.3.1 Mackenzie Shelf hydrography	133
4.4 Materials and methods	135
4.4.1 Coring, sedimentology, sampling	135
4.4.2 Microfossil sample processing and assemblage analysis	136
4.4.3 Stable isotope analyses	136
4.4.4 Biogenic silica (opal)	138
4.4.5 Chronology	139
4.4.6 Statistical analyses	141
4.5 Results	141
4.5.1 Correlation of radioisotopes and AMS ¹⁴ C dating	141
4.5.2 Ostracode and foraminifera faunal assemblages	142
4.5.2.1 Zone 1 (0-800 years CE)	143
4.5.2.2 Zone 2 (MCA, 800-1200 CE)	144
4.5.2.3 Zone 3 (LIA, 1300-1850 CE)	144
4.5.2.4 Zone 4 (1850-2013 CE)	144
4.5.3 Biogenic silica (opal)	145
4.5.4 Ostracode and foraminifera $\delta^{18}\text{O}$ and $\delta^{13}\text{C}$	146
4.6 Discussion	147
4.6.1 Cold Arctic bottom water during Zone 1 (0-800 years CE)	147
4.6.2 Variable warming, fluctuating conditions with Atlantic water incursions during Zone 2 (MCA, 800-1200 CE)	148
4.6.3 Cooling and episodic sediment disturbance during Zone 3 (LIA, 1300-1850 CE)	150
4.6.4 Continued near-freezing conditions and shifts in organic carbon and seafloor environment during Zone 4 (1850-2013 CE)	151
4.7 Conclusions and summary	154
4.8 Data availability	156
4.9 Acknowledgments	156
Figures	157
Tables	166
Chapter 5: Overall Conclusions	169
5.1 Review of project goals and key findings	169
5.2 Future work	171
Bibliography	173

List of Tables

Chapter 1

No tables

Chapter 2

Table 2.1 Ecoregion names and respective bounding coordinates of sample groups and transects investigated in this study. Samples were grouped by ecoregions based on established Distributed Biological Observatory (DBO) station grids, which include four biological hotspot locations in the Bering and Chukchi Seas along a latitudinal gradient and sampled interannually: DBO1-south of St. Lawrence Island polynya (SLIP); DBO2-Chirikov Basin, north of St. Lawrence Island; DBO3-southern Chukchi Sea, southwest of Point Hope; and DBO5-Barrow Canyon in the northeast Chukchi Sea. Two other transects, sampled only in 2018, are also examined: Ledyard Bay (LB) and Icy Cape (ICY). Two other areas are defined in this study: northeast Chukchi (C-NE) that included sample locations in the northeast not specifically part of DBO4 or DBO5 transects; and Hanna Shoal (C-HS), an offshore region around Hanna Shoal. The symbol “*” represents that a few sample locations are located in deeper water (72, 104 and 130m) north of Hanna Shoal. The Alaskan Beaufort Sea was treated as one ecoregion. DBO station mean bottom water temperature, salinity, and sediment chlorophyll, with \pm standard deviation, are provided for years 2000-2012, from March to July at DBO1, May to August at DBO2, July to September at DBO3, and May to September at Northeast Chukchi. From Grebmeier et al., 2015a; Grebmeier and Cooper, 2014a and Okkonen, 2013. Ranges for sediment chlorophyll-a are provided for transects LB, ICY and DBO5 from the present study because values at a given location were very divergent from neighboring stations.

Table 2.2 List of 47 species and five genera found in the study region ($\geq 1\%$ of cumulative assemblage and/or occurred in 5 or more samples). Abbreviations of species are used in stack plots. According to the International Commission on Zoological Nomenclature, authors' names are in parentheses if the assignment listed was not the first description of the species.

Table 2.3 DCA results based on the relative abundance of 49 ostracode species (including three genera, *Argilloecia*, *Cytheropteron* and *Semicytherura*) in 289 surface sediment samples from continental shelf regions of the Bering Chukchi and Beaufort Seas collected primarily in summer 1970-2018. Four assemblages related to average summer bottom water properties, and several species' preferences of bottom sediment texture, organic sediment food types, are established. Because this area is a broad continental shelf, there is overlap of taxa between Alaska Coastal Water and Bering Sea Water, which is bridged by *S. bradii* and secondary taxa that include *E. concinna*.

Chapter 3

Table 3.1 The summer temperature and salinity range for each water mass taken from Coachman et al., 1975; Gong and Pickart, 2015; seawater $\delta^{18}\text{O}$ values from Cooper et al, 1997; and mean data with average standard deviation (stdev) from the present study.

Table 3.2 List of surface samples used in this study, including year of the cruise, expedition, geographic location, water depth, $\delta^{18}\text{O}_{\text{water}}$, bottom water temperature, salinity, water mass, species measured, and $\delta^{18}\text{O}_{\text{ost}}$ results. Juvenile measurements are listed below the adult samples. Abbreviations: “Year” = Year sample collected; “Expedition” = expedition name includes either “HLY” for USCGC Healy or “SWL” for CCGS Sir Wilfrid Laurier and the year and leg; “Name” = sampling name, first letter refers to expedition vessel, “H” for Healy or “L” for Sir Wilfrid Laurier, then the two digit year of collection followed by the sampling station name; “Lat” = Latitude; “Long” = Longitude; “Depth” = bottom water depth as recorded by the CTD; “ $\delta^{18}\text{O}_{\text{water}}$ ” = bottom $\delta^{18}\text{O}_{\text{water}}$ ‰ VSMOW; “Temp” = near-bottom water temperature; “Sal” = near-bottom salinity; “Water mass” = designated water mass based on properties listed in Table 3.1; “Species” = species measured (N= *N. leioderma*, P= *P. pseudopunctillata*, S= *S. bradii*, HF= *H. fascis*, HS= *H. sorbyana*); “ $\delta^{18}\text{O}_{\text{ost}}$ ” = ostracode shell calcite result ‰ VPDB.

Table 3.3 Average bottom seawater $\delta^{18}\text{O}$ values at sampling stations during years 2014-2018 and standard deviation of those values. Shaded rows list average seawater $\delta^{18}\text{O}$ value and standard deviation for the DBO transect indicated. Note "*" represents station sites where only three years of data within the 2014-2018 period were available.

Table 3.4 Average $\delta^{18}\text{O}$ and average expected $\delta^{18}\text{O}$ values of equilibrium calcite for adult ostracode taxa from surface samples in this study (shaded blue) and other studies (not shaded) and their respective vital offsets determined by the equations cited in Methods section 3.3.4. Other studies include: [1] Ingram, 1998; [2] Simstich et al., 2004; [3] Didié and Bauch, 2002.

Chapter 4

Table 4.1. Dominant ostracode species used in the HLY1302 composite cores (multicore [MC29], gravity core [GGC30], and piston core [JPC32]) to infer water mass changes at the Mackenzie shelf site. SEM photos taken from Gemery et al., 2015.

Table 4.2 List of radiocarbon dates for the HLY1302 composite cores and calibrations using CALIB 8.2 software (Stuiver et al., 2021), the Marine20 calibration curve (Heaton et al., 2020) and a marine reservoir correction of $\Delta R = 477 \pm 60$ years (Pearce et al., 2017). Yellow highlight denotes seven new samples measured to improve the age model of Seidenstein et al (2018).

Table 4.3 Summary of $\delta^{18}\text{O}$ and $\delta^{13}\text{C}$ isotopic data.

List of Supplementary Tables

Chapter 2

S2.1 Table. Six ecologically defined species in the northern Bering, Chukchi, and Beaufort Seas based on multivariate correlations with environmental factors (*=from listed ecological references). Scanning electron microscope (SEM) photos of species are taken from Gemery et al., 2015.

Chapter 3

No supplementary tables

Chapter 4

No supplementary tables

List of Figures

Chapter 1

Figure 1.1 Map of Distributed Biological Observatory (DBO) sampling transects indicated by the red boxes (<https://dbo.cbl.umces.edu>). Many samples used in this study are derived from this program.

Chapter 2

Figure 2.1 Locations of samples used for the biogeographical study. (n=289 sediment aliquots with ≥ 30 specimens per sediment sample, 34,369 total specimens, 1970-2018) The blue “DBO” areas denote Distributed Biological Observatory stations. (Geographic coordinates are provided in Table 2.1.) Note that some stations along established DBO transects are not represented due to low or no ostracode abundance (i.e. DBO3-6 to 3-8 and DBO4). Smaller inset map shows context of the study area. Figure made with GeoMapApp (www.geomapapp.org) / CC BY / CC BY (Ryan et al., 2009).

Figure 2.2 Location of sample sites in the northern Bering and Chukchi Seas used for ecoregion transect (nearshore to offshore) study (n=147 surface sediment aliquots with ≥ 30 specimens per sediment sample, 19,300 total specimens, 1990-2018). Schematic of summertime surface current flow patterns and water mass type that can affect seafloor conditions (Anadyr Water [AW], Alaska Coastal Water [ACW], Bering Sea Water [BSW]; properties denoted in Table 2.3) adapted from Danielson et al. (2017, 2020). Figure made with GeoMapApp (www.geomapapp.org) / CC BY / CC BY (Ryan et al., 2009).

Figure 2.3 Location of samples used in Beaufort Sea ecological transect study from years 1971-2018 (n=55 surface sediment aliquots with ≥ 30 specimens per sediment sample, 20-100mwd, 6,617 total specimens). Figure made with GeoMapApp (www.geomapapp.org) / CC BY / CC BY (Ryan et al., 2009).

Figure 2.4 Summer bottom water temperature at ecoregions. Comparison of summer bottom temperatures in studied ecoregions and months at stations nearest to shore (e.g. DBO3-1, DBO5-1) that are locations affected by Alaska Coastal Water, and more central or middle-shelf stations (DBO3-5 or DBO5-10) that are affected by Bering Sea Water (winter or summer variants). This subset of data was derived from the Pacific Marine Arctic Regional Synthesis (PacMARS) Project (Grebmeier and Cooper, 2014a; <http://dx.doi.org/10.5065/D6VM49BM>; Okkonen, 2013; <https://data.eol.ucar.edu/dataset/10339>) and recent expedition data (2014-2018) taken aboard USCGS Healy and CCGS Sir Wilfrid Laurier and archived at the National Science Foundation's Arctic Data Center.

Figure 2.5 Principal correspondence analysis (PCA). PCA of ostracode assemblages in the northern Bering, Chukchi, and Beaufort Sea region (locations on Fig. 2.1; geographic coordinates in Table 2.1), with sites designated by DBO areas and other ecoregions (legend symbols) and major taxa (green lines with species names labeled in blue). Three species dominate the assemblage groups: *N.*

leioderma, *S. bradii*, and *P. pseudopunctillata*. The proximity of the symbols in the plot reflects the level of similarity in taxa present at each sampling station.

Figure 2.6a Detrended correspondence analysis (DCA). DCA using the northern Bering, Chukchi, and Beaufort Seas biogeographic dataset (1970–2018), describes relationships between ostracode assemblage structure and geographic ecoregions in the region. Ostracode biofacies differed among ecoregions within the study area (described in Table 2.3) and grouped primarily on summer water mass characteristics (temperature and salinity).

Figure 2.6b Canonical correspondence analysis (CCA). CCA of ostracode assemblages in the northern Bering-Chukchi Sea region, with sampling ecoregion sites (noted by symbol on legend), major taxa (names are labeled in blue), and eight environmental parameters (green lines and labels in black: temperature, salinity, sediment total organic carbon [TOC], sediment nitrogen [TON], sediment chlorophyll-a [sedchla], phi ≥ 5 [fine silt], and phi 0-4 [gravel pebbles to sands]). Samples in the Hanna Shoal region (red dots) were separated from the larger northeastern Chukchi Sea sample set (inverted red triangle). Dataset includes the 14 most abundant species in 153 surface sediment aliquots (23,939 total specimens) from the northern Bering and Chukchi Seas during summers 1990-2018 for which sediment data was available.

Figure 2.7a Primary species, DBO2 - Chirikov Basin. Stack plot of dominant species in DBO2-Chirikov Basin region (Fig. 2.2 map) in the northern Bering Sea (various years from 2001 to 2018; n=15, 1,314 specimens with ≥ 30 specimens/sample). The 11 species presented in the stack plot comprise 98% of the biofacies in this ecoregion. (Note the boundary between Anadyr water on the western side of Chirikov Basin and Bering Sea Water on the eastern side is generalized in this graphic.)

Figure 2.7b Summer bottom water salinity at western and eastern DBO2 - Chirikov Basin sampling sites. Time series plot of summer bottom salinity at sampling stations on the western and eastern side of the Chirikov Basin (Source: Grebmeier and Cooper, 2014a; Okkonen, 2013; and recent expedition data (2014-2018) taken aboard USCGS Healy and CCGS Sir Wilfrid Laurier archived at the Arctic Data Center).

Figure 2.8 Primary species, DBO3 - Southern Chukchi Sea. Stack plot of the 12 most abundant species and one genus (*Semicytherura*), comprising 92% of the ostracode assemblage, in DBO3 region (sites on Fig. 2.2 map) from years ranging from 1998 to 2018, (n=32 samples with ≥ 30 specimens/sample, 7,514 total specimens).

Figure 2.9 Primary species, Central Chukchi Sea – Ledyard Bay. Stack plot of the 12 most abundant species and one genus (*Semicytherura*), comprising $>90\%$ of the ostracode assemblage at the 2018 Ledyard Bay transect (sites on Fig. 2.2 map), southeast Chukchi Sea, (n=5 surface sediment samples, all with ≥ 50 specimens/sample, 558 total specimens).

Figure 2.10 Primary species, Northeast Chukchi Sea - Icy Cape. Stack plot of the 9 most abundant species comprising $\sim 90\%$ of the ostracode assemblage at the 2018 Icy Cape (ICY) sampling transect (sites on Fig. 2.2 map), northeast Chukchi Sea, (n=10 samples with ≥ 75

specimens/sample [except ICY2 that contained 22 specimens], 1,554 total specimens). Species not included on plot that each represent >1-2% of transect assemblage total include *A. dunelmensis*, *Argilloecia* sp., and *E. concinna*.

Figure 2.11 Primary species, Northeast Chukchi Sea – Hanna Shoal. Stack plot of the 11 most abundant species and one genus (*Argilloecia* spp.) comprising ~96% of the ostracode assemblage in the Hanna Shoal region offshore in the northeast Chukchi Sea (sites on Fig. 2.2 map) from years 2012 to 2013, (n=21 surface sediment samples with ≥ 30 specimens/sample, 2,647 total specimens in an average water depth of 51m).

Figure 2.12 Primary species, DBO5 – Barrow Canyon. Stack plot of the 11 most abundant species and one genus (*Finmarchinella*), comprising ~80% of the ostracode assemblage, in DBO5-Barrow Canyon region (sites on Fig. 2.2 map) from years ranging from 2011 to 2018 (n=31 surface sediment samples with ≥ 30 specimens/sample, 2,951 total specimens). Other faunas at stations 5-9 and 5-10 that account for the species not shown on the stack plot include *A. dunelmensis*, *J. acuminata* and *H. fascis*, and *R. tuberculatus*.

Figure 2.13 Primary species, Alaskan Beaufort Sea. Stack plot of the 12 most abundant species comprising ~85% of the ostracode assemblage in a narrow band of the Alaskan Beaufort Sea (sites on Fig. 2.3 map) within 100 km of shore at 20-90m water depth from years 1971 to 2018, (n=55 surface sediment samples with ≥ 30 specimens/sample, 6,617 total specimens). Samples collected in 2018 are highlighted in yellow. Other species not shown on the stack plot that account for 1-2% of the assemblage include *Rabilimis septentrionalis*, *Pteroloxa chaunensis*, *E. concinna*, and several *Cytheropteron* species. Important species in the Bering and Chukchi that exhibited either very low abundance (<1%) or are absent in the Beaufort Sea at 20-90m water depth are: *S. ikeyai*, *M. mananensis*, *Finmarchinella* spp., *K. arctoborealis*, *H. clathrata*, *H. emarginata*, *J. acuminata*, *S. affinis*, *S. mainensis*, and *S. undata*.

Figure 2.14 Principal correspondence analysis of ostracode assemblages by year groups. Synoptic PCAs using the biogeographic dataset (samples located on Fig 2.1 map) from the BCB grouped by the three regions and two collection periods, a.) 1970-2012 and b.) 2013-2018.

Figure 2.15 Time series of key species in Chukchi Sea. a.) *N. leioderma*, b.) *P. pseudopunctillata*, c.) *S. bradii*, d.) *S. ikeyai*, e.) *M. mananensis*

Chapter 3

Figure 3.1 Location of sediment and near-bottom water sampling stations (n=78) in the northern Bering and Chukchi Seas used in this study. The primary summer surface currents, which can mix to the bottom to affect the sample site's water mass, are labeled (flow patterns adapted from Stabeno et al., 2018 and Danielson et al., 2017).

Figure 3.2 a.) $\delta^{18}\text{O}$ values of seawater from sampling stations (listed in Table 3.2), sorted by water mass properties versus temperature; b.) $\delta^{18}\text{O}$ values of seawater, sorted by water mass properties versus salinity. Simple regression analysis was conducted on all samples overall ($R^2=$

0.04 for temperature and $R^2=0.45$ for salinity) and for samples labeled by water mass represented with the coefficient of determination, R^2 , cited in the legend. The analytical error of the mass spectrometric measurement is $\sim 0.1\%$, which is similar to the symbol size.

Abbreviations: AW= Anadyr water; ACW = Alaska coastal water; BSW= Bering Sea water; RWW= remnant winter water

Figure 3.3 a., d., g., j., l.) $\delta^{18}\text{O}_{\text{ost}}$ results for each species from each sample; b., e., h., k., m.) calculated adult vital offset (difference between $\delta^{18}\text{O}_{\text{ost}}$ - $\delta^{18}\text{O}_{\text{expected}}$) values for each respective species with average values cited to the right; Figure 3.3 c., f., i.) calculated juvenile vital offset values for each species and average value cited to the right.

Figure 3.4 Principal component analysis results for factor loadings that include temperature, $\delta^{18}\text{O}_{\text{ost}}$, salinity, and $\delta^{18}\text{O}_{\text{water}}$. Species are color coded as follows: *N. leioderma* (red); *P. pseudopunctillata* (green); *S. bradii* (blue); *H. sorbyana* (purple); and *H. fascis* (orange); and symbols of each respective color indicate the water mass in which the sample was collected. The pink circular highlight represents samples primarily in the southeast Chukchi Sea (DBO3-1 to DBO3-4) in ACW. The yellow highlight represents samples located in the northern Chukchi Sea (DBO4, DBO5) in BSW and RWW. The blue highlight represents samples located in the western Chirikov Basin that are influenced by AW (DBO2) and samples located offshore in BSW.

Figure 3.5 a.) $\delta^{18}\text{O}_{\text{ost}}$ results of *N. leioderma* (red circles) and *P. pseudopunctillata* (green squares) sorted by water mass of sample versus temperature; b.) $\delta^{18}\text{O}_{\text{ost}}$ results sorted by water mass of sample versus salinity; c.) $\delta^{18}\text{O}_{\text{water}}$ results sorted by water mass of sample versus $\delta^{18}\text{O}_{\text{ost}}$. (Values are not corrected for vital offsets.) Simple linear regression analysis was conducted on samples shown in each plot (*N. leioderma*: $R^2=0.67$ for temperature, $R^2=0.58$ for salinity, $R^2=0.47$ for $\delta^{18}\text{O}_{\text{water}}$; *P. pseudopunctillata*: $R^2=0.52$ for temperature, $R^2=0.52$ for salinity, $R^2=0.06$ for $\delta^{18}\text{O}_{\text{water}}$) and for samples identified in ACW because, in some cases, the R^2 value supported a significant relationship.

Figure 3.6 $\delta^{18}\text{O}_{\text{ost}}$ results of *S. bradii* (blue triangles) sorted by water mass of sample versus temperature; b.) $\delta^{18}\text{O}_{\text{ost}}$ results sorted by water mass of sample collection versus salinity; c.) $\delta^{18}\text{O}_{\text{water}}$ results sorted by water mass of sample versus $\delta^{18}\text{O}_{\text{ost}}$ values. (Values are not corrected for vital offsets.) Simple linear regression analysis was conducted on samples shown in each plot, which show no significant relationships between one variable to predict the other variable ($R^2=0.09$ for temperature, $R^2=0.14$ for salinity, $R^2=0.03$ for $\delta^{18}\text{O}_{\text{water}}$).

Figure 3.7 $\delta^{18}\text{O}_{\text{ost}}$ results of *H. sorbyana* (purple squares) and *H. fascis* (orange circles) sorted by water mass of sample versus temperature; b.) $\delta^{18}\text{O}_{\text{ost}}$ results sorted by water mass of sample versus salinity; c.) $\delta^{18}\text{O}_{\text{water}}$ results sorted by water mass of sample versus $\delta^{18}\text{O}_{\text{ost}}$. (Values are not corrected for vital offsets. Regression tests were not conducted because of too few samples.)

Chapter 4

Figure 4.1 Schematic circulation of Chukchi and Beaufort Seas and geographic names. The HLY1302 MC29, GGC30 and JPC32 (69.97°N, 137.24°W) core site (magenta circle) on the

Mackenzie shelf in 60 m water depth. The green arrows denote the main pathway of Pacific-origin water exiting Chukchi Sea shelf and contributing to the Chukchi Slope Current to the west and Beaufort Shelfbreak Jet to the east. The blue arrow represents the Shelf Current in the vicinity of Mackenzie Canyon. The Beaufort Gyre (yellow arrow) situates in the Canada Basin. The bathymetry (in meters) is from The International Bathymetric Chart of the Arctic Ocean (IBCAO) v3.

Figure 4.2 Near-bottom summer a.) salinity and b.) temperature measurements (n=238) from a subset of CTD collections during August and September, 1990-2012 (Okkonen, 2013), with the core site denoted by a white circle. Archived data sets from which the CTD summary data were derived are detailed in Grebmeier et al. (2015), Appendix G1. Figure created using Ocean Data View software (Schlitzer, 2018).

Figure 4.3 Correlation of multicore 29 (MC29B) chronology to activities of ^{210}Pb and ^{137}Cs in the top 37cm of sediment.

Figure 4.4a.) Age-depth model of HLY1302 composite cores, MC29, GGC30, JPC32. Seventeen median radiocarbon dates shown with 2-sigma error bars (~95% of the measurements fall within the bar range) in years before present (BP) and calendar years (in red parentheses). b.) the regression model $y = 4.0683(x) + 196.91$ used to linearly tie the 10 most recent dates of the undisturbed sequence.

Figure 4.5a&b. Principal component analyses of (a.) ostracode assemblages and (b.) foraminifera assemblages colored by major time periods.

Figure 4.6. Stack plot of ostracode species that make up 98% of the assemblages by composite depth.

Figure 4.7. Stack plot of primary foraminifera species that make up ~95% of the assemblages by composite depth.

Figure 4.8a.) Number of ostracode specimens per binned sample; MC29 was binned every 5 cm, GGC30 every 10 cm and JPC32 every 20 cm. Two samples contained <25 specimens/binned sample, and these are indicated by yellow highlights. b.) Percent abundance of selected benthic ostracode and c.) foraminifera species (of total specimens/sample) against composite core depth. Selected foraminifera faunal data from Seidenstein et al (2018). Foraminifera species abundance in MC29 (black lines) are plotted separately from GGC30/JPC32. General periods of the LIA (1300-1850; ~36-160 cm composite depth) and MCA (800-1200; 195-294 cm), per our age model, are shown by blue and red shaded vertical bars, respectively. The beginning of each time zone is labeled 1, 2, 3, and 4. Confidence limits (95%) shown on the faunal plots were calculated using the algorithm for binomial probability (Raup, 1991).

Figure 4.9a.) Percent of sediment biogenic silica against age (calendar years, CE); b.) Measurements of ostracode $\delta^{18}\text{O}$ (green) and foraminifera $\delta^{18}\text{O}$ (blue) against age; c.) Measurements of ostracode $\delta^{13}\text{C}$ (green) and foraminifera $\delta^{13}\text{C}$ (blue) against age. Carbon

isotope values are binned (averaged) in 25-year intervals from 1800 to 2013 and binned by 100-year intervals from 0 to 1800 CE to smooth the large variability of measured values; d.) Modeled Mackenzie River outflow per Wickert (2016), and modern value representing 1990s from Carson et al. (1998). Shaded horizontal bars on plots indicate average standard deviation values.

List of Supplementary Figures

Chapter 2

S2.1 Figure. a. Faunal abundance of selected taxa in relation to near-bottom temperature during summer sediment collection in the northern Bering and Chukchi Seas (n=211, 26,170 total specimens, 1990-2018, ≥ 30 specimens/sample).

b. Faunal abundance in relation to salinity.

c. Faunal abundance in relation to sediment type. Ostracode species abundance plotted against the percent sediment modal grain size of phi 0-4, where 0 represents gravel and rocks, 1 = coarse sand, 2 = medium sand, 3-4 = finer sand. Phi ≥ 5 (not shown) represents the very fine silty mud and clay sediment fraction typical of offshore or interior areas of the continental shelf.

S2.2 Figure. Faunal abundance plotted against three different sources of sediment carbon, which may suggest preferred food sources: a. sediment chlorophyll-a (sedchla), b. total organic carbon (TOC) and c. carbon to nitrogen (C/N) ratios.

S2.3 Figure. Principal correspondence analysis (PCA) of Alaskan Beaufort Sea ostracode assemblages. Sample sites are designated by collection years (legend symbols) and major taxa (green lines with species names labeled in blue).

Chapter 3

S3.1 Figure. Percent abundance of *N. leioderma* (n=158) in AOD samples (with >10 specimens of the given taxa in a sample) plotted versus bottom water temperature, salinity, water depth and latitude.

S3.2 Figure. Modern distribution of *N. leioderma* from the AOD.

S3.3 Figure. Percent abundance of *P. pseudopunctillata* (n=210) in AOD samples (with >10 specimens of the given taxa in a sample) plotted versus bottom water temperature, salinity, water depth and latitude.

S3.4 Figure. Modern distribution of *P. pseudopunctillata* from the AOD.

S3.5 Figure. Percent abundance of *S. bradii* (n=246) in AOD samples (with >10 specimens of the given taxa in a sample) plotted versus bottom water temperature, salinity, water depth and latitude.

S3.6 Figure. Modern distribution of *S. bradii* from the AOD.

S3.7 Figure. Percent abundance of *H. sorbyana* (n=152) and *H. fascis* (n=45) in AOD samples (with >10 specimens of the given taxa in a sample) plotted versus bottom water temperature, salinity, water depth and latitude.

S3.8 Figure. Modern distribution of *H. sorbyana* and *H. fascis* from AOD.

S3.9a. Figure. Predicted temperature using paleotemperature equation by Epstein et al. (1953) versus actual sample temperature; 3.9b. Predicted temperature using paleotemperature equation by Shackleton (1974) versus actual sample temperature.

Chapter 4

No supplementary figures

Chapter 1: Introduction and Background

1.1 General aspects of ostracode life history

Ostracodes are a meiofaunal bivalved Crustacea class, with adult shells ranging in size from 0.5 to ~2.0 mm in length (Higgins and Thiele, 1988). Marine ostracode species investigated in this study are in the subclass Podocopa, order Podocopida, and live on (epifaunal) or within a few centimeters (infaunal) of seafloor sediment. Species are identified based on morphological characteristics of their shells, which are related to a particular species' ideal habitat. Infaunal ostracodes have carapaces that are smaller, smooth, tapered or elongated (Benson, 1961, 1974; Coles et al., 1994; Tanaka, 2009) while epifaunal ostracodes tend to have boxy or triangular outlines with more heavily calcified shell features that can include wing-like alae, carinae (ridges), tubercles or spines (Benson, 1961). Generally, species found in higher energy environments on coarse or gravely sediments have more robust, ornamented or reticulated carapaces (Benson, 1961, 1984).

In Arctic and subarctic regions where my investigations took place, ostracode abundance and diversity are greatest during summer months when temperatures are warmest and organic productivity is more available to facilitate reproduction (Horne, 1983). A full ostracode lifecycle includes eight molts before reaching adulthood (Horne, 1983; Cohen and Morin, 1990; Horne et al., 2002). Most marine ostracode species reproduce sexually (Horne, 1983). Females brood their eggs inside their carapace and early molts hatch with hardened shells (Horne, 1983; Cohen and Morin, 1990). Cold-water ostracode species appear to have seasonal lifecycles, and produce one or more generations per year in spring and summer, and commonly reach adulthood in late

summer/early autumn (Horne, 1983). Since benthic ostracodes are non-swimmers, their dispersal is dependent on ocean currents. Most ostracodes are scavengers, feeding on detritus (particulate organic carbon, POC), algae, and bacteria (Elofson, 1941). Ostracodes also serve as food for higher trophic organisms, and play a role in biogeochemical processes as nutrient recyclers through excretion, and indirectly by physically disturbing the sediments.

Specific life history details for many species, such as the number of broods per season, lifespan and food preferences, are difficult to ascertain since most species have not been directly observed in nature. However, a few controlled laboratory experiments of cold-water marine ostracodes (e.g. Elofson, 1941; Majoran and Agrenius, 1995; Majoran et al., 2000; Ikeya and Kato, 2000) have been conducted to constrain some of these aspects. Through culturing studies, Elofson (1941) found that shallow water ostracodes possess wider temperature tolerances than deep-sea species. He estimated the total life span for a few frigid continental shelf species (*Sarsicytheridea bradii*, *Robertsonites tuberculatus* and *Acanthocythereis dunelmensis*) to be a few years. In arctic and subarctic areas, ostracode diversity exceeds 100 species (Gemery et al., 2015; Cronin et al., 2021). Worldwide, more than 20,000 extant species live in numerous aquatic environments (Morin and Cohen, 1991; Horne et al., 2012), and some 33,000 are described in the fossil record that spans nearly 500 million years (Horne et al., 2002).

1.2 Reference literature on ostracode taxa

The primary taxonomic authorities I used for the study of cryophilic podocopid ostracodes include: Sars (1866, 1922-28), Elofson (1941), Neale and Howe (1975), Joy and Clark (1977), Cronin (1981, 1988), Brouwers (1981, 1982a, 1982b, 1990, 1993, 1994), Whatley

(1982), Hazel (1970), Penney (1989), Hartmann (1992), Whatley et al (1998), Freiwald and Mostafawi (1998), Whatley and Coles (1987), Stepanova (2006), Stepanova et al. (2003, 2004, 2007), Mackiewicz (2006), Schornikov and Zenina (2006), Frenzel et al. (2010), Gemery et al. (2015). Species identification is based on carapace morphology (shape and size), pore size and distribution, hinge characteristics, and shell ornamentation.

1.3 Applications of ostracodes as indicators of benthic environments and change

In my dissertation studies, I use ostracode assemblages and their carbonate shell stable isotope composition (expressed as $\delta^{18}\text{O}$ and $\delta^{13}\text{C}$ values) to infer ecological and water mass conditions, anthropogenic effects and as a tool for paleoceanographic reconstruction. Many benthic marine species of ostracodes inhabit a narrow range of hydrochemical conditions. Assemblage composition in any given area is constrained by a combination of environmental gradients such as depth, water mass structure (temperature, salinity), habitat (bottom topography, sediment type), and productivity (food, nutrients, light). Consequently, living assemblages serve as proxies of specific environments. Ostracodes provide a number of ways to evaluate the effects of changing environmental conditions in different types of areas/ecotones, for instance from nearshore to offshore and over climatic zones (e.g. Hazel, 1970; Stepanova, 2006; Yasuhara et al., 2012). In addition to distinct species' ecology, their small size, abundant fossil record, species-level identification and limited stratigraphic ranges makes ostracodes useful tools for paleoecologic, paleoceanographic reconstructions and biostratigraphy (e.g. Brouwers, 1992; Cronin et al., 1993; Ikeya and Cronin, 1993; Stepanova et al., 2007; Horne et al., 2012; Gemery et al., 2017).

Carbonate shell stable isotope measurements add to the value of ostracodes as proxies for benthic oceanographic change. Stable oxygen isotopes ($\delta^{18}\text{O}$) of calcareous microfossil tests – primarily planktic and benthic foraminifera – have been used to reveal changes in global ice volume, ocean circulation, and temperatures over decadal to millennial timescales (e.g. Shackleton, 1974; Lisiecki and Raymo, 2005). Likewise, stable carbon isotopes ($\delta^{13}\text{C}$) are primarily used to identify glacial to interglacial changes in surface primary productivity products exported to the seafloor. Marine ostracode isotopic records are underutilized, but the controls on isotope incorporation are similar to those of benthic foraminifers (Didié and Bauch, 2002). However, unlike molluscs or foraminifera that secrete their shells over their lifespans, ostracodes secrete their CaCO_3 shells rapidly, within a few days (Turpen and Angell, 1971; Peypouquet et al., 1988; Chivas et al., 1983; Roca and Wansard, 1997). Therefore, analysis of their shell $\delta^{18}\text{O}$ and $\delta^{13}\text{C}$ provide a “snapshot” record of the water conditions at the time of calcification. This enables oceanographic reconstructions of short-term regional hydrographic variability as well as long-term glacial to interglacial water mass change, depending on the study goals.

The $\delta^{18}\text{O}$ of non-marine ostracode valves have been widely used for paleoenvironmental studies of lakes, but to date, only a few studies have investigated marine ostracode $\delta^{18}\text{O}$ values in relation to oceanographic parameters: Didié and Bauch, 2002 (Iceland Plateau in the north Atlantic); Simstich et al., 2004 (Kara Sea); Mazzini, 2005 (Tasman Sea and Campbell Plateau off New Zealand, deep Southern Ocean); Bornemann et al., 2012 (Mediterranean Sea). Each study conducted $\delta^{18}\text{O}$ analyses of their chosen taxa from modern surface sediment specimens and established species-specific vital offsets from those isotope ratios expected from equilibrium-based composition of calcite. Results confirmed that ostracode species do not precipitate calcite in equilibrium with the temperature and the $\delta^{18}\text{O}$ composition of seawater, and that species-

specific vital effects cause this disequilibrium. Keatings et al. (2002) suggested that vital-effect offsets may be influenced by different rates of calcification. Most of the above-cited studies found positive vital-effect offsets in the $\delta^{18}\text{O}$ of the taxa examined (Didié and Bauch, 2002; Simstich et al., 2004; Mazzini, 2005).

Stable carbon isotope values of microfossil shells reflect the carbon isotopic composition of the dissolved inorganic carbon (DIC) pool in seafloor seawater or the upper-most sediment pore water in which the organism lives and calcifies its shell (e.g. von Grafenstein et al, 1999). In addition to specific bottom water $\delta^{13}\text{C}$ microhabitats where the organism lives, microfossil $\delta^{13}\text{C}$ may also be affected by its food sources and species-specific vital effects during shell calcification processes (Xia et al., 1997a, b; von Grafenstein et al., 1999; e.g. foraminifera: Wefer and Berger, 1991; Rohling and Cooke, 1999; Mackensen et al., 2000). Interpretations of $\delta^{13}\text{C}$ shell values are challenging. The $\delta^{13}\text{C}$ of dissolved inorganic carbon of phytodetritus on the seafloor has varying carbon signatures depending on the kinds of organic matter (marine- or terrestrial-derived) that settles out to the benthos and the amount of photosynthesis or microbial respiration and decomposition that took place. Also, living closer to shore with greater inputs of terrestrial material would tend to create a microhabitat with greater proportions of isotopically light carbon relative to marine organic carbon (Grebmeier and McRoy, 1989). This is consistent with the findings of Simstich et al. (2004) who found $\delta^{13}\text{C}$ values in ostracode calcite increased with depth and distance from the Ob and Yenisei river mouths.

Limited investigations of marine ostracode stable isotope chemistry underscore the need for additional study. An improved understanding of ostracode biology, ecology, and controls on isotopic shell composition facilitate interpretations of isotopic data to supplement downcore

paleoenvironmental reconstructions. These are topics that I explore further in subsequent chapters of this dissertation.

1.4 Study motivation: Recent physical and biological changes in the Pacific Arctic

During the last half century, the Arctic region has changed in ways and at a pace not previously seen in recorded data (Overland et al., 2018). This includes the focus region of my dissertation: the continental shelves of the Pacific-Arctic, specifically the northern Bering, Chukchi, and Beaufort Seas. Here, freshwater fluxes, ocean and air temperatures have increased (Woodgate, 2018; Danielson et al., 2020) while sea-ice extent, concentration and persistence have decreased (Jeffries et al., 2013; Overland et al. 2013; Strove et al., 2012, 2014; Frey et al., 2017). Since 1979, the open-water period in Chukchi Sea has increased 80 days (Serreze et al., 2016). Earlier spring sea ice retreat and later fall sea ice formation alters the timing of primary production and, in turn, the export of organic matter that settles to feed benthic organisms (Ji et al. 2013; Grebmeier et al., 2015a; Frey et al, 2017). Changes in ice also soften the arctic–subarctic ecotone boundary (Mueter and Litzow, 2008), which is allowing some cold temperate and boreal species to expand their ranges further north (Stevenson and Lauth, 2019). These physical and chemical changes create biological and ecological consequences in carbon cycling and food web dynamics that drive changes in abundance, composition and distribution of biological communities (Huntington et al., 2020; Mueter et al., 2021). Shifts in species distribution patterns, biomass, productivity and new species are already being documented (Wassmann et al., 2011; Arrigo et al., 2008, 2011; Bluhm et al., 2011; Grebmeier, 2012; Grebmeier et al., 2006, 2010, 2018; Goethel et al., 2019; Iken et al, 2013; Post et al., 2013). Recent rapid changes in the Pacific-

Arctic ecosystem also motivate the need to better understand past natural variability with respect to current anthropogenic changes.

1.5 Environmental data collection in the Pacific Arctic

During the 1960s, 1970s and early 1980s, researchers from the U.S. Geological Survey (USGS) Coastal and Marine Geology Program were actively surveying the Pacific Arctic during environmental studies and for mineral, oil and gas resources. During these expeditions, short cores and surface grabs were collected. Following this, a series of coordinated research programs, including SBI (Shelf-Basin Interactions, 1998–2008), RUSALCA (Russian American Long-Term Census of the Arctic, 2004–2014), the Bering Sea Program (2007–2012) sampled the northern Bering and/or the Chukchi Seas to track biological response to sea ice loss and associated environmental changes. Most recently, the Distributed Biological Observatory (DBO; 2010-present; Fig. 1.1) has been designed as an ecosystem observation and change detection array, with sampling stations in the Northern Bering, Chukchi, and Beaufort Seas that integrate biological measurements at multiple trophic levels with physical oceanographic sampling from ships, satellites and moorings (Moore and Grebmeier, 2018). This dissertation utilizes hydrographic and sediment data collected from these programs and other sampling efforts in the region. Ostracode assemblages from many of these collections are compiled in the Arctic Ostracode Database (Cronin et al., 2021).

1.6 The Arctic Ostracode Database

Cronin et al. (1991) compiled a comprehensive Arctic Ostracode Database (AOD) on extant species of Arctic and subarctic ostracodes. It was updated by Cronin et al. (2010), Gemery et al. (2015) and further expanded by Cronin, myself and colleagues (2021) to include new samples collected during 2014-2018 from Bering, Chukchi, and Beaufort Sea expeditions, several in which I participated. As part of my dissertation study, Cronin and I supplemented this database to apply it to investigations in Chapter 2. It is a vital tool to evaluate how recent large-scale environmental change is affecting the Arctic and subarctic benthic ecosystems via ostracode proxies. The AOD provides census data for 96 species of marine Ostracoda from ~1600 modern surface sediments from the Arctic Ocean and subarctic seas. It is an open-sourced file available at NOAA's National Centers for Environmental Information (NCEI) World Data Service for Paleoclimatology (<https://www.ncdc.noaa.gov/paleo/study/32312>), and includes latitude, longitude, water depth, bottom water temperature and collection year for most samples. Specifically, this database provides:

- Baseline benthic ostracode data for comparative future faunal surveys and past paleoecological studies of fossil assemblages from sediment cores;
- Hypotheses testing about the extent to which ongoing ecosystem changes in the Arctic and subarctic can be attributed to anthropogenic climate change;
- Understanding of how ostracodes, at the base of the food web, change in response to climate related changes, such as increases or decreases in surface productivity/sea-ice dynamics, temperature, salinity, and other factors.

1.7 Dissertation objectives and outline

Over geologic time, and particularly during the last few decades, the Arctic Ocean has experienced significant environmental change. A record of these changes is preserved at least in part by microorganisms, such as ostracodes, which are fossilized in marine sediments. The overall objective of my dissertation is to utilize benthic marine ostracode assemblages and isotope geochemistry of their shells from sediments of the Bering, Chukchi, and Beaufort (BCB) Seas as proxies to evaluate oceanographic change during the last 40 years and during the late Holocene from a sediment core record.

Chapter 2 (Gemery et al., 2021a) examines the distributions of ostracode species from surface sediment samples from the BCB Seas collected between 1970 and 2018 to assess how environmental variables and changes in those variables affect benthic meiofauna. Very few observational biogeographical and time-series studies have been conducted on benthic marine ostracodes in the Pacific-Arctic, and this study complements one other study in this region (Gemery et al., 2013). Statistical analyses and environmental time-series data (e.g. temperature, salinity, primary production indicators, and sediment grain size) are applied to identify factors related to ostracode species assemblage composition and to establish and/or further refine specific ecological preferences of dominant indicator taxa.

The goals of this chapter are to:

- Identify biogeographic-scale ostracode patterns in the BCB Seas 1970-2018;
- Establish the primary environmental factors related to ostracode biofacies, especially among dominant and “indicator” species;
- Establish species to be used for future biomonitoring;

- Evaluate if recent anthropogenic changes have affected ostracode species distributions, e.g. species' migration from the North Pacific through the Bering Strait.

Chapter 3 (Gemery et al., 2021b) is a calibration study of the stable oxygen isotope compositions of carbonates in ostracode shells ($\delta^{18}\text{O}$) in relation to the $\delta^{18}\text{O}$ values of ambient seawater from the northern Bering and Chukchi Seas. Specifically, this study compares the $\delta^{18}\text{O}$ values of water with the $\delta^{18}\text{O}$ values of ostracode shells from surface sediments collected in recent years from a range of water temperatures to infer water mass properties. Species analyzed include *Sarsicytheridea bradiei*, *Paracyprideis pseudopunctillata*, *Normanicythere leioderma* and *Heterocyprideis fascis* and *Heterocyprideis sorbyana*. This study determines baseline $\delta^{18}\text{O}$ values for the investigated taxa and their species-specific vital offsets. It also answers the following questions:

- Using regression analyses, what factors most control the $\delta^{18}\text{O}_{\text{ost}}$ values of the species?
- What is the variability of $\delta^{18}\text{O}_{\text{ost}}$ values from the same species within the same sediment sample?
- Is ostracode species' $\delta^{18}\text{O}$ a recorder of water mass properties on the Pacific-Arctic continental shelf? If so, which species are most reliable?

Chapter 4 (Gemery et al., 2022, submitted to *Micropaleontology*) uses the ecological and isotopic insights gained from Chapters 2 and 3 and applies them to support paleoceanographic interpretations from proxies preserved in a sediment core record from the Beaufort Sea. Specifically, this study uses ostracode and foraminifera assemblages, shell isotope ($\delta^{18}\text{O}$ and $\delta^{13}\text{C}$) data and sediment biogenic silica to reconstruct 2,000 years of paleoceanography on the

Mackenzie Shelf and establish a baseline for pre-anthropogenic ocean variability. In order to contextualize recent Arctic change and to distinguish human from natural ecosystem-ocean variability, longer-term data are needed to extend instrumental and observational records. This study compares pre- and post-anthropogenic ostracode and foraminifera taxa and their shell stable carbon and oxygen isotope variability to answer the following questions:

- Have benthic ostracodes in the Beaufort Sea been affected by oceanographic changes in the past and present?
- Is there evidence in the proxy data for changes in: Pacific current inflow, Atlantic water (>200m) penetration onto shelf, sea ice, Beaufort Gyre strength, Mackenzie River inputs, productivity (due to light, nutrient, ice changes)?

The overarching aim of this dissertation research is to improve the use of ostracodes as tools to better understand the Arctic benthic ecosystem and its response to changing climate and oceanographic conditions during the past 50 years and over longer timescales.

Figures Chapter 1

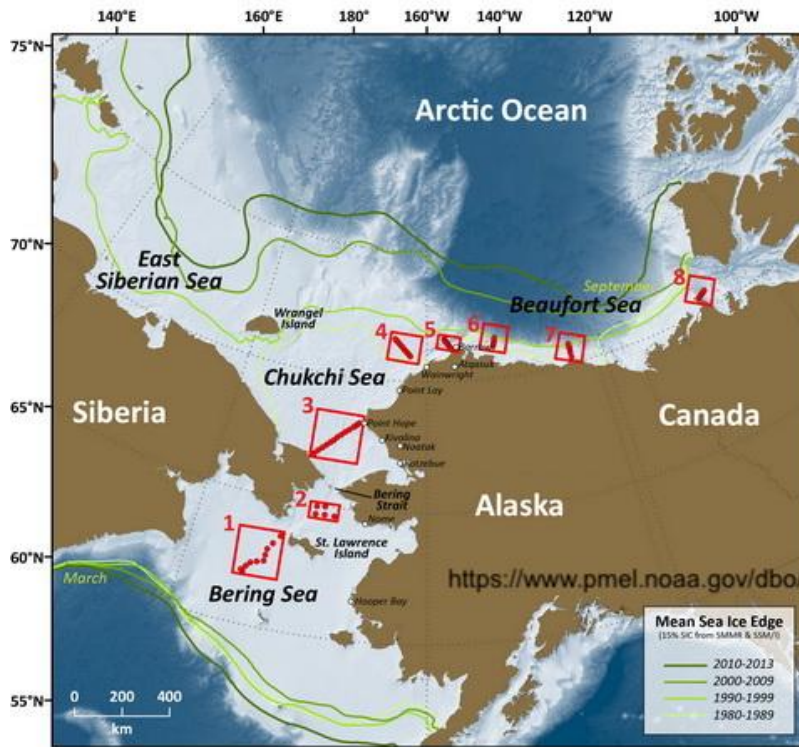


Figure 1.1 Map of Distributed Biological Observatory (DBO) sampling transects indicated by the red boxes (<https://dbo.cbl.umces.edu>). Many samples used in this study are derived from this program.

Chapter 2: Biogeography and Ecology of Ostracoda in the U.S. northern Bering, Chukchi, and Beaufort Seas

Published in PLoS ONE, May 2021, <https://doi.org/10.1371/journal.pone.0251164>

Laura Gemery, Thomas M. Cronin, Lee W. Cooper, Harry J. Dowsett, Jacqueline M. Grebmeier

Contribution: lead responsibility for the study, including experimental design, ostracode taxonomy, sample processing, data analysis and interpretation, all text and figures, writing of original draft. Text has been edited by all co-authors and reviewed for quality assurance.

2.1 Abstract

Ostracoda (bivalved Crustacea) comprise a significant part of the benthic meiofauna in the Pacific-Arctic region, including more than 50 species, many with identifiable ecological tolerances. These species hold potential as useful indicators of past and future ecosystem changes. In this study, we examined benthic ostracodes from nearly 300 surface sediment samples, >34,000 specimens, from three regions -- the northern Bering, Chukchi, and Beaufort Seas -- to establish species' ecology and distribution. Samples were collected during various sampling programs from 1970 through 2018 on the continental shelves at 20 to ~100m water depth. Ordination analyses using species' relative frequencies identified six species, *Normanicythere leioderma*, *Sarsicytheridea bradii*, *Paracyprideis pseudopunctillata*, *Semicytherura complanata*, *Schizocythere ikeyai*, and *Munseyella mananensis*, as having diagnostic habitat ranges in bottom water temperatures, salinities, sediment substrates and/or food sources. Species relative abundances and distributions can be used to infer past bottom environmental conditions in sediment archives for paleo-reconstructions and to characterize potential changes in Pacific-Arctic ecosystems in future sampling studies. Statistical analyses further showed ostracode assemblages grouped by the summer water masses influencing the area. Offshore-to-nearshore transects of samples across different water masses showed that

complex water mass characteristics, such as bottom temperature, productivity, as well as sediment texture, influenced the relative frequencies of ostracode species over small spatial scales. On the larger biogeographic scale, synoptic ordination analyses showed dominant species—*N. leioderma* (Bering Sea), *P. pseudopunctillata* (offshore Chukchi and Beaufort Seas), and *S. bradii* (all regions)—remained fairly constant over recent decades. However, during 2013-2018, northern Pacific species *M. mananensis* and *S. ikeyai* increased in abundance by small but significant proportions in the Chukchi Sea region compared to earlier years. It is yet unclear if these assemblage changes signify a meiofaunal response to changing water mass properties and if this trend will continue in the future. Our new ecological data on ostracode species and biogeography suggest these hypotheses can be tested with future benthic monitoring efforts.

2.2 Introduction

Biological systems of the Pacific-influenced Arctic Ocean are currently undergoing rapid climate-related transformations (e.g. Huntington et al., 2020; Grebmeier et al. 2006; Grebmeier, 2012; Wassmann et al., 2011). This is attributed to ocean warming in the North Pacific, Bering, and Chukchi Seas (Wood et al., 2015a; Woodgate, 2018), which is accelerating sea-ice loss and extending the open water season (Frey et al., 2015; Serreze et al., 2016). Changes in sea-ice cover further alter stratification, hydrography, and circulation patterns, all of which influence primary productivity (Stabeno et al., 2017; Lewis et al., 2020; Hill et al., 2018; Arrigo and van Dijken, 2015) and trophic relationships (Nelson et al., 2014; Stabeno et al., 2019). The quality, quantity, and timing of production reaching the sea floor ultimately affects benthic marine species abundance, distribution, and food web dynamics (Grebmeier, 2012; Grebmeier et al., 2006, 2015a, 2018). In this study, we examine a component of the benthic ecosystem: meiobenthic ostracodes

and the primary factors that influence their ecology and biogeography in response to changing conditions in the Bering, Chukchi, and Beaufort Seas.

This study has three primary objectives. The first is to examine large-scale biogeographic ostracode patterns and species diversity in the BCB Seas. The second objective is to identify primary environmental factors related to ostracode faunal distributions, particularly among dominant and diagnostic species. For this, we used ordination analyses of a series of nearshore-to-offshore transects (primarily the DBO lines) to spatially assess species abundance patterns across different water masses. Lastly, we use distribution and abundance patterns of dominant and/or ecologically significant taxa as proxies for species response to environmental changes and consider whether recent temperature, sea ice, and productivity changes are affecting ostracode distributions.

2.2.1 Ostracodes as indicators of environmental change

Ostracodes are a bivalved group of Crustacea, ranging in size from ~0.5 to 2.0 mm, that secrete a calcareous (CaCO_3) shell commonly preserved in sediments. Because individual marine ostracode species have ecological limits controlled by temperature, salinity, oxygen, sea ice, food, and other habitat-related factors, they are useful ecologic indicators (e.g. Ikeya and Cronin, 1993; Frenzel and Boomer, 2005; Stepanova et al., 2003, 2007; Horne et al., 2012). Ostracodes provide ways to evaluate the effects of changing environmental conditions in different types of areas/ecotones and through geologic time. In addition to distinct species' ecology, their small size, abundant fossil record, limited stratigraphic ranges, species-level identification, and shell isotope geochemistry, ostracodes are multi-proxy tools for paleoecologic, paleoceanographic reconstructions and biostratigraphy (e.g. Brouwers, 1992; Ikeya and Cronin, 1993; Stepanova et al., 2007; Gemery et al., 2017).

2.2.2 Controls on marine ecosystems and benthic ostracode species

The distribution of biological communities—from plankton and invertebrates to epibenthic fish and sea birds—has largely been found to reflect the distribution of water masses (Grebmeier et al., 2018; Sigler et al., 2017). While the temperature required for survival and reproduction primarily controls the distribution of cryophilic ostracode species on large biogeographic scales (Hazel, 1970; Hutchins, 1947), other local factors also influence species spatial dynamics, such as depth, sediment properties, and primary productivity exported to the benthos (Elofson, 1941; Ikeya and Cronin, 1993; Ozawa, 2003, 2004; Yasuhara et al., 2012). Assemblage composition in any given area is constrained by a combination of these environmental gradients. In addition to water mass properties, this study examines other parameters that affect dominant and indicator ostracode species over south to north gradients (Fig 2.1), as well as nearshore to offshore transects (Fig 2.2 and Fig 2.3), to better understand the ecological preferences of important indicator species.

2.2.3 Environmental setting

The continental shelves in the northern BCB Seas include several water masses with different origins that differ in properties, including temperature, salinity, nutrients (Coachman et al., 1975). The Bering Sea is the major source of nutrients, heat, and freshwater flowing into the Chukchi Sea through the Bering Strait (Woodgate, 2018), including three distinct summer water masses: Anadyr Water, Alaska Coastal Water, and Bering Sea Water (Fig 2.2; Coachman et al.,

1975; Weingartner et al., 2005, 2013). Anadyr Water (AW; $-1.0^{\circ} < T < 1.5^{\circ}$, $S \geq 32.5$) is relatively saline, cold, and nutrient-rich and flows along the Russian coast and the western side of the northern Bering Sea. Alaska Coastal Water (ACW; $3^{\circ} < T < 9^{\circ}$, $S \leq 32$) in summer contains warmer and fresher water derived in part from Alaskan river runoff (Weingartner et al., 2005). Bering Shelf Water (BSW; $0^{\circ} < T < 3.0^{\circ}$, $31.8 < S < 33$) is an intermediate water type that is lower in macro-nutrients but with higher salinity contributions from the Bering Slope Current (Coachman et al., 1975). It runs northward and bifurcates at St. Lawrence Island to enter the Bering Strait between the westerly AW and easterly ACW.

In summer, currents flowing through the Bering Strait drive oceanographic properties in the Chukchi Sea, where water is made up of ACW and Bering Sea Water (BSW), which is a combination of both Bering Shelf Water and AW (Weingartner et al., 2013; Woodgate et al., 2005a&b). Bering Sea Water has a higher salinity and nutrient levels than ACW (Walsh et al., 1989; Woodgate et al., 2005a). In the central Chukchi basin, BSW contains the highest primary production and chlorophyll standing stock (Danielson et al., 2017). This water mass follows bathymetric contours of the Chukchi Sea shelf, flowing northwest to Herald Canyon and northeast across the mid-shelf Central Channel to flank Hanna Shoal to the northern tip of Alaska (Barrow Canyon; Fig 2.2; Weingartner et al., 2013; Danielson et al., 2017). Year-round, when the prevailing northeast winds are weak, outflowing water from the Chukchi Sea is advected toward the eastern Canadian Basin along the Beaufort shelfbreak jet (Fig 2.2; Pickart et al., 2009).

These seasonal ocean currents are key in transporting nutrients and phytodetritus into the western Arctic Ocean and maintaining high productivity and biomass (Grebmeier et al., 2015a). In winter and early spring, the shelf areas are uniformly comprised of cold Winter Water (WW;

$T \leq -1.0^\circ$, $S > 31.5$; Gong and Pickart, 2015; Danielson et al., 2020). In summer and fall, WW remains present in the bottom waters of the northern Chukchi Sea (Danielson et al., 2020).

2.3 Materials and Methods

2.3.1 Sample collection and processing

The AOD-2020 compiles ostracode census data collected from circum-Arctic and subarctic sites between 1970 to 2018 from a number of programs and expeditions. Geographical coordinates, depth, temperature, salinity, and original source methodology for all samples in the database are based on original published studies. Most samples were obtained from the uppermost 0-2 cm of surface sediments. For collections during 2009-2018, including the Distributed Biological Observatory (DBO) program, surface sediments were taken from the tops of multicores or Van Veen grabs prior to opening. Most sampling occurred during the months of June, July, August, or September. Corresponding bottom water temperature and salinity were collected at the time of sampling or if shipboard expedition data were not available, as was the case for some older Beaufort Sea samples from the 1970s and 1980s, measurements were derived from World Ocean Atlas 2001 (Stephens et al., 2002; Boyer et al., 2002) and World Ocean Database 2013 (Boyer et al. 2013; as cited in Cronin et al., 2021). Salinity is given without units using the Practical Salinity Scale (Millero, 1993).

Sediments ranging in wet weight from 20 to 150g were washed with tap water through a 63 μ m sieve, oven-dried in paper filters at 40–50°C, and then dry sieved over a mesh-size of >125 μ m. In most cases, all ostracode specimens present in a sample were picked. Living and dead specimens were counted together; however, the majority of samples contained well-preserved shells

and carapaces with chitinous appendages that indicated specimens were alive at or near the time of collection. The number of specimens refers to valves and articulated carapaces each counted as one specimen (Cronin et al., 1991).

2.3.2 Surface sediment characteristics

Because sediment composition and organic carbon content impact benthic faunal biofacies in the Pacific-Arctic (Grebmeier 2012; Grebmeier et al., 2015b), we used ancillary, corresponding surface sediment data, where available, to help characterize benthic ostracode habitat in the northern Bering and Chukchi Seas. Surface sediment total organic carbon (TOC), total organic nitrogen (TON), carbon to nitrogen ratios (C/N), sediment chlorophyll-a (sedchla, as a function of newly settled organic matter), and sediment grain size (0-4 phi = coarse pebbles to sands, ≥ 5 phi = fine silts and clay) used in this study have been previously reported (see Cooper et al., 2002, 2015; Cooper and Grebmeier, 2018 and methodology therein) and are available in public data archives (PacMARS EOL data portal, <http://pacmars.eol.ucar.edu/>, Grebmeier and Cooper, 2014b, 2016; and Arctic Data Center, <https://arcticdata.io/>).

2.3.3 Statistical analyses

Multivariate statistical analyses were carried out using the Paleontological Statistics (PAST) software package, version 3.24 (Hammer et al., 2001). Relative frequencies (percent abundance of total assemblage) were calculated for each ostracode species. Species relative abundance data are expressed as a percentage of an individual species relative to the total number of individuals in a sample. Our studies focused on ostracode samples yielding more than 30 total specimens. Both species (R-mode) and samples (Q-mode) were grouped by several

different correspondence analyses. A principal component analysis (PCA) was used to group ostracode species by their similarities/differences in dominance based on samples designated by ecoregions. A detrended correspondence analysis (DCA) described relationships between ostracode assemblage structure and geographic DBO/other ecoregions. A canonical correspondence analysis (CCA) was used to explore multivariate relationships between the most common ostracode species and their associations with major environmental variables, and sample locations were color-coded by ecoregion. The benthic environment at each station in the northern Bering and Chukchi Seas was characterized by eight variables that could affect ostracode habitat and survival: bottom water temperature; bottom salinity; grain sizes 0-4 phi; grain size ≥ 5 phi; sediment chlorophyll-a; TOC; TON; C/N ratios. The Shannon Weaver “H” Index was used to measure ostracode diversity (Shannon and Weaver, 1949). The values of “H” typically range from 0.0 to 5.0, and increases with increases in both richness (or the number of different species) and evenness (how close in abundance each species is in an environment). In general, values above 3.0 suggest a habitat structure that stable and balanced. Values less than 1.0 indicate a more challenging or impoverished habitat for survival and reproduction.

2.4 Results

Benthic ostracodes were abundant and diverse at continental shelf depths (20-~100m water depth) in Pacific Arctic surface sediments analyzed (ranging from 30 to 562 specimens/sample; Fig 2.1, Table 2.1). A total of 47 ostracode species and five genera were identified in 289 samples (34,369 total specimens) collected from 1970-2018 in the BCB Seas (Table 2.2). Ostracode species identified represent a mixture of Arctic, subarctic, and cold-temperate taxa. At the sampling sites, summer bottom water temperatures were highly variable,

ranging from 12°C off Nome to 6-9°C near the Alaskan coast to $\leq 0^\circ\text{C}$ in Bering and Chukchi Sea middle shelf areas (Fig 2.4a-e). More specifically, ecoregion comparisons of summer near-seafloor temperatures from conductivity-temperature-depth (CTD) measurements show the northern Bering Sea, southwest of St. Lawrence Island (Fig 2.4a, in year 2018), the Chirikov Basin (Fig 2.4b, red dots = DBO2 eastern-most samples off Alaska) and nearshore regions in the southeastern Chukchi Sea (Fig 2.4c, red dots = DBO3-1 eastern samples off Pt. Hope) recently warmed by 2-4°C above historical temperatures. Summer bottom water temperatures at sample locations in Anadyr Water in the northern Bering Sea (Fig 2.4b, blue diamonds) and those more centrally located in Chukchi Sea ecoregions (Fig. 2.4c, orange squares = DBO3-8 and Fig 2.4d, navy squares = DBO5-10) have not yet manifested a sustained warming trend (Grebmeier et al, 2018). The Chukchi Ecosystem Observatory (CEO) mooring, located 70 miles offshore in northeast Chukchi Sea near Hanna Shoal, (71.6 °N and 161.5 °W) rarely recorded near-seafloor temperatures above 0°C prior to 2016. That year and each following year it recorded several months with temperatures exceeding 0°C, which lasted up to four months in 2018 (Huntington et al., 2020). Bottom water temperatures representing a similar but wider geographic area in 2015 and 2017 corroborate this finding (Fig 2.4e).

Salinity was relatively uniform across the sampling locations in that marine conditions prevailed and averaged 32 ± 2 . In the Alaskan Beaufort Sea (20-90m water depth), summer temperatures across all years of sampling averaged $0^\circ\text{C} \pm 1^\circ\text{C}$, and salinity averaged 31 ± 1 . Coarser, sandy sediments that occur in the hydrodynamically active nearshore areas did not cause lower ostracode abundances, as might have been expected (Kornicker, 1959; Kornicker and Wise, 1960).

Diversity “H” in the Chukchi Sea ranged from 1.8 to a little more than 2 during most sample years. Samples averaged 12 (± 4) different species. The Beaufort Sea samples had comparable

diversity values of 1.8, which was consistent in years 1970-2018 where sampling occurred, and 11 (± 3) distinct species per sample. Ostracode diversity in the northern Bering Sea was the lowest compared to these regions, and averaged 1.1-1.2 during the period 2009-2018 with an average of 6 (± 2) species per sample.

2.4.1 Large-scale biogeography of ostracodes in the Bering, Chukchi, Beaufort Seas

Three dominant species in BCB Seas region accounted for 20% to 50% of the total population in the study area: *Normanicythere leioderma*, *Sarsicytheridea bradii*, and *Paracyprideis pseudopunctillata* (Fig 2.5). Each of these species clearly groups with sampling regions designated by DBO ecoregions (noted by symbol on legend) in separate quadrants of the PCA (Fig 2.5). In some samples along the DBO3 and central Chukchi Sea (Ledyard Bay) transects (indicated by orange squares on the PCA), *N. leioderma* and *S. bradii* were co-dominant. Otherwise, all three taxa showed distinct spatial distribution patterns related to the path of the primary summer bottom water masses (and its respective properties) in the surveyed regions. Other ostracode species (labeled in blue around the center axes on the PCA) are secondary components in assemblages.

A DCA (Fig 2.6a) grouped ostracode samples in four distinct geographical groups (Table 2.3). These ostracode biofacies are associated with specific bottom water masses, sediment substrates and/or food sources: Group 1 is a subarctic assemblage dominated by *N. leioderma* in the vicinity of the St. Lawrence Island polynya and the western Chirikov Basin at DBO2 that is influenced in summer by Anadyr Water. Group 2 is an Arctic-subarctic assemblage dominated by *S. bradii* and *N. leioderma* found in the eastern Chirikov Basin of DBO2 and nearshore areas in the southeast Chukchi Sea. Group 2 and Group 3 is bridged by *S. bradii*. In sediments further offshore in the central and middle shelf areas, *P. pseudopunctillata* was the most abundant

species in Group 3, influenced by the BSW of the northeast Chukchi Sea. This offshore sample group includes sediments of Hanna Shoal, which is characterized by stable, cold bottom water temperatures and higher salinity from brine rejection, with WW present in bottom waters year-round (Danielson et al., 2020). Group 4 are the Beaufort Sea samples where influences by river influx and sea ice are strong, and ostracodes are dominated by *P. pseudopunctillata* and *H. sorbyana*.

Environmental factors influencing 14 of the most abundant ostracode species in the northern Bering and Chukchi Seas were examined by CCA (Fig 2.6b) and indicate that variables other than temperature and salinity water mass characteristics influence species distribution patterns. The environmental variables best correlated to ostracode assemblage structure at nearshore stations in the Chukchi Sea (orange squares in Figure 2.6b, i.e. DBO3-1 to 3-4, Ledyard Bay, and blue triangles at DBO5-1 to 5-3) are coarse, sandy sediments (0-4phi) and increased temperatures of ACW. The species most associated with these characteristics include *Schizocythere ikeyai*, *Munseyella mananensis*, *Semicytherura mainensis*, and *Elofsonella concinna*. In addition, *N. leioderma* and *S. bradii* are associated with these regions where sediments have sandy-pebbly textures and also at some locations with high sediment chlorophyll-a in the northern Bering Sea, both south of St. Lawrence Island and in the Chirikov Basin. In samples located in the offshore northern Chukchi Sea and Hanna Shoal region (red inverted triangles and red circles respectively in Fig 2.6b), sustained cold temperatures (<0°C), high salinity from brine rejection during ice formation, and finer grained sediments best align to ostracode assemblage structure and the dominant species, *P. pseudopunctillata*, *Jonesia acuminata*, *Acanthocythereis dunelmensis*, *Robertsonites tuberculatus*, *Kotoracythere arctoborealis*, and *Heterocyprideis fascis*.

The CCA yielded four axes that explained 84.4% of the variance in the relationships between ostracode assemblage structure and environmental properties. The first two axes alone explained about 52% of the variance in the data. The CCA affirms that in the northern Bering and Chukchi Sea region, continental shelf ostracode taxa are more correlated to variables associated with distance from shore and water mass than to latitude (60-71°N). These factors include sediment substrate and food type or availability which link certain species to specific environments.

Based on ordination and multivariate results of ostracode species in the study region (Figs 2.5 and 2.6b), we consider six species, *N. leioderma*, *S. bradii*, *P. pseudopunctillata*, *S. complanata*, *S. ikeyai*, and *M. mananensis*, to be most diagnostic of specific ranges in bottom water temperatures, salinities, sediment substrates and/or food sources (Figs 2.5 and 2.6a&b).

2.4.2 Ecoregions and transects: ecological-scale ostracode assemblages

We also incorporated DBO transect lines (Figs 2.2 and 2.3) in each ecoregion (Table 2.1) into our analysis of ecological preferences of dominant and ecologically significant species. Ecoregion-scale plots of species abundances across seven transects over multiple sampling years help illustrate the regional variation of ostracode biofacies and their spatial composition from nearshore to offshore (Figs 2.7-2.13). Ecoregion DBO-2 in the Chirikov Basin of the northern Bering Sea (Fig 2.7) shows a sharp faunal boundary between *N. leioderma* overlain by Anadyr Water on the western side of the Basin and *S. bradii* in Bering Shelf Water on the eastern side. The southeast DBO-3 ecoregion is dominated by *N. leioderma*, *S. bradii* and *S. ikeyai* in ACW. In samples directly north of the Bering Strait in BSW, *S. complanata* increases in proportion among these species (Fig 2.8). More complex onshore-to-offshore assemblage changes are

reflected in the Ledyard Bay and Icy Cape transects (Figs. 2.9 and 2.10) from 2018, both in the Chukchi Sea. Ledyard Bay and Ice Cape also show clear onshore-to-offshore changes in dominant species. With the exception of a few samples, the Hanna Shoal in the northeast Chukchi Sea ecoregion (Fig 2.11) is dominated by *P. pseudopunctillata* and Group 3 species (Table 2.3). The Barrow Canyon transect (Fig 2.12) shows perhaps the most complex faunal patterns reflecting the temporally and spatially complex and variable ocean water masses and depth changes in the Canyon. The Beaufort Sea west-to-east transect (Fig 2.13, sample locations on Fig 2.4 map) shows fairly consistent dominance of *H. sorbyana*, *P. pseudopunctillata*, *S. bradii* and recent contributions from *N. leioderma*, which is in sharp contrast to its abundant presence in samples of the western Chirikov Basin and southernmost Chukchi Sea. Biogeographic patterns of these species are further discussed below in the “Ecological transects” 2.5.2 section.

2.4.3 Time-series analysis

Two time periods (1970-2012 and 2013-2018) were assessed by PCA to evaluate possible temporal changes in ostracode assemblages (Fig 2.14). These groupings were chosen based on the documentation of accelerated environmental changes (Huntington et al., 2020; Grebmeier et al., 2018) during the latter years, including sea ice duration (Frey et al., 2015), ocean temperature and oceanography (Danielson et al., 2020; Woodgate et al., 2018) and primary productivity (Frey et al., 2020). We did not find that the three most dominant species, *N. leioderma* (Bering Sea), *P. pseudopunctillata* (offshore Chukchi and Beaufort Seas) and *S. bradii* (all regions), changed in relative abundance. For the more recent 2013-2018 period, northern Pacific species *Munseyella*

mananensis and *Schizocythere ikeyai* exhibited small but ecologically significant increases in abundance (~2%) and frequency in the Chukchi Sea region. Based on this evidence, we examined times series of relative frequencies of these five species, *N. leioderma*, *S. bradii*, *P. pseudopunctillata*, *S. ikeyai* and *M. mananensis* (Fig 2.15). The goal was to augment the synoptic time slice analyses to determine if the sampling was complete enough to detect decadal trends from interannual variability. The time series was limited to the last 18 years in Chukchi Sea (2000-2018) because too few repeat observations at similar locations to assess benthic change regionally.

2.5 Discussion

2.5.1 Distribution and ecology of dominant and indicator taxa

Normanicythere leioderma and *S. bradii* are ubiquitous in this region, with very broad environmental tolerances. These species are adapted to the large seasonal variations of the inner and middle continental shelf. *S. bradii* is a wide-ranging, cold temperate to frigid species with temperature tolerances of -1.7 to 18°C (Hazel, 1970), but it demonstrates a preference for mid-shelf depths in temperatures colder than 4.5°C and typical Arctic marine salinities on continental shelves (31-33 is typical; Gemery et al., 2015; S2.1 a&b Fig). Likewise, *N. leioderma* has wide temperature tolerances (-1.7 to 19°C; Hazel, 1970) in typical Arctic shelf salinity. As a dominant species in the northern Bering Sea (Gemery et al., 2013), its distribution is circum-Arctic, including the Chukchi, Beaufort, and Eastern Siberian Seas (Gemery et al., 2015), but is very rare in the Kara Sea and absent in the Laptev Sea (Stepanova et al., 2007). *Paracyprideis pseudopunctillata* is a cryophilic, littoral-sublittoral species (1-50m) with a southerly range limit of ~63°N latitude, tolerant of salinities as low as 5-10 (Hazel, 1970; Neale and Howe, 1975; Stepanova et al., 2003, Stepanova,

2006). *Semicytherura complanata* is adapted to the coldest conditions on continental shelves, including where polynyas form during winter (Stepanova, 2006). An analysis of this species in AOD-2020 reveals that its distribution is tied to near-freezing water temperatures $\leq 0^{\circ}\text{C}$ in sublittoral depths, even though it can withstand higher seasonal temperatures.

These four species, which dominate the study area, are ideally adapted to bottom water temperatures that normally range from -1.8°C to $\sim 4^{\circ}\text{C}$ across the area (S2.1 Table). This temperature range coincides with the temperature window established for benthic macrofaunal animals prevalent at hotspot areas of the Pacific Arctic (Grebmeier et al., 2015a, 2015b).

S. ikeyai and *M. mananensis* are members of genera endemic to the Pacific that have modern distributions off eastern Japan and the Okhotsk Sea and are adapted to a wider range of summer bottom water temperatures ($0-20^{\circ}\text{C}$; Ozawa, 2004; Schornikov, 2001) than the species discussed above. *M. mananensis* is also common to the cold temperate North Atlantic with bottom water temperatures from 2° to 14°C and water depths from 24 to 261m (Hazel and Valentine, 1969). Siddiqui and Grigg (1975) included this species in a list of sublittoral fauna from Halifax Harbour, Nova Scotia. Using the AOD-2020 to assess the subarctic-Arctic distribution of these species in samples with 10 or more specimens, *M. mananensis* is most commonly found in estuarine inlets, with highest abundances (2-30%) in Hudson Bay, North Star Bay (Thule, Greenland), Norton Sound (Alaska) and Chaunskaya Gulf (Eastern Siberian Sea) in bottom water temperatures ranging in summer from 0 to 7°C and salinities from 26 to 33. *S. ikeyai* is rare (one sample reported) in the Beaufort Sea before 2018. It is recorded on the Chukchi Sea shelf in 8 samples (abundance of 2-38%) before 2014 in summer bottom water temperatures from 0°C to 6°C and salinities from 31 to 33. Single specimens occurred in three samples in the Alaskan Beaufort Sea from 1971 to 1982. In the northern Bering Sea, *S. ikeyai* is rare (1.2% of the cumulative assemblage in samples collected

during 2010-2018), and *M. mananensis* is extremely rare (<1% of assemblage). Increased frequency of these species in the Arctic could reflect warming bottom water temperatures since these species reach peak abundances in lower-latitude waters that generally remain above 0°C throughout most of the year. Overall, the abundance and distribution of these six species can be used to infer benthic environmental conditions and potential change in the Pacific Arctic in future studies and in sediment archives for paleo-reconstructions.

While temperature of the bottom water mass is a dominant control on ostracode distributions (Fig 2.6a), the CCA (Fig 2.6b) showed that some species are correlated to a particular sediment texture, and type/availability of carbon food sources. For a few species, *N. leioderma* and *P. pseudopunctillata*, these factors appear to drive their abundance, as supported by the transect analyses (see “Ecoregion transects” Discussion). For example, in the northern Bering and Chukchi Seas, *N. leioderma* more commonly inhabits coarse and pebbly sediments (0-4 phi) of faster moving water, as does *S. bradii*, *S. ikeyai*, and *M. mananensis* (Fig 2.6b; S2.1c Fig). *Paracyprideis pseudopunctillata* is found in greater proportions in silty, fine-grained seafloor habitats (≥ 5 phi) as indicated by its low abundance in sediments of phi 0-4 (Fig 2.6b; S2.1c Fig). *Semicytherura complanata* does not demonstrate a sediment preference (S2.1c Fig).

Availability of organic carbon is a top-level factor that drives species survival and reproduction (Joy and Clark, 1977). *N. leioderma* is associated with areas of newly settled organic material (i.e. higher quality carbon), as indicated by its relative abundance in areas of higher sediment chlorophyll-a ($>10\text{mg/m}^2$) and lower C/N ratios (<7 ; Fig 2.6b; S2.2a&b Fig). In contrast, *P. pseudopunctillata* resides in areas with lower sediment chlorophyll-a and higher TOC ($>0.5\%$; indicating a greater amount of detritus in the surface sediments; Fig 2.6b; S2.2b Fig) and C/N values (>7 ; indicating greater terrigenous inputs; Fig 2.6b; S2.2c Fig). This may indicate *P.*

pseudopunctillata uses detritus or more refractory carbon sources for food. The widespread abundance of *S. bradii* in areas of high- and low-quality carbon further supports its eurytopic nature, and it demonstrates no clear carbon (food) preference (S2.2a&b&c Fig). Because *S. complanata*, *M. mananensis* and *S. ikeyai* are secondary components in assemblages, their proportions are lower and therefore their environmental preferences are more difficult to evaluate. *M. mananensis* and *S. ikeyai* are present in sediments with higher C/N ratios, which corresponds to their higher proportions at sampling stations nearer to shore in ACW, e.g. southern Chukchi Sea stations DBO3-1 to DBO3-4 and northern Chukchi Sea stations DBO5-1 to DBO5-3 (S2.2c Fig). In these nearshore sediments, coarse grains and gravel may be dominant, but there is fine sediment in between the large grain size. This indicates variable settling rates over various seasons, providing complexity to nearshore statistical findings. Additional sampling of these species and corresponding sediments are required to better evaluate the role that sediment and organic carbon sources may have on their abundance.

2.5.2 Ecoregion transects: spatial relationships among ostracode biofacies

Stack plots showing the primary species in sample assemblages in an ecoregion and/or along a sampling transect (Figs. 2.7-2.13) provide insight into factors that control species occurrence and frequency. Generally in the study area, bottom water temperature declines with increasing latitude and distance from shore. Sediment composition also becomes finer-grained (greater silt fraction) with increasing distance from shore (Feder et al., 1994; Grebmeier et al., 2015a). Other properties, especially in the central and northeast Chukchi Sea, involve more complex spatial patterns (Grebmeier et al., 2015b; Blanchard et al., 2013). Varying seafloor bathymetry, sediment substrate, flux of organic carbon settling to the seafloor, and current

velocities combine with water mass characteristics to create a complex habitat of varying ecological gradients. These transects show the variability of species occupying a sampling area of 0.1m² at a given location on the seafloor during a summer's day collection. At DBO2-Chirikov Basin (Fig 2.7a), Ledyard Bay (Fig 2.9), Icy Cape (Fig 2.10) and DBO5-Barrow Canyon (Fig 2.12) transects, ostracode biofacies do not show a continuous composition but instead a faunal transition from nearshore to offshore stations. The ecoregion plots show distinct abundance changes in indicator species, which were sometimes acutely distinct, based on spatial environmental changes in water mass, sediment properties and food type. These descriptions of ostracode faunal assemblages can serve as a baseline to examine future meiofaunal changes in the BCB Seas.

2.5.2.1 Chirikov Basin – DBO2

The DBO2 transect in the Chirikov Basin (Fig 2.7a) is an example of ostracode indicator species clearly divided by water masses of differing productivity. Stations DBO2-1 and 2-4 are the western-most locations, and are in the path of AW (Fig 2.2). Major differences between the water masses include higher average values of sediment chlorophyll-a and salinity (Fig 2.7b) to the west because the more eastern samples are underlain by BSW or a combination of ACW above and BSW below. Integrated primary production estimates in the Chirikov Basin range from ~80 g C m⁻² yr⁻¹ on the interior shelf to up to 480 g C m⁻² yr⁻¹ in AW (Hill et al., 2018). *N. leioderma* (red) is more prevalent in AW. The eastern side of the Basin (stations DBO2-2 and 2-5) is dominated by *S. bradii* (blue) and *E. concinna* (brown), with increasing numbers of *S. ikeyai* (light blue) in 2018 samples that may reflect slightly higher average bottom water temperatures (nearly 2°C, Fig 2.4b). The abrupt change in faunas from east to west related to water mass channels is very consistent on interannual timescales at these sampling locations, with the exception of DBO2-4. Earlier samples

from years 2001 and 2003 do not have *N. leioderma* as the dominant fauna at DBO2-4, and samples from years 2016 and 2018 do. We speculate that *N. leioderma* may have expanded its population perhaps due to increasing carbon export to the benthos and/or changes in current flow that affected sediment grain size. Since satellite monitoring began in 1979, the length of the ice-free season in the Chirikov Basin has increased by ~25 days, stimulating greater primary productivity due to a longer growing season (Brown and Arrigo, 2012; Brown et al., 2011). With *N. leioderma* as the established dominant fauna in the northern Bering Sea around the St. Lawrence Island polynya (Gemery et al., 2013), additional light and productivity may be factors that contribute to its expansion. Another major feature of this area is strong currents that create coarse seafloor sediments consisting of primarily (>75%) 0-4 phi-sized sand, which *N. leioderma* favors. Macrofaunal biomass associated with finer-grained sediments has significantly declined at sampling station DBO2.4 from 1999-2015 (Grebmeier et al., 2018). At this site, *N. leioderma* comprised >50% of the assemblage composition in 2018 and 2016 compared to <10% in 2001 and 2004 (Fig 2.7a).

2.5.2.2 Southeast Chukchi Sea – DBO3

At the nearest-to-shore stations, DBO3-1 to 3-4, the ostracode biofacies during 2014 to 2018 have been extremely consistent, not only in species present but species proportions as well (Fig 2.8). Species at DBO3-1 to 3-4 stations are in the path of ACW (temperatures 6°–10°C) that reach to the seafloor (Wood et al., 2015b). Higher sediment grain sizes at these near shore stations are consistent with the presence of the ACC. These nearshore stations experience great variability in seasonal bottom water temperatures (~10°C) and are dominated by *N. leioderma* (35%) with secondary taxa *S. bradii* (14%), *S. ikeyai* (13%), *E. concinna* (6%), *M. mananensis* (3%) and

Finmarchinella spp. (5%). *Paracyprideis pseudopunctillata* is also present in many sample years in low abundance (2%). *H. sorbyana* (3%), an extremely euryhaline species (Cronin, 1977; Neale and Howe, 1975), appears only at nearest-to-shore DBO3-1 sites, and reflects the fresher water (average 31 salinity) of ACW. DBO3-1 to 3-4 are hotspots of ostracode abundance (samples averaged 235 specimens/sample) compared to sites further south or north. Despite high current velocities at these near shore stations, as indicated by coarser sediment grain sizes (75% phi 0-4 [± 9]), sediment chlorophyll-a averaged 18 mg/m² (± 11) at DBO3-1 to DBO3-5 sites from years 2014 to 2018, which supported consistently high abundances of *N. leioderma* and other ostracode species.

Samples just north of the Bering Strait (denoted as “N of St” on Fig 2.12) and DBO3-5 are offshore in a different summer water mass than DBO3 sites closer to shore. This water mass change is indicated by a different ostracode biofacies with fewer species overall and high proportions of *N. leioderma* and *Semicytherura* spp., particularly *S. complanata* and *S. mainensis*.

Ostracodes are rare or absent in sites further offshore (DBO3-6 to DBO3-8) in the path of BSW as sediment composition shifts to finer-grained sediments (slower current speeds, ~50-93% ≥ 5 phi) and higher TOC (>1%) values. This pattern is consistent over multiple years of sampling. Benthic macrofaunal biomass is very high at these offshore sites, with abundant production settling to the sediments (Grebmeier et al., 2015b).

2.5.2.3 Central Chukchi Sea – Ledyard Bay

While the ostracode biofacies at most sampling sites along the 2018 Ledyard Bay transect are similar to those at DBO3 sites (except *S. ikeyai* is lacking at Ledyard Bay [2 individuals]), the Central Channel bearing BSW north to the shelf break (Fig 2.2) cuts across this sampling transect

and creates sediment grain size, production and temperature gradients between the sample locations that drastically change ostracode assemblage composition. The station LB-5, in the path of ACW proximal to shore, has coarse sediments (75% 0-4 phi), a summer bottom water temperature at the time of sampling of 8.7°C, and 31 salinity. Subarctic species *N. leioderma* (20%), *M. mananensis* (6%) and *Semicytherura* species (32%) occupied this site (Fig 2.9). At the next site, LB-7, sediments change to finer silt (59% ≥ 5 phi) and *P. pseudopunctillata* becomes dominant with *Palmenella limicola* and *S. complanta*. *N. leioderma* is absent. Further offshore there is a grain size shift back to coarser sediments east of Herald Shoal (62% in the 0-4 phi category at LB-13, and of that, 25% in the 0-2 phi category) where *N. leioderma*, *S. bradii*, *M. mananensis* and *Kotoracythere arctoborealis* become predominant. In addition, the highest primary productivity rates in the Chukchi Sea are consistently observed in the central part of the shelf along the dividing line between the warm Alaskan Coastal Current to the east and in the colder nutrient-rich Bering shelf waters to the west (Woodgate et al., 2015). *N. leioderma*'s increasing abundance at LB-11 and LB-13 may reflect a fresh, more ample food source. TOC increases toward the offshore stations and sediment chlorophyll-a, although seasonally and yearly highly variable is highest at LB-13 (20 mg/m²) as is *N. leioderma*'s (30%) abundance. Along the transect, temperature declined with distance from the coast from 8.7°C at LB-5 to 2.4°C at LB-13, where *N. leioderma*, *S. bradii*, *S. complanata*, *M. mananensis* and *K. arctoborealis* persist. This transect may be an example of how subtle changes in bathymetry and current flow can result in changes in food availability and sediment texture in very localized areas that affect the spatial distribution of benthic communities (Blanchard et al., 2013) and, likewise, ostracode biofacies.

2.5.2.4 Northeast Chukchi Sea – Icy Cape 2018

The 2018 Icy Cape transect shows the influence of bottom water mass and sediment texture on assemblage composition. Bottom water temperature closest to shore at ICY2 was 1.4°C, but more offshore stations were colder with temperatures of 0° to -1°C (Fig 2.10). In the northeast Chukchi Sea, sea-ice coverage usually extends into the summer months (July- August), with areas of localized persistence possible throughout the summer. Winter water was still present on the seafloor during late summer sampling. Close to shore, grain size at ICY2 to ICY5 was coarse (45% to 76% in phi 0-4 category), where *S. bradii* and *S. complanata* were predominant and *P. pseudopunctillata* was absent. The presence of *P. pseudopunctillata* beginning at ICY6 and steadily increasing to dominate (25% to 60%) the assemblages at ICY9, ICY10 and ICY11 is indicative of a seafloor sediment transition to very fine grains, ranging from 63% to 87% ≥ 5 phi. In addition to suitable habitat, persistent cold temperature supports *P. pseudopunctillata*. *Jonesia acuminata* is correlated to near-freezing temperatures and fine sediments (Gemery et al., 2013), and this species has a small but notable presence at the ICY7 to ICY11 stations.

2.5.2.5 Offshore Hanna Shoal, Northeast Chukchi Sea

Heterogeneous seafloor contours direct BSW with high nutrient concentrations to the Hanna Shoal area (Weingartner et al., 2017b). It is a hotspot for benthic productivity that supports marine mammals (Grebmeier et al., 2015a). The ostracode biofacies includes *P. pseudopunctillata* (37% of assemblage) with secondary species *S. complanata* (14%), *H. fascis* (8%), *R. tuberculatus* (7%) and *C. cluthae* (5%; Fig 2.11). It is very similar to the assemblage of offshore Icy Cape sites except this biofacies includes greater proportions of *A. dunelmensis* (6%) and *R. tuberculatus*, and *Argilloecia* sp. (4%), which are species associated with finer-grained sediments (Fig 2.6b). *Normanicocythere*

leioderma is rare (1%). *Paracyprideis pseudopunctillata* and *H. fascis* are euryhaline and can tolerate fluctuating salinities. At the time of summer collection, the average salinity at sample locations was 33, bottom temperature, -1.7°C and water depth, 51m. This area lacks any strong gradient from currents, as sea ice tends to be trapped over Hanna Shoal, so dense bottom-confined pools formed by winter water tend to stagnate (Martin and Drucker, 1997; Weingartner et al., 2005, 2013). Sustained cold temperatures, fine-grained sediments, and relatively higher salinities describe this frigid-water assemblage.

2.5.2.6 Barrow Canyon/DBO5

Sampling stations on the DBO5 transect have significant changes in depth, from ~50m at DBO 5-1 and DBO5-2, ~90m at DBO5-3 and deepening further to ~130m at DBO5-5, ~120m at DBO5-6, ~90m at DBO5-7 and ascending to 60-70m depths at DBO5-8 to DBO5-10 (Fig 2.2). Although seasonally variable, the deeper locations had much higher sediment chlorophyll-a (18-26 mean mg/m²) values measured in summer, deposited by variable strong currents flowing through the Canyon. *N. leioderma* increases in abundance at these sites, particularly DBO5-6 and 5-7 stations, which historically also have high TOC values (~2%; Fig 2.12). These offshore stations are usually characterized by bottom water temperatures <0°C, however nearshore DBO5-1 and 5-2 sites have experienced summer warming in recent years with temperatures reaching 4-7°C (Fig 2.4d). Station DBO5-1 is influenced by ACW, which can reach the seafloor. These nearshore stations are dominated by *S. bradii* and cold-temperate/subarctic taxa *M. mananensis* and *S. ikeyai*, which decline in abundance moving seaward towards DBO5-5. (Note: Sites DBO5-4 and 5-8 are not represented due to low ostracode abundance of <30 specimens/sample.) At stations DBO5-6 to 5-10, seafloor sediments are extremely fine-grained silt, typically ≥90% 5phi. These sediments are

the finest-grained of any ecoregion, and they are occupied by ostracode faunas that require this habitat along with near-freezing temperatures, notably *P. pseudopunctillata*, *S. complanata* and *C. cluthae*. At station DBO5-9 there is a distinct faunal transition to these species. Cold ($<0^{\circ}\text{C}$), dense ($\sim 33\text{-}34$ salinity) WW can remain at these stations during summer (Pickart et al., 2011). Occasionally, warm ($>-1.2^{\circ}\text{C}$), salty (>33.6) Atlantic water is upwelled into the Canyon and fills the deepest part of the area (Pickart et al., 2019).

2.5.2.7 Alaskan Beaufort Sea

The Alaskan Beaufort continental shelf is a highly variable environment, influenced by seasonal discharge from the Colville and Mackenzie rivers that supply fresh water and deposit terrigenous material but lacks strong gradients within the examined narrow area of 20-90m water depth (Fig 2.3; sample locations were limited to within 100 km of shore, and included intermittent years between 1971 and 2018). Bottom water salinity at the sampling sites during the time of collection averaged 31. In addition to river inflow, the Beaufort shelf also receives dense “winter-transformed” Pacific water (Weingartner et al., 1998; Pickart, 2004) that drains off the Chukchi shelf. This water enters the Beaufort Sea as a shelf-break current that turns eastward from Barrow (Fig 2.2; Pickart et al., 2005). As an area that experiences dramatic seasonal fluctuations, particularly in salinity, two species are overwhelmingly suited to these conditions: *P. pseudopunctillata* and *H. sorbyana*, cryophilic taxa correlated with euryhaline conditions (Fig 2.13; Stepanova et al., 2003, 2007). These two species are reported by Stepanova et al. (2003, 2007) as adapted to the inner shelf, river-affected zone of the Kara and Laptev seas where salinities range between 26 and 32. The eastern Alaskan Beaufort is influenced by the Mackenzie River, resulting in finer sediment grain sizes and better sorting in that region (Naidu, 1974; Barnes et al., 1982),

which correlates to greater abundance of *P. pseudopunctillata*. For 2018 PRW and PRB transect samples (sites on Fig 2.3 map) that are most influenced by Colville River inflow, *H. sorbyana* is more prevalent than *P. pseudopunctillata*. Secondary species in the Beaufort Sea assemblage include *S. bradii*, *S. punctillata*, *R. tuberculatus*, *H. fascis*, and *A. dunelmensis*. *S. complanata* is present in low (~2%) abundance in these Beaufort Sea assemblages.

Despite limited temporal data in this area, *N. leioderma* and *S. bradii* are more prevalent in 2018 samples than in samples collected in comparable locations during the 1970s and 1980s where *P. pseudopunctillata* and *H. sorbyana* comprised the major proportion of the assemblage (S2.3 Fig). This may be due to recent declines in ice persistence and increases in nearshore temperatures or changes in sediment composition that may be incompatible with *P. pseudopunctillata*'s preferences for near-freezing temperatures and finer grained sediments. However, sediment transport by ice rafting can be significant on the shelf, and can carry gravel and sand particles from the coast onto the shelf (Barnes et al., 1982). There are insufficient data available to determine if a change in sediment grain size is a factor. The Beaufort shelf, while not as productive as the Chukchi Sea, can have locally high primary production rates associated with the ice edge, reaching $200\text{mg C m}^{-2} \text{d}^{-1}$ (Hill et al., 2018). The retreating sea-ice edge, in addition to upwelling, provides nutrients for phytoplankton growth. The number and strength of upwelling events in the Alaskan Beaufort Sea has increased over the past 25 years (Pickart et al., 2013a, 2013b). Greater fresh phytoplankton production may be an explanation for the increasing appearance of *N. leioderma* in 2018 samples (S2.3 Fig), but our new data must be considered cautiously given the single year of samples.

2.5.3 Temporal trends in BCB Sea indicator species

Criteria used to assess whether environmental factors are driving changes in benthic communities include the arrival of taxa characteristic of a temperate climate zone or shifting dominance or abundance of taxa (Bluhm et al., 2017). Species can extend north and south (and east to west) to the point where certain maximum or minimum tolerable temperatures are reached (Hazel, 1970).

Due to temporal and spatial gaps in sampling, we could confidently evaluate temporal changes only in the dominant species, *N. leioderma*, *S. bradii* and *P. pseudopunctillata*. Two PCA comparisons by years (1970-2012 and 2013-2018) showed that the dominant species have remained fairly consistent in the BCB Seas (Fig 2.14). Interannual abundances of the dominant species in the Chukchi Sea from 2000-2018 did not reveal statistically significant changes, but two indicator species, *S. ikeyai* and *M. mananensis*, show incipient increases (Fig 2.15).

Dispersal of meiofauna into new areas likely lags behind sediment and water column changes. Benthic marine ostracodes are transported by ocean currents (Teeter, 1973). Considering that the movement of Pacific water from the Aleutian Passes to Bering Strait takes more than a year (Wood et al., 2015a) and an additional ~4 months to transit to Barrow Canyon in the Chukchi Sea (Woodgate et al., 2005b), benthic meiofaunal migration from the north Pacific to the Arctic could take a number of years. Over the shallow shelves of the northern Bering and Chukchi Seas, seasonal ice coverage cools the entire water column to temperatures below 0°C. These cold temperatures limit the northern distribution of subarctic populations of groundfish (Mueter and Litzow, 2008) and may also serve as a barrier inhibiting the mixing of Arctic and N. Pacific faunas through the Bering Strait (Joy and Clark, 1977). It is more likely that cold temperate species already inhabiting restricted inner bay areas like Norton Sound and

coastal polynyas along Alaska will increasingly be able to extend their range and abundance as conditions become more suitable for them under changing climate scenarios.

2.6 Conclusions

We examined benthic ostracode assemblages collected during research cruises from 1970-2018 in the northern Bering, Chukchi, and Alaskan Beaufort Seas. We focused on identifying indicator species and their associated ecological preferences. In particular, ostracode abundance and distribution were related to bottom temperature, salinity, organic carbon deposition (sedchla, TOC, C/N), and sediment substrate.

The variability in ostracode assemblage composition throughout the BCB Seas was linked qualitatively to localized (summer seasonal) environmental patterns. We found south-to-north (Chirikov Basin to Northern Chukchi to Beaufort) changes in dominant ostracode species and assemblage composition. Over the large biogeographic scale, four ostracode biofacies were identified in the study area primarily tied to the transit of summer water masses. Distinct changes of ostracode biofacies in nearshore to offshore transects were related to water mass properties likely in combination with food sources and sediment substrate. This study is among the first to highlight changes in ostracode abundance and species over small spatial scales in response to changes in water mass properties and productivity.

Six indicator species were identified by correspondence and multivariate analyses based upon their abundance and correlations with distinct ecological parameters by which they are defined:

Normanicythere leioderma – opportunistic subarctic species correlated with ample, high-quality production (exported phytoplankton) as food source; sandy to pebbly to gravelly sediments;

Paracyprideis pseudopunctillata – euryhaline cryophilic species associated with WW presence and sea ice, fine grained sediments, sustained frigid temperatures ($\leq 1^{\circ}\text{C}$), TOC with high phytodetritus;

Sarsicytheridea bradii – habitat generalist, eurytopic species that capitalizes in highly dynamic environments, higher frequency in sandy sediments;

Semicytherura complanata – frigid temperatures ($\leq 1^{\circ}\text{C}$), normal marine salinity, no discernable sediment preference;

Schizocythere ikeyai – cold-temperate species, warmer temperatures, ACW, sandy sediments;

Munseyella mananensis – cold-temperate species, warmer temperatures, ACW, sandy sediments.

This study found a consistent link between areas of high sediment chlorophyll, coarse sediment grain size and the abundance of *N. leioderma*. Despite wide tolerances, it may be a sensitive indicator of new production reaching the benthos and/or enhanced food supply. In future paleoceanographic studies using fossil ostracode faunal assemblage data, *N. leioderma* may signal the influence of nutrient-rich Pacific water flowing in through the Bering Strait and a food supply consisting of newly settled phytoplankton. *Paracyprideis pseudopunctillata* is positively correlated to very fine-grained sediment textures with high TOC values of refractory (detrital) organic carbon food sources.

During the last decade, we document an incipient increase in two secondary cold-temperate species, *S. ikeyai* and *M. mananensis*, that may be increasing. Preliminary interpretation of this finding may reflect recent increases in coastal and mid-shelf bottom water temperatures and/or carbon flux to the benthos.

Continued monitoring of temperature-sensitive ostracode species in the BCB Seas is necessary to provide information on annual and decadal variability in species distributions. This analysis of modern species ecology can help interpretation of ostracode faunal data from

sediment cores in relation to past and future ocean changes. This study contributes new species ecology and further validates the sensitivity and application of ostracode fauna as biomonitors and proxies for specific environmental conditions. These results provide a baseline for assessing the effects of future water mass changes and productivity on benthic ostracode communities in the Pacific Arctic.

2.7 Acknowledgements

We thank A. Ruefer, N. Vaka and S. Watson for assistance with sample processing and E. Fachon for collection of 2018 Beaufort Sea samples during the HLY18-03 expedition. We also thank the field technicians in the Grebmeier/Cooper laboratory at CBL/UMCES for water column and sediment collections from multiple time-series cruises used in this study. We would also like to thank J. Keith, M. Robinson, G. L. Wingard, and two anonymous reviewers for critical comments that improved earlier versions of the manuscript. Any use of trade, firm, or product names is for descriptive purposes only and does not imply endorsement by the U.S. Government. Financial support for sample collections was provided by grants to JMG and LWC from the NSF Arctic Observing Network program (1204082, 1702456 and 1917469) and the NOAA Arctic Research Program (CINAR 22309.07 and 25984.02, <https://arctic.noaa.gov/>). Support was also provided by the USGS Climate & Land Use R&D Program. The funders had no role in study design, data collection and analysis, decision to publish, or preparation of the manuscript.

Figure 2.2 Location of sample sites in the northern Bering and Chukchi Seas used for ecoregion transect (nearshore to offshore) study. (n=147 surface sediment aliquots with ≥ 30 specimens per sediment sample, 19,300 total specimens, 1990-2018) Schematic of summertime surface current flow patterns and water mass type that can affect seafloor conditions (Anadyr Water [AW], Alaska Coastal Water [ACW], Bering Sea Water [BSW]; properties denoted in Table 2.3) adapted from Danielson et al. (2017, 2020). Figure made with GeoMapApp (www.geomapapp.org) / CC BY / CC BY (Ryan et al., 2009).

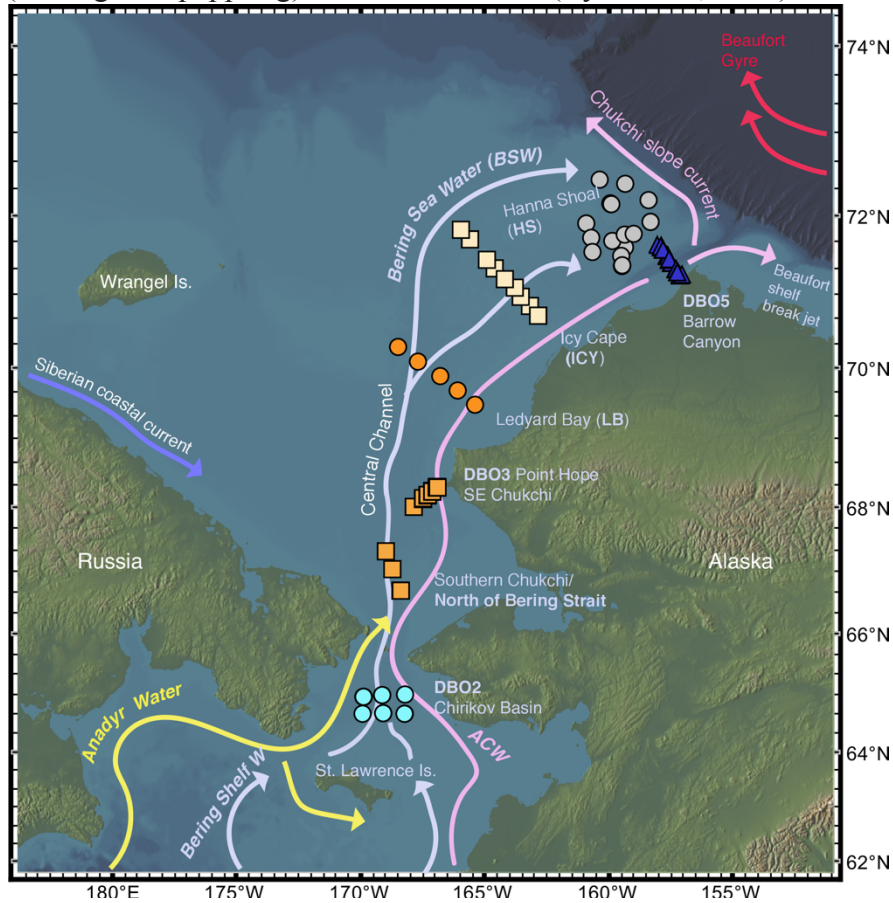


Figure 2.3 Location of samples used in Beaufort Sea ecological transect study from years 1971-2018 (n=55 surface sediment aliquots with ≥ 30 specimens per sediment sample, 20-100mwd, 6,617 total specimens). Figure made with GeoMapApp (www.geomapapp.org) / CC BY / CC BY (Ryan et al., 2009).

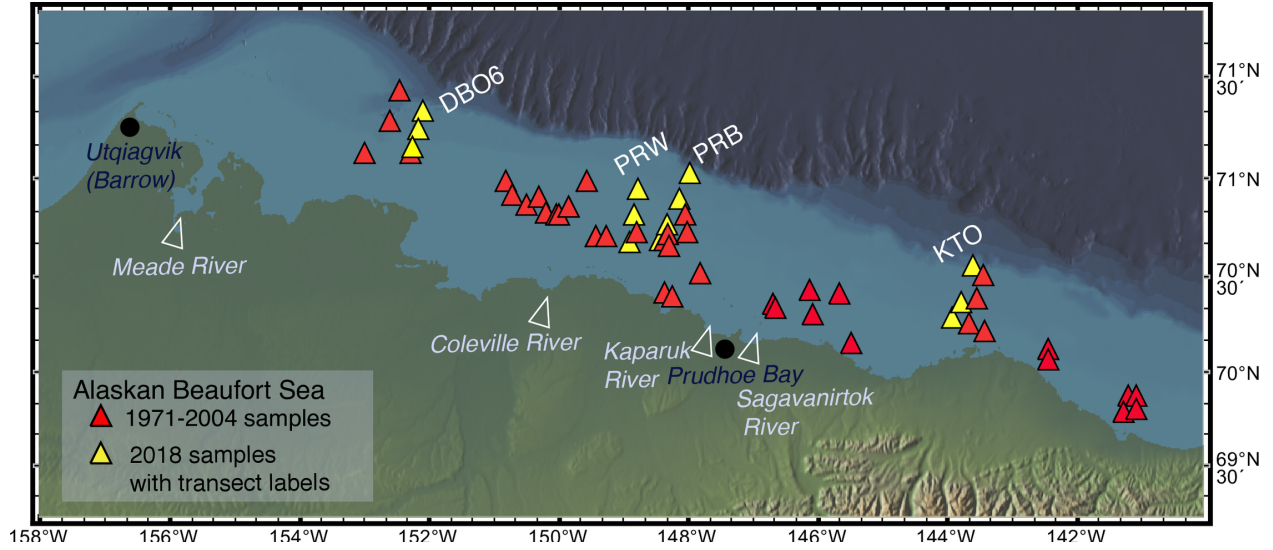


Figure 2.4 Summer bottom water temperature at ecoregions. Comparison of summer bottom temperatures in studied ecoregions and months at stations nearest to shore (e.g. DBO3-1, DBO5-1) that are locations affected by Alaska Coastal Water, and more central or middle-shelf stations (DBO3-5 or DBO5-10) that are affected by Bering Sea Water (winter or summer variants). This subset of data was derived from the Pacific Marine Arctic Regional Synthesis (PacMARS) Project (Grebmeier and Cooper, 2014a; <http://dx.doi.org/10.5065/D6VM49BM>; Okkonen, 2013; <https://data.eol.ucar.edu/dataset/10339>) and recent expedition data (2014-2018) taken aboard USCGS Healy and CCGS Sir Wilfrid Laurier and archived at the National Science Foundation's Arctic Data Center.

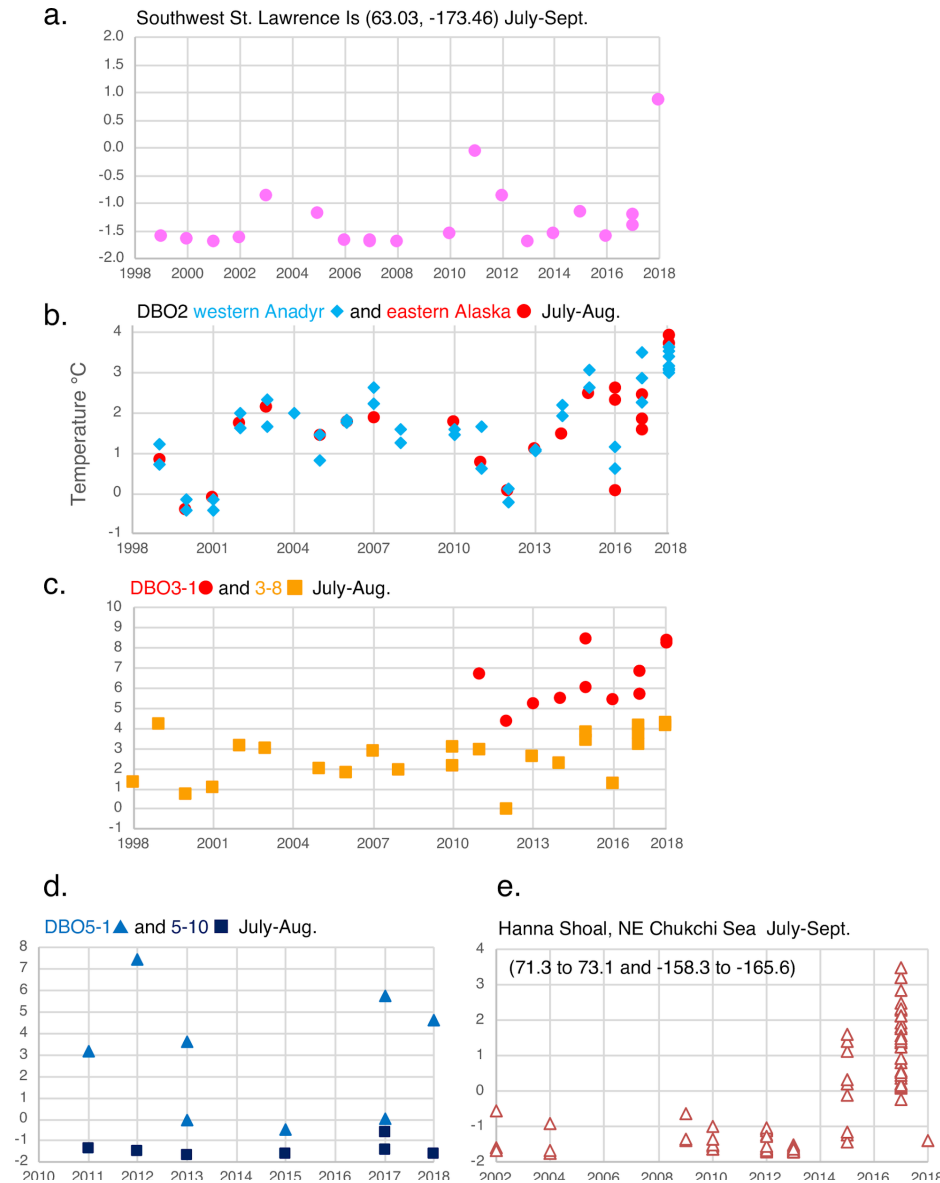


Figure 2.5 Principal correspondence analysis (PCA). PCA of ostracode assemblages in the northern Bering, Chukchi, and Beaufort Sea region (locations on Fig 2.1; geographic coordinates in Table 2.1), with sites designated by DBO areas and other ecoregions (legend symbols) and major taxa (green lines with species names labeled in blue). Three species dominate the assemblage groups: *N. leioderma*, *S. bradii*, and *P. pseudopunctillata*. The proximity of the symbols in the plot reflects the level of similarity in taxa present at each sampling station.

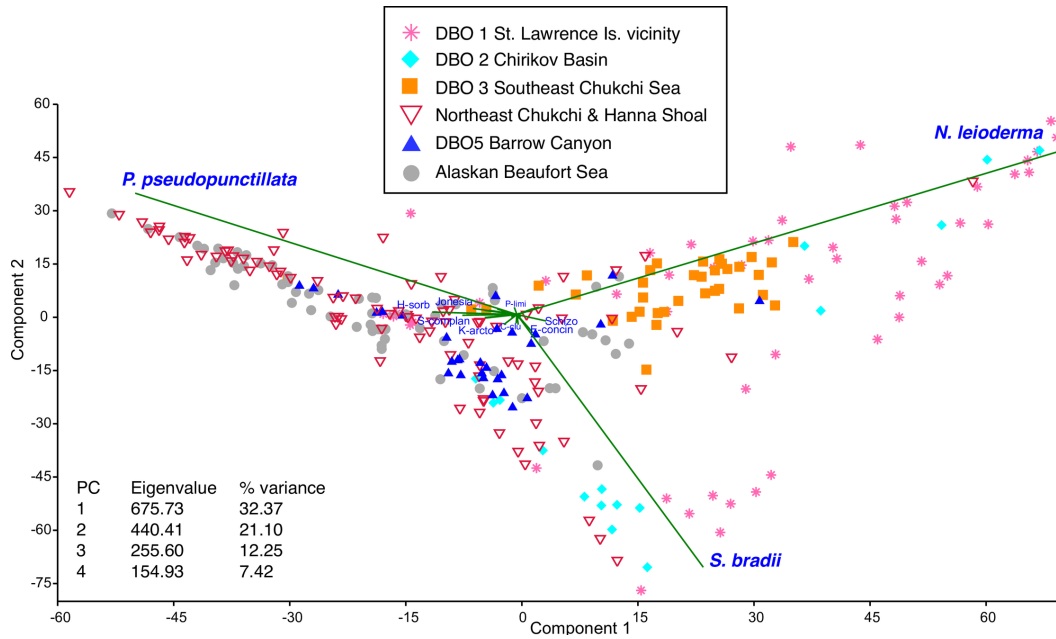


Figure 2.6a Detrended correspondence analysis (DCA). DCA using the northern Bering, Chukchi, and Beaufort Seas biogeographic dataset (1970–2018), describes relationships between ostracode assemblage structure and geographic ecoregions in the region. Ostracode biofacies differed among ecoregions within the study area (described in Table 2.3) and grouped primarily on summer water mass characteristics (temperature and salinity).

Figure 2.6b Canonical correspondence analysis (CCA). CCA of ostracode assemblages in the northern Bering-Chukchi Sea region, with sampling ecoregion sites (noted by symbol on legend), major taxa (names are labeled in blue), and eight environmental parameters (green lines and labels in black: temperature, salinity, sediment total organic carbon [TOC], sediment nitrogen [TON], sediment chlorophyll-a [sedchla], phi ≥ 5 [fine silt], and phi 0-4 [gravel pebbles to sands]). Samples in the Hanna Shoal region (red dots) were separated from the larger northeastern Chukchi Sea sample set (inverted red triangle). Dataset includes the 14 most abundant species in 153 surface sediment aliquots (23,939 total specimens) from the northern Bering and Chukchi Seas during summers 1990-2018 for which sediment data was available.

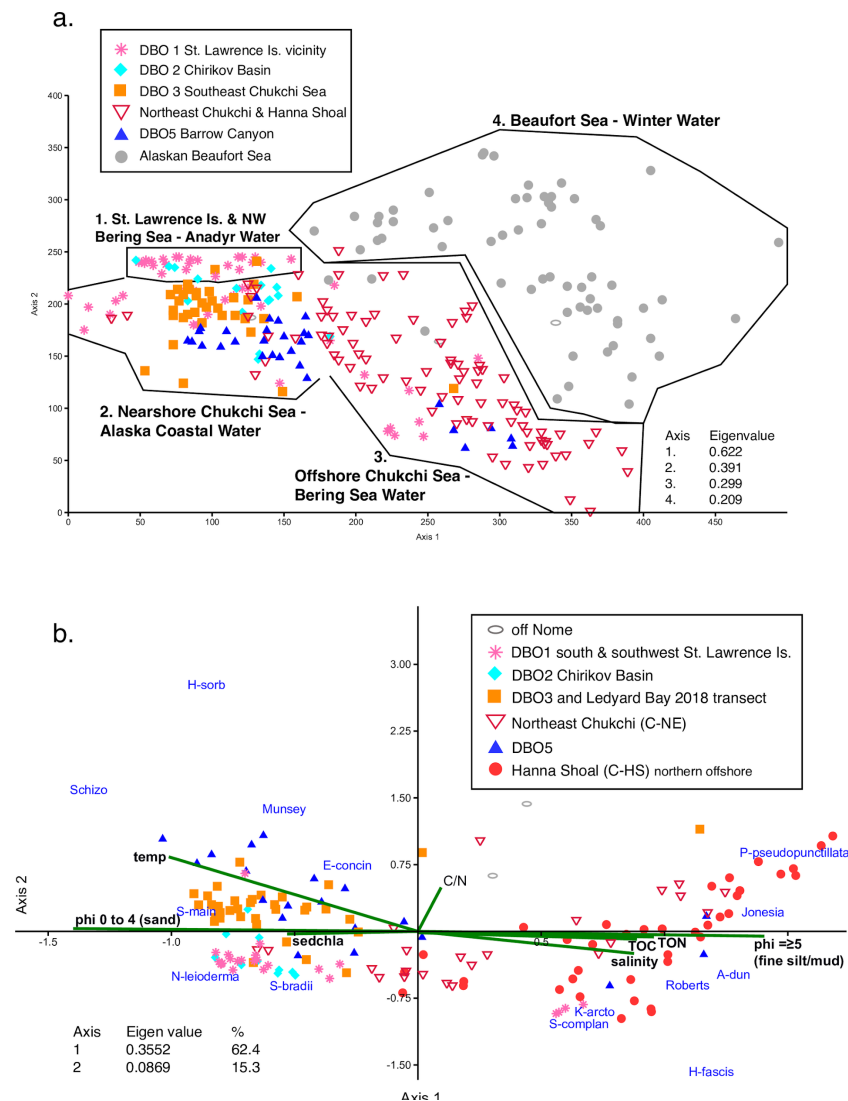
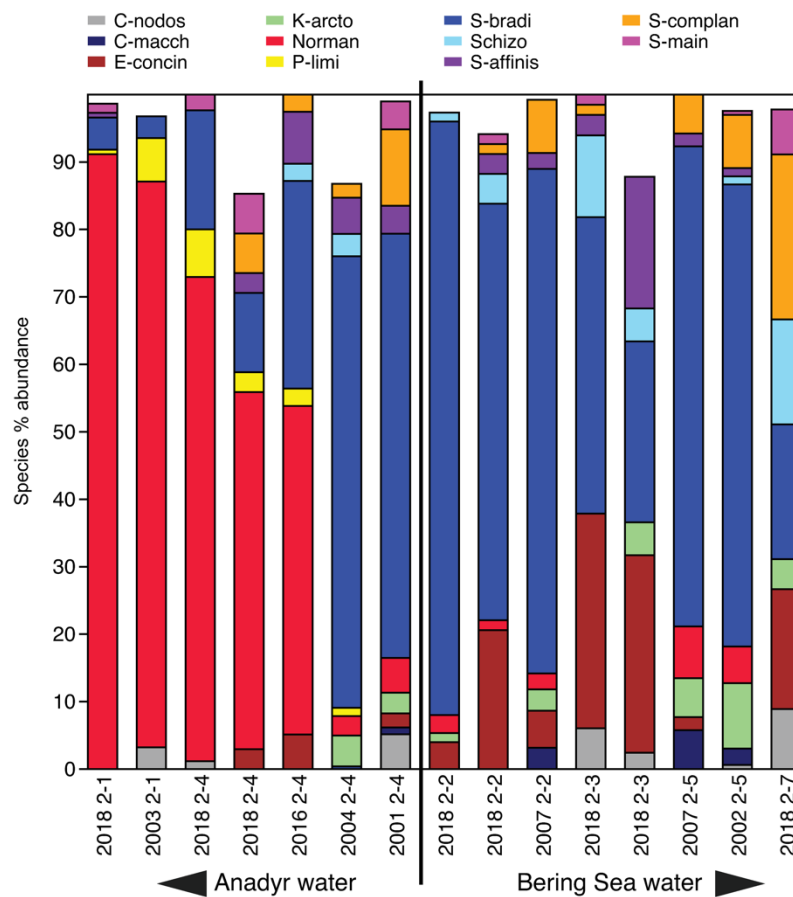


Figure 2.7a Primary species, DBO2 - Chirikov Basin. Stack plot of dominant species in DBO2-Chirikov Basin region (Fig 2.2) in the northern Bering Sea (various years from 2001 to 2018; n=15, 1,314 specimens with ≥ 30 specimens/sample). The 11 species presented in the stack plot comprise 98% of the biofacies in this ecoregion. (Note the boundary between Anadyr water on the western side of Chirikov Basin and Bering Sea Water on the eastern side is generalized in this graphic.)

Figure 2.7b Summer bottom water salinity at western and eastern DBO2 - Chirikov Basin sampling sites. Time series plot of summer bottom salinity at sampling stations on the western and eastern side of the Chirikov Basin (Source: Grebmeier and Cooper, 2014a; Okkonen, 2013; and recent expedition data (2014-2018) taken aboard USCGS Healy and CCGS Sir Wilfrid Laurier archived at the Arctic Data Center)

a. Chirikov Basin - DBO2



b. DBO2 western Chirikov \blacklozenge and eastern Chirikov \bullet July-Aug. salinity

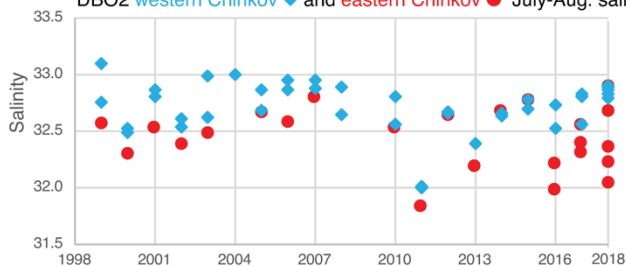


Figure 2.8 Primary species, DBO3 - Southern Chukchi Sea. Stack plot of the 12 most abundant species and one genus (*Semicytherura*), comprising 92% of the ostracode assemblage, in DBO3 region (sites on Fig 2.2 map) from years ranging from 1998 to 2018, (n=32 samples with ≥ 30 specimens/sample, 7,514 total specimens).

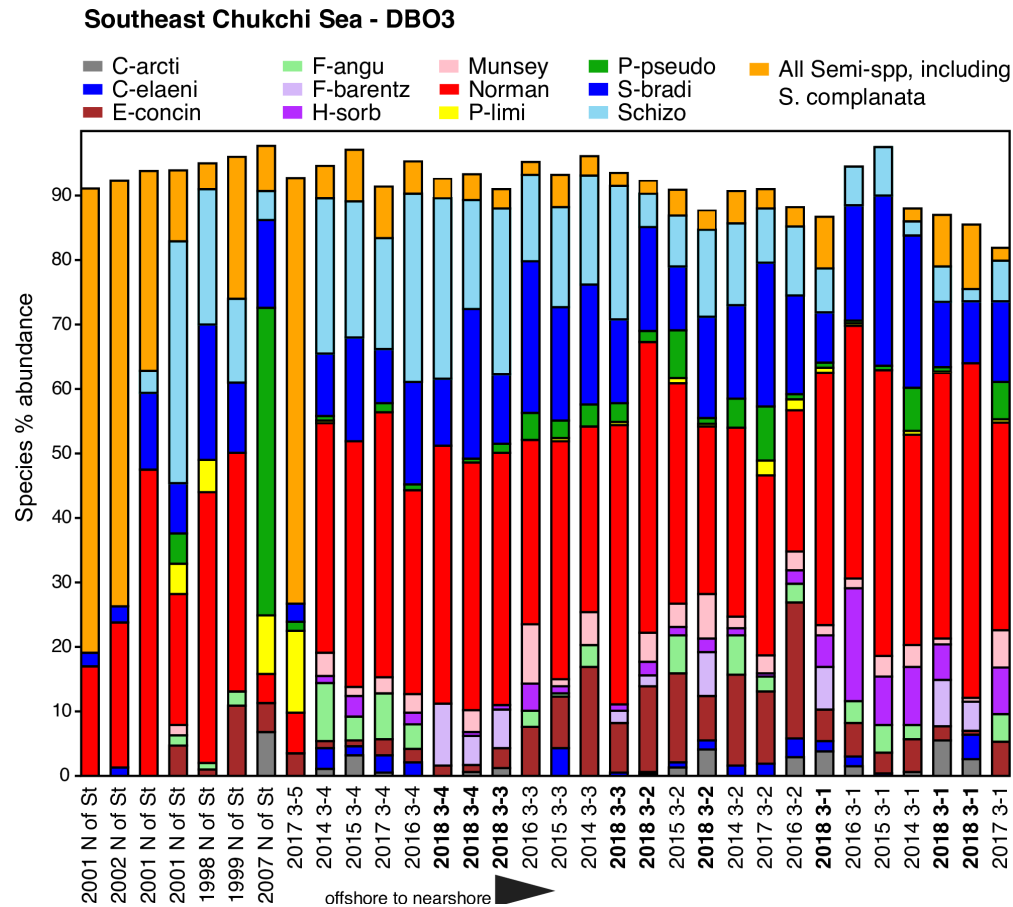


Figure 2.9 Primary species, Central Chukchi Sea – Ledyard Bay. Stack plot of the 12 most abundant species and one genus (*Semicytherura*), comprising >90% of the ostracode assemblage at the 2018 Ledyard Bay transect (sites on Fig 2.2 map), southeast Chukchi Sea, (n=5 surface sediment samples, all with ≥ 50 specimens/sample, 558 total specimens).

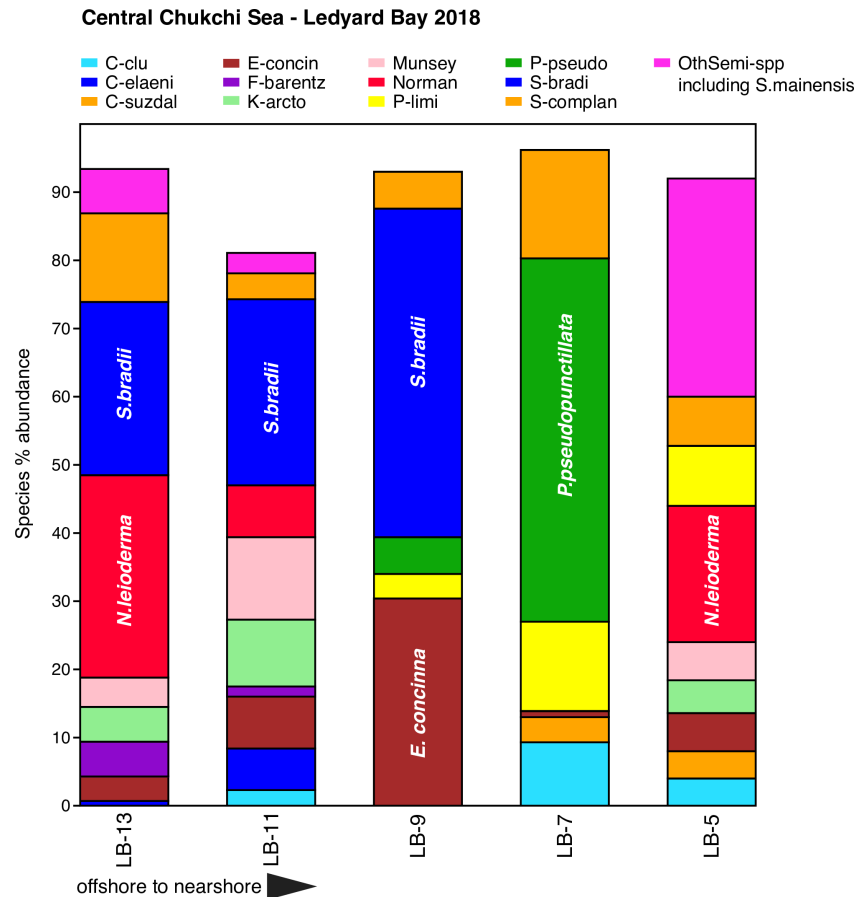


Figure 2.10 Primary species, Northeast Chukchi Sea - Icy Cape. Stack plot of the 9 most abundant species comprising ~90% of the ostracode assemblage at the 2018 Icy Cape (ICY) sampling transect (sites on Fig 2.2 map), northeast Chukchi Sea, (n=10 samples with ≥ 75 specimens/sample [except ICY2 that contained 22 specimens], 1,554 total specimens). Species not included on plot that each represent $>1-2\%$ of transect assemblage total include *A. dunelmensis*, *Argilloecia* sp., and *E. concinna*.

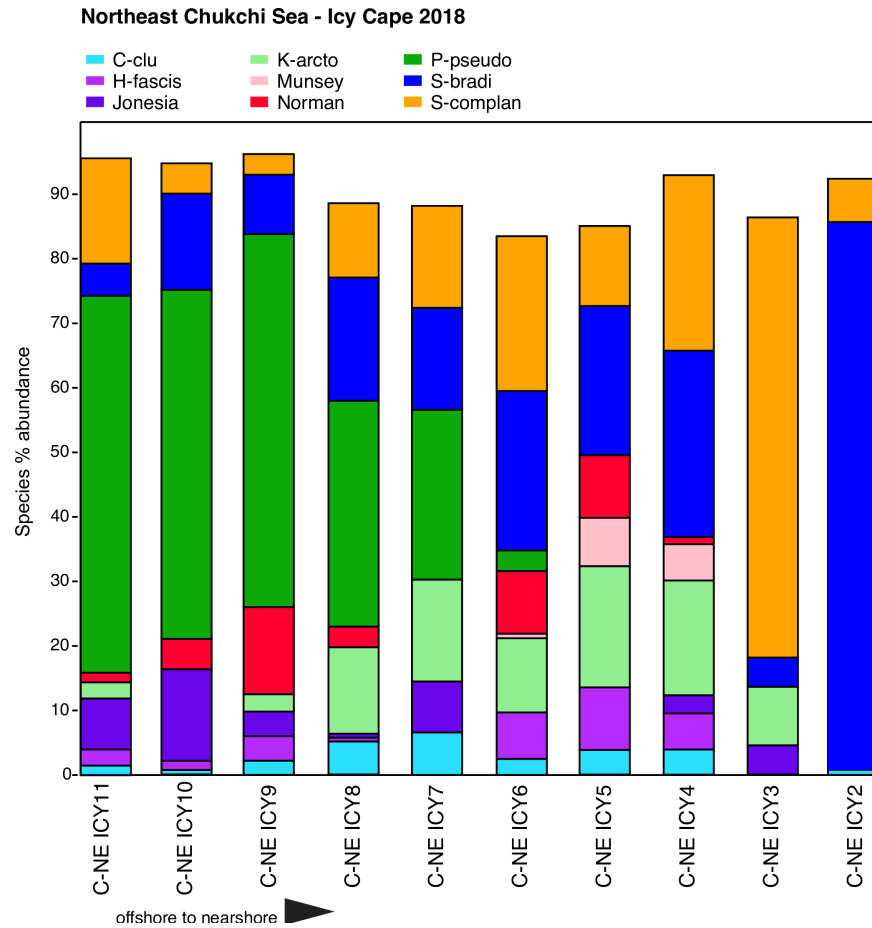


Figure 2.11 Primary species, Northeast Chukchi Sea – Hanna Shoal. Stack plot of the 11 most abundant species and one genus (*Argilloecia* spp.) comprising ~96% of the ostracode assemblage in the Hanna Shoal region offshore in the northeast Chukchi Sea (sites on Fig 2.2 map) from years 2012 to 2013, (n=21 surface sediment samples with ≥ 30 specimens/sample, 2,647 total specimens in an average water depth of 51m).

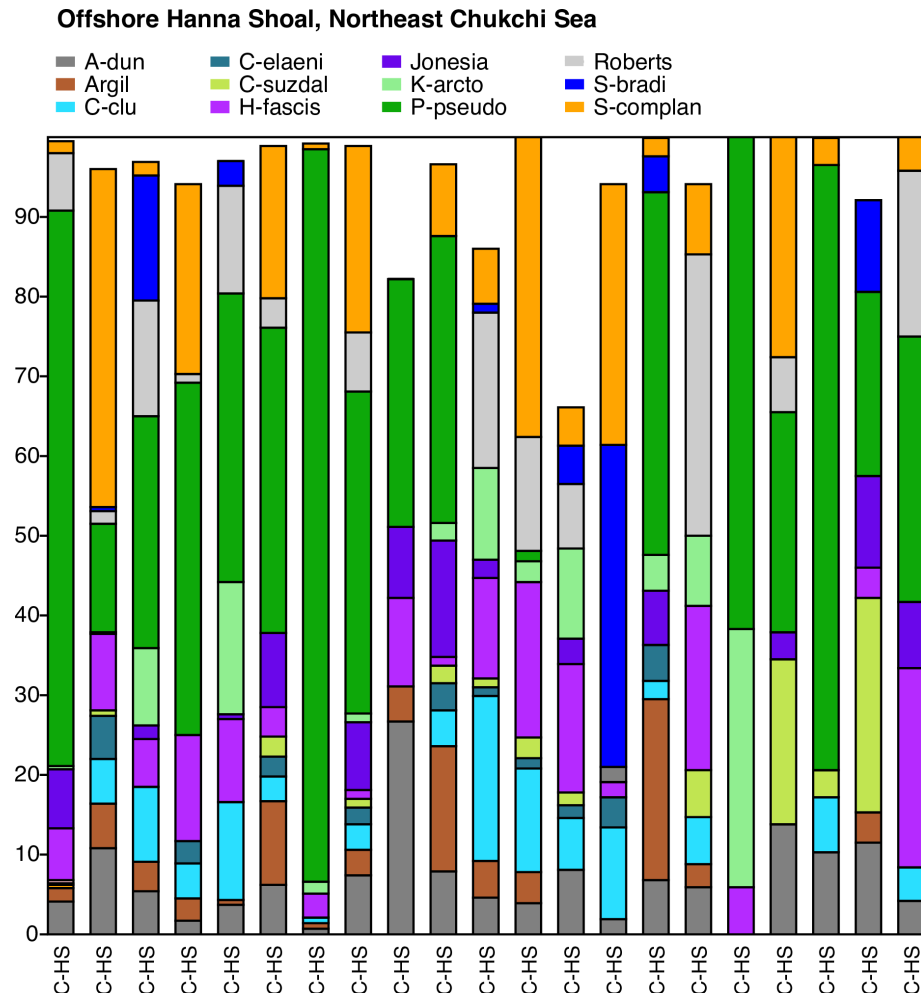


Figure 2.12 Primary species, DBO5 – Barrow Canyon. Stack plot of the 11 most abundant species and one genus (*Finmarchinella*), comprising ~80% of the ostracode assemblage, in DBO5-Barrow Canyon region (sites on Fig 2.2 map) from years ranging from 2011 to 2018 (n=31 surface sediment samples with ≥ 30 specimens/sample, 2,951 total specimens). Other faunas at stations 5-9 and 5-10 that account for the species not shown on the stack plot include *A. dunelmensis*, *J. acuminata* and *H. fascis*, and *R. tuberculatus*.

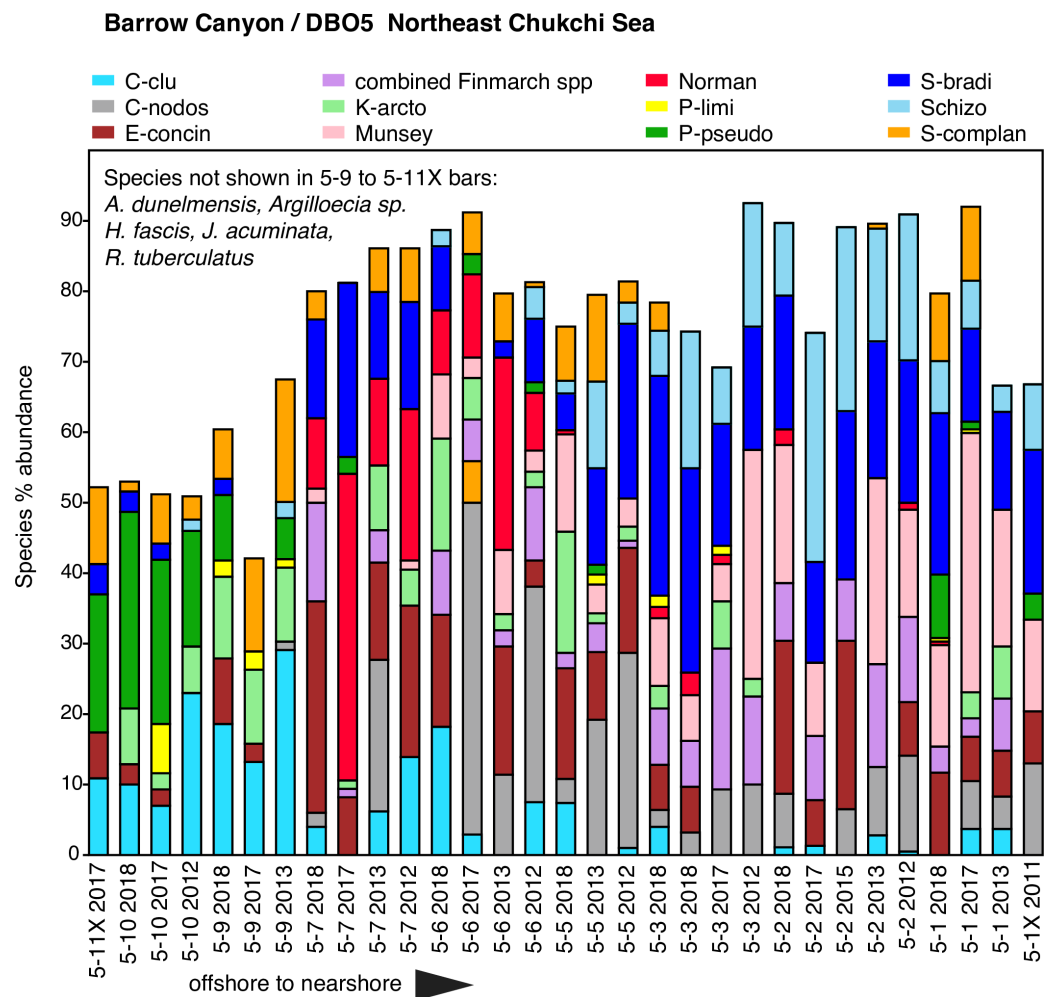


Figure 2.13 Primary species, Alaskan Beaufort Sea. Stack plot of the 12 most abundant species comprising ~85% of the ostracode assemblage in a narrow band of the Alaskan Beaufort Sea (sites on Fig. 2.4 map) within 100 km of shore at 20-90m water depth from years 1971 to 2018, (n=55 surface sediment samples with ≥ 30 specimens/sample, 6,617 total specimens). Samples collected in 2018 are highlighted in yellow. Other species not shown on the stack plot that account for 1-2% of the assemblage include *Rabilimis septentrionalis*, *Pteroloxa chaunensis*, *E. concinna*, and several *Cytheropteron* species. Important species in the Bering and Chukchi that exhibited either very low abundance (<1%) or are absent in the Beaufort Sea at 20-90m water depth are: *S. ikeyai*, *M. mananensis*, *Finmarchinella* spp., *K. arctoborealis*, *H. clathrata*, *H. emarginata*, *J. acuminata*, *S. affinis*, *S. mainensis*, and *S. undata*.

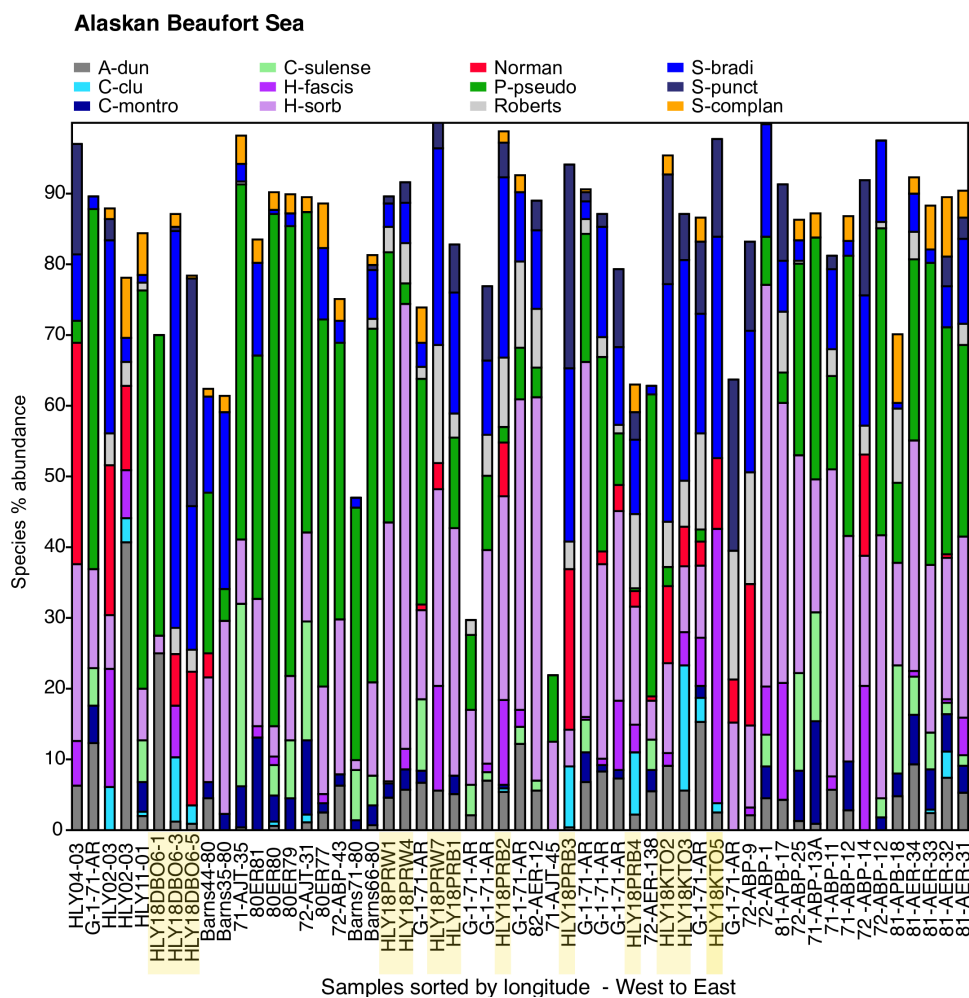


Figure 2.14 Principal correspondence analysis of ostracode assemblages by year groups. Synoptic PCAs using the biogeographic dataset (samples located on Fig 2.1 map) from the BCB grouped by the three regions and two collection periods, a.) 1970-2012 and b.) 2013-2018.

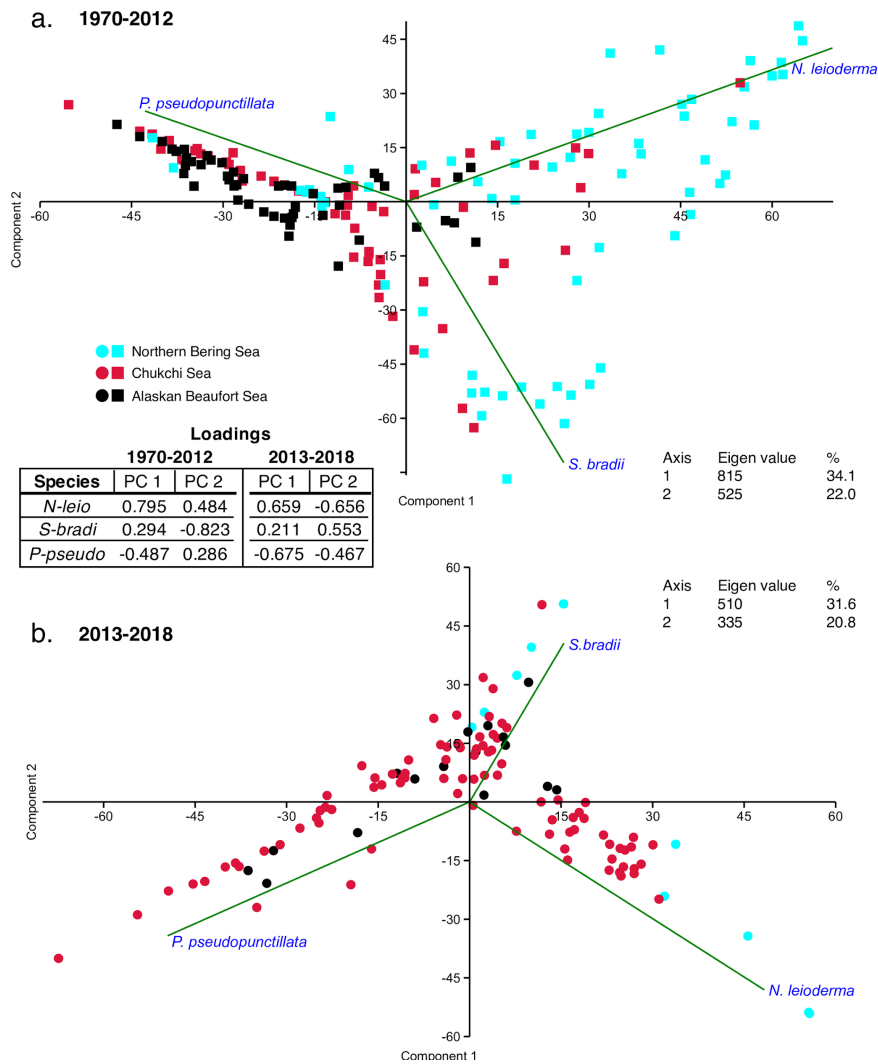
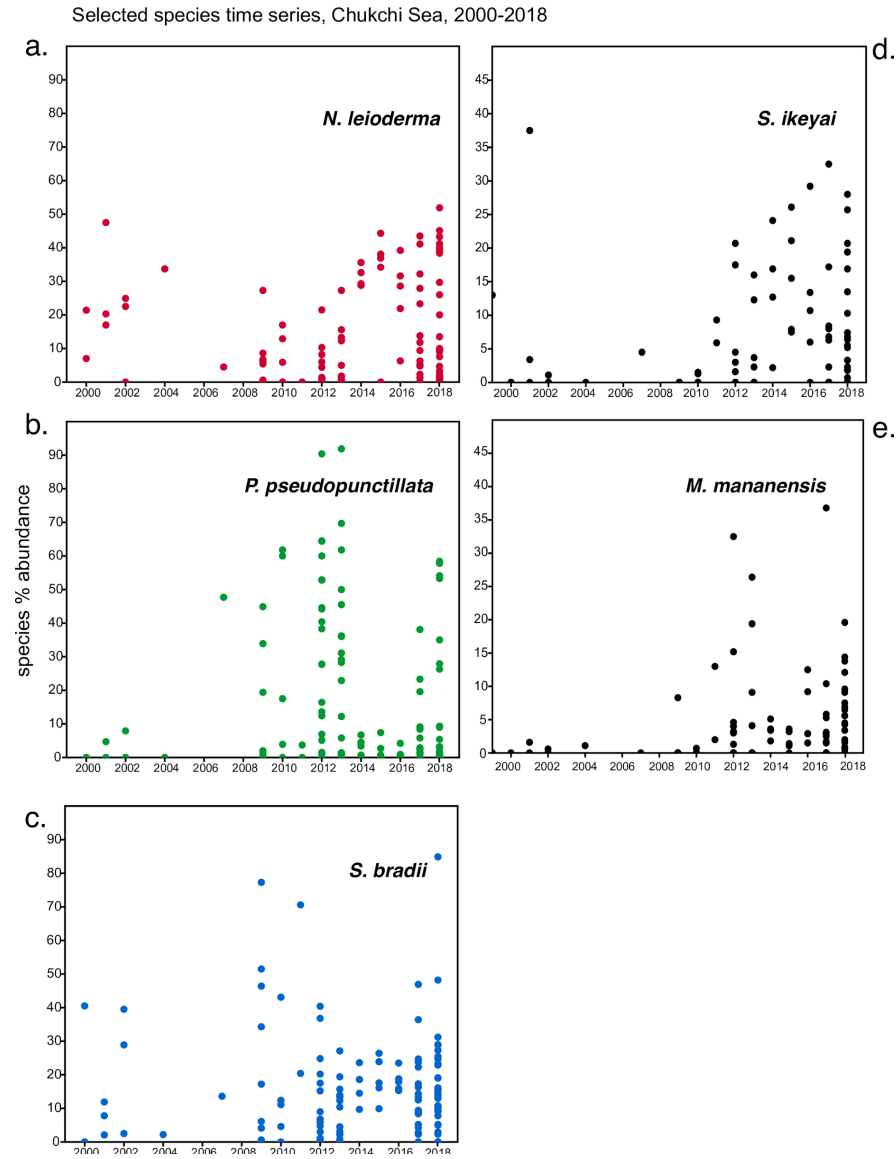


Figure 2.15 Time series of key species in Chukchi Sea. a.) *N. leioderma*, b.) *P. pseudopunctillata*, c.) *S. bradii*, d.) *S. ikeyai*, e.) *M. mananensis*

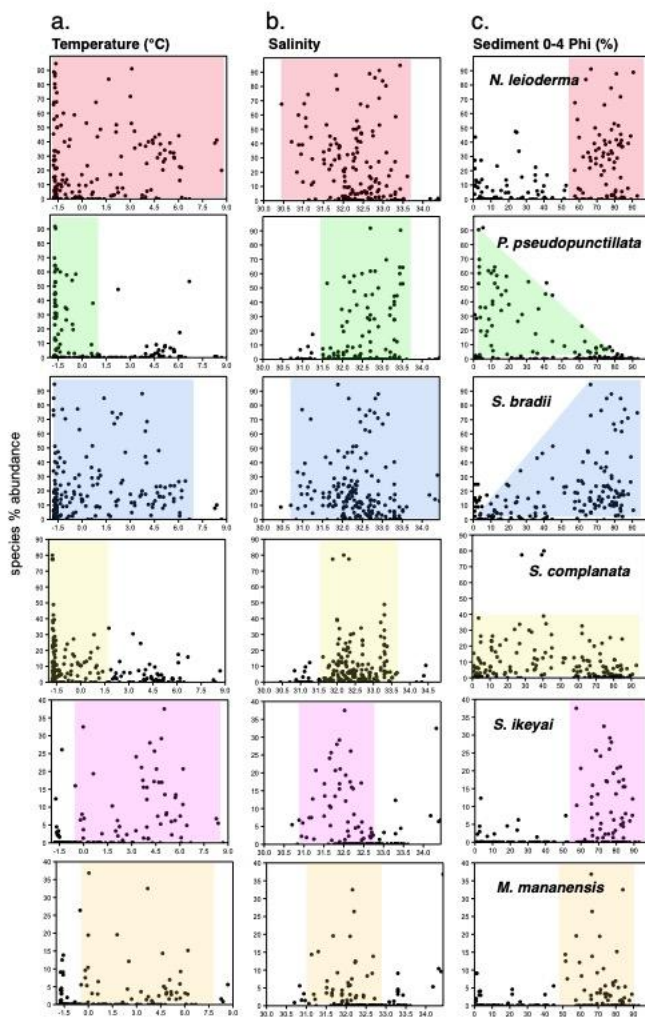


Supplementary Figures Chapter 2

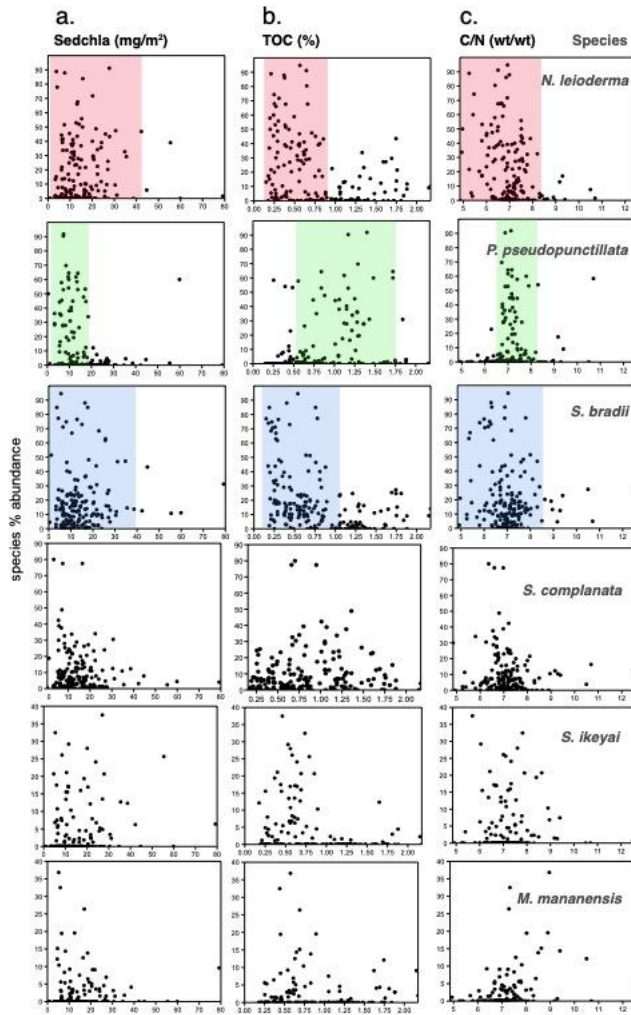
S2.1 Figure. a. Faunal abundance of selected taxa in relation to near-bottom temperature during summer sediment collection in the northern Bering and Chukchi Seas (n=211, 26,170 total specimens, 1990-2018, ≥ 30 specimens/sample).

b. Faunal abundance in relation to salinity.

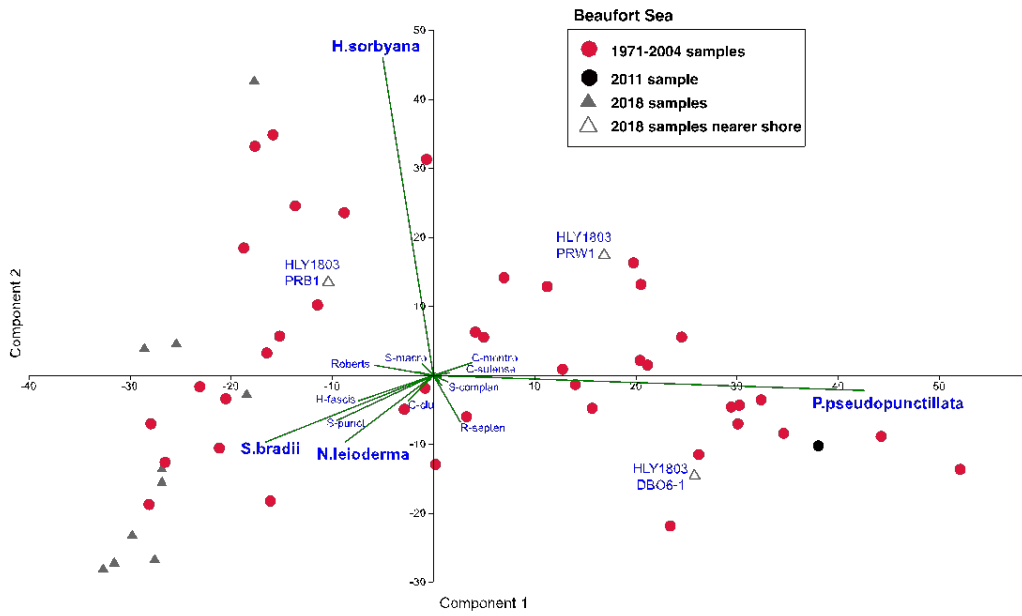
c. Faunal abundance in relation to sediment type. Ostracode species abundance plotted against the percent sediment modal grain size of phi 0-4, where 0 represents gravel and rocks, 1 = coarse sand, 2 = medium sand, 3-4 = finer sand. Phi ≥ 5 (not shown) represents the very fine silty mud and clay sediment fraction typical of offshore or interior areas of the continental shelf.



S2.2 Figure. Faunal abundance plotted against three different sources of sediment carbon, which may suggest preferred food sources: a. sediment chlorophyll-a (sedchla), b. total organic carbon (TOC) and c. carbon to nitrogen (C/N) ratios.



S2.3 Figure. Principal correspondence analysis (PCA) of Alaskan Beaufort Sea ostracode assemblages. Sample sites are designated by collection years (legend symbols) and major taxa (green lines with species names labeled in blue).



Tables Chapter 2

Table 2.1 Ecoregion names and respective bounding coordinates of sample groups and transects investigated in this study.

Ecoregions	DBO1 - South and west of St. Lawrence Island, Bering Sea	DBO2 - Chirikov Basin, Northern Bering Sea	DBO3 - Southern Chukchi Sea	Ledyard Bay (LB) transect, Chukchi Sea	Icy Cape (ICY) transect, Chukchi Sea	C-NE - Northeast Chukchi Sea	DBO5 - Barrow Canyon, Chukchi Sea	C-HS - Hanna Shoal, Chukchi Sea	Alaskan Beaufort Shelf
Latitude °N	63.77	65.111	68.60	70.30	71.83	71.00	71.808	73.30	70.60
°S	61.84	64.482	66.752	69.50	70.72	69.00	71.111	71.37	71.70
Longitude °E	-172.18	-167.86	-166.48	-165.40	-162.86	-159.40	-155.93	-158.30	-131.90
°W	-176.14	-170.49	-171.41	-168.50	-165.97	-173.80	-158.84	-165.60	-140.00
Depth range (m)	32-66	38-50	30-51	35-50	43-46	31-55	41-131	37-60*	20-90
Mean summer bottom temp. (°C)	-1.64 ±0.26	2.01 ±2.37	2.20 ±1.64	8.7 to 2.4	1.4 to -0.4	-0.70 ±1.54	0.1±2.3	-1.7	-0.9 ±0.7
Mean bottom salinity	32.47 ±0.32	32.2 ±0.61	32.36 ±0.56	31.7 ±0.53	32.1 ±0.1	32.59 ±0.84	32.6±0.9	33.0 ±0.3	31.4 ±1.0
Sediment chla (mg m ⁻²)	13.31 ± 6.51	15.74 ± 8.15	19.16 ± 9.80	6.1 to 20.4	6.2 to 26.6	12.74 ± 7.73	5.2 to 38.6	8.7 ±4.1	not avail

Table 2.2. List of 43 species and five genera found in the study region and abbreviations used in stack plot figures. According to the International Commission on Zoological Nomenclature, authors' names are in parentheses if the assignment listed was not the first description of the species.

A-dun	<i>Acanthocythereis dunelmensis</i> (Norman 1869) sensu lato
Argil	<i>Argilloecia</i> spp.
C-clu	<i>Cluthia cluthae</i> (Brady, Crosskey & Robertson 1874)
C-tesh	<i>Cytheretta teshepkukensis</i> Swain 1963
C-macch	<i>Cytheromorpha macchesneyi</i> (Brady and Crosskey 1871)
C-angul	<i>Cytheropteron angulatum</i> Brady and Robertson 1872
C-arcti	<i>Cytheropteron arcticum</i> Neale and Howe 1973
C-champ	<i>Cytheropteron champlainum</i> Cronin 1981
C-elaeni	<i>Cytheropteron elaeni</i> Cronin 1989
C-inflat	<i>Cytheropteron inflatum</i> Brady, Crosskey & Robertson 1874
C-montro	<i>Cytheropteron montrosiense</i> Brady, Crosskey & Robertson 1874
C-nodos	<i>Cytheropteron nodosoalatum</i> Neale and Howe 1973
C-sulense	<i>Cytheropteron sulense</i> Lev 1972
C-suzdal	<i>Cytheropteron suzdalskyi</i> Lev 1972
C- tumefact	<i>Cytheropteron tumefactum</i> Lev 1972
Cyth-spp	<i>Cytheropteron</i> spp.
E-concin	<i>Elofsonella concinna</i> (Jones 1857)
F-angu	<i>Finmarchinella angulata</i> (Sars 1866)
F-barentz	<i>Finmarchinella barentzovoensis</i> (Mandelstam 1957)
F-logani	<i>Finmarchinella logani</i> (Brady and Crosskey 1871)
H-emarg	<i>Hemicythere emarginata</i> (Sars 1866)
H-clathrata	<i>Hemicytherura clathrata</i> (Sars 1866)
H-fascis	<i>Heterocyprideis fascis</i> (Brady and Norman 1889)
H-sorb	<i>Heterocyprideis sorbyana</i> (Jones 1857)
Jonesia	<i>Jonesia acuminata</i> (Sars 1866) sensu lato
K-arcto	<i>Kotoracythere arctoborealis</i> Schornikov and Zenina 2006
K-hunti	<i>Krithe hunti</i> Yasuhara, Stepanova, Okahashi, Cronin and Brouwers 2014
Loxo	<i>Loxoconcha venepidermoidea</i> Swain 1963
Munsey	<i>Munseyella mananensis</i> Hazel and Valentine 1969
Norman	<i>Normanicythere leioderma</i> (Norman 1869)
P-limi	<i>Palmenella limicola</i> (Norman 1865)
P-pseudo	<i>Paracyprideis pseudopunctillata</i> Swain 1963
Paracytherois	<i>Paracytherois</i> spp.
P-chaun	<i>Pteroloxa chaunensis</i> Schornikov and Zenina 2006
R-mirab	<i>Rabilimis mirabilis</i> (Brady 1868)

R-septen	<i>Rabilimis septentrionalis</i> (Brady 1866)
Roberts	<i>Robertsonites tuberculatus</i> (Sars 1866)
Roundstonia	<i>Roundstonia globulifera</i> (Brady 1868)
S-bradi	<i>Sarsicytheridea bradii</i> (Norman 1865)
S-macro	<i>Sarsicytheridea macrolaminata</i> (Elofson 1939)
S-punct	<i>Sarsicytheridea punctillata</i> (Brady 1865)
Schizo	<i>Schizocythere ikeyai</i> Tsukagoshi and Briggs 1998
Sclero	<i>Sclerochilus</i> spp.
S-affinis	<i>Semicytherura affinis</i> (Sars 1866)
S-complan	<i>Semicytherura complanata</i> (Brady, Crosskey & Robertson 1874)
S-main	<i>Semicytherura mainensis</i> (Hazel and Valentine 1969)
Semi-spp	<i>Semicytherura</i> spp.
S-undata	<i>Semicytherura undata</i> (Sars 1866)

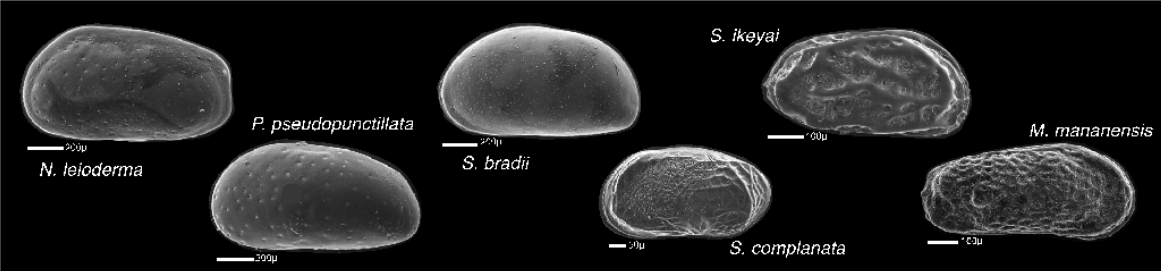
Table 2.3 DCA results based on the relative abundance of 49 ostracode species (including three genera, *Argilloecia*, *Cytheropteron* and *Semicytherura*) in 289 surface sediment samples from continental shelf regions of the Bering, Chukchi, and Beaufort Seas collected primarily in summer 1970–2018. Four assemblages related to average summer bottom water properties, and several species’ preferences of bottom sediment texture, organic sediment food types, are established. Because this area is a broad continental shelf, there is overlap of taxa between Alaska Coastal Water and Bering Sea Water, which is bridged by *S. bradii* and secondary taxa that include *E. concinna*.

Group	Ecoregion	Distinguishing features	Typical bottom summer water mass*	Dominant species	Associated taxa in assemblage
1	Northern Bering Sea -- Western Chirikov Basin (DBO2), St. Lawrence Isl polyna	Subarctic-Arctic, polyna open water, high sediment chlorophyll-a, hot spot areas of high-quality production, gravel-sandy sediments	Anadyr (-1.0 to 1.5°C, ≥32.5 salinity)	<i>Normanicythere leioderma</i>	<i>Sarsicytheridea bradii</i> , <i>Palmenella limicola</i> , <i>Semicytherura mainensis</i> , <i>Semicytherura affinis</i>
2	Nearshore Chukchi Sea (DBO3-1 to 3-5 and DBO5-1 to 5-7)	Cold-temperate, subarctic, arctic; gravel to sandy sediments	Alaska Coastal Water (~ 3-9°C, ≥30 salinity)	<i>Normanicythere leioderma</i> and <i>Sarsicytheridea bradii</i>	<i>Schizocythere ikeyai</i> , <i>Munseyella mananensis</i> , <i>Semicytherura</i> spp. (i.e. <i>S. undata</i>), <i>Finmarchinella</i> spp., <i>Heterocyprideis sorbyana</i> , <i>Cytheropteron nodosalatum</i> , <i>Elofsonella concinna</i>
3	Eastern Chirikov Basin (DBO2) and central Bering Sea (middle shelf LB, ICY stations)	Arctic-subarctic; normal marine salinity	Bering Sea Water (0-3°C, 31.8-33.6 salinity)	<i>Sarsicytheridea bradii</i>	<i>Elofsonella concinna</i> , <i>Semicytherura complanata</i> , <i>Kotoracythere arctoborealis</i> , <i>Semicytherura affinis</i>

3	Offshore NE Chukchi and Hanna Shoal DBO5-9 and 5-10	Arctic, marine euryhaline, hot spot areas of high TOC detritus, fine-grained sediments	Bering Sea Water/ Winter Water ($\leq -1.0^{\circ}\text{C}$, ≤ 31.5 salinity avg. 33 salinity)	<i>Paracyprideis pseudopunctillata</i>	<i>Semicytherura complanata</i> , <i>Heterocyprideis fascis</i> , <i>Robertsonites tuberculatus</i> , <i>Acanthocythereis dunelmensis</i> , <i>Cluthia chuthae</i> , <i>Argilloecia spp.</i> , <i>Kotoracythere arctoborealis</i> , <i>Jonesia acuminata</i>
4	Alaskan Beaufort Sea	Arctic, marine euryhaline, river influenced	Bering Sea Water/ Winter Water ($\leq -1.0^{\circ}\text{C}$, ≤ 31.5 salinity avg. 33 salinity)	<i>Paracyprideis pseudopunctillata</i> and <i>Heterocyprideis sorbyana</i>	<i>Sarsicytheridea bradii</i> , <i>Sarsicytheridea punctillata</i> , <i>Cytheropteron sulense</i> , <i>Heterocyprideis fascis</i> , <i>Acanthocythereis dunelmensis</i> , <i>Robertsonites tuberculatus</i>

Supplementary Table Chapter 2

S2.1 Table. Six ecologically defined species in the northern Bering, Chukchi, and Beaufort Seas based on multivariate correlations with environmental factors (*=from listed ecological references). Scanning electron microscope (SEM) photos of species are taken from Gemery et al., 2015.



Species	ideal temperature	salinity	watermass	sediment substrate	food preference	representative climata zone	primary modern distribution*	mode of life	primary ecological reference(s)
<i>Normanicythere leioderma</i>	wide (-1.8 to 9°C)	normal marine (31-33)	AW, ACW, BSW	pebbly-sandy	newly settled production	subarctic-arctic / circum-Arctic	Sea of Japan, waters off eastern Japan, Bering Sea, polynya south of St. Lawrence Island (northern Bering), Chukchi Sea, Bay areas in North Atlantic (Gulf of St. Lawrence, Nova Scotia), Ellesmere Island, Iceland, northwestern Scotland, Gulf of Maine, Spitsbergen, Russian Harbor, Novaya Zemlya (Barents Sea)	epifaunal	Hazel 1967; Ikoya and Cronin 1993; Gemery et al., 2013; this study
<i>Paracythereis pseudopunctilata</i>	cold (<1°C)	euryhaline	HSW, WW	fine silty muds	phytodetritus	arctic subarctic / circum-Arctic	Beaufort Sea and nearshore waters off Greenland, Norwegian, Kara, Laptev, East Siberian, Norton Sound in Bering Sea, Chukchi Sea	infaunal	Stepanova, 2006
<i>Sarsicytheridea bradii</i>	eurythermic but more common in ≤4.5°C	normal marine	AW, ACW, BSW	wide	wide	arctic-subarctic / circum-Arctic	North Atlantic (north of Cape Cod and Georges Bank), Ungava Bay, Frobisher Bay, Hudson Bay, Gulf of Maine, straits of the Canadian Arctic Archipelago, Newfoundland, Labrador Sea, waters off Great Britain, Ireland, Norway, Green and Franz Josef I and Spitsbergen, Novaya Zemlya, White, Baltic, North, Barents, Kara, Laptev, East Siberian, Chukchi nearshore waters off Aleutian Islands, Anadyr Bay, Bering, Norton Sound, nearshore waters off Alaska	infaunal	Stepanova, 2006; Freiwald and Mostafaei, 1998; Hazel, 1970
<i>Sarsicytherura complanata</i>	cold (<1°C)	normal marine, but high abundance in ≥33	BSW, WW	wide	unknown	arctic subarctic / circum-Arctic	Areas where a polynya forms during wintertime; Greenland, White (southern inlet of the Barents Sea), Barents, Norwegian, Kara, Laptev, East Siberian, Chukchi, Bering, Beaufort Seas; Labrador seas, Ungava, Frobisher, and Hudson bays, straits of the Canadian Arctic Archipelago, Ireland	infaunal	Stepanova, 2006; Brouwers et al., 2000; Cronin et al. 1994
<i>Schizocythere ikoyai</i>	warm (0-20°C)	lower salinity areas <32	ACW	sandy	unknown	cold-temperate to subarctic	Waters off eastern Japan, Cook Inlet, Gulf of Alaska, Kocisk Shelf, Pribilof Islands, Norton Sound, Chukchi Sea	unknown	Tsukagoshi and Briggs, 1998; Ozawa, 2004; Cronin et al., 2021
<i>Munseyella mananensis</i>	warm (0-14°C)	lower salinity areas <32	ACW	sandy	unknown	cold-temperate to subarctic	Sea of Japan, Okhotsk Sea, Bering Sea, Gulf of Alaska; Ungava, Frobisher, Krieland Bays off Canada and Baffin Bay off western Greenland, Halifax Inlet off Nova Scotia	unknown	Hazel and Valentine, 1969; Schornikov, 2001; 2006; Cronin et al., 2021

Chapter 3: Stable oxygen isotopes in shallow marine ostracodes from the northern Bering and Chukchi Seas

Published in *Marine Micropaleontology*, May 2021,

<https://doi.org/10.1016/j.marmicro.2021.102001>

Laura Gemery, Lee W. Cooper, Thomas M. Cronin, Cédric Magen, Jacqueline M. Grebmeier

Contribution: lead responsibility for the study, including experimental design, sample selection and preparation, sample analysis, data analysis and interpretation, all text and figures, writing of original draft. Other contributions: C. Magen for sample analysis and data generation; Text has been edited by all co-authors and reviewed for quality assurance.

3.1 Abstract

Stable oxygen isotope measurements on calcitic valves of benthic ostracodes ($\delta^{18}\text{O}_{\text{ost}}$) from the northern Bering and Chukchi Seas were used to examine ecological and hydrographic processes governing ostracode and associated seawater $\delta^{18}\text{O}$ values. Five cryophilic taxa were analyzed for $\delta^{18}\text{O}_{\text{ost}}$ values: *Sarsicytheridea bradleyi*; *Paracyprideis pseudopunctillata*; *Heterocyprideis sorbyana*; *Heterocyprideis fascis*; and the subarctic species *Normanicypther leioderma*. Controls on the stable oxygen isotope composition of ostracode calcite were investigated by first establishing species' vital effects and then comparing $\delta^{18}\text{O}_{\text{ost}}$ to seawater $\delta^{18}\text{O}$ values (that ranged from -2.7 to -0.5‰), CTD temperature (-1.7 to 8.7°C) and salinity (30-34) measured at sampling stations in the Bering and Chukchi Seas during the six summers of 2013-2018. Results from 297 $\delta^{18}\text{O}_{\text{ost}}$ measurements from 53 sites on the Bering and Chukchi Sea continental shelves are consistent with the temporal and spatial variation in $\delta^{18}\text{O}$ values of continental shelf bottom water, as impacted by seasonality, regional hydrography, and physical processes (i.e., sea-ice melt and extent, vertical mixing, precipitation/evaporation). Regression statistics for $\delta^{18}\text{O}_{\text{ost}}$ values of two species, *N. leioderma* and *P. pseudopunctillata*, showed

correlations to temperature and salinity that may facilitate prediction of water-mass characteristics when applied to sediment core records. Specifically, a significant linear regression relationship was found between $\delta^{18}\text{O}_{\text{ost}}$ values of *N. leioderma* and *P. pseudopunctillata* and temperature ($R^2 = 0.67$ and 0.52 , respectively). A principal component analysis confirmed temperature as the main controlling factor in the $\delta^{18}\text{O}_{\text{ost}}$ values of all species except *S. bradii*, with samples of distinct water masses grouping together. The $\delta^{18}\text{O}_{\text{ost}}$ values of *S. bradii* exhibited a narrow range of values (~ 3 to 4.5‰) across a temperature range of 10°C . Due to strong vital effects and possibly other undetermined factors, the incorporation of $\delta^{18}\text{O}_{\text{ost}}$ in *S. bradii* was not driven by any obvious predominant environmental factors.

3.2 Introduction

Stable oxygen isotopes of calcareous microfossil tests – primarily planktic and benthic foraminifera – have been used to reveal changes in global ice volume, ocean circulation, and temperatures over decadal to millennial timescales (e.g., Shackleton, 1974; Lisiecki and Raymo, 2005). Ostracodes, small bivalved crustaceans, are an underexploited group for isotopic proxy applications. Not only do benthic ostracode stable oxygen isotopic records display similar trends to those of benthic foraminifers (e.g., Didié and Bauch, 2002), but they also secrete their calcium carbonate (CaCO_3) shells within a few hours (Turpen and Angell, 1971) or up to a few days (Peypouquet et al., 1988; Chivas et al., 1983; Roca and Wansard, 1997). Alternatively, molluscs and foraminifera secrete their shells continuously over their entire lifespan, and at different water depths for some planktic species. Because ostracodes use bicarbonate and carbonate ions from the surrounding water to build their shells very rapidly (Turpen and Angell, 1971), calcite $\delta^{18}\text{O}$ values of their shells (hereafter $\delta^{18}\text{O}_{\text{ost}}$) provide a “snapshot” record of the water conditions at the

discrete time of calcification (Holmes and DeDecker, 2012 and references therein). The primary factors controlling the fractionation of oxygen isotopes in biogenic carbonates (CaCO_3) are water temperature and the isotopic composition of seawater (Urey, 1947; Epstein et al., 1951; 1953). Thermodynamically, ^{18}O is favored at equilibrium during calcite formation over ^{16}O (Urey, 1947). Epstein et al. (1953) established the temperature relationship in molluscs of approximately 0.2‰ change in $\delta^{18}\text{O}$ per 1°C , and this has been found to be fairly consistent for other calcium-carbonate-shelled organisms when calcite is precipitated in isotopic equilibrium with water (e.g., Bemis et al., 1998, Shackleton, 1974). The incorporation of ^{18}O due to water temperature and the $\delta^{18}\text{O}$ of the surrounding water is further complicated in different species by biologically or metabolically driven “vital effects” that create offsets in the expected oxygen isotope fractionation between CaCO_3 and water (Epstein et al., 1953). This disequilibrium fractionation drives deviations from the expected isotopic equilibrium value of calcite outside of and separate from temperature and $\delta^{18}\text{O}$ of the surrounding water. In ostracodes, species-specific vital-effect offsets, relative to that of expected equilibrium inorganic calcite precipitation, can range from a few tenths to several per mil and must first be established. Benthic ostracodes display more positive vital offsets than expected equilibrium values (Xia et al, 1997a; von Grafenstein et al, 1999; Simstich et al., 2004).

3.2.1 Goals of the study

The overarching goal of this study is to evaluate the feasibility of using ostracode carbonate as stable oxygen isotope tracers of temperature or water mass tracers in the northern Bering and Chukchi Seas. If successful, this proxy may be applied to other regions where the investigated species are found (Supplement Figs 3.1-3.8). This study presents 297 benthic $\delta^{18}\text{O}_{\text{ost}}$

measurements from five cryophilic (able to thrive at low temperatures) taxa representing different ecological preferences. Associated seawater $\delta^{18}\text{O}$ (hereafter $\delta^{18}\text{O}_{\text{water}}$) was measured from the same sites as those for collected ostracode samples from expeditions in the Bering and Chukchi Seas primarily during the summer (July – September) months of 2013-2018 (Fig. 3.1). We evaluate the temporal and spatial variability of the oxygen isotopic composition of bottom water (section 3.4.1), and in relation to benthic ostracode ecology (section 3.4.2) and $\delta^{18}\text{O}_{\text{ost}}$ values (section 3.4.3). The study confirms that calcite $\delta^{18}\text{O}_{\text{ost}}$ is not secreted in equilibrium with ambient $\delta^{18}\text{O}_{\text{water}}$, and vital-effect isotopic fractionations for each species are significant (section 3.4.4). Adult and juvenile $\delta^{18}\text{O}_{\text{ost}}$ values are compared to test if isotopic signatures vary with age (section 3.4.5). In order to examine the variability of $\delta^{18}\text{O}_{\text{ost}}$ values from the same species within the same sediment sample, 205 replicate analyses were conducted (section 3.4.6). Based on the $\delta^{18}\text{O}_{\text{water}}$, temperature and salinity at the time of collection, each sample was designated as representative of a particular bottom water mass (Table 3.2) to determine if $\delta^{18}\text{O}_{\text{ost}}$ is correlated with distinct water mass properties (section 3.4.7). This study investigates the multiple factors controlling $\delta^{18}\text{O}_{\text{ost}}$ values of the species via regression analyses. Water temperature effects on $\delta^{18}\text{O}_{\text{ost}}$ are also tested to determine if the expected temperature sensitivity for biogenic carbonates applies in a similar way for ostracode calcite.

3.2.2 Previous Work

Although the $\delta^{18}\text{O}_{\text{ost}}$ values of non-marine ostracode calcite has been widely used for modern and paleoenvironmental studies of lakes (e.g., von Grafenstein et al., 1999; Holmes et al., 2010; Ito and Forester, 2017; Roberts et al., 2020), to date, only a few studies have investigated marine ostracode $\delta^{18}\text{O}$ values in relation to oceanographic parameters: Didié and

Bauch, 2002 (the Iceland Plateau surrounding Iceland); Simstich et al., 2004 (Kara Sea); Erlenkeuser and von Grafenstein, 1999 (Laptev Sea); Mazzini, 2005 (Tasman Sea, southeast of New Zealand, and the deep Southern Ocean); Bornemann et al., 2012 (Mediterranean Sea). These studies determined the $\delta^{18}\text{O}_{\text{ost}}$ values of common taxa from modern surface sediments and established species-specific vital offsets from equilibrium calcite oxygen isotope values. In a few of these studies, baseline $\delta^{18}\text{O}_{\text{ost}}$ values were applied to downcore records, with $\delta^{18}\text{O}_{\text{ost}}$ values used as water mass tracers to identify deglaciation changes in river inputs to offshore areas (Simstich et al., 2004) or glacial-interglacial cycles in the deep North Atlantic (Didié and Bauch, 2002). For additional background of methods applied and results obtained by stable isotope studies using non-marine and marine Ostracoda, the reader is referred to Holmes and DeDeckker (2012).

3.2.3 Cryophilic ostracode life history

Little is known of the specific life histories of the ostracode species used in this study because relatively few direct observations have been made. Factors such as lifespan, food sources, and reproductive and metabolic ecology should be considered because they may affect the incorporation of ^{18}O into ostracode calcite or the interpretation of $\delta^{18}\text{O}_{\text{ost}}$ measurements. Several controlled laboratory experiments of cold-water marine ostracodes (e.g., Elofson, 1941; Majoran and Agrenius, 1995; Majoran et al., 2000; Ikeya and Kato, 2000) have constrained some of these uncertainties. For podocopan ostracodes (the taxonomic subclass investigated in this study), a full lifecycle includes eight molts before reaching adulthood (Horne, 1983; Cohen and Morin, 1990; Horne et al., 2002), so instar (juvenile) shells representing successive life stages are also preserved in sediments. Keyser and Walter (2004) proposed the process of shell secretion in

ostracodes involves dissolved inorganic carbon species and calcium being concentrated in an outer epidermal layer that gives rise to the shell. Through culturing studies, Elofson (1941) estimated that an ostracode lifespan may extend over multiple years, while development from the first instar to adult occur in as little as 30-35 days. The majority of cold-water, marine ostracode species appear to have seasonal lifecycles, and produce one or more generations per year in late spring, summer and early autumn (Horne, 1983; Athersuch et al., 1989). Temperature and food supply are likely the controlling factors that restrict cryophilic ostracode reproduction and development to this brief seasonal window when temperatures are warmest and organic matter produced as the result of primary productivity settles to the seafloor. The molt cycle is hormonally cued, with warming temperature being the most important environmental stimulus (Majoran et al., 2000). Ostracode growth rates are positively correlated with temperature. Majoran et al. (2000) reported higher temperatures were associated with later ontogenetic stages of *Krithe praetexta praetexta*. Likewise, in a study of temporal variation in a shallow water benthic community in Nova Scotia, Levings (1975) found a correlation between bottom temperature and abundance of *Normanicythere leioderma* during summer months. Most podocopan ostracode species reproduce sexually, and many brood eggs inside the adult female's carapace that hatch as juveniles with hardened shells (Horne, 1983; Cohen and Morin, 1990). Eggs or early instars brood within female adults and overwinter in delayed development until hatching is triggered (Horne 1983; Horne et al., 2002). Temperature is the likely cue for eggs to hatch (Theisen, 1966; Ganning, 1971; Levings, 1975). Adults and late-stage juveniles also overwinter until the following spring to perpetuate the population as well, and may enter diapause during winter (Majoran et al., 2000). Based on these inferences from previous studies, we therefore presume that the $\delta^{18}\text{O}$ values of ostracode calcite should reflect the $\delta^{18}\text{O}$ values of

seawater and water mass properties of the mean summer season (the sampling period) when the environment is most productive and the majority of ostracodes reach maturity.

3.2.4 Assumptions to address life history uncertainties

It is possible that some adult specimens selected for this study's analysis calcified their shells the previous summer or autumn season, and overlap from year to year is impossible to constrain. We employ the assumption that seawater $\delta^{18}\text{O}$, temperature and salinity measured at the time of ostracode collection best correspond to the environmental conditions during which the majority of ostracodes reach adulthood and build their final shell. Additionally, in continental shelf environments, changes in water $\delta^{18}\text{O}$ values can occur over short periods. To address these uncertainties, $\delta^{18}\text{O}_{\text{ost}}$ replicates from the same species in the same sample were analyzed to determine the range of variability in measured $\delta^{18}\text{O}_{\text{ost}}$ values at a given location (section 4.6). Lastly, we adhered to strict criteria (section 3.2) when selecting shells for analysis. For the regression analyses comparing $\delta^{18}\text{O}_{\text{ost}}$ with temperature, salinity and $\delta^{18}\text{O}_{\text{water}}$, only shells from adult carapaces were used, and many contained the chitinous bodies of the animal, indicating it was alive at the time of collection. Second, only the most pristine shells were chosen; in a continental shelf environment, dead individuals quickly show signs of reworking or deterioration, such as shell whitening or abrasion.

3.2.5 Regional setting

The continental shelf waters of the Bering and Chukchi Seas represent a mixture of water masses primarily differentiated by their salinity, temperature and nutrient concentrations. During the July-August-September sampling periods in the northern Bering and Chukchi Seas, there

were several distinct bottom water types, as outlined below, with distinct temperature and salinity ranges and $\delta^{18}\text{O}_{\text{water}}$ signatures (Table 3.1). Because the Bering Sea is in many respects a northern extension of the North Pacific Ocean, it is a major transport mechanism for heat, freshwater and nutrients through the Bering Strait into the Chukchi Sea. Waters from several origins comprise this flow into the Bering Sea: Anadyr Water (AW; upwelled from the western Bering continental slope, is cold, high salinity and high nutrient water); Alaska Coastal Current water (ACW; warmer, nutrient-poor, fresher water); and Bering Shelf Water (an intermediate mixture of these two water masses; Coachman et al., 1975; Weingartner et al., 2005, 2013; Gong and Pickart, 2015).

Northward flow through the ~80km-wide Bering Strait heavily influences oceanographic properties in the Chukchi Sea. Water through the Bering Strait is made up of ACW in the east and mostly Bering Sea Water (BSW) in the center and west, which comprises both Bering Shelf Water and AW. Its path is directed by the bottom topography of the Chukchi shelf (Hunt et al., 2013; Weingartner et al., 2005, 2013; Woodgate et al., 2005b). The Central Channel is the bathymetric depression between Herald Shoal and Hanna Shoal that steers BSW north over the shelf (Weingartner et al., 2005). Along the Alaskan coast, the seasonal (April-December) ACW is a narrow (10–20 km wide) wind- and buoyancy-forced current (Weingartner et al., 2005). It transits north along the coast and exits the Chukchi Sea via Barrow Canyon, where it bifurcates east to the Beaufort Sea to form the Beaufort shelf-break jet (Pickart, 2004) and west to form the Chukchi slope current (Li et al., 2019).

The seasonality of these water masses is important to note. During winter and early spring, most of the shelf is filled with cold ($<0^{\circ}\text{C}$) winter water (Pickart et al., 2016). In late spring and summer as the water warms seasonally, sharper distinctions among the water mass

become observable. There is also cold, dilute ice melt water (<31.5 salinity) in the upper water column. Bottom winter water is either newly ventilated (with a higher nutrient concentration) or remnant water with temperatures of $\sim -1.6^{\circ}\text{C}$ (collectively referred to herein as RWW, remnant winter water; Pickart et al., 2016; Li et al., 2019). We consider RWW ($\sim -1.4/-1.5\text{‰}$) a component of BSW because it is colder albeit not isotopically distinct. The oxygen isotope composition of each of these water masses was established as follows from Cooper et al. (1997): AW = -0.4 to -0.6‰ ; ACW = -4 to -1.5‰ ; BSW = -1.5 to -0.4‰ (Table 3.1).

A major characteristic of this area is the seasonal and interannual variability of sea-ice coverage. In the last few years, the Chukchi Sea has become nearly ice-free late in the summer season. A lack of ice would potentially allow storm and wind action to mix water masses vertically and/or more deeply, creating greater regional-scale variability in $\delta^{18}\text{O}_{\text{water}}$ values.

3.3 Materials and Methods

3.3.1 Ostracode surface sediment samples

Ostracodes from surface sediment samples ($\sim 0\text{-}2$ cm) were collected during summer (July, August, September) expeditions aboard U.S. Coast Guard Cutter (USCGC) Healy in 2013 and 2017-2018 and Canadian Coast Guard Ship (CCGS) Sir Wilfrid Laurier in 2001, 2014-2018 (Fig. 3.1; Table 3.2) using a van Veen grab (0.1 m^2) or a multi- or single-HAPS benthic corer (133 cm^2) to obtain the uppermost few centimeters of sediment. Samples were scraped from the top of surface grabs before the grab was opened through a trap-door, or from the top one to two centimeters of multicores. Wet sediment sample weight ranged from 20 g to > 100 g. To process for ostracodes, sediments were washed with tap water through a $63\text{ }\mu\text{m}$ sieve. The $> 63\text{ }\mu\text{m}$ size

fraction was dried in an oven overnight at 50°C. Using a light microscope, ostracode shells were hand-picked from the >125 µm size fraction of dried sediment using a finely tipped brush and transferred to a slide. Adult and juvenile target species for this study are found in this size range.

Sample station names presented in subsequent text, Table 3.2 and figures are abbreviated, with the first letter, “H” or “L” representing the expedition vessel, Healy or Laurier, the following two numbers designate the year of the cruise and the following letters/numbers represent the transect line and sample station name. For example, H18DBO3-1 represents the Healy 2018 expedition at the station DBO3-1. DBO station numbers increase from nearshore to further offshore.

3.3.2 Ostracode selection and preparation for isotope analysis

For specimen screening criteria, selection and preparation, the recommendations presented in Holmes and Chivas (2002) were followed, and are outlined here:

- Shells were visually inspected for excellent preservation to minimize impurity effects resulting from diagenesis, dissolution or remineralization and obtain clean shell carbonate for analysis. Selected shells were “glassy” or translucent/transparent, with well-preserved morphology, such as clearly defined muscle scars and ornamentation, fully developed inner lamellae, and non-granular surfaces. In many cases, specimens selected were alive at the time of collection. This was determined by shell quality, preserved chitinous appendages, and articulated carapaces.
- Shells were cleaned using distilled water and dried quickly. Sediment adhering to the shells was generally fine grained and easily removed using a brush. Closed carapaces

were opened to two single valves, and soft parts from within the shell were removed with a fine tweezer, brush, and needle tool.

- Only adult-stage valves and carapaces were used for main study analyses. Juvenile valves (instar molts) are smaller, thinner and less calcified than adults. A separate, minor examination was conducted on juvenile shells of various molt stages of *N. leioderma* (n=3), *P. pseudopunctillata* (n=9), and *S. bradii* (n=13), to determine their $\delta^{18}\text{O}$ values.
- To generate an average $\delta^{18}\text{O}$ calcite measurement representative of the summer season, three to four shells from different individuals (of the same species in the same sample) were used to achieve a mass of ~150-225 μg . In a second analysis, several months later in 2019, one adult valve (or ~5-15 juvenile shells) was used to achieve a weight of 40-90 μg .
- To test measurement precision, reproducibility and the variability of shell $\delta^{18}\text{O}$ values within the same sample, a number of duplicate analyses were analyzed in all runs.

3.3.3 Collection and analysis of $\delta^{18}\text{O}_{\text{water}}$ and $\delta^{18}\text{O}_{\text{ost}}$

Seawater was collected at the same stations as ostracode sediment samples via a conductivity-temperature-depth (CTD) rosette, which also measured near-bottom water temperature and salinity. Samples for $\delta^{18}\text{O}_{\text{water}}$ (Table 3.3) and $\delta^{18}\text{O}_{\text{ost}}$ were analyzed at the University of Maryland Center for Environmental Science in Solomons, Maryland, USA using a Thermo Fisher Scientific™ Delta V Plus stable isotope mass spectrometer coupled to a GasBench® peripheral preparation device. The precision of the measurements, based upon repeated measurements of an internal water standard and carbonate standards, was determined to be $\sim \pm 0.1\text{‰}$. The oxygen isotope bottle data used is archived at the University Corporation for

Atmospheric Research/National Center for Atmospheric Research (UCAR/NCAR) Earth Observing Laboratory (<https://www.eol.ucar.edu/>) and the National Science Foundation's Arctic Data Center (<https://arcticdata.io/catalog/portals/DBO>).

3.3.4 Ostracode $\delta^{18}\text{O}$, notation, and analyses

Oxygen isotope values are reported in parts per thousand, or per mil (‰) deviations of the $^{18}\text{O}/^{16}\text{O}$ isotope ratios relative to the VPDB (Vienna Pee Dee Belemnite) scale using laboratory standards calibrated against NBS19 and NBS18 (National Bureau of Standards). The ratios between $^{18}\text{O}/^{16}\text{O}$ are expressed in delta notation as follows:

$$\delta^{18}\text{O} \text{ ‰} = [(R_{\text{sample}}/R_{\text{standard}}) - 1] * 1000 \quad (1)$$

where $R = ^{18}\text{O}/^{16}\text{O}$ for $\delta^{18}\text{O}$ values in the sample vs. the standard (Craig, 1961; Coplen, 1994).

To convert between $\delta^{18}\text{O}$ water on the Vienna Standard Mean Ocean Water (VSMOW) scale to $\delta^{18}\text{O}$ water on VPDB scale as per mil, we followed Hut (1987):

$$\delta^{18}\text{O}_{\text{water, VPDB}} = 0.99973 * \delta^{18}\text{O}_{\text{water, VSMOW}} - 0.27 \quad (2)$$

The average expected $\delta^{18}\text{O}$ value of equilibrium calcite was determined using the equation established by O'Neil et al. (1969) and used by Didié and Bauch (2002) and Simstich et al. (2004):

$$\delta^{18}\text{O}_{\text{expected}} (\text{VPBD}) = [21.9 - 3.16 * (31.061 + T)^{0.5}] + \delta^{18}\text{O}_{\text{water VPDB}} \quad (3)$$

This equation calculates the expected $\delta^{18}\text{O}$ value of inorganic calcite precipitated in isotopic equilibrium with surrounding water of known temperature calibrated to 0°C and $\delta^{18}\text{O}_{\text{water}}$ (converted to VPBD scale). This equation was chosen because it encompasses the

closest temperature range to samples in this study. Furthermore, other ostracode studies used equations 2 and 3 so results from this study can be readily compared.

Species-specific vital effect fractionations were estimated using the measured $\delta^{18}\text{O}_{\text{ost}}$ value minus the corresponding expected equilibrium calcite value ($\delta^{18}\text{O}_{\text{ost}} - \delta^{18}\text{O}_{\text{expected}}$) for that species in the sample. Because the expected equilibrium calcite equation of O'Neil (1969) accounts for the temperature at the sampling site, an average vital offset was determined for each adult species from all measured values for that species.

Basic linear regression statistics were used to examine the influence of independent variables on the $\delta^{18}\text{O}$ values of water and/or ostracode calcite (dependent variables) to elucidate relationships among the $\delta^{18}\text{O}$ values of dominant species and oceanographic factors defining regional areas of the continental shelf environment. A value of $p < 0.05$ was used as the threshold for statistical significance. A principal component analysis (PCA) was used to examine relationships between the $\delta^{18}\text{O}_{\text{ost}}$ of specific species and water mass characteristics of the associated sample locations. The PCA was carried out using the statistics software package PAST v3.2 (PAleontological STatistics; Hammer et al., 2001). Adult replicate samples ($n=142$) were averaged so one value represents a sampling station for a given species in a given year.

3.4 Results and Discussion

In order to assess the applicability of $\delta^{18}\text{O}_{\text{ost}}$ of five benthic Arctic shelf ostracode species for proxy reconstructions, we made a total of 297 ostracode and 78 corresponding seawater $\delta^{18}\text{O}$ measurements from 53 sampling locations in the N. Bering and Chukchi Seas off northwest Alaska (Fig.3.1; Table 3.2). Our overall results, to be discussed in the following sections, indicate that $\delta^{18}\text{O}_{\text{ost}}$ values of several species reliably reflect the $\delta^{18}\text{O}_{\text{water}}$ and temperature

associated with defined water masses of the region. Thus, it may be feasible to use these species in downcore reconstructions to calculate paleotemperature of the water at the time of shell secretion. In the sections to follow, we'll present each species' specific offset relative to the expected equilibrium value of inorganic calcite. We show that interannual and intrasample variability of $\delta^{18}\text{O}_{\text{ost}}$ is minimal, and adult valves at a sample location represent the mean summer water condition of $\delta^{18}\text{O}_{\text{water}}$ and temperature within $\pm 0.2\text{‰}$. Results of a multiple regression analysis (PCA) attribute 83% of the variance in $\delta^{18}\text{O}_{\text{ost}}$ values (explained by the first two principal components) to summer bottom water temperature of the sample's corresponding water mass.

3.4.1 The relationships among $\delta^{18}\text{O}_{\text{water}}$ and water mass characteristics

Water mass characteristics vary widely in summer on the northern Bering and Chukchi Sea continental shelves. During summer months of 2013-2018, bottom-water $\delta^{18}\text{O}_{\text{water}}$ values across the shelf ranged from -2.7 to -0.5‰ with respect to VSMOW and summer bottom water temperatures ranged from -1.7 to 8.7°C (Fig. 3.2a). Salinity varied little from an average of 32 (standard deviation [stdev] ± 0.6 ; Fig. 3.2b), but a small number of stations nearest to shore in the southeast Chukchi Sea (DBO3-1, 3-2, 3-3, 3-4) and northeast Chukchi Sea (DBO4-1) had average bottom water salinity values one unit lower, ~ 31 . Bottom warming and mixing as well as freshwater runoff was most evident at shallower depths nearer to shore. At location, DBO5-1 in 2017, the highest salinity of 34 was recorded, with a temperature of 0°C (Fig. 3.2b), and the water mass was classified as RWW. The following year during the same month, that same site had a salinity of 31 with a higher temperature of 4.6°C and classified as ACW. The DBO5 transect, especially DBO5-1 closest to shore, showed the highest year-to-year variability in

temperature and the lowest seawater $\delta^{18}\text{O}_{\text{water}}$ values (Table 3.3) compared to other DBO lines. Such large temporal variation was typical at station locations close to shore along the DBO3 transect, particularly those in the flow path of the ACW where it reaches the shallow seafloor. For example, DBO3-1, sampled during July and/or August in 2014, 2015, 2016, 2017, 2018, had bottom water temperatures, respectively, of 5.5, 6.0, 5.5, 5.7 and 8.3°C, and bottom seawater $\delta^{18}\text{O}$ ranging from -2.7‰ to -1.6‰. Overall, the greatest variability from year to year in temperature and $\delta^{18}\text{O}_{\text{water}}$ was at DBO3-1 and DBO5-1, which are both closest to the coast on each transect.

Despite temporal temperature and salinity variability at near-shore sample locations, properties of the ambient water masses are reflected in the $\delta^{18}\text{O}_{\text{water}}$ profiles (Table 3.1; Figs. 3.2a & 3.2b; Cooper et al., 1997). On a global basis, for every 1 unit decrease in salinity, a corresponding 0.6‰ decrease in $\delta^{18}\text{O}_{\text{water}}$ value is expected (Craig and Gordon, 1965). The most negative $\delta^{18}\text{O}_{\text{water}}$ value of -2.5‰ was observed in the warmest, least saline bottom water (8.4°C, salinity 30.7, H18DBO3-1), which was comprised of ACW. The least negative/highest $\delta^{18}\text{O}_{\text{water}}$ value of -0.45‰ (0°C, salinity 34, H17DBO5-1) was likely made up of brine-injected RWW that was trapped in August 2017 on the shallow shelf. These end members demonstrate the expected trend, as generally, $\delta^{18}\text{O}_{\text{water}}$ values increase with lower temperature and higher salinity. Overall, regression statistics of ACW $\delta^{18}\text{O}_{\text{water}}$ samples (n= 23), show a significant correlation to temperature ($R^2= 0.53$; Fig. 3.2a) and salinity ($R^2= 0.68$; Fig. 3.2b). The $\delta^{18}\text{O}_{\text{water}}$ value of the ACW has a strong relationship to both variables because the water mass originates much further south with a $\delta^{18}\text{O}_{\text{water}}$ reflective of less saline, warmer, ^{18}O -depleted water embedded in the northward flowing current. The transit time of water advected from the Bering Strait to Barrow Canyon has been estimated to be ~4 months (Woodgate et al., 2005a) implying water masses

from the south move quickly across the shelf with lighter isotopic values indicative of its Pacific provenance.

Salinity is correlated to $\delta^{18}\text{O}_{\text{water}}$ values and reflects similar sources. A linear relationship between salinity and $\delta^{18}\text{O}_{\text{water}}$ is expected because processes that increase or decrease $\delta^{18}\text{O}_{\text{water}}$ values (evaporation, rainfall, ice melt, run-off) also correspondingly increase or decrease with salinity (Epstein et al., 1951; LeGrande and Schmidt, 2006). Fig. 3.2b shows an overall significant relationship ($R^2= 0.45$) for all samples. The few samples representing AW (indicated by the symbol “X” on Fig. 3.2b) have among the highest $\delta^{18}\text{O}_{\text{water}}$ values. Salinity and $\delta^{18}\text{O}_{\text{water}}$ have particularly significant relationships in the ACW ($R^2=0.68$, gray-colored regression line) and BSW ($R^2= 0.61$, orange-colored regression line), which are potentially influenced by contributions of melted sea ice. A subset of BSW is RWW that transited through the Bering Strait or formed during winter vs. summer. We chose to separate this water mass because it has distinctive properties (high salinity and low temperature) and can remain on shelf regions until the following summer (Woodgate et al., 2005b). During the formation of sea ice, the release of brine breaks down water column stratification. This can lead to mixing of isotopically lighter water towards the seafloor (Cooper et al., 1997; Bauch and Bauch, 2001). Our data show that most samples representing RWW have $\delta^{18}\text{O}_{\text{water}}$ values in a similar range as BSW. But a lighter signature is discernable in two samples from the Hanna Shoal region (samples H13H108 and H13H29, values circled on Fig. 3.2b). Also, during the past few decades, freshwater through the Bering Strait has increased by ~40% due to intensification of the hydrological system in the Pacific-Arctic (Woodgate, 2018). This overall freshening may help explain why BSW $\delta^{18}\text{O}$ is more strongly correlated to salinity than temperature. Based on the correlations in Figure 3.2,

every 0.5‰ change in BSW $\delta^{18}\text{O}_{\text{water}}$ corresponds with a change in salinity of ~ 0.5 , while similar changes in BSW $\delta^{18}\text{O}_{\text{water}}$ are not necessarily associated with any change in temperature.

3.4.2 Distribution and ecology of investigated ostracode species

Five common, circum-polar continental shelf ostracode species were chosen for investigation: the subarctic *Normanicythere leioderma*; the eurytopic species *Sarsicytheridea bradii*; the euryhaline species *Paracyprideis pseudopunctillata*; *Heterocyprideis sorbyana*; and the cryophilic *Heterocyprideis fascis*. All of these taxa are tolerant of considerable seasonal changes on highly variable continental shelves. Furthermore, the biogeography and ecology of these taxa were examined using the Arctic Ostracode Database (AOD) of extant species, which currently includes ~ 1600 modern surface samples from all areas of the Arctic Ocean and subarctic seas (Cronin, 1981; Cronin et al., 1991; Gemery et al., 2015; Cronin et al., 2021, AOD2020 is available from <https://www.ncdc.noaa.gov/paleo/study/32312>). The abundance of each investigated species in AOD samples (with >10 specimens of the given taxa in a sample) was plotted versus bottom water temperature, salinity, water depth and latitude (Supplement Figs 3.1, 3.3, 3.5, 3.7). Corresponding maps show each species' modern distribution from this database (Supplement Figs 3.2, 3.4, 3.6, 3.8).

Off Alaskan, Canadian and Siberian coasts, typical nearshore Arctic assemblages are dominated, in varying proportions, by *P. pseudopunctillata*, *Sarsicytheridea* spp., *H. sorbyana* (Cronin et al., 1991; Brouwers et al., 1991; Stepanova 2006; Gemery et al., 2013). These species are frequently preserved in sediment cores and in cold-temperate to high-latitude deposits in both the Atlantic and Pacific sectors of the Arctic and can represent different paleoenvironments (e.g., Cronin and Ikeya, 1987; Stepanova et al., 2011, 2019; Simstich et al., 2004). In particular, *P.*

pseudopunctillata (Supplement Figs 3.3, 3.4) and *H. sorbyana* (Supplement Figs 3.7, 3.8) are littoral-sublittoral species (1-50 m) with a southerly range limit of ~63°N latitude, tolerant of salinities as low as 5-10 (Hazel, 1970; Neale and Howe, 1975; Cronin, 1977; Stepanova et al., 2007, 2019) and temperatures from -1.7 to upwards of 10°C. Although *H. sorbyana* belongs to the same genus as *H. fascis*, its ecological preferences are distinct. *H. fascis* is more restricted in its distribution above 69°N latitude in normal Arctic marine salinity (31-34), frigid temperatures (0°C and below) and in slightly deeper offshore water depths (>40 m; Supplement Figs 3.7, 3.8). *Sarsicytheridea bradii* is a wide-ranging, cold temperate to frigid species with seafloor temperature tolerances of -1.7 to 18°C (Hazel, 1970), but demonstrates a preference for mid-shelf depths and normal Arctic marine salinity (31-33; Supplement Figs 3.5, 3.6). Likewise, *N. leioderma* has wide temperature tolerances (-1.7 to 19°C; Hazel, 1970) in normal Arctic salinity (Supplement Fig. 3.1). It mainly inhabits depths of 50 m or less in latitudes >61°N, and is a dominant species in the northern Bering Sea, while becoming less abundant in the Chukchi and Beaufort Sea region, to rare in the Kara and Laptev Seas (Stepanova et al., 2007; Gemery et al., 2013; 2015).

3.4.3 Stable oxygen isotopes of Arctic ostracodes

On the northern Bering and Chukchi Sea shelves, $\delta^{18}\text{O}_{\text{ost}}$ values across the region and a 10°C temperature gradient reflected the highly variable oceanographic regime on a continental shelf. However, an average $\delta^{18}\text{O}_{\text{ost}}$ value (\pm standard deviation) was generated for each species: 2.6‰ (± 1.1) for *N. leioderma*; 4.4‰ (± 0.4) for *P. pseudopunctillata*; 3.9‰ (± 0.4) for *S. bradii*; 3.3‰ (± 0.5) for *H. sorbyana*; 3.7‰ (± 0.3) for *H. fascis* (Table 3.4). The $\delta^{18}\text{O}_{\text{ost}}$ values for *N. leioderma* showed the largest range of up to 4‰ (Fig. 3.3a) but the range of $\delta^{18}\text{O}_{\text{ost}}$ values for

other species was narrower: 1.8‰ for *P. pseudopunctillata*; 2‰ for *S. bradii*; 1.5‰ for *H. sorbyana*; 1‰ for *H. fascis* (Figs. 3.3d, g, j, l). These $\delta^{18}\text{O}_{\text{ost}}$ values presented are not corrected for vital effect fractionations, so part of the difference in $\delta^{18}\text{O}_{\text{ost}}$ values for each species is due to this effect, which varies by taxon.

3.4.4 Species-specific vital effect fractionations

The observed difference between shell calcite $\delta^{18}\text{O}_{\text{ost}}$ and expected inorganic calcite formed in isotopic equilibrium ($\delta^{18}\text{O}_{\text{ost}} - \delta^{18}\text{O}_{\text{expected}}$) represents a species-specific isotopic fractionation broadly referred to as vital effects or offsets. Results confirmed that, relative to the expected (or equilibrium) value of inorganic calcite, ostracodes do not secrete their carapace in equilibrium with ambient water. Rather, each species showed a species-specific positive offset (Figs. 3.3b, e, h, k, m), which is consistent with values established by other studies that ranged from +1.5‰ to +0.5‰ (e.g., Simstich et al., 2004; Table 3.4). Heavier than expected isotopic offsets have also been found in deep-sea marine species (Didié and Bauch, 2002) and in non-marine ostracodes (e.g., Xia et al., 1997a & b; von Grafenstein et al., 1999).

Certain factors have been proposed to explain vital offsets. The studies of Erlenkeuser and von Grafenstein (1999) and Simstich et al. (2004) observed that higher hydrographic variability in shallow water caused wider deviations of calcite $\delta^{18}\text{O}_{\text{ost}}$ values from equilibrium. In order to separate effects from hydrographic variability, and to better estimate vital offsets, Simstich et al. (2004) used only stations from >40m water depth. We used a similar strategy in this study. Our average water depth sampled was 49m (stdev ± 13 m), with only a few sites representing end member station depths of 33 m (DBO3-1, the shallowest station), and 131 m

(DBO5-5 in Barrow Canyon, the deepest). Therefore, depth and the high environmental variability of shallow depths are better constrained.

Several strong species-specific vital effect offsets were observed in our results. The average vital effects isotopic fractionations for *N. leioderma* and *H. fascis* were lowest (+1.1‰ and +1.0‰ respectively) compared to *S. bradleyi*, *P. pseudopunctillata* and *H. sorbyana* (+2.2‰, +2.3‰ and +2.4‰, respectively), which exhibited the highest offsets from equilibrium calcite (Table 3.4). To attempt to understand various factors that could be contributing to these offsets, it is first necessary to discuss vital effects in more detail.

The mechanisms that cause vital offsets are not well understood. While isotope fractionation between marine ostracodes and the ambient water they use to build their shell has not been measured in controlled laboratory settings, results from a freshwater ostracode culturing study (Xia et al., 1997a) and a natural environmental study (Keatings et al., 2002) suggest the degree of fractionation in ostracodes may be related to the rate and temperature of calcification. Xia et al. (1997a) found that fractionation increased by 2‰ as water calcification temperatures decreased from 25°C to 15°C. Keatings et al. (2002) proposed that slower rates of calcification resulted in calcification closer to equilibrium, while faster rates of calcification led to higher fractionation (i.e., greater vital offsets). However, it is unclear whether these effects apply to the natural marine environment where calcification occurs at much lower temperatures. Because the rate of inorganic calcite precipitation has no effect on oxygen isotope fractionation (Kim and O'Neil, 1997), the measured vital offsets in ostracodes indicates isotopic fractionation resulting from some biological process (Decrouy, 2012).

Xia et al. (1997a) suggested physiological factors such as the rate of metabolism, food quantity, light penetration, and environmental stress during calcification may contribute to

nonequilibrium fractionation, or variability in shell composition. The alkalinity of water or the degree of calcite saturation in the water may also influence oxygen isotope fractionation (Decrouy, 2012; Devriendt et al., 2017). Furthermore, in a study evaluating published vital effects in freshwater and brackish ostracodes, Decrouy and Vennemann (2013) suggested that differences in vital offsets within a given freshwater or brackish taxon from different localities may be due to differences in water chemistry, citing salinity, alkalinity, Mg/Ca, and calcite saturation state [the carbonate ion concentration (CO_3^{2-}) of seawater]. These prior observations indicate that many factors must be considered to fully explain the species-specific $\delta^{18}\text{O}_{\text{ost}}$ offsets measured in this study.

The vital offset results of this study were compared with those of Simstich et al. (2004), who investigated two of the same species in offshore, river-influenced waters of the Kara Sea. Using the same equations, they reported a 1.5‰ ($\pm 0.29\%$, $n=55$) vital offset for *P. pseudopunctillata*, which is lower compared to this study's value of 2.28‰ ($\pm 0.71\%$, $n=45$). However, the average $\delta^{18}\text{O}_{\text{ost}}$ values measured for *P. pseudopunctillata* were similar in both studies (+4.35‰ [$\pm 0.42\%$] for this study) versus +4.95‰ [$\pm 0.41\%$] (Simstich et al. 2004). The expected calcite values in the Simstich et al. (2004) study were based upon water temperatures from sites that were on average much colder (-1.5°C) and less saline (~ 31). Therefore, the difference in vital offset values between our study results and those of Simstich et al. (2004) is likely due to the different hydrographic conditions and $\delta^{18}\text{O}_{\text{water}}$ composition of the sampled waters. When averaging values from areas with colder temperatures and higher river inputs, the offset average would shift. Also, instead of using direct measurements of $\delta^{18}\text{O}_{\text{water}}$ at the time of sampling, Simstich et al. (2004) estimated almost half of the $\delta^{18}\text{O}_{\text{water}}$ values from salinity, which may add a source of error because the $\delta^{18}\text{O}_{\text{water}}$ -salinity relationship varies based on distance

from runoff sources and on seasonal, annual and interannual timescales, as river inputs, wind forcing and sea-ice processes vary (Bauch and Bauch 2001; Bauch et al., 2003; 2010; Cooper et al., 2008).

For *H. sorbyana*, Simstich et al. (2004) reported a vital offset of 1.0‰ (± 0.24 ‰, n= 42) while this study found an offset of 2.4‰ (± 1.3 ‰, n=12). Because vital offsets have been found to be generally constant for closely related freshwater ostracode species (e.g., von Grafenstein et al., 1999; Decrouy, 2012; Devriendt et al., 2017), measurements from the two species in the *Heterocyprideis* genus, *H. sorbyana* and *H. fascis*, were combined in Fig. 3.3n to average a larger number of offset values over the study area and from different water masses. The station locations where *H. fascis* was found were mostly in RWW, with 11 of 16 samples from localized areas off Icy Cape and Ledyard Bay in the northeastern Chukchi Sea (Fig. 3.1). Furthermore, of the 16 *H. fascis* measurements, six were replicate measurements of valves from the same sample site in the same year. *H. sorbyana* inhabits a wider range of temperatures and lower salinities than *H. fascis*, and it is also distributed at lower latitudes (63-71°N; Supplement Fig. 3.7). The combined offset value for the genus *Heterocyprideis* in the northern Bering-Chukchi Sea region from expected equilibrium-based isotopic fractionation was +1.6‰, which may better represent the variability of water masses in the study area and is closer to the vital effect of +1.0‰ observed by Simstich et al. (2004). The difference in average $\delta^{18}\text{O}_{\text{ost}}$ values between these two studies, again, likely reflects different water properties and/or the low number of samples measured in this study. Vital offsets for the frigid, deep-sea marine (>1500 m water depth) genera *Henryhowella* and *Kriithe* from Didié and Bauch (2002), cited in Table 3.4, show generally higher average $\delta^{18}\text{O}_{\text{ost}}$ values and species vital offsets.

3.4.5 Comparison of juvenile vs. adult $\delta^{18}\text{O}_{\text{ost}}$ and vital offsets

Conflicting data have been published about $\delta^{18}\text{O}_{\text{ost}}$ values of juvenile and adult specimens, which this study has not resolved. Mazzini (2005) found differences between measured $\delta^{18}\text{O}_{\text{ost}}$ values of adults and juveniles in the genus *Krithe*. Similarly, Bornemann et al. (2012) reported that the variability of isotope values increased when juveniles were included in analyses. However, Didié and Bauch (2002) reported no difference in shell $\delta^{18}\text{O}_{\text{ost}}$ results from various *Krithe* molt stages. Studies of non-marine ostracodes show that juveniles and adults can have different $\delta^{18}\text{O}$ signatures, which may reflect different seasons of calcification (Xia et al., 1997b) and/or different calcification (Keatings et al., 2002) and metabolic rates (Xia et al., 1997a). Due to this ambiguity, we sought to determine if there were any differences in offsets between adult and instar molts of our species.

Comparing juvenile $\delta^{18}\text{O}_{\text{ost}}$ and adult $\delta^{18}\text{O}_{\text{ost}}$ offsets, the isotopic fractionation in juvenile shells is similar to adults of *N. leioderma* (n=3) and *P. pseudopunctillata* (n=9), with an average offset difference between juvenile and adults of 0.2‰ and 0.1‰, respectively (Figs. 3.3c & f). These values are within the range of analytical error. For *S. bradii*, the average offset difference is 0.6‰ (n=13; Fig. 3.3i). It is notable that all juvenile $\delta^{18}\text{O}_{\text{ost}}$ values are in the same range as adult values, with the exception of one *N. leioderma* outlier. However, despite these observations of similar offset values between adults and juveniles, the low number of juvenile measurements necessitates further testing before conclusions can be drawn.

3.4.6 Intra-sample replicate measurements

Most cryophilic ostracodes calcify their adult tests during summer months (Horne, 1983). Yet at the same sampling location, coexisting ostracodes may have different $\delta^{18}\text{O}_{\text{ost}}$ values

because overlapping generations attain maturity at different times and thus experience different environmental conditions during calcification. This is expected if an individual secreted its adult shell early in spring because it overwintered as a pre-adult (A-1) or if it matured in late autumn and kept its adult shell until the next year and was, in turn, sampled in summer. The $\delta^{18}\text{O}_{\text{ost}}$ value can be expected to be more or less heavy isotope enriched depending on seasonal variation of $\delta^{18}\text{O}_{\text{water}}$ and water temperature at the time the ostracode secreted its final shell. In order to examine the variability of $\delta^{18}\text{O}_{\text{ost}}$ values from the same species within the same sample, 205 replicate analyses were conducted on specimens from the same sediment sample.

The measured $\delta^{18}\text{O}_{\text{ost}}$ of individual species in individual samples showed minimal deviation from the taxon's average value in a given sample; intra-sample $\delta^{18}\text{O}_{\text{ost}}$ ranged from $\pm 0.16\text{‰}$ to $\pm 0.65\text{‰}$. The $\delta^{18}\text{O}_{\text{ost}}$ values for replicate samples of *P. pseudopunctillata* (n= 39) had the smallest average standard deviation of $\pm 0.16\text{‰}$, while *N. leioderma* (n= 52) and *S. bradii* (n= 96) averaged the highest standard deviations of $\pm 0.30\text{‰}$ and $\pm 0.28\text{‰}$, respectively. The average standard deviation for all intra- $\delta^{18}\text{O}_{\text{ost}}$ values was $\pm 0.24\text{‰}$, which suggests that measurements were not only precise but $\delta^{18}\text{O}_{\text{ost}}$ values were fairly consistent within a sample. This confirms that interannual and intrasample variability of $\delta^{18}\text{O}_{\text{ost}}$ values is nearly as small as analytical error, and adult valves at a sample location represent the mean summer water condition $\pm 0.2\text{‰}$. These results are consistent with the conclusion by Roberts et al. (2018) that if specimens in the same sample calcified at different times or seasons, their $\delta^{18}\text{O}$ may vary by $\pm 0.2\text{‰}$.

3.4.7 The relationship of species $\delta^{18}\text{O}_{\text{ost}}$ to temperature, salinity and $\delta^{18}\text{O}_{\text{water}}$

3.4.7.1 *Normanicythere leioderma*

Oxygen isotope values of *N. leioderma* exhibited the widest range ($\sim 4\text{‰}$, or from +0.6 to +4.4‰) and were negatively correlated ($p = 0.00$) with summer temperature when the samples were collected (Fig. 3.5a; overall $R^2 = 0.67$), and significantly correlated with salinity (Fig. 3.5b; overall $R^2 = 0.58$) and $\delta^{18}\text{O}_{\text{water}}$ values (Fig. 3.5c; $R^2 = 0.47$). This species demonstrated temperature-dependent fractionation that is generally similar in slope to the predicted temperature sensitivity for carbonates of -0.23‰ per 1°C (Epstein et al., 1953). The samples collected from ACW (red-filled circles) were specifically distinguished by the $\delta^{18}\text{O}_{\text{ost}}$ values of *N. leioderma* in warm ($>4^\circ\text{C}$), less saline (<32), lower $\delta^{18}\text{O}_{\text{water}}$, which are characteristic properties of this water mass (Figs. 3.5a & b). The $\delta^{18}\text{O}_{\text{ost}}$ values representative of RWW were more narrowly clustered in this colder, more saline water mass.

After the calculated vital offset was subtracted from the *N. leioderma* $\delta^{18}\text{O}_{\text{ost}}$ measurements, the $\delta^{18}\text{O}_{\text{ost}}$ value was close to expected equilibrium calcite values after accounting for expected temperature effects. Therefore, the oxygen isotopic composition of *N. leioderma* may be a valid proxy indicator of water temperature at the time of shell calcification. In order to test this relationship, we used the following paleotemperature equation (Epstein et al., 1951, 1953; modified by Craig, 1965), which was calibrated for biogenic carbonates in a temperature range of ~ 7 to 29°C . Although this temperature range is higher than observed for most of our samples, we used it to test its applicability:

$$T = 16.9 - 4.2 * (\delta^{18}\text{O}_{\text{ost}} - \delta^{18}\text{O}_{\text{water}}) + 0.13 * (\delta^{18}\text{O}_{\text{ost}} - \delta^{18}\text{O}_{\text{water}})^2$$

(Note: the Epstein et al. [1953] equation was standardized with PDB-derived CO_2 , so conversion of $\delta^{18}\text{O}_{\text{water}}$ VSMOW to VPDB uses the currently accepted value of -0.27‰ .)

To test how closely this predicted temperature equation matched the actual temperature at the ostracode collection sites, the equation was solved for temperature using the measured $\delta^{18}\text{O}_{\text{water}}$ values and $\delta^{18}\text{O}_{\text{ost}}$ values. The predicted temperature for the *N. leioderma* samples averaged within $\pm 1.70^\circ\text{C}$ ($R^2 = 0.57$) of the actual measured temperature (Table 3.2) at the site of collection (Supplement Fig. 3.9a).

In addition, we tested *N. leioderma* sample data with the Shackleton (1974) paleotemperature equation:

$$T = 16.9 - 4.38 (\delta^{18}\text{O}_{\text{ost}} - \delta^{18}\text{O}_{\text{water}}) + 0.1 (\delta^{18}\text{O}_{\text{ost}} - \delta^{18}\text{O}_{\text{water}})^2$$

(Note: $\delta^{18}\text{O}_{\text{water}}$ is on the VSMOW scale so 0.20 is subtracted for the conversion to VPDB, which was the conversion at the time this equation was calibrated.)

Using this equation, the average predicted temperature was within $\pm 0.77^\circ\text{C}$ ($R^2 = 0.58$) of the actual temperature at the sample sites (Supplement Fig. 3.9b). This suggests that the $\delta^{18}\text{O}_{\text{ost}}$ values of this species may have application in downcore reconstructions for use in estimating water temperatures. At sites where bottom water temperatures reached $>8^\circ\text{C}$, both equations predicted temperatures that were much lower than recorded temperatures. It is likely that in these cases the ostracodes secreted their shells earlier in the season and prior to our sampling and temperature measurement, when temperatures were cooler. At some sampling sites nearer to shore, it is possible for temperatures to increase quickly in summer, by $3\text{-}5^\circ\text{C}$ during a single month in the Chirikov Basin and along the southeastern Chukchi coast. Part of this temperature increase, which is higher at the sea surface, can extend to the seafloor. The correlation of this species $\delta^{18}\text{O}_{\text{ost}}$ value with temperature would likely be stronger if we could better constrain the particular month of shell secretion because bottom temperatures in the summer can change so rapidly. Nevertheless, these exercises show the potential for this species to be used as a

paleotemperature proxy for the summer season. Ultimately, we conclude that oxygen isotope fractionation in *N. leioderma* calcite is strongly tied to ambient water temperatures.

3.4.7.2 *Paracyprideis pseudopunctillata*

Despite $\delta^{18}\text{O}_{\text{ost}}$ values of *P. pseudopunctillata* varying in a narrow range (<2‰, or from +3.4 to +5.1‰), a relationship between $\delta^{18}\text{O}_{\text{ost}}$ and temperature (Fig. 3.5a; overall $R^2 = 0.52$) and salinity (Fig. 3.5b; overall $R^2 = 0.52$; Table 3.2) was found. There was no overall correlation of $\delta^{18}\text{O}_{\text{ost}}$ to $\delta^{18}\text{O}_{\text{water}}$ (Fig. 3.5c; $R^2 = 0.06$) but ACW can be distinguished from the $\delta^{18}\text{O}_{\text{ost}}$ values in most samples. The $\delta^{18}\text{O}_{\text{ost}}$ of this species in ACW samples was typically <4‰ while the $\delta^{18}\text{O}_{\text{ost}}$ of BSW and RWW was >4‰. Particularly in ACW samples, the $\delta^{18}\text{O}_{\text{ost}}$ values of *P. pseudopunctillata* showed relationships to temperature ($R^2 = 0.58$), salinity ($R^2 = 0.65$) and $\delta^{18}\text{O}_{\text{water}}$ ($R^2 = 0.43$; five sample locations and 14 measurements). As with *N. leioderma*, we tested the paleotemperature equations with *P. pseudopunctillata* data and found better temperature prediction at lower temperatures. While individual influences of temperature and $\delta^{18}\text{O}_{\text{water}}$ are challenging to deconvolve, as is the case with *N. leioderma*, the $\delta^{18}\text{O}_{\text{ost}}$ of this species also demonstrated a clear relationship to water mass properties.

3.4.7.3 *Sarsicytheridea bradii*

Sarsicytheridea bradii, in its wide, pan-Arctic distribution, displays very broad environmental tolerances (Supplement Figs. 3.5, 3.6; Neale and Howe, 1975; Gemery et al., 2015), and the sample locations where it was found in our study support its eurytopic nature. Its $\delta^{18}\text{O}_{\text{ost}}$ values exhibited a narrow range of values (~+3 to 4.5‰) across a temperature range of 10°C (Fig. 3.6a) and a salinity range of four units (Fig. 3.6b; Table 3.2). Due to strong vital effects and possibly other undetermined factors, the isotopic fractionation of ^{18}O in *S. bradii* was

not strongly driven by any environmental factors that could be distinguished. For example, regression analysis showed its $\delta^{18}\text{O}_{\text{ost}}$ values were not significantly related to temperature, salinity or $\delta^{18}\text{O}_{\text{water}}$ ($R^2 = 0.09$, $R^2 = 0.14$ $R^2 = 0.03$ respectively; Figs. 3.6a, b, c).

3.4.7.4 *Heterocyprideis* spp.

The two cryophilic *Heterocyprideis* species measured (12 samples *H. sorbyana*, 16 samples *H. fascis*) had average $\delta^{18}\text{O}_{\text{ost}}$ values within 0.4‰ of each other, but the average expected calcite isotopic composition, based upon thermodynamic equilibrium considerations, diverged. *H. fascis* was found mostly in locations of frigid water (<0°C; Fig. 3.7a, c), so equilibrium isotopic fractionation led to higher expected $\delta^{18}\text{O}$ values, but species vital offsets were low. This species was not found in ACW. By comparison, *H. sorbyana* was found in warmer, lower salinity sample locations (Fig. 3.7a, b) and its $\delta^{18}\text{O}_{\text{ost}}$ reflects the more heavy-isotope depleted composition of ACW. Because the environmental conditions, especially temperature, were so different for these two species, it is difficult to determine if the two species fractionate oxygen isotopes in similar ways and if the species vital offsets are actually so distinct from each other. A key limitation preventing interpretation is the small sample size for these species.

3.5 Conclusions

This study determined calcite stable oxygen isotope values for five common high latitude continental shelf ostracode species and investigated the environmental factors that influence shell $\delta^{18}\text{O}_{\text{ost}}$ values. Because most Arctic ostracodes calcify their adult tests during summer months, we compared $\delta^{18}\text{O}_{\text{ost}}$ values with summer water mass properties and the measured salinity, temperature and $\delta^{18}\text{O}_{\text{water}}$ values at the time of sampling. Measured water properties may not

reflect the exact timing of shell calcification but intra-sample $\delta^{18}\text{O}_{\text{ost}}$ variability was only slightly larger than analytical precision, averaging $\pm 0.2\text{‰}$. This suggests that multiple $\delta^{18}\text{O}_{\text{ost}}$ measurements within an individual sample reflects an acceptably low degree of variation. The continental shelf environment is highly variable with rapid and short-term changes in water masses, both seasonally and regionally. This variability, for instance, is reflected by a 4‰ range in the $\delta^{18}\text{O}_{\text{ost}}$ values of a widely distributed species (*N. leioderma*) over areas of the N. Bering Sea into the Chukchi Sea. Such divergent values indicate that this species occurs in a variety of near-shore environments that experience large degrees of temperature and $\delta^{18}\text{O}_{\text{water}}$ values.

We conclude that $\delta^{18}\text{O}_{\text{ost}}$ values of some species can be reliable recorders of changes in temperature and isotopic composition of seawater (as reflected in salinity) and, in turn, provenance of the water mass. Such relationships might also be present in the other studied species but are difficult to constrain without additional research. Seasonal hydrography of warmer and less saline ACW and very cold, saline RWW is reflected in stable isotope records of $\delta^{18}\text{O}_{\text{water}}$ values and particularly in $\delta^{18}\text{O}_{\text{ost}}$ values of two species, *N. leioderma* and *P. pseudopunctillata*. After accounting for vital effects and a constant offset for temperature, *N. leioderma* $\delta^{18}\text{O}_{\text{ost}}$ appears to best reflect the oxygen isotope composition of the ambient water. The $\delta^{18}\text{O}_{\text{ost}}$ values of *S. bradii* reveal further influences on the isotopic composition of this species' shell calcite, affected by metabolic and/or environmental factors that could not be determined. This study indicates that the isotopic composition of benthic ostracode calcite has the potential to be used to reconstruct mean summer water mass conditions in high latitude continental shelf environments. Future research can apply $\delta^{18}\text{O}_{\text{ost}}$ results to down-core sediments in order to reconstruct Pleistocene and Holocene Arctic paleoceanography and support the use of

$\delta^{18}\text{O}_{\text{ost}}$ values to help identify regional-scale changes in $\delta^{18}\text{O}_{\text{water}}$, water masses, circulation patterns, and ocean responses to climate variability.

3.6 Acknowledgements

We thank the scientists and crews of USCGC Healy and CCGS Sir Wilfrid Laurier expeditions for facilitating sample collections. We gratefully acknowledge two very helpful reviews of an earlier version of the manuscript by R. Seal and R. Poirier. L. Roberts and an anonymous reviewer are thanked for providing constructive comments that improved this manuscript. LG appreciates the time and useful feedback of A. Mix and M. Gonsior at an Ocean Sciences conference poster session in February 2020. Thanks to S. Bergstresser for mapping graphics and A. Ruefer, S. Watson and N. Vaka for lab assistance. Any use of trade, firm, or product names is for descriptive purposes only and does not imply endorsement by the U.S. Government. Financial support for this research project was provided by the USGS Land Change Science Program / Florence Bascom Geoscience Center. Expedition funding and associated science activities by JMG and LWC was provided by BOEM through the COMIDA Hanna Shoal project (UTA11-000872), NOAA Arctic Research Program (CINAR 22309.07), and the NSF Office of Polar Programs (OPP-0125082) and Arctic Observing Network program (1204082, 1702456, and 1917434).

Figures Chapter 3

Figure 3.1 Location of sediment and near-bottom water sampling stations (n=78) in the northern Bering and Chukchi Seas used in this study. The primary summer surface currents, which can mix to the bottom to affect the sample site's water mass, are labeled (flow patterns adapted from Stabeno et al., 2018 and Danielson et al., 2017).

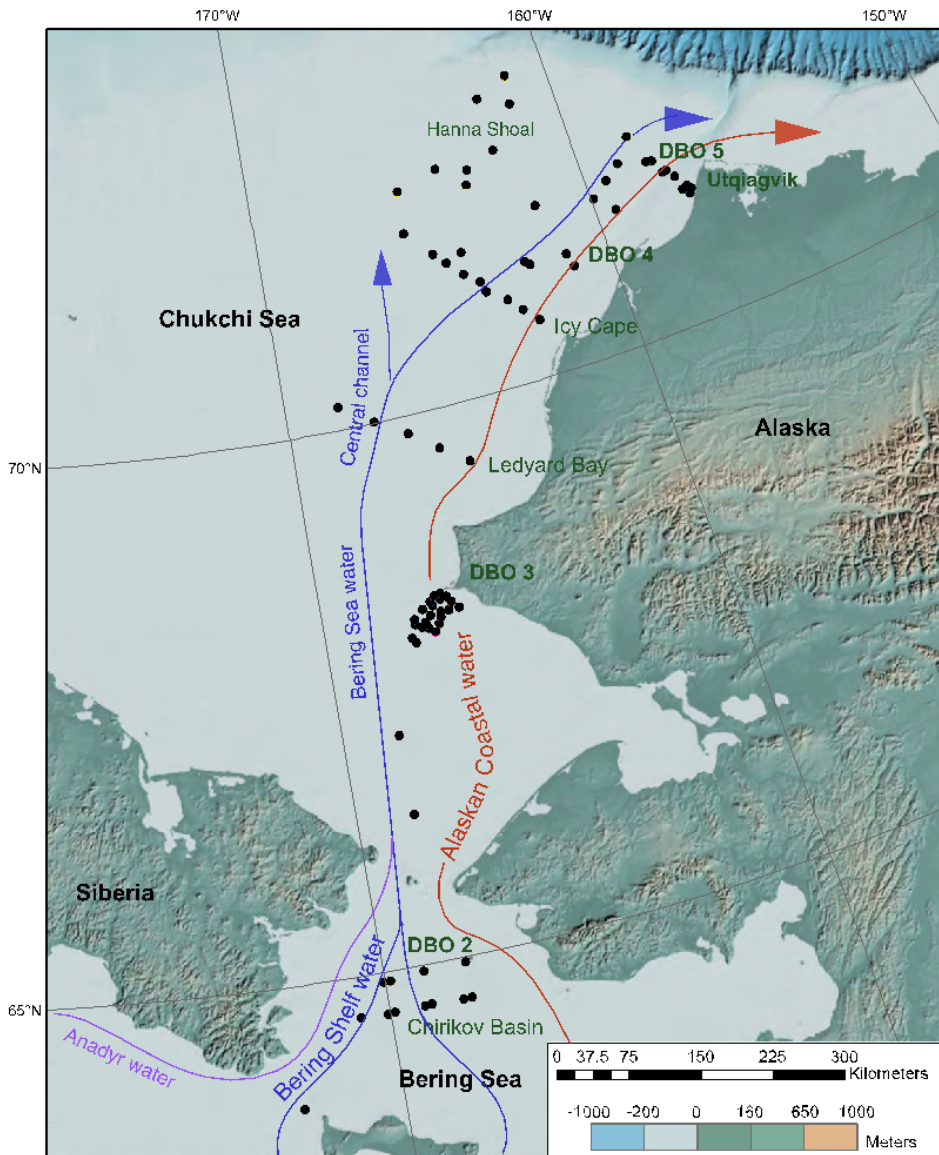
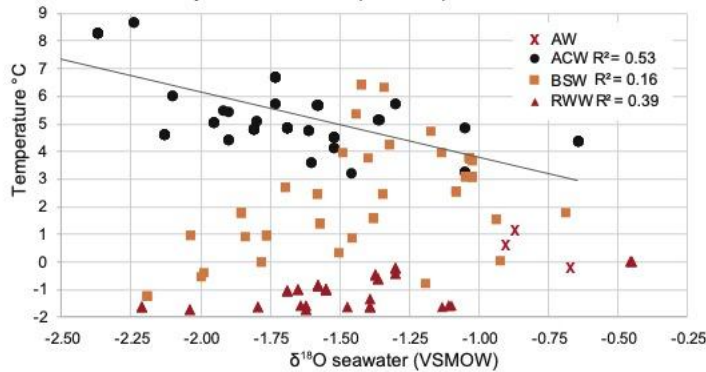


Figure 3.2 a.) $\delta^{18}\text{O}$ values of seawater from sampling stations (listed in Table 3.2), sorted by water mass properties versus temperature; b.) $\delta^{18}\text{O}$ values of seawater, sorted by water mass properties versus salinity. Simple regression analysis was conducted on all samples overall ($R^2=0.04$ for temperature and $R^2=0.45$ for salinity) and for samples labeled by water mass represented with the coefficient of determination, R^2 , cited in the legend. The analytical error of the mass spectrometric measurement is $\sim 0.1\text{‰}$, which is similar to the symbol size. Abbreviations: AW= Anadyr water; ACW = Alaska coastal water; BSW= Bering Sea water; RWW= remnant winter water

a. $\delta^{18}\text{O}$ seawater by water mass v Temperature (Years 2013-2018, n=78, $R^2=0.04$)



b. $\delta^{18}\text{O}$ seawater by water mass v Salinity (Years 2013-2018, n=78, $R^2=0.45$)

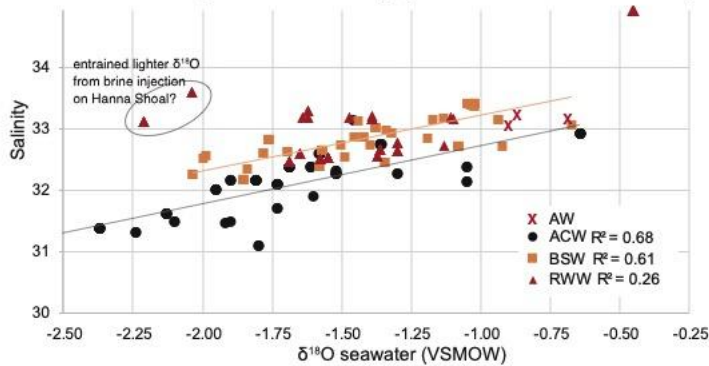


Figure 3.3 a., d., g., j., l.) $\delta^{18}\text{O}_{\text{Ost}}$ results for each species from each sample; b., e., h., k., m.) calculated adult vital offset (difference between $\delta^{18}\text{O}_{\text{Ost}}$ - $\delta^{18}\text{O}_{\text{expected}}$) values for each respective species with average values cited to the right; Figure 3. c., f., i.) calculated juvenile vital offset values for each species and average value cited to the right.

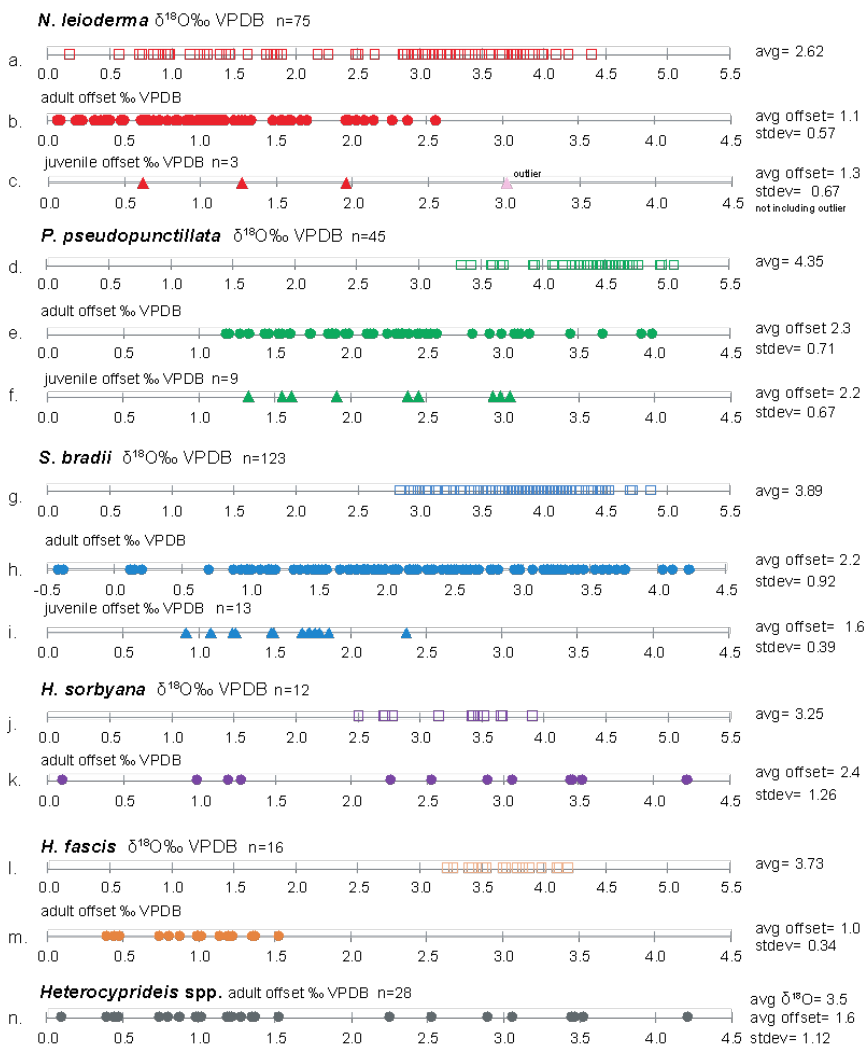


Figure 3.4 Principal component analysis results for factor loadings that include temperature, $\delta^{18}\text{O}_{\text{ost}}$, salinity, and $\delta^{18}\text{O}_{\text{water}}$. Species are color coded as follows: *N. leioderma* (red); *P. pseudopunctillata* (green); *S. bradii* (blue); *H. sorbyana* (purple); and *H. fascis* (orange); and symbols of each respective color indicate the water mass in which the sample was collected. The pink circular highlight represents samples primarily in the southeast Chukchi Sea (DBO3-1 to DBO3-4) in ACW. The yellow highlight represents samples located in the northern Chukchi Sea (DBO4, DBO5) in BSW and RWW. The blue highlight represents samples located in the western Chirikov Basin that are influenced by AW (DBO2) and samples located offshore in BSW.

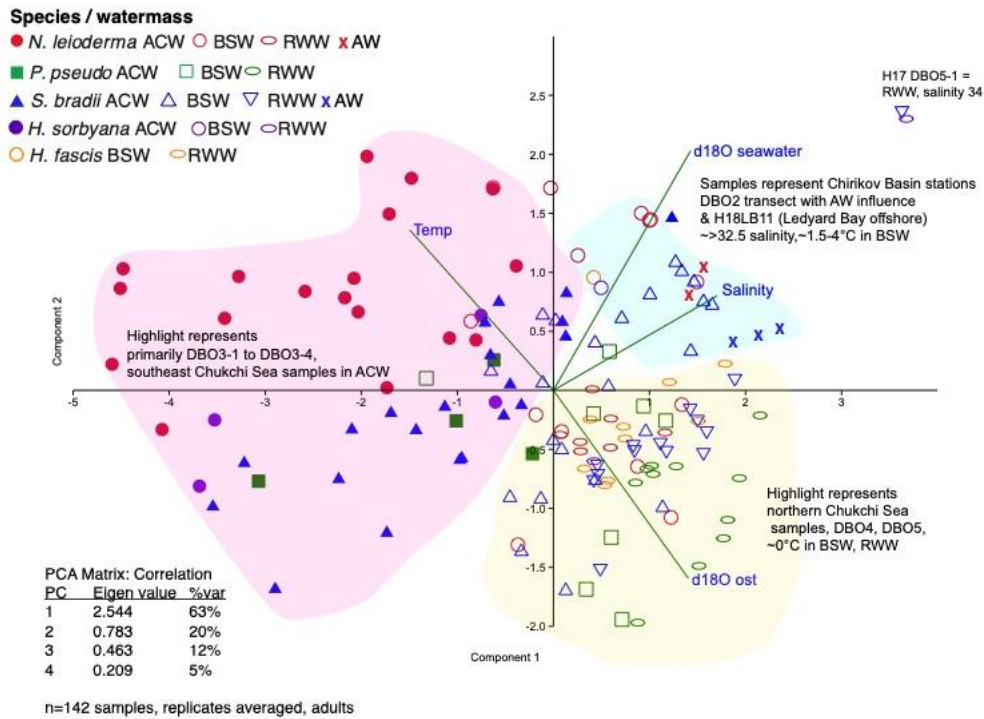


Figure 3.5 a.) $\delta^{18}\text{O}_{\text{ost}}$ results of *N. leioderma* (red circles) and *P. pseudopunctillata* (green squares) sorted by water mass of sample versus temperature; b.) $\delta^{18}\text{O}_{\text{ost}}$ results sorted by water mass of sample versus salinity; c.) $\delta^{18}\text{O}_{\text{water}}$ results sorted by water mass of sample versus $\delta^{18}\text{O}_{\text{ost}}$. (Values are not corrected for vital offsets.) Simple linear regression analysis was conducted on samples shown in each plot (*N. leioderma*: $R^2= 0.67$ for temperature, $R^2= 0.58$ for salinity, $R^2= 0.47$ for $\delta^{18}\text{O}_{\text{water}}$; *P. pseudopunctillata*: $R^2= 0.52$ for temperature, $R^2= 0.52$ for salinity, $R^2= 0.06$ for $\delta^{18}\text{O}_{\text{water}}$) and for samples identified in ACW because, in some cases, the R^2 value supported a significant relationship.

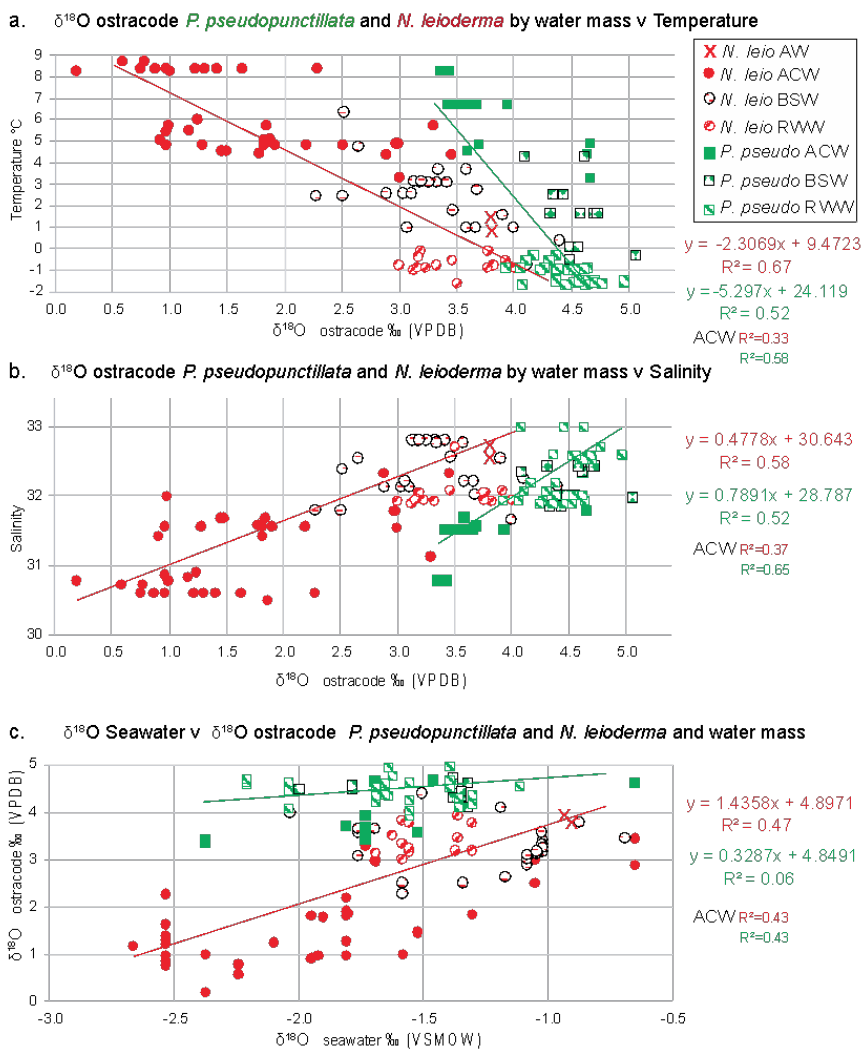


Figure 3.6 $\delta^{18}\text{O}_{\text{ost}}$ results of *S. bradii* (blue triangles) sorted by water mass of sample versus temperature; b.) $\delta^{18}\text{O}_{\text{ost}}$ results sorted by water mass of sample collection versus salinity; c.) $\delta^{18}\text{O}_{\text{water}}$ results sorted by water mass of sample versus $\delta^{18}\text{O}_{\text{ost}}$ values. (Values are not corrected for vital offsets.) Simple linear regression analysis was conducted on samples shown in each plot, which show no significant relationships between one variable to predict the other variable ($R^2 = 0.09$ for temperature, $R^2 = 0.14$ for salinity, $R^2 = 0.03$ for $\delta^{18}\text{O}_{\text{water}}$).

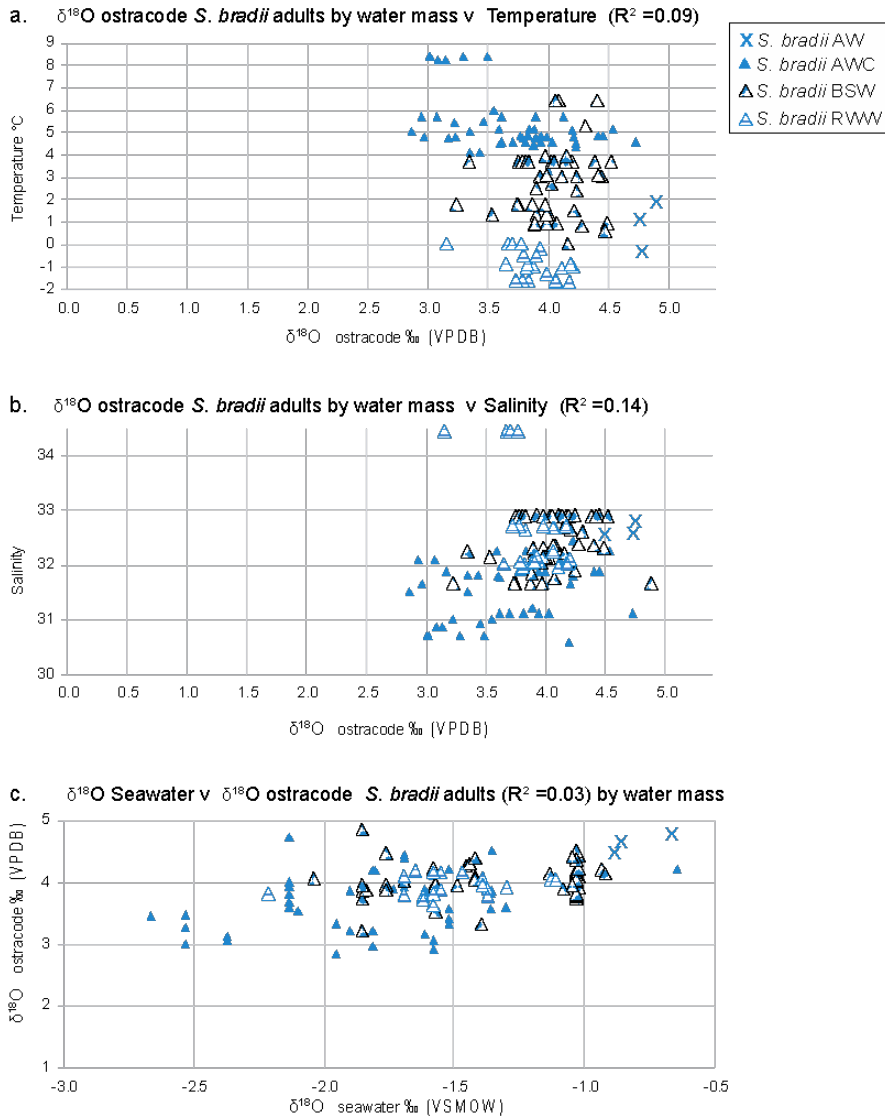
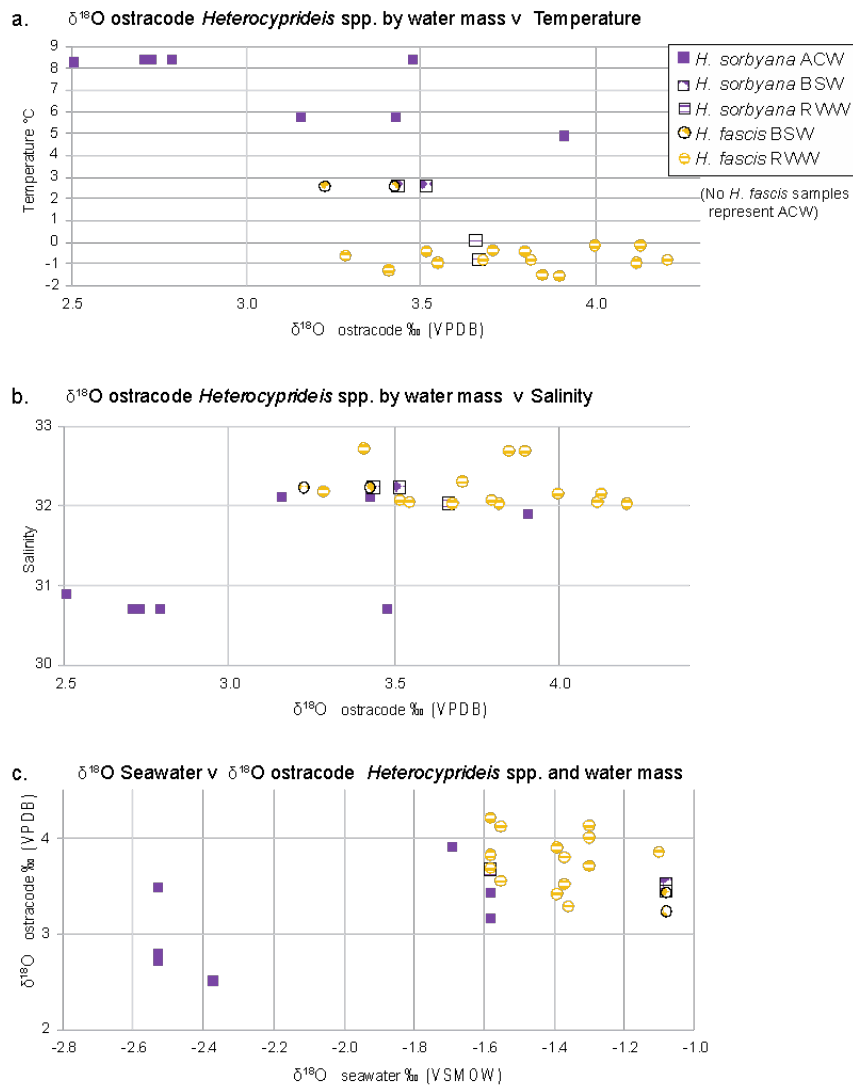
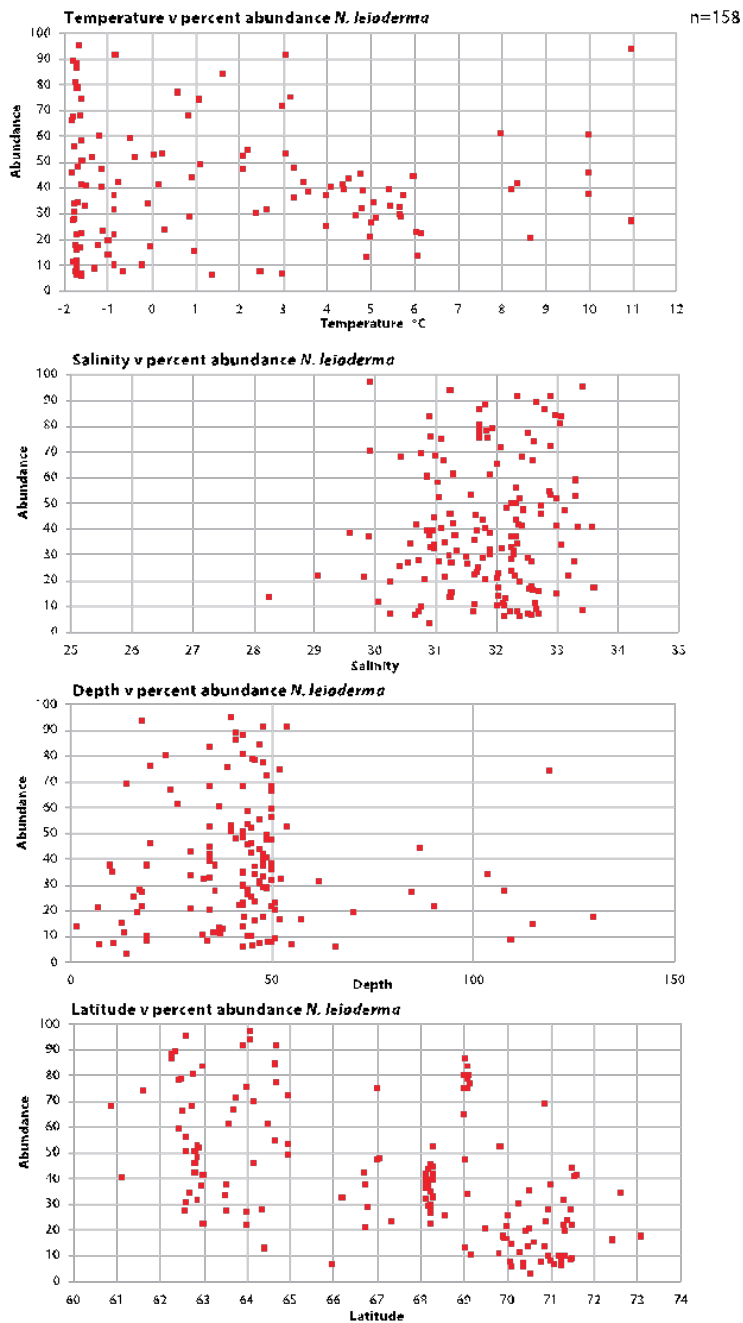


Figure 3.7 $\delta^{18}\text{O}_{\text{ost}}$ results of *H. sorbyana* (purple squares) and *H. fascis* (orange circles) sorted by water mass of sample versus temperature; b.) $\delta^{18}\text{O}_{\text{ost}}$ results sorted by water mass of sample versus salinity; c.) $\delta^{18}\text{O}_{\text{water}}$ results sorted by water mass of sample versus $\delta^{18}\text{O}_{\text{ost}}$. (Values are not corrected for vital offsets. Regression tests were not conducted because of too few samples.)

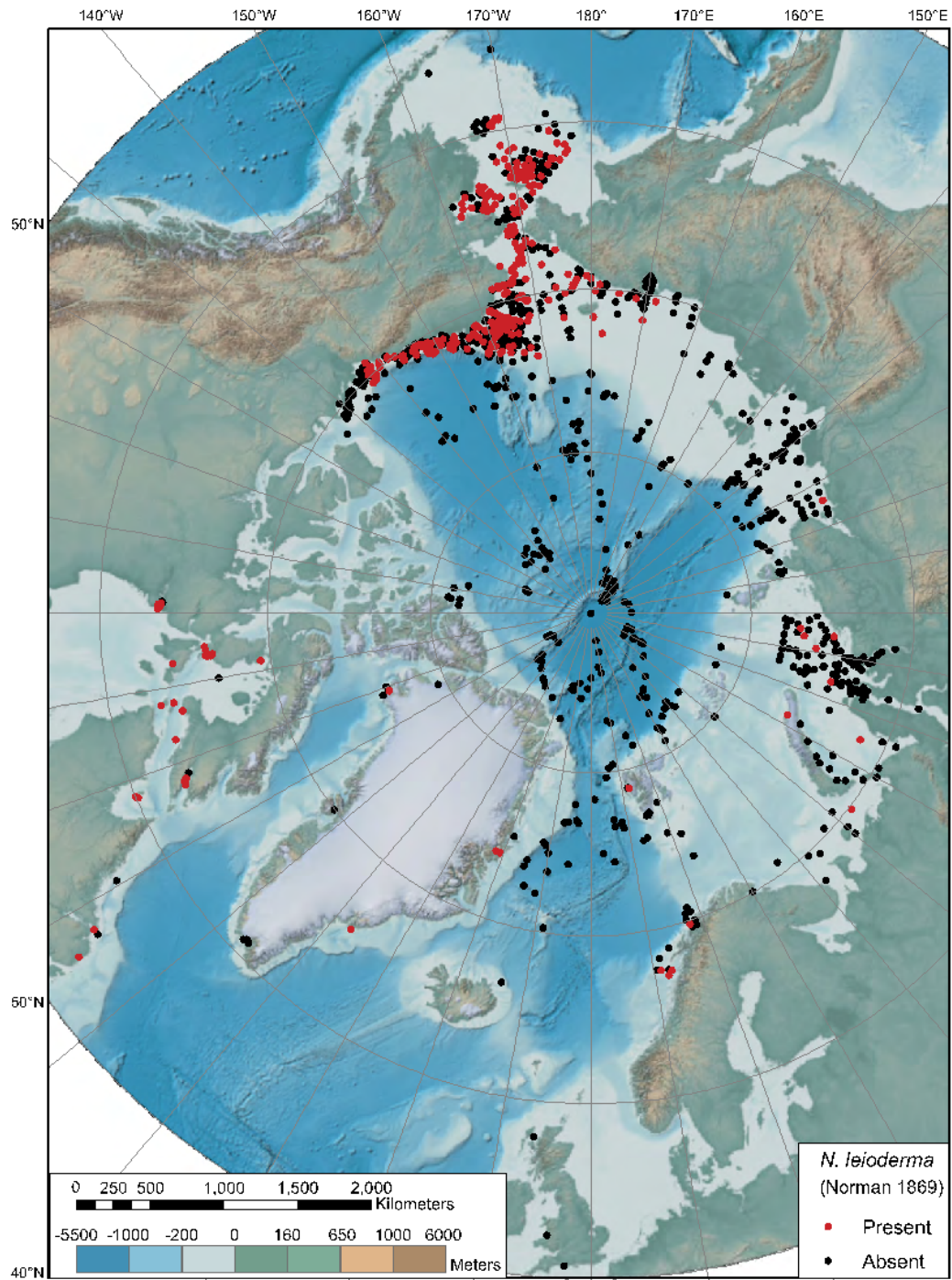


Supplementary Figures Chapter 3

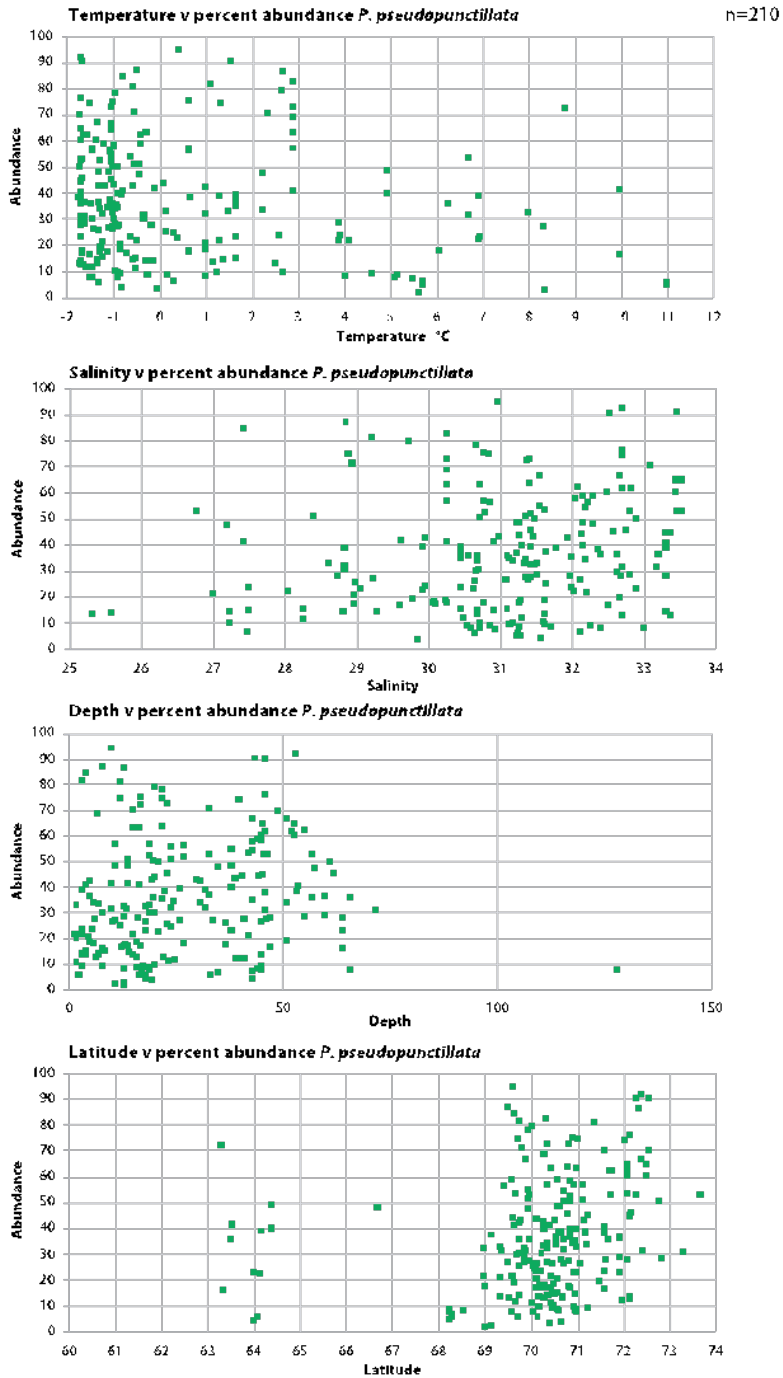
S3.1 Percent abundance of *N. leioderma* (n=158) in AOD samples (with >10 specimens of the given taxa in a sample) plotted versus bottom water temperature, salinity, water depth and latitude.



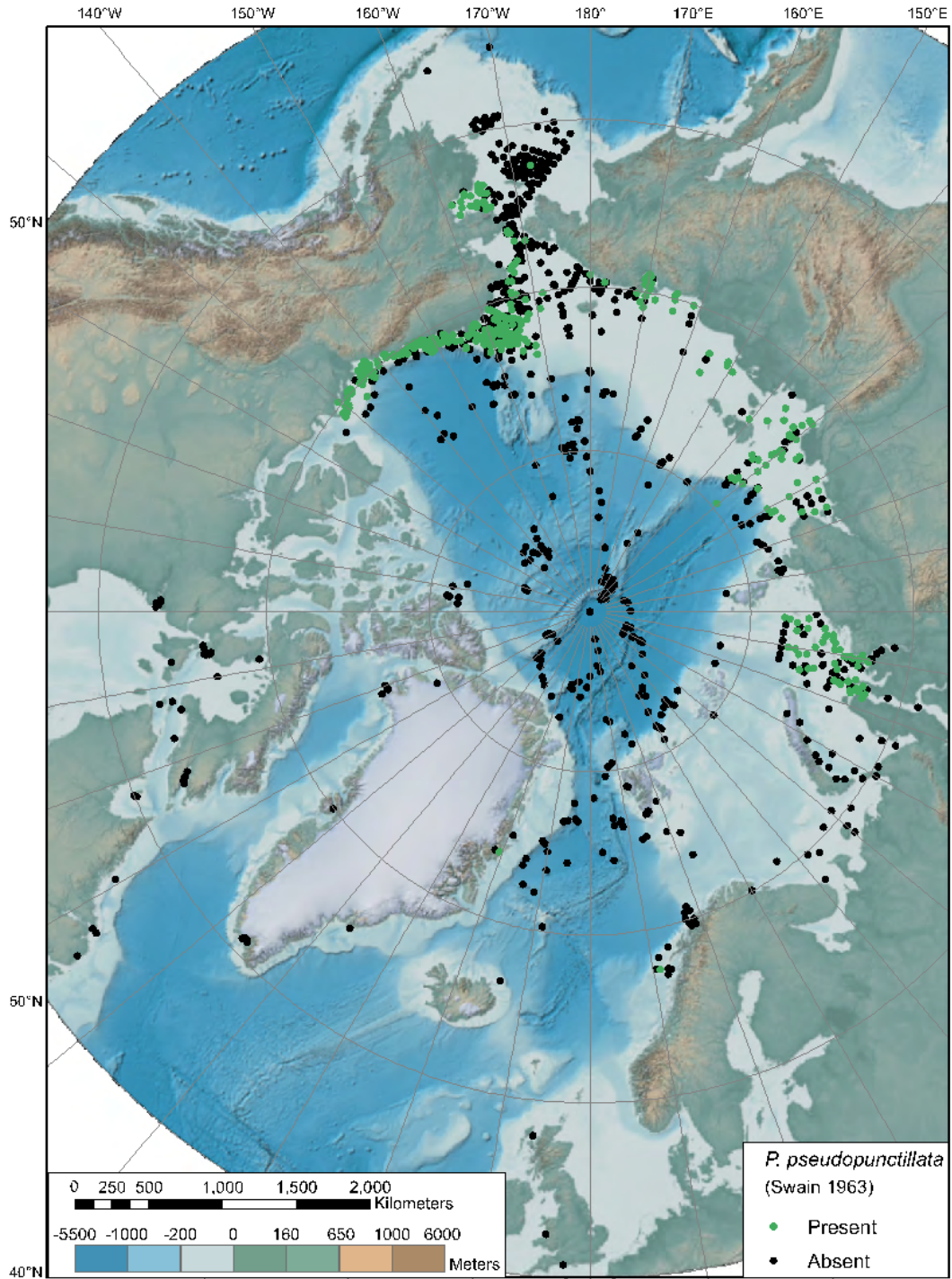
S3.2 Modern distribution of *N. leioderma* from the AOD.



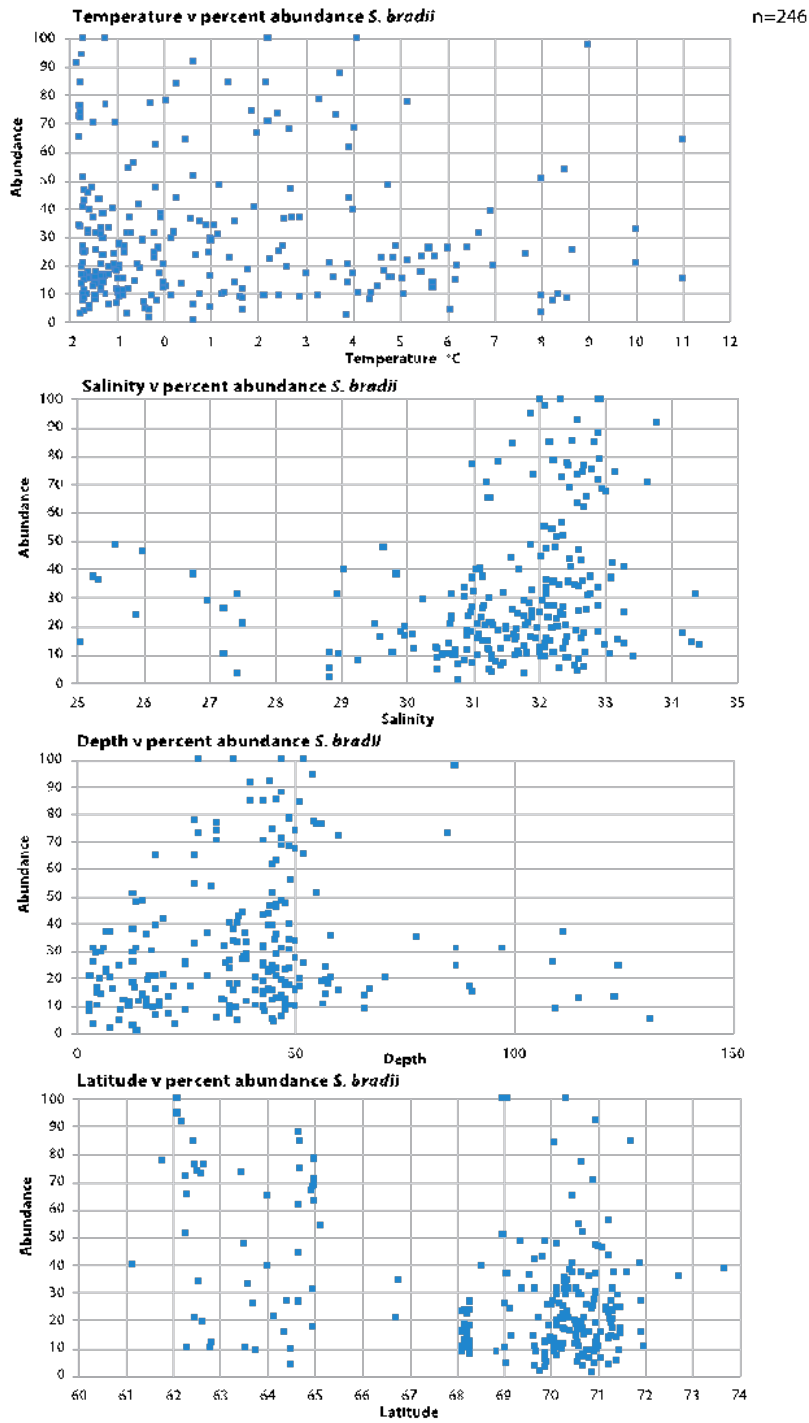
S3.3 Percent abundance of *P. pseudopunctillata* (n=210) in AOD samples (with >10 specimens of the given taxa in a sample) plotted versus bottom water temperature, salinity, water depth and latitude.



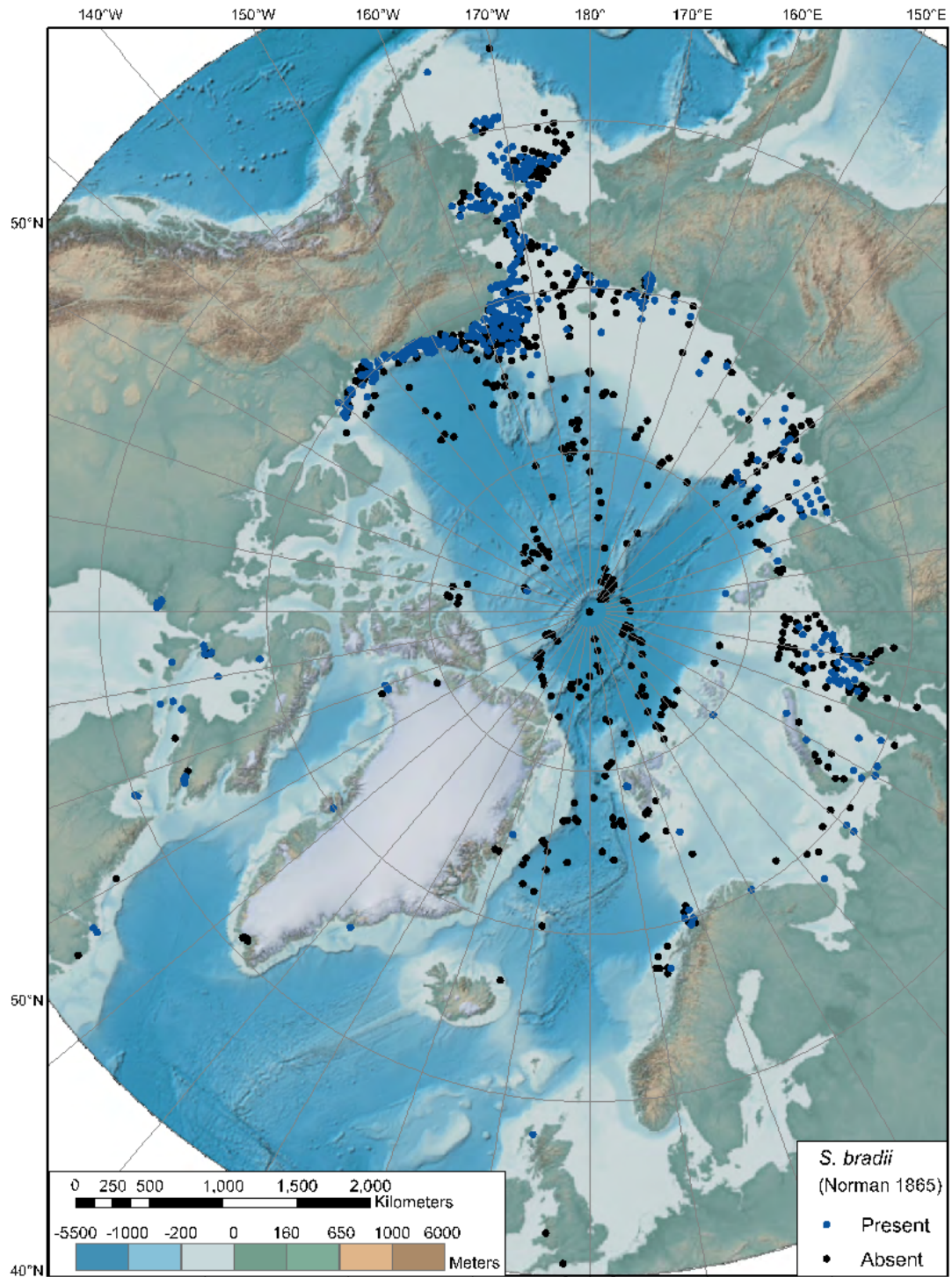
S3.4 Modern distribution of *P. pseudopunctillata* from the AOD.



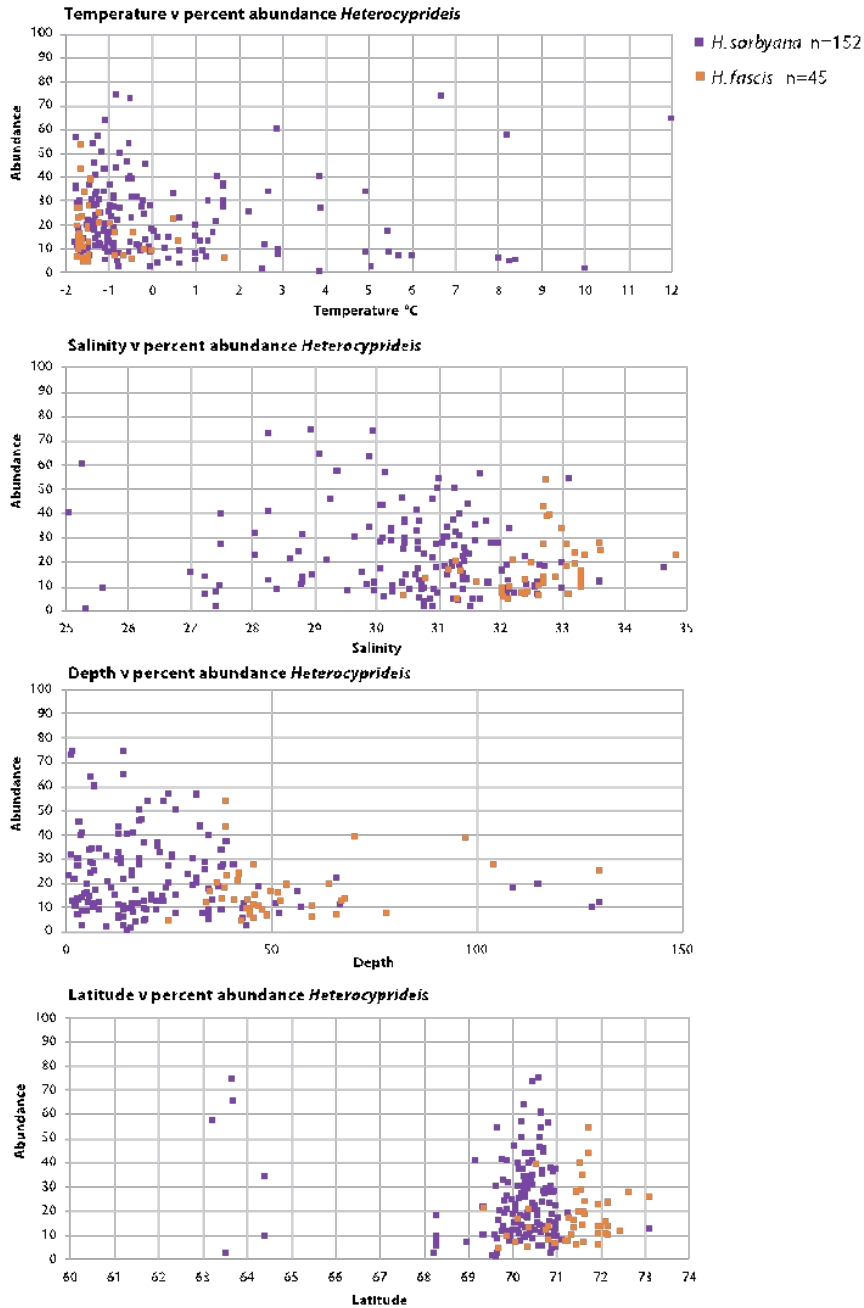
S3.5 Percent abundance of *S. bradii* (n=246) in AOD samples (with >10 specimens of the given taxa in a sample) plotted versus bottom water temperature, salinity, water depth and latitude.



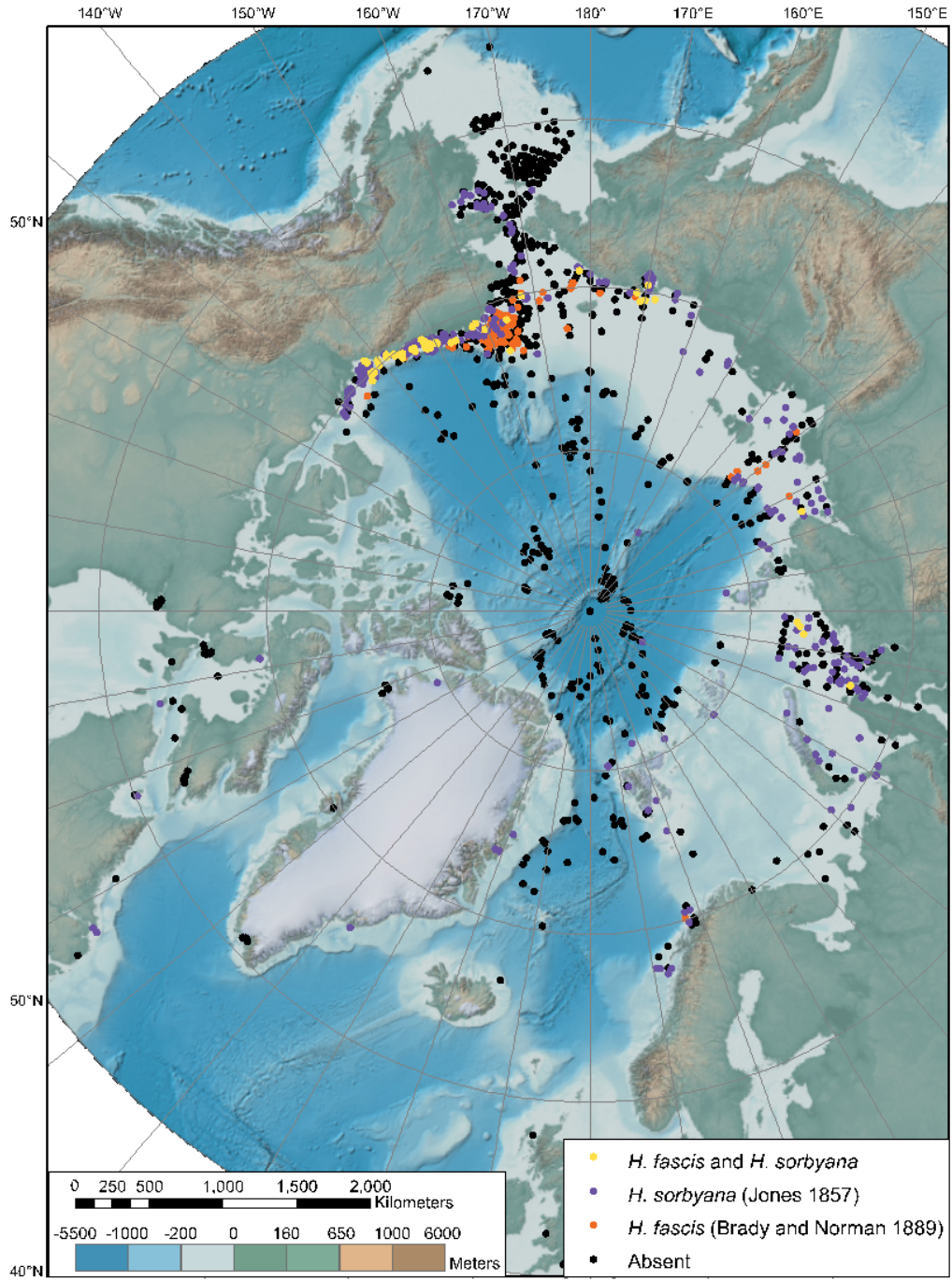
S3.6 Modern distribution of *S. bradii* from the AOD.



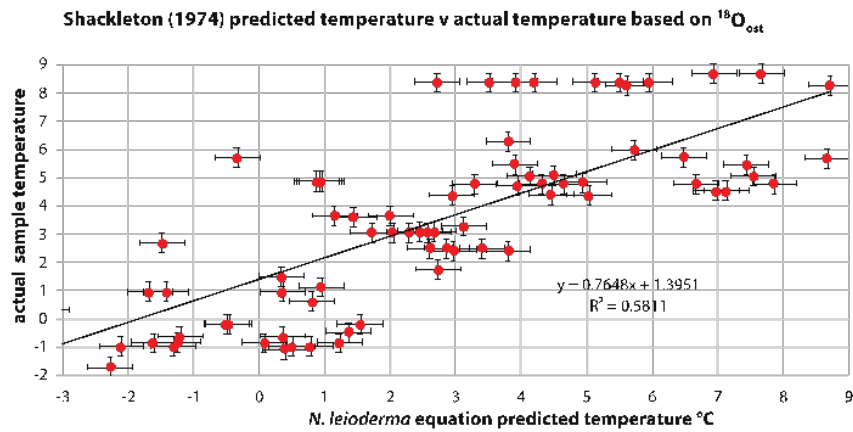
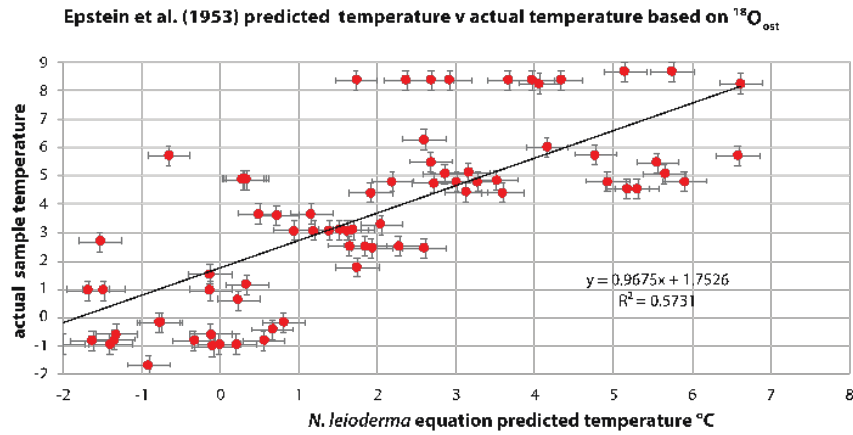
S3.7 Percent abundance of *H. sorbyana* (n=152) and *H. fascis* (n=45) in AOD samples (with >10 specimens of the given taxa in a sample) plotted versus bottom water temperature, salinity, water depth and latitude.



S3.8 Modern distribution of *H. sorbyana* and *H. fascis* from AOD.



S3.9a. Predicted temperature using paleotemperature equation by Epstein et al. (1953) versus actual sample temperature; 3.9b. Predicted temperature using paleotemperature equation by Shackleton (1974) versus actual sample temperature.



Tables Chapter 3

Table 3.1 The summer temperature and salinity range for each water mass taken from Coachman et al., 1975; Gong and Pickart, 2015; seawater $\delta^{18}\text{O}$ values from Cooper et al, 1997; and mean data with average standard deviation (stdev) from the present study.

Water mass	Avg. Temp. range °C	Salinity	$\delta^{18}\text{O}_{\text{water}}$ ‰ VSMOW and stdev	n= (This study)
Anadyr Water (AW)	-1.0 to 1.5	≥ 32.5	~-0.4 to -0.6	3
Alaska Coastal Water (ACW)	≥ 3 avg 5	≥ 30	-4 to -1.5 avg -1.8 (stdev ± 0.48)	23
Bering Sea Water (BSW)	0 to 3 avg 2	31.8-32.5	-1.5 to -0.4 avg -1.3 (stdev ± 0.35)	31
Winter Water (RWW)	< -1.0 avg -1.2	>31.5	-1.4/-1.5 (stdev ± 0.35)	21
Melt water (MW)	<2 to 4	24-30	-1.9	0

Table 3.2 List of surface samples used in this study, including year of the cruise, expedition, geographic location, water depth, $\delta^{18}\text{O}_{\text{water}}$, bottom water temperature, salinity, water mass, species measured, and $\delta^{18}\text{O}_{\text{ost}}$ results. Juvenile measurements are listed below the adult samples. Abbreviations: “Year” = Year sample collected; “Expedition” = expedition name includes either “HLY” for USCGC Healy or “SWL” for CCGS Sir Wilfrid Laurier and the year and leg; “Name” = sampling name, first letter refers to expedition vessel, “H” for Healy or “L” for Sir Wilfrid Laurier, then the two digit year of collection followed by the sampling station name; “Depth” = bottom water depth as recorded by the CTD; “ $\delta^{18}\text{O}_{\text{water}}$ ” = bottom $\delta^{18}\text{O}_{\text{water}}$ ‰ VSMOW; “Temp” = near-bottom water temperature; “Sal” = near-bottom salinity; “Water mass” = designated water mass based on properties listed in Table 3.1; “Species” = species measured (N= *N. leioderma*, P= *P. pseudopunctillata*, S= *S. bradii*, HF= *H. fascis*, HS= *H. sorbyana*); “ $\delta^{18}\text{O}_{\text{ost}}$ ” = ostracode shell calcite result ‰ VPDB.

Year	Expedition	Name	Latitude °N	Longitude °W	Depth (m)	$\delta^{18}\text{O}_{\text{water}}$ ‰ VSMOW	$\delta^{18}\text{O}_{\text{seawater}}$ ‰ VPDB	Temp (°C)	Sal	Water mass	Species	$\delta^{18}\text{O}_{\text{ost}}$ ‰ VPDB
2018	HLY1801	H18D5-10	71.63	-157.90	64	-1.4	-1.7	-1.6	32.7	RWW	HF	3.9
2018	HLY1801	H18D5-5	71.41	-157.45	131	-1.1	-1.4	-1.6	32.7	RWW	HF	3.9
2018	HLY1801	H18D5-7	71.50	-157.63	96	-1.4	-1.7	-1.3	32.7	RWW	HF	3.4
2018	HLY1801	H18IC11	71.83	-165.97	45	-1.5	-1.8	-0.4	32.3	RWW	HF	3.7
2018	HLY1801	H18IC10	71.71	-165.60	43	-1.6	-1.8	-0.6	32.2	RWW	HF	3.3
2018	HLY1801	H18IC9	71.71	-165.60	43	-1.4	-1.6	-1.0	32.0	RWW	HF	4.1
2018	HLY1801	H18IC9	71.71	-165.60	43	-1.4	-1.6	-1.0	32.0	RWW	HF	3.6
2018	HLY1801	H18IC6	71.20	-164.20	45	-1.6	-1.8	-0.8	32.0	RWW	HF	3.7
2018	HLY1801	H18IC6	71.20	-164.20	45	-1.6	-1.8	-0.8	32.0	RWW	HF	4.2
2018	HLY1801	H18IC5	71.09	-163.80	44	-1.7	-1.9	-0.2	32.1	RWW	HF	4.1
2018	HLY1801	H18IC5	71.09	-163.80	44	-1.7	-1.9	-0.2	32.1	RWW	HF	4.0
2018	HLY1801	H18IC4	70.97	-163.56	46	-1.7	-2.0	-0.4	32.1	RWW	HF	3.5
2018	HLY1801	H18IC4	70.97	-163.56	46	-1.7	-2.0	-0.4	32.1	RWW	HF	3.8
2018	HLY1801	H18LB11	70.06	-167.66	50	-1.1	-1.3	2.5	32.2	BSW	HF	3.4
2018	HLY1801	H18LB11	70.06	-167.66	50	-1.1	-1.3	2.5	32.2	BSW	HF	3.2
2017	HLY1702	H17D3-1	68.30	-166.91	33	-1.6	-1.8	5.7	32.1	ACW	HS	3.2
2017	HLY1702	H17D3-1	68.30	-166.91	33	-1.6	-1.8	5.7	32.1	ACW	HS	3.4
2017	HLY1702	H17D5-1	71.25	-157.16	46	-0.5	-0.7	0.0	34.4	RWW	HS	3.7
2018	HLY1801	H18D3-1	68.30	-166.93	35	-2.5	-2.8	8.4	30.7	ACW	HS	2.7
2018	HLY1801	H18D3-1	68.30	-166.93	35	-2.5	-2.8	8.4	30.7	ACW	HS	2.7
2018	HLY1801	H18D3-1	68.30	-166.93	35	-2.5	-2.8	8.4	30.7	ACW	HS	3.5
2018	HLY1801	H18D3-1	68.30	-166.93	35	-2.5	-2.8	8.4	30.7	ACW	HS	2.8

2018	HLY1801	H18D3-4	68.14	-167.49	48	-1.7	-2.0	4.9	31.9	ACW	HS	3.9
2018	HLY1801	H18IC6	71.20	-164.20	45	-1.6	-1.8	-0.8	32.0	RWW	HS	3.7
2018	HLY1801	H18LB11	70.06	-167.66	50	-1.1	-1.3	2.5	32.2	BSW	HS	3.5
2018	HLY1801	H18LB11	70.06	-167.66	50	-1.1	-1.3	2.5	32.2	BSW	HS	3.4
2018	SWL18	L18D3-1	68.30	-166.94	35	-2.4	-2.6	8.3	30.9	ACW	HS	2.5
2013	HLY13-01	H13H27	72.86	-161.22	55	-1.6	-1.9	-1.7	32.8	RWW	N	3.5
2017	HLY1702	H17D3-1	68.30	-166.91	33	-1.6	-1.8	5.7	32.1	ACW	N	1.0
2017	HLY1702	H17D3-4	68.13	-167.49	48	-0.6	-0.9	4.4	32.4	ACW	N	2.9
2017	HLY1702	H17D5-7	71.50	-157.68	87	-1.8	-2.0	1.0	32.3	BSW	N	3.6
2017	HLY1702	H17D5-7	71.50	-157.68	87	-1.8	-2.0	1.0	32.3	BSW	N	3.1
2017	HLY1702	H17D5-7	71.50	-157.68	87	-1.8	-2.0	1.0	32.3	BSW	N	3.7
2017	HLY1702	H17NW6	72.73	-162.98	58	-0.9	-1.2	1.5	32.7	BSW	N	3.9
2017	HLY1702	H17S6	70.96	-161.08	46	-1.7	-2.0	2.7	32.1	BSW	N	3.7
2017	HLY1702	H17SE1	71.33	-159.40	55	-2.0	-2.3	0.9	31.8	BSW	N	4.0
2017	HLY1702	H17SW3	71.40	-164.09	46	-1.5	-1.8	0.3	32.2	BSW	N	4.4
2018	HLY1801	H18D2-4	64.96	-169.90	44	-1.0	-1.3	3.1	32.9	BSW	N	3.4
2018	HLY1801	H18D2-4	64.96	-169.90	44	-1.0	-1.3	3.1	32.9	BSW	N	3.3
2018	HLY1801	H18D2-4	64.96	-169.90	44	-1.0	-1.3	3.1	32.9	BSW	N	3.2
2018	HLY1801	H18D2-4	64.96	-169.90	44	-1.0	-1.3	3.1	32.9	BSW	N	3.3
2018	HLY1801	H18D3-1	68.30	-166.93	35	-2.5	-2.8	8.4	30.7	ACW	N	1.3
2018	HLY1801	H18D3-1	68.30	-166.93	35	-2.5	-2.8	8.4	30.7	ACW	N	1.6
2018	HLY1801	H18D3-1	68.30	-166.93	35	-2.5	-2.8	8.4	30.7	ACW	N	1.4
2018	HLY1801	H18D3-1	68.30	-166.93	35	-2.5	-2.8	8.4	30.7	ACW	N	0.9
2018	HLY1801	H18D3-1	68.30	-166.93	35	-2.5	-2.8	8.4	30.7	ACW	N	0.8
2018	HLY1801	H18D3-1	68.30	-166.93	35	-2.5	-2.8	8.4	30.7	ACW	N	1.0
2018	HLY1801	H18D3-2	68.25	-167.13	44	-1.8	-2.1	4.8	31.7	ACW	N	2.2
2018	HLY1801	H18D3-2	68.25	-167.13	44	-1.8	-2.1	4.8	31.7	ACW	N	1.9
2018	HLY1801	H18D3-2	68.25	-167.13	44	-1.8	-2.1	4.8	31.7	ACW	N	1.8
2018	HLY1801	H18D3-2	68.25	-167.13	44	-1.8	-2.1	4.8	31.7	ACW	N	1.0
2018	HLY1801	H18D3-2	68.25	-167.13	44	-1.8	-2.1	4.8	31.7	ACW	N	1.3
2018	HLY1801	H18D3-3	68.19	-167.30	47	-1.5	-1.8	4.5	31.8	ACW	N	1.5
2018	HLY1801	H18D3-3	68.19	-167.30	47	-1.5	-1.8	4.5	31.8	ACW	N	1.5
2018	HLY1801	H18D3-4	68.14	-167.49	48	-1.7	-2.0	4.9	31.9	ACW	N	3.0
2018	HLY1801	H18D3-4	68.14	-167.49	48	-1.7	-2.0	4.9	31.9	ACW	N	3.0
2018	HLY1801	H18D3-4	68.14	-167.49	48	-1.7	-2.0	4.9	31.9	ACW	N	3.0
2018	HLY1801	H18D3-5	68.02	-167.88	51	-1.2	-1.4	4.7	32.6	BSW	N	2.7
2018	HLY1801	H18IC10	71.71	-165.60	43	-1.6	-1.8	-0.6	32.2	RWW	N	3.5
2018	HLY1801	H18IC10	71.71	-165.60	43	-1.6	-1.8	-0.6	32.2	RWW	N	3.9
2018	HLY1801	H18IC9	71.71	-165.60	43	-1.4	-1.6	-1.0	32.0	RWW	N	4.0
2018	HLY1801	H18IC9	71.71	-165.60	43	-1.4	-1.6	-1.0	32.0	RWW	N	3.2
2018	HLY1801	H18IC9	71.71	-165.60	43	-1.4	-1.6	-1.0	32.0	RWW	N	3.8
2018	HLY1801	H18IC9	71.71	-165.60	43	-1.4	-1.6	-1.0	32.0	RWW	N	3.2
2018	HLY1801	H18IC8	71.45	-164.92	43	-1.4	-1.6	-1.0	32.0	RWW	N	3.1
2018	HLY1801	H18IC6	71.20	-164.20	45	-1.6	-1.8	-0.8	32.0	RWW	N	3.8

2018	HLY1801	H18IC6	71.20	-164.20	45	-1.6	-1.8	-0.8	32.0	RWW	N	3.0
2018	HLY1801	H18IC6	71.20	-164.20	45	-1.6	-1.8	-0.8	32.0	RWW	N	3.3
2018	HLY1801	H18IC5	71.09	-163.80	44	-1.7	-1.9	-0.2	32.1	RWW	N	3.8
2018	HLY1801	H18IC5	71.09	-163.80	44	-1.7	-1.9	-0.2	32.1	RWW	N	3.8
2018	HLY1801	H18IC5	71.09	-163.80	44	-1.7	-1.9	-0.2	32.1	RWW	N	3.2
2018	HLY1801	H18IC4	70.97	-163.56	46	-1.7	-2.0	-0.4	32.1	RWW	N	3.2
2018	HLY1801	H18LB11	70.06	-167.66	50	-1.1	-1.3	2.5	32.2	BSW	N	2.9
2018	HLY1801	H18LB11	70.06	-167.66	50	-1.1	-1.3	2.5	32.2	BSW	N	3.0
2018	HLY1801	H18LB11	70.06	-167.66	50	-1.1	-1.3	2.5	32.2	BSW	N	3.1
2018	HLY1801	H18LB13	70.26	-168.54	43	-1.6	-1.8	2.4	31.9	BSW	N	2.3
2018	HLY1801	H18LB13	70.26	-168.54	43	-1.6	-1.8	2.4	31.9	BSW	N	2.5
2018	HLY1801	H18LB5	69.50	-165.38	35	-2.2	-2.5	8.7	30.8	ACW	N	0.8
2018	HLY1801	H18LB5	69.50	-165.38	35	-2.2	-2.5	8.7	30.8	ACW	N	0.6
2018	HLY1801	H18T2	67.16	-168.66	47	-1.3	-1.6	6.3	32.5	BSW	N	2.5
2014	SWL14	L14D3-1	68.30	-166.94	35	-2.7	-2.9	5.5	30.9	ACW	N	1.2
2014	SWL14	L14D3-2	68.24	-167.12	43	-1.7	-2.0	5.7	31.2	ACW	N	3.3
2014	SWL14	L14D3-4	68.13	-167.50	50	-1.0	-1.3	3.3	31.6	ACW	N	3.0
2015	SWL15	L15D3-1	68.30	-166.94	35	-2.1	-2.4	6.0	31.0	ACW	N	1.2
2015	SWL15	L15D3-2	68.24	-167.12	43	-1.8	-2.1	5.1	31.5	ACW	N	1.9
2015	SWL15	L15D3-4	68.13	-167.50	50	-1.6	-1.9	3.6	31.9	ACW	N	2.9
2015	SWL15	L15D4-2	71.10	-162.27	46	-1.8	-2.1	-1.6	32.7	RWW	N	4.2
2016	SWL16	L16BCL6	63.92	-172.10	54	-1.2	-1.5	-0.8	32.3	BSW	N	4.1
2016	SWL16	L16D2-1	64.67	-169.92	48	-0.9	-1.2	0.6	32.5	AW/BSW	N	3.8
2016	SWL16	L16D2-4	64.96	-169.89	49	-0.9	-1.1	1.1	32.7	AW/BSW	N	3.8
2016	SWL16	L16D3-1	68.30	-166.94	35	-1.9	-2.2	5.5	31.0	ACW	N	1.0
2016	SWL16	L16D3-3	68.19	-167.31	49	-1.3	-1.6	5.7	31.8	ACW	N	1.8
2016	SWL16	L16D3-4	68.13	-167.49	50	-1.1	-1.3	4.8	31.9	ACW	N	2.5
2018	SWL18	L18D2-0	64.67	-170.64	48	-1.0	-1.3	3.7	32.9	BSW	N	3.6
2018	SWL18	L18D2-0	64.67	-170.64	48	-1.0	-1.3	3.7	32.9	BSW	N	3.3
2018	SWL18	L18D2-1	64.67	-169.93	48	-1.0	-1.3	3.1	32.9	BSW	N	3.1
2018	SWL18	L18D2-1	64.67	-169.93	48	-1.0	-1.3	3.1	32.9	BSW	N	3.2
2018	SWL18	L18D3-1	68.30	-166.94	35	-2.4	-2.6	8.3	30.9	ACW	N	1.0
2018	SWL18	L18D3-1	68.30	-166.94	35	-2.4	-2.6	8.3	30.9	ACW	N	0.2
2018	SWL18	L18D3-2	68.24	-167.12	44	-2.0	-2.2	5.1	31.5	ACW	N	1.8
2018	SWL18	L18D3-2	68.24	-167.12	44	-2.0	-2.2	5.1	31.5	ACW	N	0.9
2018	SWL18	L18D3-3	68.19	-167.31	48	-1.9	-2.2	4.4	31.7	ACW	N	1.8
2013	HLY1301	H13CBL11	72.10	-165.46	46	-1.6	-1.9	-1.6	32.7	RWW	P	5.0
2013	HLY1301	H13H108	71.61	-159.38	49	-2.0	-2.3	-1.7	33.1	RWW	P	4.6
2013	HLY1301	H13H108	71.61	-159.38	49	-2.0	-2.3	-1.7	33.1	RWW	P	4.5
2013	HLY1301	H13H27	72.86	-161.22	55	-1.6	-1.9	-1.7	32.8	RWW	P	4.8
2013	HLY1301	H13H29	71.93	-158.33	60	-2.2	-2.5	-1.6	32.6	RWW	P	4.6
2017	HLY1702	H17D3-4	68.13	-167.49	48	-0.6	-0.9	4.4	32.4	ACW	P	4.6
2017	HLY1702	H17E10	71.64	-158.06	59	-2.0	-2.3	-0.6	32.0	BSW	P	4.5
2017	HLY1702	H17E8	71.72	-158.88	55	-2.0	-2.3	-0.4	32.1	BSW	P	5.1

2017	HLY1702	H17NNE4	72.59	-161.36	46	-1.4	-1.6	1.6	32.5	BSW	P	4.7
2017	HLY1702	H17NNE4	72.59	-161.36	46	-1.4	-1.6	1.6	32.5	BSW	P	4.7
2017	HLY1702	H17NNE4	72.59	-161.36	46	-1.4	-1.6	1.6	32.5	BSW	P	4.3
2017	HLY1702	H17NNE4	72.59	-161.36	46	-1.4	-1.6	1.6	32.5	BSW	P	4.6
2017	HLY1702	H17SE3	71.49	-159.91	50	-1.8	-2.1	0.0	32.1	BSW	P	4.5
2017	HLY1702	H17SE3	71.49	-159.91	50	-1.8	-2.1	0.0	32.1	BSW	P	4.6
2017	HLY1702	H17SE9	71.98	-162.08	33	-1.3	-1.6	2.5	31.9	BSW	P	4.3
2017	HLY1702	H17SE9	71.98	-162.08	33	-1.3	-1.6	2.5	31.9	BSW	P	4.4
2017	HLY1702	H17W4	72.21	-164.16	41	-1.5	-1.7	3.2	32.6	ACW	P	4.7
2018	HLY1801	H18D3-2	68.25	-167.13	44	-1.8	-2.1	4.8	31.7	ACW	P	3.7
2018	HLY1801	H18D3-3	68.19	-167.30	47	-1.5	-1.8	4.5	31.8	ACW	P	3.6
2018	HLY1801	H18D3-4	68.14	-167.49	48	-1.7	-2.0	4.9	31.9	ACW	P	4.7
2018	HLY1801	H18D4-5N	71.61	-161.62	47	-1.1	-1.4	-1.6	32.7	RWW	P	4.6
2018	HLY1801	H18D5-10	71.63	-157.90	64	-1.4	-1.7	-1.6	32.7	RWW	P	4.5
2018	HLY1801	H18D5-10	71.63	-157.90	64	-1.4	-1.7	-1.6	32.7	RWW	P	4.7
2018	HLY1801	H18D5-10	71.63	-157.90	64	-1.4	-1.7	-1.6	32.7	RWW	P	5.0
2018	HLY1801	H18IC11	71.83	-165.97	45	-1.5	-1.8	-0.4	32.3	RWW	P	4.2
2018	HLY1801	H18IC11	71.83	-165.97	45	-1.5	-1.8	-0.4	32.3	RWW	P	4.4
2018	HLY1801	H18IC10	71.71	-165.60	43	-1.6	-1.8	-0.6	32.2	RWW	P	4.3
2018	HLY1801	H18IC10	71.71	-165.60	43	-1.6	-1.8	-0.6	32.2	RWW	P	4.1
2018	HLY1801	H18IC9	71.71	-165.60	43	-1.4	-1.6	-1.0	32.0	RWW	P	4.7
2018	HLY1801	H18IC9	71.71	-165.60	43	-1.4	-1.6	-1.0	32.0	RWW	P	3.9
2018	HLY1801	H18IC9	71.71	-165.60	43	-1.4	-1.6	-1.0	32.0	RWW	P	4.3
2018	HLY1801	H18IC8	71.45	-164.92	43	-1.4	-1.6	-1.0	32.0	RWW	P	4.5
2018	HLY1801	H18IC8	71.45	-164.92	43	-1.4	-1.6	-1.0	32.0	RWW	P	4.2
2018	HLY1801	H18IC8	71.45	-164.92	43	-1.4	-1.6	-1.0	32.0	RWW	P	4.4
2018	HLY1801	H18IC7	71.34	-164.61	45	-1.3	-1.6	-1.0	32.1	RWW	P	4.5
2018	HLY1801	H18IC7	71.34	-164.61	45	-1.3	-1.6	-1.0	32.1	RWW	P	4.4
2018	HLY1801	H18IC7	71.34	-164.61	45	-1.3	-1.6	-1.0	32.1	RWW	P	4.6
2018	HLY1801	H18LB7	69.68	-166.09	42	-1.7	-2.0	6.7	31.6	ACW	P	3.6
2018	HLY1801	H18LB7	69.68	-166.09	42	-1.7	-2.0	6.7	31.6	ACW	P	3.6
2018	HLY1801	H18LB7	69.68	-166.09	42	-1.7	-2.0	6.7	31.6	ACW	P	3.7
2018	HLY1801	H18LB7	69.68	-166.09	42	-1.7	-2.0	6.7	31.6	ACW	P	3.9
2018	SWL18	L18D3-1	68.30	-166.94	35	-2.4	-2.6	8.3	30.9	ACW	P	3.4
2018	SWL18	L18D3-1	68.30	-166.94	35	-2.4	-2.6	8.3	30.9	ACW	P	3.4
2018	SWL18	L18D3-5	68.01	-167.87	54	-1.3	-1.6	4.3	32.4	BSW	P	4.6
2018	SWL18	L18D3-5	68.01	-167.87	54	-1.3	-1.6	4.3	32.4	BSW	P	4.1
2013	HLY1301	H13H17	71.99	-163.38	41	-1.5	-1.7	-1.6	32.7	RWW	S	4.2
2013	HLY1301	H13H29	71.93	-158.33	60	-2.2	-2.5	-1.6	32.6	RWW	S	3.8
2017	HLY1702	H17D3-1	68.30	-166.91	33	-1.6	-1.9	5.7	32.1	ACW	S	4.1
2017	HLY1702	H17D3-1	68.30	-166.91	33	-1.6	-1.8	5.7	32.1	ACW	S	2.9
2017	HLY1702	H17D3-1	68.30	-166.91	33	-1.6	-1.8	5.7	32.1	ACW	S	3.1
2017	HLY1702	H17D3-2	68.24	-167.12	44	-1.4	-1.6	5.2	32.3	ACW	S	4.5
2017	HLY1702	H17D3-2	68.24	-167.12	44	-1.4	-1.6	5.2	32.3	ACW	S	3.9

2017	HLY1702	H17D3-2	68.24	-167.12	44	-1.4	-1.6	5.2	32.3	ACW	S	3.6
2017	HLY1702	H17D3-2	68.24	-167.12	44	-1.4	-1.6	5.2	32.3	ACW	S	3.8
2017	HLY1702	H17D3-4	68.13	-167.49	48	-0.6	-0.9	4.4	32.4	ACW	S	4.2
2017	HLY1702	H17D5-1	71.25	-157.16	46	-0.5	-0.7	0.0	34.4	RWW	S	3.7
2017	HLY1702	H17D5-1	71.25	-157.16	46	-0.5	-0.7	0.0	34.4	RWW	S	3.7
2017	HLY1702	H17D5-1	71.25	-157.16	46	-0.5	-0.7	0.0	34.4	RWW	S	3.8
2017	HLY1702	H17D5-1	71.25	-157.16	46	-0.5	-0.7	0.0	34.4	RWW	S	3.2
2017	HLY1702	H17D5-7	71.50	-157.68	87	-1.8	-2.0	1.0	32.3	BSW	S	4.5
2017	HLY1702	H17D5-7	71.50	-157.68	87	-1.8	-2.0	1.0	32.3	BSW	S	4.0
2017	HLY1702	H17D5-7	71.50	-157.68	87	-1.8	-2.0	1.0	32.3	BSW	S	3.9
2017	HLY1702	H17NW10	72.23	-162.30	37	-1.8	-2.1	0.9	31.9	BSW	S	3.9
2017	HLY1702	H17NW6	72.73	-162.98	58	-0.9	-1.2	1.5	32.7	BSW	S	4.2
2017	HLY1702	H17S6	70.96	-161.08	46	-1.7	-2.0	2.7	32.1	BSW	S	4.0
2017	HLY1702	H17SE1	71.33	-159.40	55	-2.0	-2.3	0.9	31.8	BSW	S	4.1
2017	HLY1702	H17W2	72.12	-163.24	41	-1.5	-1.7	0.9	32.4	BSW	S	4.3
2018	HLY1801	H18D2-2	64.68	-169.10	47	-1.0	-1.3	3.7	32.9	BSW	S	4.2
2018	HLY1801	H18D2-2	64.68	-169.10	47	-1.0	-1.3	3.7	32.9	BSW	S	4.2
2018	HLY1801	H18D2-2	64.68	-169.10	47	-1.0	-1.3	3.7	32.9	BSW	S	3.8
2018	HLY1801	H18D2-2	64.68	-169.10	47	-1.0	-1.3	3.7	32.9	BSW	S	4.0
2018	HLY1801	H18D2-2	64.68	-169.10	47	-1.0	-1.3	3.7	32.9	BSW	S	3.8
2018	HLY1801	H18D2-2	64.68	-169.10	47	-1.0	-1.3	3.7	32.9	BSW	S	3.8
2018	HLY1801	H18D2-2	64.68	-169.10	47	-1.0	-1.3	3.7	32.9	BSW	S	3.8
2018	HLY1801	H18D2-2	64.68	-169.10	47	-1.0	-1.3	3.7	32.9	BSW	S	4.1
2018	HLY1801	H18D2-2	64.68	-169.10	47	-1.0	-1.3	3.7	32.9	BSW	S	4.1
2018	HLY1801	H18D2-2	64.68	-169.10	47	-1.0	-1.3	3.7	32.9	BSW	S	4.1
2018	HLY1801	H18D2-2	64.68	-169.10	47	-1.0	-1.3	3.7	32.9	BSW	S	4.1
2018	HLY1801	H18D2-2	64.68	-169.10	47	-1.0	-1.3	3.7	32.9	BSW	S	3.8
2018	HLY1801	H18D2-2	64.68	-169.10	47	-1.0	-1.3	3.7	32.9	BSW	S	4.5
2018	HLY1801	H18D2-2	64.68	-169.10	47	-1.0	-1.3	3.7	32.9	BSW	S	4.4
2018	HLY1801	H18D2-3	64.67	-168.23	39	-1.4	-1.7	6.4	32.4	BSW	S	4.1
2018	HLY1801	H18D2-3	64.67	-168.23	39	-1.4	-1.7	6.4	32.4	BSW	S	4.1
2018	HLY1801	H18D2-3	64.67	-168.23	39	-1.4	-1.7	6.4	32.4	BSW	S	4.4
2018	HLY1801	H18D2-4	64.96	-169.90	44	-1.0	-1.3	3.1	32.9	BSW	S	4.1
2018	HLY1801	H18D2-4	64.96	-169.90	44	-1.0	-1.3	3.1	32.9	BSW	S	3.9
2018	HLY1801	H18D2-4	64.96	-169.90	44	-1.0	-1.3	3.1	32.9	BSW	S	4.5
2018	HLY1801	H18D2-4	64.96	-169.90	44	-1.0	-1.3	3.1	32.9	BSW	S	4.2
2018	HLY1801	H18D3-1	68.30	-166.93	35	-2.5	-2.8	8.4	30.7	ACW	S	3.5
2018	HLY1801	H18D3-1	68.30	-166.93	35	-2.5	-2.8	8.4	30.7	ACW	S	3.0
2018	HLY1801	H18D3-1	68.30	-166.93	35	-2.5	-2.8	8.4	30.7	ACW	S	3.0
2018	HLY1801	H18D3-1	68.30	-166.93	35	-2.5	-2.8	8.4	30.7	ACW	S	3.3
2018	HLY1801	H18D3-2	68.25	-167.13	44	-1.8	-2.1	4.8	31.7	ACW	S	4.2
2018	HLY1801	H18D3-2	68.25	-167.13	44	-1.8	-2.1	4.8	31.7	ACW	S	3.0
2018	HLY1801	H18D3-2	68.25	-167.13	44	-1.8	-2.1	4.8	31.7	ACW	S	3.2
2018	HLY1801	H18D3-3	68.19	-167.30	47	-1.5	-1.8	4.5	31.8	ACW	S	4.2
2018	HLY1801	H18D3-3	68.19	-167.30	47	-1.5	-1.8	4.5	31.8	ACW	S	3.6

2018	HLY1801	H18D3-4	68.14	-167.49	48	-1.7	-2.0	4.9	31.9	ACW	S	3.9
2018	HLY1801	H18D3-4	68.14	-167.49	48	-1.7	-2.0	4.9	31.9	ACW	S	3.8
2018	HLY1801	H18D3-4	68.14	-167.49	48	-1.7	-2.0	4.9	31.9	ACW	S	3.8
2018	HLY1801	H18D3-4	68.14	-167.49	48	-1.7	-2.0	4.9	31.9	ACW	S	4.5
2018	HLY1801	H18D3-4	68.14	-167.49	48	-1.7	-2.0	4.9	31.9	ACW	S	4.4
2018	HLY1801	H18D4-1N	71.09	-161.19	48	-1.6	-1.9	-1.6	32.7	RWW	S	3.8
2018	HLY1801	H18D4-1N	71.09	-161.19	48	-1.6	-1.9	-1.6	32.7	RWW	S	3.7
2018	HLY1801	H18D4-5N	71.61	-161.62	47	-1.1	-1.4	-1.6	32.7	RWW	S	4.1
2018	HLY1801	H18D5-1	71.25	-157.14	45	-2.1	-2.4	4.6	31.1	ACW	S	4.0
2018	HLY1801	H18D5-1	71.25	-157.14	45	-2.1	-2.4	4.6	31.1	ACW	S	3.6
2018	HLY1801	H18D5-1	71.25	-157.14	45	-2.1	-2.4	4.6	31.1	ACW	S	3.7
2018	HLY1801	H18D5-1	71.25	-157.14	45	-2.1	-2.4	4.6	31.1	ACW	S	3.9
2018	HLY1801	H18D5-1	71.25	-157.14	45	-2.1	-2.4	4.6	31.1	ACW	S	4.7
2018	HLY1801	H18D5-1	71.25	-157.14	45	-2.1	-2.4	4.6	31.1	ACW	S	3.8
2018	HLY1801	H18D5-10	71.63	-157.90	64	-1.4	-1.7	-1.6	32.7	RWW	S	4.1
2018	HLY1801	H18D5-2	71.29	-157.22	56	-1.9	-2.1	1.8	31.7	BSW	S	3.8
2018	HLY1801	H18D5-2	71.29	-157.22	56	-1.9	-2.1	1.8	31.7	BSW	S	3.2
2018	HLY1801	H18D5-2	71.29	-157.22	56	-1.9	-2.1	1.8	31.7	BSW	S	3.9
2018	HLY1801	H18D5-2	71.29	-157.22	56	-1.9	-2.1	1.8	31.7	BSW	S	4.9
2018	HLY1801	H18D5-2	71.29	-157.22	56	-1.9	-2.1	1.8	31.7	BSW	S	3.7
2018	HLY1801	H18D5-2	71.29	-157.22	56	-1.9	-2.1	1.8	31.7	BSW	S	4.0
2018	HLY1801	H18D5-7	71.50	-157.63	96	-1.4	-1.7	-1.3	32.7	RWW	S	4.0
2018	HLY1801	H18IC2	70.72	-162.86	43	-1.4	-1.6	1.4	32.2	BSW	S	3.9
2018	HLY1801	H18IC2	70.72	-162.86	43	-1.4	-1.6	1.4	32.2	BSW	S	3.5
2018	HLY1801	H18IC2	70.72	-162.86	43	-1.4	-1.6	1.4	32.2	BSW	S	4.0
2018	HLY1801	H18IC2	70.72	-162.86	43	-1.4	-1.6	1.4	32.2	BSW	S	4.0
2018	HLY1801	H18IC9	71.71	-165.60	43	-1.4	-1.6	-1.0	32.0	RWW	S	4.2
2018	HLY1801	H18IC9	71.71	-165.60	43	-1.4	-1.6	-1.0	32.0	RWW	S	3.9
2018	HLY1801	H18IC8	71.45	-164.92	43	-1.4	-1.6	-1.0	32.0	RWW	S	4.1
2018	HLY1801	H18IC8	71.45	-164.92	43	-1.4	-1.6	-1.0	32.0	RWW	S	3.8
2018	HLY1801	H18IC7	71.34	-164.61	45	-1.3	-1.6	-1.0	32.1	RWW	S	4.2
2018	HLY1801	H18IC6	71.20	-164.20	45	-1.6	-1.8	-0.8	32.0	RWW	S	4.2
2018	HLY1801	H18IC6	71.20	-164.20	45	-1.6	-1.8	-0.8	32.0	RWW	S	3.8
2018	HLY1801	H18IC6	71.20	-164.20	45	-1.6	-1.8	-0.8	32.0	RWW	S	3.7
2018	HLY1801	H18IC5	71.09	-163.80	44	-1.7	-1.9	-0.2	32.1	RWW	S	3.9
2018	HLY1801	H18IC4	70.97	-163.56	46	-1.7	-2.0	-0.4	32.1	RWW	S	3.9
2018	HLY1801	H18IC4	70.97	-163.56	46	-1.7	-2.0	-0.4	32.1	RWW	S	3.8
2018	HLY1801	H18LB11	70.06	-167.66	50	-1.1	-1.3	2.5	32.2	BSW	S	3.9
2018	HLY1801	H18LB13	70.26	-168.54	43	-1.6	-1.8	2.4	31.9	BSW	S	4.2
2018	HLY1801	H18LB9	69.88	-166.82	47	-1.6	-1.9	4.8	31.9	ACW	S	3.8
2018	HLY1801	H18LB9	69.88	-166.82	47	-1.6	-1.9	4.8	31.9	ACW	S	3.9
2018	HLY1801	H18LB9	69.88	-166.82	47	-1.6	-1.9	4.8	31.9	ACW	S	3.2
2018	HLY1801	H18T1	66.42	-168.68	57	-1.4	-1.7	5.3	32.6	BSW	S	4.3
2001	SWL01	L01D2-4	64.99	-169.14	46	-0.7	-0.9	-0.2	32.6	AW/BSW	S	4.7

2014	SWL14	L14D3-1	68.30	-166.94	35	-2.7	-2.9	5.5	30.9	ACW	S	3.5
2014	SWL14	L14D3-2	68.24	-167.12	43	-1.7	-2.0	5.7	31.2	ACW	S	3.9
2014	SWL14	L14D3-4	68.13	-167.50	50	-1.0	-1.3	3.3	31.6	ACW	S	4.0
2015	SWL15	L15D3-1	68.30	-166.94	35	-2.1	-2.4	6.0	31.0	ACW	S	3.6
2015	SWL15	L15D3-2	68.24	-167.12	43	-1.8	-2.1	5.1	31.5	ACW	S	4.2
2015	SWL15	L15D3-4	68.13	-167.50	50	-1.6	-1.9	3.6	31.9	ACW	S	3.8
2015	SWL15	L15D4-2	71.10	-162.27	46	-1.8	-2.1	-1.6	32.7	RWW	S	4.1
2015	SWL15	L15D5-2	71.29	-157.25	57	-2.2	-2.5	-1.3	32.2	RWW	S	3.9
2016	SWL16	L16D2-1	64.67	-169.92	48	-0.9	-1.2	0.6	32.5	AW/BSW	S	4.5
2016	SWL16	L16D2-4	64.96	-169.89	49	-0.9	-1.1	1.1	32.7	AW/BSW	S	4.7
2016	SWL16	L16D2-5	64.99	-169.14	49	-0.9	-1.2	0.0	32.2	BSW	S	4.2
2016	SWL16	L16D3-1	68.30	-166.94	35	-1.9	-2.2	5.5	31.0	ACW	S	3.2
2016	SWL16	L16D3-3	68.19	-167.31	49	-1.3	-1.6	5.7	31.8	ACW	S	3.6
2016	SWL16	L16D3-4	68.13	-167.49	50	-1.1	-1.3	4.8	31.9	ACW	S	4.0
2016	SWL16	L16D4-2	71.10	-162.26	49	-1.1	-1.4	-1.6	32.2	RWW	S	4.1
2018	SWL18	L18D2-1	64.67	-169.93	48	-1.0	-1.3	3.1	32.9	BSW	S	4.4
2018	SWL18	L18D2-1	64.67	-169.93	48	-1.0	-1.3	3.1	32.9	BSW	S	4.0
2018	SWL18	L18D2-2	64.68	-169.10	45	-1.1	-1.4	3.9	32.7	BSW	S	4.2
2018	SWL18	L18D2-3	64.67	-168.24	38	-1.5	-1.8	3.9	32.0	BSW	S	4.0
2018	SWL18	L18D2-7	65.00	-168.22	46	-1.4	-1.7	3.7	32.2	BSW	S	3.3
2018	SWL18	L18D3-1	68.30	-166.94	35	-2.4	-2.6	8.3	30.9	ACW	S	3.1
2018	SWL18	L18D3-1	68.30	-166.94	35	-2.4	-2.6	8.3	30.9	ACW	S	3.1
2018	SWL18	L18D3-2	68.24	-167.12	44	-2.0	-2.2	5.1	31.5	ACW	S	2.9
2018	SWL18	L18D3-2	68.24	-167.12	44	-2.0	-2.2	5.1	31.5	ACW	S	3.4
2018	SWL18	L18D3-3	68.19	-167.31	48	-1.9	-2.2	4.4	31.7	ACW	S	3.9
2018	SWL18	L18D3-3	68.19	-167.31	48	-1.9	-2.2	4.4	31.7	ACW	S	3.9
2018	SWL18	L18D3-4	68.13	-167.49	49	-1.5	-1.8	4.1	31.8	ACW	S	3.4
2018	SWL18	L18D3-4	68.13	-167.49	49	-1.5	-1.8	4.1	31.8	ACW	S	3.4
	Juveniles											
2018	HLY1801	H18D2-2j	64.68	-169.10	47	-1.0	-1.3	3.7	32.9		S	3.8
2018	HLY1801	H18D2-2j	64.68	-169.10	47	-1.0	-1.3	3.7	32.9		S	3.7
2018	HLY1801	H18D2-2j	64.68	-169.10	47	-1.0	-1.3	3.7	32.9		S	3.6
2018	HLY1801	H18D2-2j	64.68	-169.10	47	-1.0	-1.3	3.7	32.9		S	3.2
2018	HLY1801	H18D2-2j	64.68	-169.10	47	-1.0	-1.3	3.7	32.9		S	3.7
2018	HLY1801	H18D2-2j	64.68	-169.10	47	-1.0	-1.3	3.7	32.9		S	3.7
2017	HLY1702	H17D3-4j	68.13	-167.49	48	-0.6	-0.9	4.4	32.4		S	4.5
2018	HLY1801	H18IC6j	71.20	-164.20	45	-1.6	-1.8	-0.8	32.0		S	4.2
2018	HLY1801	H18IC6j	71.20	-164.20	45	-1.6	-1.8	-0.8	32.0		S	3.9
2018	HLY1801	H18IC2j	71.70	-165.60	43	-1.6	-1.8	1.4	32.2		S	3.9
2013	HLY1301	H13H29j	71.93	-158.33	60	-2.2	-2.5	-1.6	32.6		S	3.8
2013	HLY1301	H13H17j	71.99	-163.38	41	-1.5	-1.7	-1.6	32.7		S	4.1
2013	HLY1301	H13H27j	72.86	-161.22	55	-1.6	-1.9	-1.7	32.8		S	3.8
2013	HLY1301	H13CBL11	72.10	-165.46	46	-1.6	-1.9	-1.6	32.7		P	4.4
2013	HLY1301	H13H108j	71.61	-159.38	49	-2.0	-2.3	-1.7	33.1		P	4.1

2013	HLY1301	H13H29j	71.93	-158.33	60	-2.2	-2.5	-1.6	32.6		P	4.6
2013	HLY1301	H13H29j	71.93	-158.33	60	-2.2	-2.5	-1.6	32.6		P	4.7
2017	HLY1702	H17D3-4j	68.13	-167.49	48	-0.6	-0.9	4.4	32.4		N	3.5
2018	HLY1801	H18D3-1j	68.30	-166.93	35	-2.5	-2.8	8.4	30.7		N	2.3
2018	HLY1801	H18D3-1j	68.30	-166.93	35	-2.5	-2.8	8.4	30.7		N	1.2
2018	HLY1801	H18IC9j	71.71	-165.60	43	-1.4	-1.6	-1.0	32.0		P	4.1
2018	HLY1801	H18IC8j	71.45	-164.92	43	-1.4	-1.6	-1.0	32.0		P	4.5
2018	HLY1801	H18IC6j	71.20	-164.20	45	-1.6	-1.8	-0.8	32.0		HF	3.8
2018	HLY1801	H18LB7j	69.68	-166.09	42	-1.7	-2.0	6.7	31.6		P	3.5
2018	HLY1801	H18LB7j	69.68	-166.09	42	-1.7	-2.0	6.7	31.6		P	3.4
2018	HLY1801	H18LB7j	69.68	-166.09	42	-1.7	-2.0	6.7	31.6		P	3.5
2001	SWL01	L01UTN3j	67.33	-169.00	47	-0.7	-1.0	1.8	32.7		N	3.5

Table 3.3 Average bottom seawater $\delta^{18}\text{O}$ values at sampling stations during years 2014-2018 and standard deviation of those values. Shaded rows list average seawater $\delta^{18}\text{O}$ value and standard deviation for the DBO transect indicated. Note "*" represents station sites where only three years of data within the 2014-2018 period were available.

Station	Avg $\delta^{18}\text{O}\text{‰}$ VSMOW	stdev $\delta^{18}\text{O}\text{‰}$
DBO2-1	-1.0	0.15
DBO2-2	-1.1	0.15
* DBO2-3	-1.4	0.09
DBO2-4	-1.0	0.12
DBO2-5	-1.2	0.25
DBO2 line	-1.1	0.15
DBO3-1	-2.2	0.41
DBO3-2	-1.7	0.22
DBO3-3	-1.5	0.24
DBO3-4	-1.3	0.44
DBO3-5	-1.2	0.21
DBO3-6	-1.0	0.30
DBO3-7	-1.1	0.37
DBO3-8	-1.1	0.27
DBO3 line	-1.4	0.31
DBO4-1	-1.7	0.51
DBO4-2	-1.5	0.34
DBO4-3	-1.5	0.34
DBO4-4	-1.4	0.74
DBO4-5	-1.5	0.33
DBO4-6	-1.4	0.18
DBO4 line	-1.5	0.41
* DBO5-1	-2.1	0.96
* DBO5-2	-2.0	0.77
DBO5-3	-1.4	0.54
DBO5-4	-1.5	0.50
DBO5-5	-1.5	0.52
* DBO5-6	-1.7	0.48
* DBO5-7	-2.0	0.73
* DBO5-8	-1.9	0.37
* DBO5-9	-1.9	0.51
* DBO5-10	-2.1	0.84
DBO5 line	-1.8	0.62

Table 3.4 Average $\delta^{18}\text{O}$ and average expected $\delta^{18}\text{O}$ values of equilibrium calcite for adult ostracode taxa from surface samples in this study (shaded blue) and other studies (not shaded) and their respective vital offsets determined by the equations cited in Methods section 3.3.4. Other studies include: [1] Ingram, 1998; [2] Simstich et al., 2004; [3] Didié and Bauch, 2002.

Taxon	Avg. adult ostracode $\delta^{18}\text{O}\text{‰}$ VPDB and stdev (This study)	n=	Comparable studies avg. ostracode $\delta^{18}\text{O}\text{‰}$ VPDB and stdev [Source other studies]	Avg. expected adult $\delta^{18}\text{O}\text{‰}$ VPDB and stdev. (This study and [other study])	Avg. adult vital offset ‰ and stdev (This study)	Comparable studies' avg. vital offset ‰ and stdev [Source other studies]
<i>N. leioderma</i>	2.62 (± 1.10)	75		1.52 (± 1.15)	1.1 (± 0.57)	
<i>P. punctillata</i>	4.35 (± 0.42)	45	4.95 (± 0.41)[2]	2.08 (± 0.95)	2.3 (± 0.71)	1.5 (± 0.29)[2]
<i>S. bradii</i>	3.89 (± 0.41)	123		1.71 (± 1.01)	2.2 (± 0.92)	
<i>S. bradii</i> and <i>S. punctillata</i>			2.18 to 3.35 [1]			
<i>S. punctillata</i>			4.83 (± 0.27)[2]			1.0 (± 0.26)[2]
<i>H. sorbyana</i>	3.25 (± 0.46)	12	4.65 (± 0.26)[2]	0.83 (± 1.56)	2.4 (± 1.26)	1.0 (± 0.24)[2]
<i>H. fascis</i>	3.73 (± 0.30)	16		2.77 (± 0.28)	1.0 (± 0.34)	
combined <i>H. fascis</i> and <i>H. sorbyana</i>	3.52 (± 0.44)	28		1.91 (± 1.43)	1.6 (± 1.14)	
<i>Krithe</i>			5.91 (± 0.15)[3]	4.57[3]		1.3 (± 0.26)[3]
<i>Henryhowella</i>			4.96 (± 0.05)[3]	4.57[3]		0.5 (± 0.04)[3]

Chapter 4: Multi-proxy record of ocean-climate variability during the last two millennia on the Mackenzie Shelf, Beaufort Sea

Submitted to Micropaleontology, February 2022

Laura Gemery, Thomas M. Cronin, Lee W. Cooper, Lucy R. Roberts, Lloyd W. Keigwin, Jason

A. Addison, Melanie J. Leng, Peigen Lin, Cédric Magen, Marci E. Marot, Valerie Schwartz

Contribution: lead responsibility for the study, including experimental design, sample selection and preparation, data analysis and interpretation, text and figures, writing of original draft.

Other contributions: J. Addison, M. Leng, C. Magen, M. Marot, L. Roberts, V. Schwartz for sample analysis and data generation; P. Lin for Figure 1 visualization; Text has been reviewed for quality assurance and/or edited by all co-authors.

4.1 Abstract

A 2,000 year-long oceanographic history, in sub-centennial resolution, from a Canadian Beaufort Sea continental shelf site (60-meters water depth) near the Mackenzie River outlet is reconstructed from ostracode and foraminifera faunal assemblages, shell stable isotopes ($\delta^{18}\text{O}$, $\delta^{13}\text{C}$) and sediment biogenic silica. The chronology of three sediment cores making up the composite section was established using ^{137}Cs and ^{210}Pb dating for the most recent 150 years and combined with linear interpolation of radiocarbon dates from bivalve shells and foraminifera tests. Continuous centimeter-sampling of the multicore and high-resolution sampling of a gravity and piston core yielded a time-averaged faunal record of every ~40 years from 0 to 1850 CE and every ~24 years from 1850 to 2013 CE. Proxy records were consistent with temperature oscillations and related changes in organic carbon cycling associated with the Medieval Climate Anomaly (MCA) and the Little Ice Age (LIA). Abundance changes in dominant microfossil species, such as the ostracode *Paracyprideis pseudopunctillata* and agglutinated foraminifers *Spiroplectammina biformis* and *S. earlandi*, are used as indicators of less saline, and possibly disturbed/turbid bottom conditions associated with the MCA (~800-1200 CE) and the most

recent ~60 years (1950-2013). During these periods, pronounced fluctuations in these species suggest that prolonged seasonal sea-ice melting, changes in riverine inputs and sediment dynamics affected the benthic environment. Taxa analyzed for stable oxygen isotope composition of carbonates show the lowest $\delta^{18}\text{O}$ values during intervals within the MCA and the highest during the late LIA, which is consistent with a 1° to 2°C cooling of bottom waters. Faunal and isotopic changes during the cooler LIA (1300-1850 CE) are most apparent at ~1500-1850 CE and are particularly pronounced during 1850 to ~1900 CE, with a ~0.5 per mil increase in $\delta^{18}\text{O}$ values of carbonates from median values in the analyzed taxa. This very cold 50-year period suggests that enhanced summer sea ice suppressed productivity, which is indicated by low sediment biogenic silica values and lower $\delta^{13}\text{C}$ values in analyzed species. From 1900 CE to present, declines in calcareous faunal assemblages and changes in dominant species (*Cassidulina reniforme* and *P. pseudopunctillata*) are associated with inhospitable bottom water conditions, such as turbidity or acidification, indicated by a peak in agglutinated foraminifera from 1950-1990 CE.

4.2 Introduction

The recent acceleration of Arctic Ocean warming (Timmermans et al., 2018), freshwater storage (Proshutinsky et al., 2019), river discharge (Rawlins et al., 2010; Rood et al., 2017) and declines in sea ice extent, concentration and duration (Frey et al., 2015; Wood et al., 2015; Comiso et al., 2017) provide motivation to better understand past natural climate variability in the Arctic. Proxy data from natural archives can provide a context for anthropogenically influenced climate change, and extend climate records back in time from the available instrumental observations (e.g. PAGES 2k Consortium, 2013). However, understanding the

Arctic's response to Holocene climate change is difficult due to limited records with high spatial and temporal resolutions.

In this study, we infer paleoenvironmental signals from multiple proxy records at a continental shelf site in the Canadian Beaufort Sea over the past 2 millennia. The data were obtained using a set of composite cores collected from a mean water depth of 60m – a jumbo piston core (JPC32), a gravity core (GGC30) and a multicore (MC29) – that were collected during a U.S. Coast Guard Cutter Healy 2013 (HLY1302) expedition (Fig. 4.1). We constrain the timing of Medieval Climate Anomaly (MCA) and Little Ice Age (LIA) climatic fluctuations in this region using biogenic silica (opal), microfossil faunal assemblages and stable oxygen and carbon isotope ratios from a dominant ostracode species, *Paracyprideis pseudopunctillata*, and a benthic foraminiferal species, *Cassidulina teretis* s.l.

Oxygen isotopes ($\delta^{18}\text{O}$) of ostracode and foraminifera shell calcite can provide insights into benthic environmental change, including recording temperature variability and possibly sea ice change (such as increased salinity due to brine rejection from ice formation) or river water mixing to the seafloor. Water masses, and thus $\delta^{18}\text{O}$ values, in this region are affected not only by Pacific Water advected from the Bering and Chukchi Sea shelves but by localized processes, such as upwelling/downwelling, vertical mixing, sea ice freeze-up and melt-back, and Mackenzie River discharge. Since cryophilic ostracodes calcify and molt their shells during warmer months to an adult stage in order to reproduce (Horne, 1983; Athersuch et al., 1989), the $\delta^{18}\text{O}$ values of ostracodes reflect a summer water mass (Gemery et al., 2021b). Carbon isotope variation (expressed as $\delta^{13}\text{C}$) reflects the composition of dissolved inorganic carbon (DIC) in seawater in which the shell calcified. In addition to specific bottom water microhabitats where the animal lives, $\delta^{13}\text{C}$ values may also be influenced by the organism's food sources and, like calcite $\delta^{18}\text{O}$,

species-specific vital effects from shell calcification processes (stemming from the incorporation of metabolic CO₂ into the shell; Xia et al., 1997a,b; von Grafenstein et al., 1999; Wefer and Berger 1991; Rohling and Cooke, 1999; Mackensen et al., 2000). Marine ostracodes are herbivores and detritivores (Smith & Horne, 2002), feeding on particulate organic matter that reaches the sea floor and/or microbial components (Elofson, 1941). $\delta^{13}\text{C}$ values at the sediment interface are affected by organic carbon flux rates to the sea floor (Buzas et al., 1993). Generally, higher productivity results in higher $\delta^{13}\text{C}$ values in the dissolved inorganic carbon that is incorporated into the shell. Lower (more negative) $\delta^{13}\text{C}$ values may indicate periods with less export of productivity to the seafloor and DIC from terrestrial carbon sources or microbial reworking. Reviews of stable oxygen and carbon isotopes in benthic ostracodes and foraminifera can be found in Holmes and Chivas (2002) and Ravelo and Hillaire-Marcel (2007).

4.2.1 Arctic climate variability during the last 2,000 years

Proxy records and models that examine the middle-late Holocene, north of 60°N, support a long cooling trend (i.e. the Neoglacial) beginning between 6 and 3 kyr ago, depending on the particular proxy examined, and extending until the late 20th century (Kaufman et al., 2009; Miller et al., 2010). The cooling during the late Holocene has been linked to the orbitally driven decrease in summer insolation, sulfates from volcanic eruptions, and the Maunder sunspot Minimum, 1650-1710 CE (Ammann et al., 2007). This declining temperature pattern is supported by a dataset of 59 Arctic/subarctic time-series multi-proxy records with annual-decadal resolution covering the last 2,000 years (PAGES 2k Consortium, 2013; McKay and Kaufman, 2014; <https://www.ncdc.noaa.gov/paleo-search/study/16973>). The increase in sea ice extent during the late Holocene appears to be circum-Arctic, although there are different regional

patterns of temperature and ice variability (e.g. de Vernal et al., 2005, 2013; Farmer et al., 2011; Bringué and Rochon, 2012; Stranne et al., 2014; Stein et al., 2017; Hörner et al., 2016).

Superimposed within the overall cooling trend are many multi-decadal to centennial-scale warmer or colder summer intervals that vary by region, as revealed in records from, for example, tree rings, Greenland ice cores, and lake sediments (Kaufman et al., 2009; PAGES 2k Consortium, 2013).

A period of milder climate identified in many records is the MCA, from ~800-1200 CE (e.g. Broecker, 2001; Bradley et al., 2003b), but it is not synchronous in all regions (Bradley et al., 2003a&b; Kaufman et al., 2009; PAGES 2k Consortium, 2013). Proxy data are insufficient to determine if this was an Arctic-wide or wholly northern hemisphere event (Kaufman et al., 2009). Neoglacial summer cooling reached a maximum during the LIA (~1300–1850 CE; Miller et al., 2010). In many areas of the Arctic, glaciers and ice caps began to re-advance ~1300 CE (Anderson et al., 2008), with the coldest period between ~1550-1900 CE (Bradley et al., 2003a), ± 50 years (Kaufman et al., 2009). Despite decreasing summer insolation through the 20th century, instrumental and proxy data show a “hockey-stick” shaped increase in temperature attributed to greenhouse gas emissions during the late 20th to early 21st centuries (Mann et al., 2008; Miller et al., 2010; IPCC, 2021). This warming is globally ubiquitous and amplified in the Arctic (e.g. McKay and Kaufman, 2014; PAGES 2k Consortium, 2013 and references therein).

4.2.2 Environmental significance of microfossil species

Micropaleontological studies of benthic ostracodes and foraminifera have demonstrated that faunal biofacies record regional-scale and short-term ecosystem changes linked to sea-ice cover, surface productivity, and bottom temperature (e.g. Scott et al., 2009; Cronin et al., 2010;

Poirier et al., 2012; Polyak et al., 2013; Gemery et al., 2017, 2021a). These benthic faunal records are interpreted by comparison with modern species distributions and their affinities. This comparison allowed us to consider environmental changes in temperature, salinity, productivity, sea ice, sediment substrate, the strength of Pacific water inflows and river inputs, and storm events as possible conditions that can alter species abundance and distribution. Many of these factors also affect stable isotope ratios.

All taxa discussed here are typical representatives of Arctic-subarctic shallow-water continental shelf fauna (Cronin et al., 2021). Specifically, in order to identify changes in water mass characteristics of Arctic-Pacific water vs. Atlantic water vs. freshened water from river inputs, we relied on published preferences concerning a taxon's ecological/environment habitats, which are commonly associated with temperature and salinity. For purposes of this study, we distinguish three water mass categories and the foraminifera and ostracode taxa used as indicators of each water mass:

- 1.) Indicators of Atlantic water are species commonly found in relatively warm water ($>0^{\circ}\text{C}$) and high salinities (33-35), with wider depth tolerances (shelf and slope waters). Species indicating Atlantic water suggest considerably less influence of river inputs and sea ice melt. These species are: *Cassidulina teretis* s.l., *Cassidulina reniforme*, and *Semicytherura complanata* (see Note on *C. teretis* s.l. taxonomy, below).
- 2.) Indicators of Arctic shelf water are versatile species more adapted to cold ($\leq 0-3^{\circ}\text{C}$) water and typically shelf salinity of 31-33. These species include *Elphidium excavatum forma clavatum*, *Sarsicytheridea bradleyi*, and *Kotoracythere arctoborealis*. The ecological affinities of *C. reniforme* also align with this group when it appears in an assemblage with *E. excavatum forma clavatum* (Hald et al., 1994).

3.) Low-salinity tolerant species are adapted to environments with high variability, with seasonal fluxes of salinity, food supply and temperature. Indicators of cold Arctic waters ($\leq 1^{\circ}\text{C}$) influenced by river inputs at polar surface water depths are *Paracyprideis pseudopunctillata* and two agglutinated species *Spiroplectammina biformis* and *S. earlandi*.

A more detailed ecological overview of the foraminifera and ostracode species in each water mass group is provided below, with dominant ostracode species summarized in Table 4.1.

4.2.2.1 Atlantic water species

Foraminifera *C. teretis* s.l. and *C. reniforme* inhabit Arctic continental shelves, however they occur together more commonly in slope sediments of intermediate depths (400-1500 m), which suggests Atlantic-modified water (0 to 3°C) and uniformly high salinity (34-35; Ishman and Foley, 1996; Schröder-Adams et al., 1990; Scott et al., 2008). The use of these species as indicators of the presence of Atlantic water with warm and saline attributes is well established in many studies using high latitude foraminifera (e.g., Ishman and Foley, 1996; Seidenkrantz 1995; Mackensen and Hald, 1988; Polyak et al., 2002; Jennings et al., 2011; Perner et al., 2011, 2013; Cage et al., 2021). *C. reniforme* is a key taxon used in reconstructing seasonal sea-ice coverage because it is common on Arctic shelves and in glacially influenced fjord environments (Polyak et al. 2002; Jennings et al., 2011). This species seems to prefer cold-water areas (temperatures below ca. 2°C), and is not found in salinities ≤ 30 (Polyak et al., 2002).

The ostracode species *S. complanata* inhabits areas with frigid temperatures ($\leq 0-3^{\circ}\text{C}$) and normal marine salinity, but is found in greater abundance in higher salinity (>33) waters (Gemery et al., 2021a) and areas with winter polynyas (Stepanova et al., 2003). It has wide depth tolerances, as it is found in Arctic Intermediate Water, 220-1000 meters deep, in the Greenland,

Norwegian and Kara Seas (Cronin et al., 1994). This species shows no discernable sediment preference (Gemery et al., 2021a). As an infaunal species, it appears to tolerate bottom waters with faster moving currents, as its abundance increases in coarse sediments directly north of the Bering Strait and in Icy Cape region, northeast Chukchi Sea (Gemery et al., 2021a).

4.2.2.2 Eurytopic Arctic shelf species

Like *C. reniforme*, *E. excavatum forma clavatum* is a common and widespread foraminifera on shallow Arctic continental shelves. Noted for its habitat versatility, *E. clavatum* is considered an opportunistic taxon (Hald et al., 1994) typical in muddy sediments (Polyak et al., 2002).

S. bradii is a eurytopic ostracode species with broad temperature and salinity tolerances, taking advantage of highly dynamic environments (Gemery et al., 2021a). Hazel (1970) categorized *S. bradii* as living in frigid to mild-temperate climatic zones, with a temperature range of <0-18°C in depths of 3-750 m. This species is a generalist, as it lives in shallow and deep open sea locations in both coarsely and finely grained sediments, with higher frequency in sandy sediments and most typically in neritic, but fully marine environments (Stepanova et al., 2007; Gemery et al., 2021a).

Ostracode species *K. arctoborealis* has been observed in highest abundances in Chaunskaya Bay (Eastern Siberian Sea), a fairly protected and shallow bay, with a maximum depth of 31m its greatest depth (Cronin et al., 2021). This area is covered with ice most of the year and bottom waters are subject to brine rejection but also freshwater inputs from rivers in summer. Here *K. arctoborealis* was collected in salinities of 19 to 25 (Cronin et al., 2021). In addition, it is found in lower abundances (2-16% of total species assemblage) in normal marine

shelf salinity (31-33) and very cold waters ($\leq 0-3^{\circ}\text{C}$) of the Bering, Chukchi, and Eastern Siberian Seas (Cronin et al., 2021). It typically occurs in assemblages that include *S. bradii*, at depths of 40-100 m (Gemery et al., 2021a). *K. arctoborealis* is not present on the Eurasian shelves (Kara, Laptev and Barents Seas). It is not found in Norton Sound of the Bering Sea, which is seasonally some of the warmest and freshest coastal waters in the Bering Sea.

4.2.2.3 Low-salinity tolerant species

Explicit bottom water changes are signaled by changes in the abundance of several agglutinated foraminifera, *S. biformis* and *S. earlandi*. Agglutinated taxa are considered to have low trophic requirements that can withstand low food supplies (Alve, 2010; Jennings et al., 2001; Jernas et al., 2018). *S. biformis* and *S. earlandi* are found in low-salinity/estuarine and very cold bottom waters that persist year-round, often in shallow (50-200 m) glaciomarine environments (Scott et al., 2008; Perner et al., 2013; 2015) or semi-enclosed bays where turbidity and/or anaerobic and/or acidic conditions are inferred (Schröder-Adams et al., 1990; Hayward et al., 2007). They are indicators of Arctic Surface Water and glacial meltwater in Arctic fjords (Jennings and Helgadottir, 1994). Increased abundance of agglutinated foraminifera may be a response to conditions that hinder carbonate preservation (Schröder-Adams et al., 1990), since these protists do not have a calcareous shell but instead create a shell by assembling particles from the sediment. In a culture experiment that tested several agglutinated foraminifera species' tolerance and responses when exposed to different dysoxia or acidified conditions, *S. biformis* had the highest survivorship and chamber addition rates in high CO_2 and low oxygen conditions (van Dijk et al., 2017).

P. pseudopunctillata is a cryophilic ostracode that inhabits shallow (<50 mwd), nearshore environments, often near river mouths such as in Norton Sound (northern Bering Sea), and offshore areas characterized by cold bottom water temperatures, such as the Hanna Shoal region of the northern Chukchi Sea (Cronin et al., 2021; Gemery et al., 2021a). It is particularly tolerant of seasonally fluctuating salinities (Stepanova et al., 2007; Gemery et al., 2015; Gemery et al., 2021a) to as low as 5–10 (Neale and Howe, 1975; Cronin, 1977). It is associated with sea ice, sustained frigid temperatures ($\leq 0^{\circ}\text{C}$), and sediments with relatively high total organic carbon (TOC)/phytodetritus (Gemery et al., 2021a). While the distribution of some ostracode species is not restricted by bottom surface sediment types, this species is positively correlated to very fine-grained sediment textures (Gemery et al., 2021a), which is useful for inferring sediment grain size changes as current flows shift. *P. pseudopunctillata* is found in high proportions in modern shallow (<20 m) surface sediments of the E. Siberian, Kara and Laptev Seas (Stepanova, 2006; Stepanova et al., 2007).

4.2.3 Note on *Cassidulina teretis* taxonomy

Cassidulina teretis Tappan was first described from the northern Alaskan Coastal Plain, and it has consistently been used as an indicator of Atlantic Water in mid-depths of the Arctic Ocean. As detailed in Cronin et al. (2019), there are varying views on the taxonomy of *C. teretis* from the Nordic Seas and eastern Arctic Ocean due to interpretations of an evolutionary transition from *Cassidulina teretis* Tappan (Tappan, 1951) to *Cassidulina neoteretis* Seidenkrantz (Seidenkrantz, 1995) during the Pleistocene. Based on morphological re-examination studies of Lazar et al. (2016) and Cronin et al (2019), a *C. teretis/C. neoteretis* transition was time-transgressive and these foraminifers may be ecophenotypes rather than different species. As

noted by Scott et al (2008), within a population group, high variability exists in the aperture of this species (See plate 6 in Scott et al., 2008). Due to unresolved questions about *C. teretis* populations from the Arctic Ocean representing a single species (Cage et al., 2021), we use the name *Cassidulina teretis* s.l. where “s.l.” refers to sensu lato, or “in the wide sense.”

4.3 Regional setting

4.3.1 Mackenzie Shelf hydrography

The Mackenzie Shelf, a broad rectangular-shaped platform in the southeastern Beaufort Sea (Fig. 4.1; width ~120 km; length ~530 km), is one of most estuarine of all the panarctic shelves (Macdonald et al. 1989). The Mackenzie River is the fourth largest of the Arctic rivers, discharging ~280 km³ (±25) annually (Melling, 2000) to the Mackenzie Shelf, mostly between May and September (Macdonald et al. 1998). During summer, this equates to a 3.7- to 10-meter-thick freshwater surface layer across the shelf (Macdonald et al. 1998; Carmack et al., 1989; Jackson et al., 2015) that is separated from the underlying cold saline water by a seasonal (summer) halocline (average salinity 20; Carmack et al., 1989).

Beaufort Sea shelf waters are mainly derived from relatively nutrient-rich Pacific Ocean waters advected from the Bering Strait and Chukchi Sea. Flowing northeastward closest to shore (~50-m isobath) is the Alaska Coastal Current (ACC) that mainly transports warm ($T > 3^{\circ}\text{C}$), low-salinity ($S = 30-32$) and nutrient-poor Alaskan Coastal Water in summer (Fig. 4.1; Weingartner et al., 2005; Nikolopoulos et al., 2009). Most of the Pacific-origin waters (including warm and fresh Pacific Summer Water and cold and salty Pacific Winter Water) from the other pathways in Chukchi Sea eventually rejoin to the ACC before draining off the shelf via Barrow Canyon (Lin

et al., 2016, 2019b). The Barrow Canyon outflow then forms the Beaufort Shelfbreak Jet to the east. The Beaufort Shelfbreak Jet is surface-intensified in summer with significant seasonal variation (Nikolopoulos et al., 2009). It progresses eastward to the Canadian Beaufort Sea through the Mackenzie Canyon (Lin et al., 2020, 2021). Besides the Shelfbreak jet, the primary circulation on the Mackenzie Shelf, the Shelf Current, is predominantly wind-driven (Kulikov et al., 1998; Lin et al., 2020), and the anticyclonic Beaufort Gyre is dominant further offshore in the Canada Basin. Driven by wind, upwelling and downwelling commonly occur in both the Alaskan and Canadian Beaufort Sea, and play an important role in shelf-basin interactions (e.g., Foukal et al., 2019; Lin et al., 2019a; 2021). Upwelling commonly brings up warm and salty Atlantic water (T -1°C to 3°C and S 34-35) that generally resides at depth (below 150m on the slope and even deeper in the basin, Nikolopoulos et al., 2009), while downwelling can transport waters in the lower shelf layer into the basin (Lin et al., 2021). Mackenzie Shelf waters are modified by multiple factors, including vertical mixing, winds, ice and river runoff (Fig. 4.1; Macdonald et al., 1987; Williams et al., 2008). Hence, water mass analyses on the Mackenzie Shelf are not necessarily straightforward (Carmack et al., 1989; Macdonald et al., 1989).

Sea surface temperature varies during summer (1°C to 10°C), but below $\sim 40\text{m}$, water temperatures remain ~ -1 to -2°C year-round (Macdonald et al., 1987) and salinities are between 30.4 and 34.4 (Carmack et al., 1989). These general patterns are also consistent with recent bottom salinity and temperature measurements from conductivity-temperature-depth (CTD) profiling system collections (Okkonen, 2013; as shown in Fig. 4.2a & b). During fall and winter (November-April), winds, cooling and freezing flush out low-salinity surface water and break down the shelf stratification so the water column is vertically well-mixed and uniform in temperature and salinity (Macdonald et al., 1987). Sea ice covers the Mackenzie Shelf from

September/October to May and can reach 2–3m thick (Melling and Riedel, 1996). In the vicinity of our core site in winter, mean salinity is 32.15 (± 0.05) and mean temperature is -1.76°C ($\pm 0.01^{\circ}\text{C}$; Jackson et al., 2015).

4.4 Materials and methods

4.4.1 Coring, sedimentology, sampling

The MC29, GGC30, JPC32 cores (69.97°N , -137.24°W , 60m) were collected during expedition HLY1302 in summer 2013 onboard USCGC *Healy*. The site, in which all cores were collected, was located in the moat of a diapiric-like feature caused by methane gas hydrate decomposition during a prior warming period, which enabled recent, well-laminated sedimentation to occur. Additional description of the site is available elsewhere (Seidenstein et al., 2018). Cores were sub-sampled in September of 2016, 2018 and again in May 2019, including a second multicore, at Woods Hole Oceanographic Institution (WHOI). The sediment was primarily dark gray clay-mud. Altogether, core samples were taken every centimeter from MC29A and MC29B, and at 2-cm intervals from GGC30 and every 6cm from JPC32. Samples of 1-cm-thick slices at 1-cm intervals were taken from MC29A and MC29B, 2-cm³ aliquots were taken every 2cm from GGC30 and 4-cm³ aliquots were taken every 6cm from JPC32. Subsamples representing every 1cm increment of MC29B and each 10-cm interval in GGC30 and JPC32 were used for biogenic silica analysis. In addition, subsamples of MC29B in 2-cm intervals from 1cm to 37cm were assayed for the radioisotopes ²¹⁰Pb and ¹³⁷Cs in order to assess sedimentation rates and chronology in combination with the ¹⁴C-dated intervals.

4.4.2 Microfossil sample processing and assemblage analysis

Sediments were washed through a 63-micron sieve and the residue oven-dried. Because the full round diameter of core MC29 was used, the average weight before processing was 30g and the dry weight (after processing) of these 1-cm samples averaged 0.07g. In GGC30 and JPC32, half of the core was sampled, and for each 2-cm interval, half of the half-round was taken. Sample weight before processing ranged from 30 to 44g and after processing averaged 0.03g. Ostracodes were picked from all sediments greater than 125-micron size fraction to a microslide, sorted and identified using the taxonomy of Stepanova (2006) and Gemery et al. (2015). In accordance with counting protocols (Seidenstein et al., 2018), up to 200 foraminiferal specimens were picked per sample. All ostracode specimens found in the samples were picked and counted. Sample binning was done by combining count data from adjacent samples into one grouped sample comprising a larger depth interval; for ostracodes, samples from core MC29 were binned every 5cm, from core GGC30 every 10cm and from core JPC32 every 20cm (Supplementary Table 4.2; ostracode counts are expressed as number of valves; articulated carapaces were counted as two valves). For foraminifera data, individual samples contained sufficient specimen numbers (~200, with a few exceptions in core JPC32) and binning was not necessary. To identify significant changes in the faunal assemblages, 95% confidence limits were calculated using the algorithm for binomial probability from Raup (1991).

4.4.3 Stable isotope analyses

Stable oxygen and carbon isotope ratios were determined for calcium carbonate tests of *C. teretis* s.l. (n= 61) and *P. pseudopunctillata* (n=50; Gemery, 2021). Data are reported in parts per thousand, or per mil (‰) deviations of the $^{18}\text{O}/^{16}\text{O}$ and $^{13}\text{C}/^{12}\text{C}$ ratios relative to the V-PDB

(Vienna Peedee Belemnite) standard using laboratory standards calibrated against NBS19 and NBS18 (National Institute of Science and Technology). The ratios between $^{18}\text{O}/^{16}\text{O}$ and $^{13}\text{C}/^{12}\text{C}$ are expressed as delta values ($\delta^{18}\text{O}$ and $\delta^{13}\text{C}$) as follows:

$$\delta^{18}\text{O} \text{ and } \delta^{13}\text{C} \text{ ‰} = [(R_{\text{sample}}/R_{\text{standard}})-1]*1000$$

where $R = ^{18}\text{O}/^{16}\text{O}$ for $\delta^{18}\text{O}$ values or $^{13}\text{C}/^{12}\text{C}$ for $\delta^{13}\text{C}$ in the sample vs. the standard (Craig, 1961; Coplen, 1994). Values presented are not corrected for species vital effects, and are used as a relative measure for changes in water mass characteristics and/or meltwater/river inputs to the area. Analyses of ostracode shell $\delta^{18}\text{O}$ and $\delta^{13}\text{C}$ values were conducted at the University of Maryland Center for Environmental Science in Solomons, Maryland, USA using a Thermo Fisher Scientific™ Delta V Plus stable isotope mass spectrometer coupled to a GasBench® peripheral preparation device. The precision of the measurements, based upon repeated measurements of carbonate standards, was determined to be $\sim \pm 0.1\text{‰}$ for $\delta^{18}\text{O}$ and $\sim \pm 0.06\text{‰}$ for $\delta^{13}\text{C}$. Each isotope measurement consisted of two adult valves from the same sample interval that were cleaned of debris with water to achieve a weight of 40-90 μg . Only adult ostracode specimens were used for geochemical analyses due to possible ontogenetic differences in shell chemistry during the life cycle. This also minimizes differences in shell weights due to varying shell size.

Foraminifera *C. teretis* s.l. $\delta^{18}\text{O}$ and $\delta^{13}\text{C}$ values were measured on an Elementar IsoPrime dual inlet mass spectrometer with a Multiprep peripheral at the National Environmental Isotope Facility at the British Geological Survey, Nottingham, UK. The precision of the data, based upon repeated measurements of the internal standard (Keyworth Carrara Marble calibrated against NBS), was determined to be $\sim \pm 0.04\text{‰}$ for $\delta^{18}\text{O}$ and $\sim \pm 0.03\text{‰}$ for $\delta^{13}\text{C}$. Each isotopic

measurement comprised between 4-20 tests from the same sample interval. Tests from each sample were cleaned of debris with water to achieve a weight of 30-120 μg .

The intervals from which shells were derived depended on the abundance and preservation of specimens available in the sample. Because post-mortem processes can alter the original shell chemistry, only shells that were translucent or translucent-white were selected with no signs of early diagenetic effects.

4.4.4 Biogenic silica (opal)

Subsamples of HLY1302-MC29, -GGC30, and -JPC32 (n=79; Gemery, 2021) were analyzed for biogenic silica (opal) at the USGS Biogenic Silica Lab in Menlo Park, CA, USA following the modified procedure of Mortlock and Froehlich (1989). This method is considered reliable for quantifying biogenic opal in opal-poor deposits. Briefly, samples were treated with 1N HCl overnight to remove carbonates and rinsed with distilled Nanopure water three times. Sediments were then freeze-dried, and 100 mg per sample was placed in a 0.1 M Na_2CO_3 solution at 85°C for four hours and cooled to room temperature overnight. 100 μL were reacted with a molybdate blue complex. Absorbances were measured at 812nm wavelength using a Thermo Scientific GeneSys 10S spectrophotometer. Biogenic silica measurements were converted to opal concentrations using a 2.4 multiplication factor assuming 10% hydration ($\text{SiO}_2 \cdot 0.4 \text{H}_2\text{O}$). To estimate error, we measured a subset of replicates; the average 1-sigma standard deviation for all replicates was 0.05 wt%. These assessments of precision and accuracy, in addition to comparisons of internal standards, suggest the estimate of error for the analysis is 0.06 wt%. Sample values are reported as a proportion of the sediment mass.

4.4.5 Chronology

Consecutive subsamples of MC29B in 2-cm intervals (0-38cm) were analyzed on a low energy, high-purity germanium well detector for activities of ^{210}Pb and ^{137}Cs (Gemery, 2021) at the St. Petersburg Coastal and Marine Science Center (SPCMSC), a United States Geological Survey lab in St. Petersburg, FL, USA. Each subsample (approximately 20-25g of wet sediment) was oven-dried at 60°C for 48 hours. The dried sediment was homogenized to a fine powder with a porcelain mortar and pestle. Dried ground sediments (6g) were sealed in polystyrene vials with epoxy to prevent gas emanation. The sample weight and counting container geometry were matched to a pre-determined calibration standard. The samples were sealed for a minimum of three weeks prior to analysis to allow ^{226}Ra to reach secular equilibrium with its daughter isotopes ^{214}Pb and ^{214}Bi . The sealed samples were then counted for 24–36 hours. Detector efficiency was determined with IAEA RGU-1 reference material. Radioactive activities were decay-corrected to the date of field collection.

^{210}Pb is a natural radioisotope derived from atmospheric deposition (a daughter product of the uranium-238 decay series) with a 22.3-year half-life. Based on this natural decay rate, ^{210}Pb should reach a baseline value at our core site at ~1880 CE, if sedimentation has not been disturbed. Cesium-137, a nuclear bomb fallout product with a 30.2-year half-life, is an independent tracer of sedimentation that can be used to validate ^{210}Pb chronologies. Given that the peak bomb fallout was in ~1963, this year should align with the peak in ^{137}Cs activity. The depth and activity of ^{137}Cs found in the sediments and the rate at which it decays can reflect specific years following the introduction of the nuclear fallout product in context of the sedimentation rate, or it can also provide evidence of bioturbation if the radionuclide is well-mixed. Because ^{137}Cs preferentially binds to clay mineral surfaces, its activity can also be

related to fine sediment content and total organic carbon (Avery, 1996; Cooper et al., 1998). Relevantly, these fine sediments are also present on the Mackenzie Shelf. The accumulation of both ^{210}Pb and ^{137}Cs is assumed to be constant from direct deposition but likely with some import from the watershed (Fig. 4.3).

Radiocarbon dates from molluscs and mixed benthic foraminifera were generated using the National Ocean Sciences Accelerator Mass Spectrometer (NOSAMS) facility at Wood Hole, MA, USA. Ages were calibrated to calendar years BP with the Marine20 radiocarbon age calibration curve (Heaton et al., 2020) using the Calib version 8.2 software (Stuiver et al., 2021; Fig. 4.4; Table 4.2). Because old Pacific waters are a component of the Beaufort Sea, we corrected for a regional reservoir age of 477 ± 60 years based on late Holocene sediments absolutely dated by 3.6 ka Aniakchak volcanic ash (Pearce et al., 2017). Radiocarbon ages are reported using the BP 1950-time ^{14}C scale, meaning years before 1950 are also converted to calendar years (CE). The age model for MC29 was fit linearly using the regression equation based on the most recent radiocarbon date at 30cm and back-dated under the assumption that the 0–1cm interval represents the year the core was collected (Fig. 4.4; calendar year 2013, -63 years BP). The activity levels of ^{137}Cs and ^{210}Pb in MC29 were used to corroborate the MC29 age model from the radiocarbon dates. By matching the foraminiferal faunal assemblages of GGC30 with MC29, it was determined by Seidenstein et al. (2018) that 20cm was missing from the top of GGC30. Likewise, we followed that study's determination that 301cm was missing from the top of JPC32 to align with the bottom of GGC30. Linear sedimentation rates were calculated by dividing the difference in depth by the difference in age between two samples. These rates do not

account for possible compaction of sediment with depth, elastic rebound of sediment cores with decreased pressure, or coring disturbance.

4.4.6 Statistical analyses

Multivariate statistical analyses were carried out using the Paleontological Statistics (PAST) software package, version 3.24 (Hammer et al., 2001). Principal component analyses (PCA) were used to determine how foraminifera and ostracode species assemblages in sample intervals group by similarities/differences in species composition (Fig. 4.5a&b).

4.5 Results

4.5.1 Correlation of radioisotopes and AMS ^{14}C dating

In MC29, a consistent logarithmic decline of ^{210}Pb shows that background activity (~ 3 dpm/g) was reached at the 23-cm core depth (Fig. 4.3a). Based on the 22.3-year half-life of ^{210}Pb , only background (“supported”) activities should be reached by the year 1880 CE. Per our age model, the 1880 CE date coincides with ~ 28 -cm depth. There are a few minor spikes of slightly higher activity sediment (~ 1 dpm/g) in the ^{210}Pb concentration after 23cm that may be a consequence of sediment transport.

The temporal change of ^{137}Cs radioactivity in MC29 shows the 1963 nuclear weapons testing maximum between 7-15cm, which is the depth of peak ^{137}Cs activity (Fig. 4.3b). Our age model aligns with the 1963 date at 11cm depth, which is the middle of the 7-15cm ^{137}Cs maximum. The first testing of nuclear weapons in 1954 aligns with 13cm, within the beginning range of peak ^{137}Cs activity. Overall, both curves support that sedimentation dominates over bioturbation at the core site (Fig. 4.3). Both curves corroborate the dates used in the MC29 section of the age model.

Seventeen radiocarbon dates show that before ~550cm composite depth, the sediments of JPC32 are disturbed (Table 4.2; Fig. 4.4a). A regression model with an $r^2 = 0.97$ is used to linearly tie the 10 most recent dates of the undisturbed sequence (Fig. 4.4b). Therefore, the record we present begins at 0 CE (2ka BP), or 490cm composite depth, and ends in the year 2013 at the top of MC29. We have confidence that the sedimentation was relatively undisturbed through this period based on sequential radiocarbon dates and ^{137}Cs and ^{210}Pb activity. Sedimentation rates ranged from 22cm (in MC29) to 24cm/century (in GGC30 and JPC32).

The age uncertainty associated with the radiocarbon dates precludes the study of decadal-scale variability, but the faunal and isotopic fluctuations enable the evaluation of sub-centennial environmental changes and comparison with modern conditions.

4.5.2 Ostracode and foraminifera faunal assemblages

A total of 11 benthic ostracode species were identified (Gemery, 2021), and are listed in order of percent abundance within the 2 kyr record (n=4356 specimens in 52 binned samples; Fig. 4.6): *Paracyprideis pseudopunctillata* (55%), *Semicytherura complanata* (12%), *Kotoracythere arctoborealis* (8%), *Cytheropteron elaei* (5%), *Acanthocythereis dunelmensis* (4%), *Cytheropteron montrosiense* (3%), *Sarsicytheridea bradii* (3%), *Cluthia cluthae* (3%), *Rabilimis mirabilis* (2%), *Palmenella limicola* (2%), *Roundstonia globulifera* (1%). These species make up 98% of the assemblage composition during the 2 kyr record. The number of specimens per binned sample ranged from 18 to 274, with an average of 84 specimens (± 50) per grouped sample. Two of the binned samples contained less than 25 ostracode specimens (Fig. 4.6). Of the benthic foraminiferal fauna, 90% of the assemblage during the last 2 kyr was comprised by varying proportions of calcareous species *Cassidulina reniforme* (32%), *Elphidium*

excavatum forma clavatum (19%), *Cassidulina teretis* s.l. (11%), *Stanforthia feylingi* (7%), *Buccella frigida* (3%), *Stanforthia loeblichii* (3%), *Elphidium incertum* (2%), and agglutinated species *Spiroplectammina biformis* (12%), and *Spiroplectammina earlandi* ([1%]; n=24,767 total specimens in 121 binned samples; selected species, Fig. 4.7).

The last 2,000 years were subdivided into four major time periods based on climate oscillations identified by other published proxy compilations (e.g. Kaufman et al., 2009; PAGES 2k Arctic, 2013; McKay and Kaufman, 2014) and fluctuations of dominant foraminifera and ostracode species abundance and isotope values (Fig. 4.8). The lowermost zone 1, from 300-490cm, covers 0-800 CE. Zone 2, 190-300cm, covers the MCA (800-1200 CE). Zone 3, 35-170cm, covers the LIA (1300-1850 CE). The uppermost Zone 4, 0-35cm covers 1850 to 2013 CE. PCA analyses (Fig. 4.5 a&b) show ostracode and, to a lesser degree, foraminifera species assemblage composition aligns with these periods, which are described below.

4.5.2.1 Zone 1 (0-800 years CE)

This period is characterized by the ostracode *P. pseudopunctillata* dominating >60-90% of the assemblages. *Kotoracythere arctoborealis* is a consistent species in the assemblage, and its abundances fluctuate from 0-12% in samples. *Sarsicytheridea bradii* and *S. complanata* are present in only some samples at very low percentages (<5%). Of the foraminifera, *C. reniforme* averages 43%, *E. clavatum* averages 24% (with a standard deviation of $\pm 8\%$, not shown, please refer to Seidenstein et al., 2018) and *C. teretis* s.l. averages 16% (standard deviation of $\pm 9\%$, Fig. 4.8c) during this period. There is an interval of very low microfossil abundance from 330-350cm (~640-670 CE) with 18 ostracode specimens denoted by a yellow highlight (Fig. 4.8a) and 24-49 foraminifera specimens (2 samples). While it appears that several faunas rapidly changed in

relative abundance within this interval, this should be considered an artifact due to low microfossil abundance.

4.5.2.2 Zone 2 (MCA, 800-1200 CE)

A notable change in the record during the MCA is signaled by distinct increases in the agglutinated species *S. biformis* to between 20% to 42% of the overall assemblage in 12 sample intervals within the depth range of 175-300cm, and this results in a decrease in *C. reniforme* to a proportion of between 5-25%. A near absence of *S. biformis* coincides with a short-term maxima of *C. teretis* at ~260-cm depth (~900 CE). *Paracyprideis pseudopunctillata* remains the dominant ostracode species (50-80% of assemblages), with some variable increases of *S. bradii* (5-15%) and the consistent presence of *K. arctoborealis* at low proportions.

4.5.2.3 Zone 3 (LIA, 1300-1850 CE)

The beginning of the LIA at ~1300 CE is marked by a precipitous decline in *P. pseudopunctillata* to between 6-30% of the assemblage. *Semicytherura complanata* reaches its highest abundances (44%) of the record during 1400 to ~1600 CE and *C. reniforme* declines from 45% to <20%. *Cassidulina teretis* increases modestly from ~4% to 26% with some variability, as does *K. arctoborealis*, which reaches 20% of the assemblage population at ~1600 CE. After 1600 CE, both *P. pseudopunctillata* and *C. reniforme* increase and remain the dominant species to 1850 CE.

4.5.2.4 Zone 4 (1850-2013 CE)

The most recent part of the record was sampled at consecutive one-centimeter resolution for benthic microfossils and represents a time-averaged faunal record of every 23 years from

1850 to 2013 CE. From 1850 to 1900 CE, dominant fauna *P. pseudopunctillata* and *C. reniforme* decline in a somewhat stair-stepped manner from abundance highs of 60% to an average of 35% and 30% by the 1950s. While these species decline (after ~1950), agglutinated foraminifera *S. biformis* and *S. earlandi* sharply increase to abundances of 30-62% and 4-14%, respectively, and reach peak abundances ~1970 to 1990 (5-10cm depth). Among the ostracode fauna, *P. pseudopunctillata* represents 19% of the assemblage ~1980 and 32% ~2000, with other taxa in the *Cytheropteron* spp. group (including *C. elaei*, *C. inflatum*, *C. paralatissimum*) representing up to 38% of the assemblage. *Kotoracythere arctoborealis* maintains an average population of 13% during the entire zone and 18% in the uppermost interval. The most recent 20 years of the record shows the agglutinated species declining with a wider diversity of foraminifera representing the assemblage, notably, *C. reniforme* (12%) and *E. clavatum* (9%) co-dominate with *S. biformis* (17%). Other foraminifera that have significant increases in abundance since ~2000 CE include *Elphidium incertum* (12%) and *Elphidium bartletti* (8%), both of which prefer riverine-influenced habitats with sandy, shallow seafloor areas off estuaries (Polyak et al., 2002).

4.5.3 Biogenic silica (opal)

Biogenic silica is used as an indicator of marine primary production in the surface water from primarily diatoms, which are the dominant photosynthesizing marine organisms (Okazaki et al., 2005; Addison et al., 2013). The biogenic silica rain rate and subsequent burial in the sediments may suggest increased/decreased primary productivity resulting from a reduced/enhanced sea ice cover. Low percentages of biogenic silica content are generally found in glacial periods with more stable sea ice cover (Stein and Fahl, 2000) and when there was no transport of Pacific surface waters through the Bering Strait. At our core site, biogenic silica concentration (n=79) averaged 1.2% \pm 0.23, with maxima (outside of the standard deviation

ranges) corresponding to a few intervals in Zone 1 between 100 and 400 CE and in Zone 4 from 1925-2013 (Fig. 4.9a). Minima corresponded to intervals within Zone 2 during the MCA from 800-1150 CE, Zone 3 during the early LIA, and Zone 4 from 1850 to 1900.

4.5.4 Ostracode and foraminifera $\delta^{18}\text{O}$ and $\delta^{13}\text{C}$

The $\delta^{18}\text{O}$ values of cryophilic ostracodes reflect summer water masses, since it is during the warmer months that ostracodes calcify their shells to an adult stage in order to reproduce (Horne, 1983). More variability in temperature and salinity would be expected in summer than winter due to warmer temperatures, Mackenzie river discharge, and sea ice melt.

The $\delta^{18}\text{O}$ of *P. pseudopunctillata* (n=50) varied from +3.0 to +4.5‰, with an average value of +3.8‰ (± 0.31), and a core-top value of +4.2‰ (Table 4.3; Fig. 4.9b). Ten replicate ostracode samples were measured from different sample intervals, and the average standard deviation of the $\delta^{18}\text{O}$ intra-sample measurements was 0.1‰ and for $\delta^{13}\text{C}$, 0.4‰. Comparing $\delta^{18}\text{O}$ of this species in the Beaufort Sea to values from modern specimens in the northern Bering and Chukchi Sea shelves (at 75–80°N), we find average values to be lower in the Beaufort Sea by 0.6‰ (+4.4‰ [± 0.4] per Gemery et al., 2021b). This suggests that $\delta^{18}\text{O}$ of bottom water on the Canadian Beaufort shelf may be lower overall due to some Mackenzie River water mixing to the 60 m seafloor. It is likely not due to temperature differences because values would be higher, and bottom temperatures have remained cold ($<0^\circ\text{C}$). The $\delta^{18}\text{O}$ of *C. teretis* s.l. (n=61) varied from +1.9 to +2.9‰, with an average value of +2.3‰ (± 0.18), and a core-top value of +2.6‰ (Table 4.3; Fig. 4.9b).

The mean $\delta^{18}\text{O}$ values of both species from the MCA to post-LIA reveal a trend toward higher isotope values that, assuming temperature is the primary control, correspond to a 1-2°C

decrease in bottom water temperature. The $\delta^{18}\text{O}$ values of *P. pseudopunctillata* ranged from +3.0‰ to +4.1‰ during the MCA and from 3.7‰ to 4.5‰ during the LIA. The $\delta^{18}\text{O}$ value for *C. teretis* s.l. varied from +2.0‰ to +2.3‰ during the MCA and from +2.3‰ to +2.6‰ during 1800-1900. Likewise, for the two species, mean $\delta^{18}\text{O}$ values during the last ~100 years (1900-2013) is higher than average values over the past 2 kyr (Table 4.3; Fig. 4.9b).

The $\delta^{13}\text{C}$ values of *P. pseudopunctillata* fluctuated from -2.6 to -0.7‰, with an average value of -1.7‰ (± 0.48), and a core-top value of -2.4‰ (Table 4.3; Fig. 4.9b). The $\delta^{13}\text{C}$ values of *C. teretis* s.l. varied from -2.0 to -0.6‰, with an average value of -1.2‰ (± 0.32), and a core-top value of -0.8‰ (Table 4.3; Fig. 4.9b). A comparison of $\delta^{13}\text{C}$ values during the MCA and late- to post-LIA showed no significant change.

4.6 Discussion

The ostracode, foraminifera, stable isotope, and biogenic silica records together demonstrate that bottom water conditions varied considerably during the past 2 kyr. Alongside species' faunal changes (Fig 4.8) intervals with lower and higher $\delta^{18}\text{O}$ (Fig. 4.9b) and $\delta^{13}\text{C}$ carbonate values (Fig. 4.9c) can be used to identify periods of changing water masses. Here, we discuss how the fluctuations in proxy records (Figs. 4.8 and 4.9) may reflect the presence of specific water mass and paleoenvironmental conditions during and within the four chronological zones established above.

4.6.1 Cold Arctic bottom water during Zone 1 (0-800 years CE)

Dominant ostracode and foraminifera species support that cold, river-influenced Arctic shelf water was primarily present on the bottom during this period. This is evident by high abundances (>70%) of *P. pseudopunctillata* and a consistent presence (5-10%) of *K.*

arctoborealis and foraminifera (24%) *E. clavatum*. Likewise, the abundance of *C. reniforme* alternates from 30 to 70% of the assemblage. However, the varying presence of *C. teretis* s.l. (>10%) implies there are some sustained Atlantic water incursions onto the shelf (Jennings and Helgadottir, 1994), especially during 370-570 CE when *C. teretis* s.l. and *C. reniforme* (Hald et al., 1994) combined comprise upwards of 60% of the assemblage. Stable isotope measurements of both species are not highly resolved during this period but do not fluctuate much from average values. The interval of low microfossil abundance (~600 CE), which is not resolved in this record, could be attributed to several possible scenarios, such as transport or dilution of the fauna from a storm event, or dissolution from diagenetic processes.

4.6.2 Variable warming, fluctuating conditions with Atlantic water incursions during Zone 2 (MCA, 800-1200 CE)

High abundances (>60% assemblage average) of *P. pseudopunctillata* continue during the MCA in addition to low and steady percentages of *S. complanata* and *K. arctoborealis*. Abundance of thermally adaptable *S. bradii* increases (~15% of assemblage) at ~870-1000 CE and 1100-1200 CE. The ostracode PCA (Fig. 4.5a) identifies the MCA and the period before 800 CE as zones in which low-salinity tolerant *P. pseudopunctillata* is most dominant.

Atlantic water upwelling is evident from the fluctuating abundance of *C. teretis* s.l. The foraminifera PCA (Fig. 4.5b) shows most samples in the MCA include more *C. teretis* s.l. and agglutinated species than the typical polar shelf species *C. reniforme*. Intervals in the early, mid-, and late part of the MCA also see short but significant increases of agglutinated foraminifera *S. biformis* from near zero to 32-42% abundance. Generally, an increased frequency of agglutinated

taxa has been attributed to harsher or less stable environmental conditions, such as turbidity, irregular food or anoxia (Jennings and Helgadottir, 1994; Perner et al., 2013, 2015).

Measurements of biogenic silica during the early and late MCA are the lowest sustained percentages of the record, suggesting extended periods of somewhat depressed productivity.

There also is a strong negative excursion of binned $\delta^{13}\text{C}$ of *P. pseudopunctillata* and lower $\delta^{13}\text{C}$ values of *C. teretis* s.l. that corroborate reduced productivity.

Stable oxygen isotopes of *P. pseudopunctillata* are the lightest of the record ($\delta^{18}\text{O} = 3.0\text{-}3.3\text{‰}$) and suggestive of less saline or warmer bottom waters, yet the $\delta^{18}\text{O}$ values of *C. teretis* s.l. show only limited changes from average values. These patterns could result from the fact that ostracodes most commonly reach adulthood in summer (Horne, 1983), so the $\delta^{18}\text{O}$ of *P. pseudopunctillata* is reflective of summer bottom temperatures (Gemery et al, 2021b) whereas the foraminifera signal integrates more of the whole year. If the lower $\delta^{18}\text{O}$ oscillations reflect bottom water warming, this may have resulted from warmer summer fluctuations or possibly changes in the extent, strength or temperature of Atlantic Water affecting the core site. Further, we conclude that the lower $\delta^{18}\text{O}$ values reflect a temperature shift because freshwater changes due to variation in the Mackenzie River outflow are not thought to be significant during the MCA (Fig. 4.9d; Wickert, 2016). Overall, variable warming during this period is corroborated by a reduction in sulfate aerosols from explosive volcanism (Crowley, 2000; Goosse et al., 2005) and high levels of total solar irradiance (Bradley et al., 2003a&b; Beer, 2000). It may also be related to circulation anomalies in the northern hemisphere, possibly involving a shift in the mode of the North Atlantic or Arctic Oscillation (Bradley et al., 2003a &b).

4.6.3 Cooling and episodic sediment disturbance during Zone 3 (LIA, 1300-1850 CE)

After 1300 CE, the abundance of *P. pseudopunctillata* declines, and from 1400 to 1600 CE, *P. pseudopunctillata* reaches its lowest presence (10-30%) of the record, which is possibly due to a sediment grain size change. Furthermore, *Semicytherura complanata* and *K. arctoborealis*, which are found in coarser sediments (Gemery et al., 2021b), increase during this 300-year period, as well as low proportions (8-24%) of agglutinated foraminifera *S. biformis*. Sediments on the Beaufort Sea shelf are generally high in silt and clay, with minimal to no sand (Scott et al., 2008). The ecological tolerances of *P. pseudopunctillata* could accommodate slight changes in temperature or salinity that would be feasible during this period and would be unlikely to affect its abundance. Also, $\delta^{18}\text{O}$ values do not suggest higher salinity or extreme temperature change. We surmise that it was stronger bottom water currents that winnowed the very fine silts to create a coarse sediment bottom texture unfavorable to *P. pseudopunctillata* (Gemery et al., 2021b).

Atlantic water upwelling is evident from the abundance of *C. teretis* s.l. (4-26%) and *C. reniforme* (17-48%) during the early and mid-LIA. After 1600 CE, the rebound of *P. pseudopunctillata* to 45-65% abundance, the steady increase in *C. reniforme* to 46-52% and continuous presence of *E. clavatum* (ranging from 13 to 35%) and *S. biformis* (ranging from 1 to 17%) all support a scenario where bottom water was generally influenced by very cold-water masses as the LIA progressed. Cold water masses are indicated by the $\delta^{18}\text{O}$ values of *P. pseudopunctillata*, recording three high values $>4.0\text{‰}$ before 1750 CE. At 1750 CE, there is one $\delta^{18}\text{O}$ measurement of 3.3‰ , just below average values, but then values increase to above or within average standard deviation ranges. $\delta^{18}\text{O}$ values of *C. teretis* s.l. remain relatively constant

within one standard deviation of variation through the LIA. Our proxy results support a cooling trend from the MCA to LIA documented, which is demonstrated in the mean-annual temperature reconstructions from the GISP2 ice core (Alley et al., 1999) and terrestrial records of arctic summer temperatures (Kaufman et al., 2009). The mean $\delta^{18}\text{O}$ values of both species from the MCA to post-LIA shows a trend toward higher values that corresponds to a 1-2°C decrease in bottom water temperature. Productivity, as reflected in biogenic silica measurements, varied from 1300-1500 CE but thereafter remained high during most of the period until 1850 CE.

4.6.4 Continued near-freezing conditions and shifts in organic carbon and seafloor environment during Zone 4 (1850-2013 CE)

Changes in faunal abundance (Fig. 4.8), shell geochemistry, and biogenic silica (Fig. 4.9) during the most recent 150 years are substantial, and align more synchronously than do changes at any other time during the previous ~1850-year records.

At 1850 CE, the Mackenzie River mean outflow starts declining from a high point (11,693 m³/s), so that by 1950 CE, it reaches a low (7,204 m³/s, outside of standard deviation ranges; Fig. 4.9d; Wickert, 2016). In addition, around 1850, sharp declines in biogenic silica and the carbonate $\delta^{13}\text{C}$ values of both analyzed species, *P. pseudopunctillata* and *C. teretis* s.l., are evidence for reduced water column productivity. *C. reniforme* (71%) reached its highest abundance with *E. clavatum* (28%) and *P. pseudopunctillata* (~60%) both responding to cold shelf waters and detrital or terrestrial carbon food sources (lower carbonate $\delta^{13}\text{C}$ values). From 1850 to 1900 CE, the $\delta^{18}\text{O}$ of both *P. pseudopunctillata* and *C. teretis* s.l. increased by 0.5‰ above standard deviation ranges, which supports not only reduced freshwater mixing from lower Mackenzie River discharge but continued cooling of 1-2°C to ~1900 CE, the coldest interval of

the record. Cooling until 1900 CE agrees with the summer Arctic temperature reconstruction of Kaufman et al. (2009), which was particularly evident in records from ice and lakes in northern Canada and Greenland. Our record shows that this 50-year cooling coincides with a steep reduction in biogenic silica and expansion of inorganic carbon storage (lower or more negative $\delta^{13}\text{C}$ values), which may have been caused by an increase in sea ice cover that limited primary production. Enhanced sea ice during this period is supported by diatom and dinocyst assemblage evidence (de Vernal et al., 2013; Ledu et al., 2008; Bringué and Rochon, 2012; Pieńkowski et al., 2017).

From ~1900 to 2013 CE, ostracode and foraminiferal community composition, biogenic silica and stable isotope values all displayed large changes, suggesting an important shift in water mass conditions. The proportion of dominant species *P. pseudopunctillata* begins a gradual decline, which is accompanied by a rise in *K. arctoborealis* (11-18%), *A. dunelmensis* (7-13%) and *Cytheropteron* species. The ostracode PCA (Fig. 4.5a) particularly highlights this subtle increase of typical polar shelf water species *K. arctoborealis* and *A. dunelmensis* in the modern (post-1950 CE) samples, which is not otherwise clearly evident. Dominant foraminifera *C. reniforme* and *E. clavatum* follow the same declining pattern as *P. pseudopunctillata*. By 1950 CE, these species are largely replaced by agglutinated species *S. biformis* (42-62%), and *S. earlandi* (5-14%), which are associated with cold, low-salinity Arctic water and sometimes less hospitable (e.g. turbid, corrosive or low oxygen) environments (Schröder-Adams et al., 1990; Jennings and Helgadottir, 1994; Korsun and Hald, 2000; Perner et al., 2012, 2015). Productivity, inferred from biogenic silica values, rebounds from depressed values between 1850-1900 CE to high levels above average standard deviation values from 1920 to 2013 CE, which suggests diminished sea ice and prolonged summer open waters with sufficient nutrients in the upper

water column. This is supported by observations that the ice-free ocean area of the Beaufort Sea in summer has increased by 70% compared to the reference climatology (1981-2010; Wood et al., 2015). After 1900 CE, our record shows slightly higher than average $\delta^{18}\text{O}$ and $\delta^{13}\text{C}$ values in biogenic carbonates, suggesting that bottom waters remained cold with a high flux of organic matter to the seafloor due to more productive waters. High primary productivity could lead to high pCO_2 , and carbonate dissolution in the sediments from decay of organic matter. The drastic change of microfossil species composition, reflected in the PCAs (Fig 4.5a&b), and rise of agglutinated species from 1950 to 1990 is an unambiguous sign that bottom waters became less hospitable for calcareous species. This inhospitality could manifest as corrosive conditions or greater turbidity from upwelling and/or downwelling that resuspended sediments or terrestrial inputs from Mackenzie River discharge (Kipp et al., 2018). The Mackenzie river delivers large amounts (~125 Mt/yr) of sediment to the shelf (Macdonald et al. 1998). Freshwater discharge from the Mackenzie River has increased by 25% over the past several decades, and particulate (terrestrial suspended particles and organic carbon) export from the river into the Beaufort Sea has increased by 50% (Doxaran et al., 2015).

After 1990 CE, there are signs of some recovery of calcareous species. Foraminifera showing significant increases in abundance since ~2000 CE include *Elphidium incertum* (12%) and *Elphidium bartletti* (8%), both of which prefer riverine-influenced habitats with sandy, shallow seafloor areas downstream of estuaries (Polyak et al., 2002). A strong increase in arctic summer temperature during the last ~100 years is evident in terrestrial archives (Kaufman et al., 2009). This pattern could support an increase in primary productivity and/or a longer growing season (Arrigo et al., 2008) as well. Considered in sum, the proxy records imply a dramatic

change post-1900 CE in the benthic environment, which may include nutrient and carbon cycling over the Beaufort continental shelf influenced by the Mackenzie River discharge.

4.7 Conclusions and summary

This study improves our understanding of late Holocene oceanographic changes on the Mackenzie Shelf based on benthic foraminifera and benthic ostracode distributions, oxygen and carbon isotope values of their shells, radiocarbon and radiometric dating and biogenic silica measurements of the sediments. Our results revealed the following:

- PCAs distinguish microfossil assemblage groupings that reflect changes in the bottom water environment particularly during 1950-2013 CE, attributed to anthropogenic influences.
- Oxygen isotope shifts appear to be correlated to the LIA, MCA, and recent periods that indicate significant alterations in bottom water mass properties. Increases in $\delta^{18}\text{O}$ reflect a ~1-2 °C decrease in temperature from the MCA to the end of the LIA.
- Comparison of $\delta^{18}\text{O}$ of *P. pseudopunctillata* in this downcore study with calibrations from modern specimens in the Bering and Chukchi Seas (Gemery et al., 2021b) indicates that mixing of river water lowers the overall $\delta^{18}\text{O}$ of bottom water masses on the Mackenzie Shelf due to the proximity to the river estuary.
- From 0 to 800 CE, microfossil faunal assemblage composition, $\delta^{18}\text{O}$ and $\delta^{13}\text{C}$ records generally reflect cold conditions with multidecadal variability and some sustained Atlantic water incursions onto the shelf. Average to high biogenic silica measurements suggest productivity was fairly stable. An anomalous interval at ~600 CE of low microfossil abundance limits interpretation.

- From 800 to 1200 CE, microfossil $\delta^{18}\text{O}$ suggest summer warming oscillations and periods of low productivity (biogenic silica) during the MCA, and pronounced increases in agglutinated species *S. biformis* suggest some instability (i.e. episodic food and/or turbidity) affected the bottom environment.
- From 1300-1600 CE, the early LIA period is marked by previously dominant *P. pseudopunctillata* declining to its lowest abundance of the record (10-30%). This suggests a period of increased current flow that winnowed its preferred fine sediment substrate. Known to inhabit sandy sediments, *S. complanata* and *K. arctoborealis* increase during this interval.
- During the mid-to-late LIA (1600-1850 CE) the abundance of *P. pseudopunctillata* rebounds with the progression of more stable, cold conditions, as indicated by high biogenic silica values and generally high $\delta^{18}\text{O}$.
- From 1850 to 1900 CE, alignments of very high microfossil $\delta^{18}\text{O}$, very low biogenic silica and low $\delta^{13}\text{C}$ shell carbonate values indicate this was the coldest interval of the record, characterized by enhanced sea ice that depressed primary productivity. The continuation of cold temperatures from 1850 to 1900 CE is consistent with the summer temperature reconstruction of Kaufman et al. (2009).
- From 1900 to ~1990, productivity, as reflected by silica and $\delta^{13}\text{C}$, steeply rebounds and remains high. Dominant species *P. pseudopunctillata* and *C. reniforme* decline while agglutinated taxa *S. biformis* and *S. earlandi* increase from 1950 to ~1990 to form up to 66% of the assemblage. The near-replacement of calcareous by agglutinated taxa during 1950 to ~1990 CE reflects bottom conditions more conducive to the ecology of agglutinated taxa.

- After 1990 CE, biogenic silica concentrations and $\delta^{18}\text{O}$ values remain high, and there are signs of a slight recovery of calcareous foraminifera, which notably include species whose distribution reflects river inputs, *Elphidium incertum* and *Elphidium bartletti*.
- Changes within the last ~60 years in all investigated proxies suggest longer periods of open water, high productivity, greater freshwater inputs and/or turbidity along the Canadian Beaufort Sea shelf.

4.8 Data Availability

Data presented in this study are available via a U.S. Geological Survey data release, <https://doi.org/10.5066/P9SRRW6T> (Gemery, 2021).

4.9 Acknowledgements

We thank the science team, and officers and crews of USCGC Healy in 2013, Leg 2 for facilitating sediment core collections. We are grateful to Steven Watson and Nick Vaka for help with sample preparation. LG appreciates conversations with Patrick De Deckker that improved proxy interpretations. We also thank Miriam Jones and Harry Dowsett for their useful USGS internal reviews of this manuscript. Financial support for this research project was provided by the USGS Land Change Science Program / Florence Bascom Geoscience Center. USCGC Healy expedition 1302 was funded by NSF Grant ARC 1204045. LWC is supported through NSF Office of Polar Programs Arctic Observing Network program (1917434). PL is funded by NSF grant OPP-1733564. Any use of trade, firm, or product names is for descriptive purposes only and does not imply endorsement by the U.S. Government.

Figures Chapter 4

Figure 4.1 Schematic circulation of Chukchi and Beaufort Seas and geographic names. The HLY1302 MC29, GGC30 and JPC32 (69.97°N, 137.24°W) core site (magenta circle) on the Mackenzie shelf in 60 m water depth. The green arrows denote the main pathway of Pacific-origin water exiting Chukchi Sea shelf and contributing to the Chukchi Slope Current to the west and Beaufort Shelfbreak Jet to the east. The blue arrow represents the Shelf Current in the vicinity of Mackenzie Canyon. The Beaufort Gyre (yellow arrow) situates in the Canada Basin. The bathymetry (in meters) is from The International Bathymetric Chart of the Arctic Ocean (IBCAO) v3.

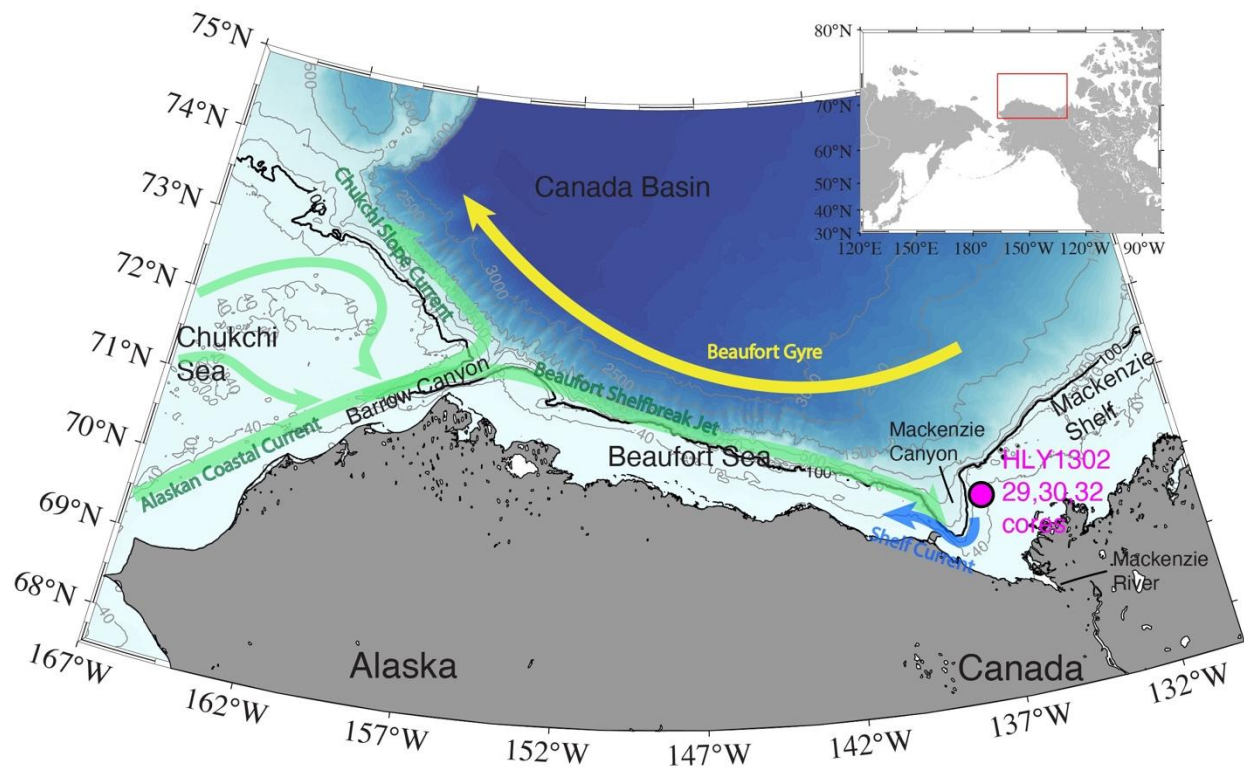


Figure 4.2 Near-bottom summer a.) salinity and b.) temperature measurements (n=238) from a subset of CTD collections during August and September, 1990-2012 (Okkonen, 2013), with the core site denoted by a white circle. Archived data sets from which the CTD summary data were derived are detailed in Grebmeier et al. (2015), Appendix G1. Figure created using Ocean Data View software (Schlitzer, 2018).

Near-bottom salinity and temperature measurements (n=238)
 subsorted from a CTD dataset collected during August and September, 1990-2012

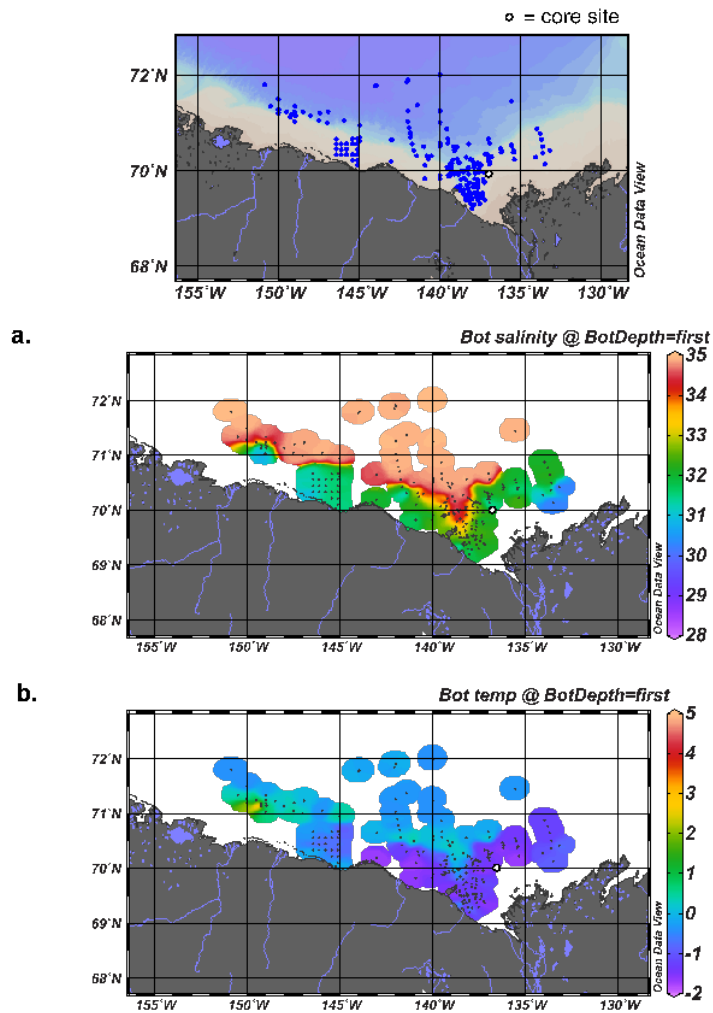


Figure 4.3 Correlation of multicore 29 (MC29B) chronology to activities of ^{210}Pb and ^{137}Cs in the top 37cm of sediment.

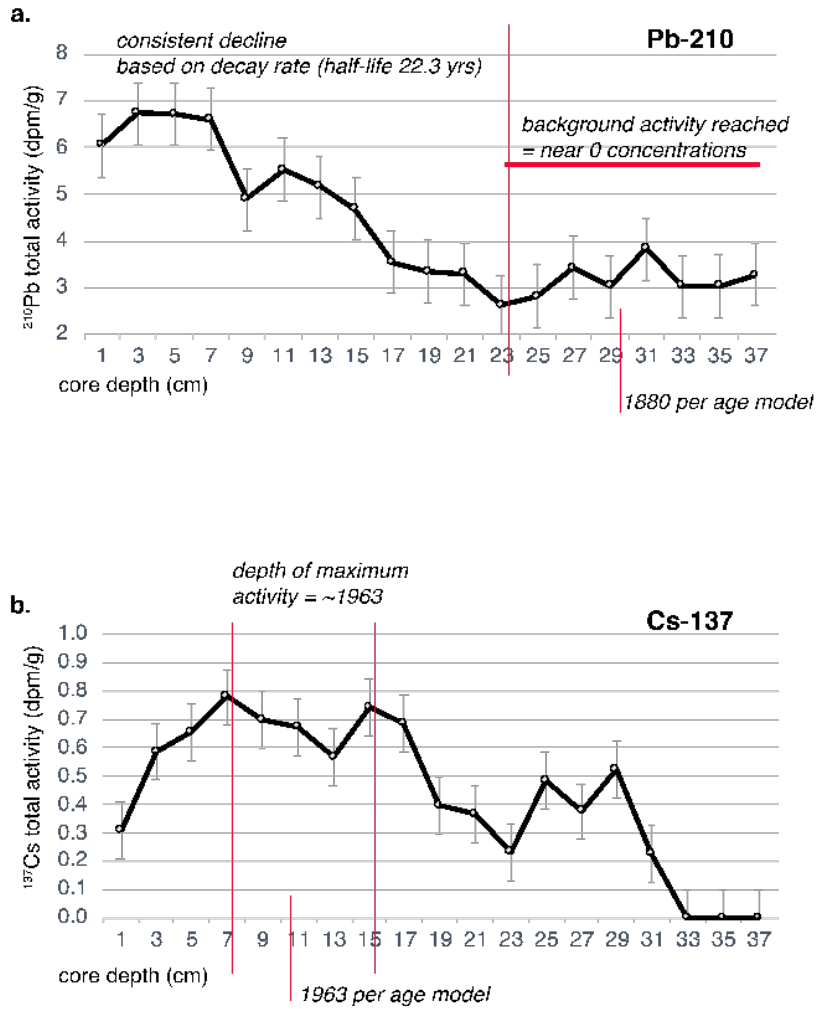


Figure 4.4a.) Age-depth model of HLY1302 composite cores, MC29, GGC30, JPC32. Seventeen median radiocarbon dates shown with 2-sigma error bars (~95% of the measurements fall within the bar range) in years before present (BP) and calendar years (in red parentheses). b.) the regression model $y = 4.0683(x) + 196.91$ used to linearly tie the 10 most recent dates of the undisturbed sequence.

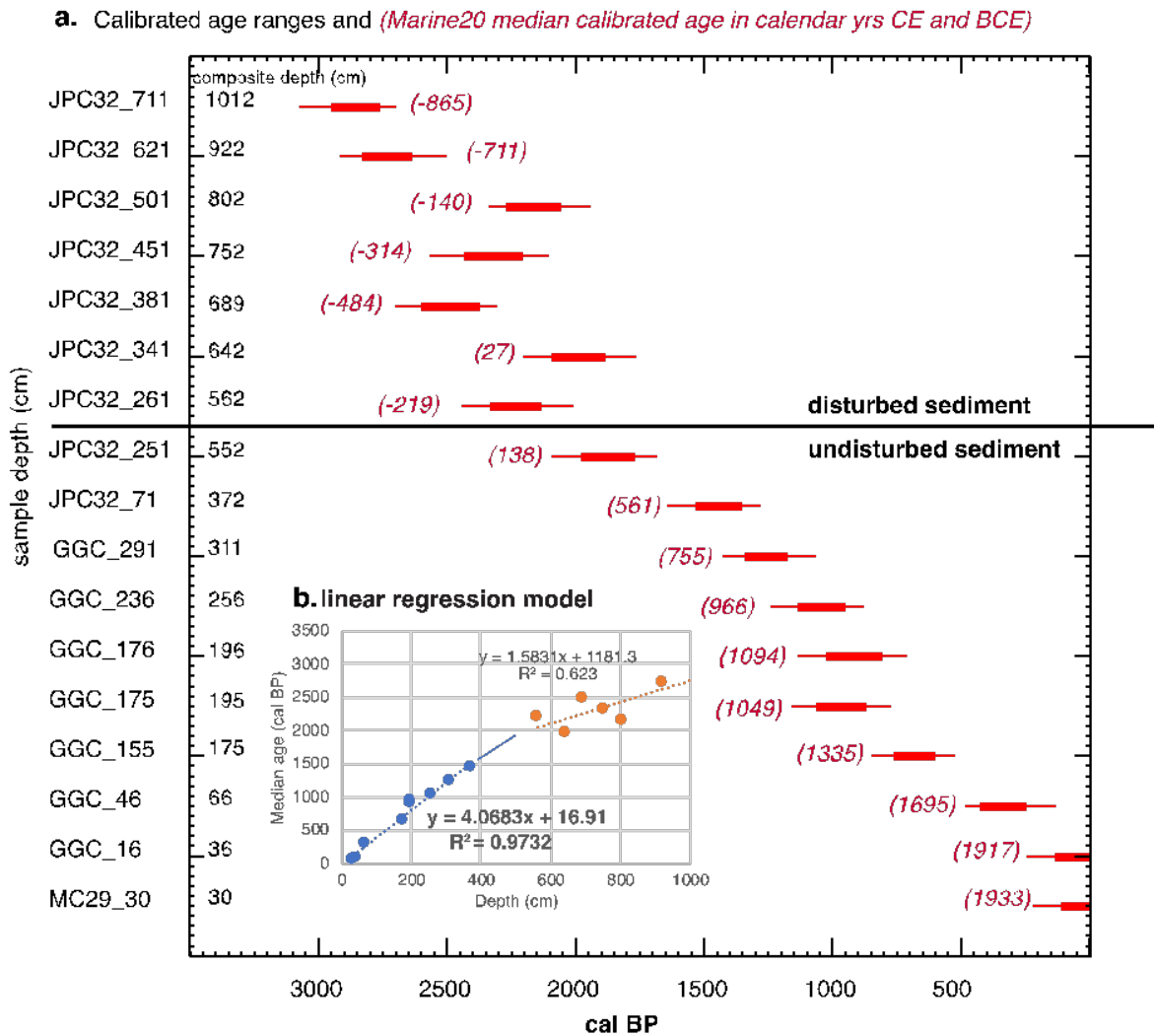


Figure 4.5a&b. Principal component analyses of (a.) ostracode assemblages and (b) foraminifera assemblages colored by major time periods.

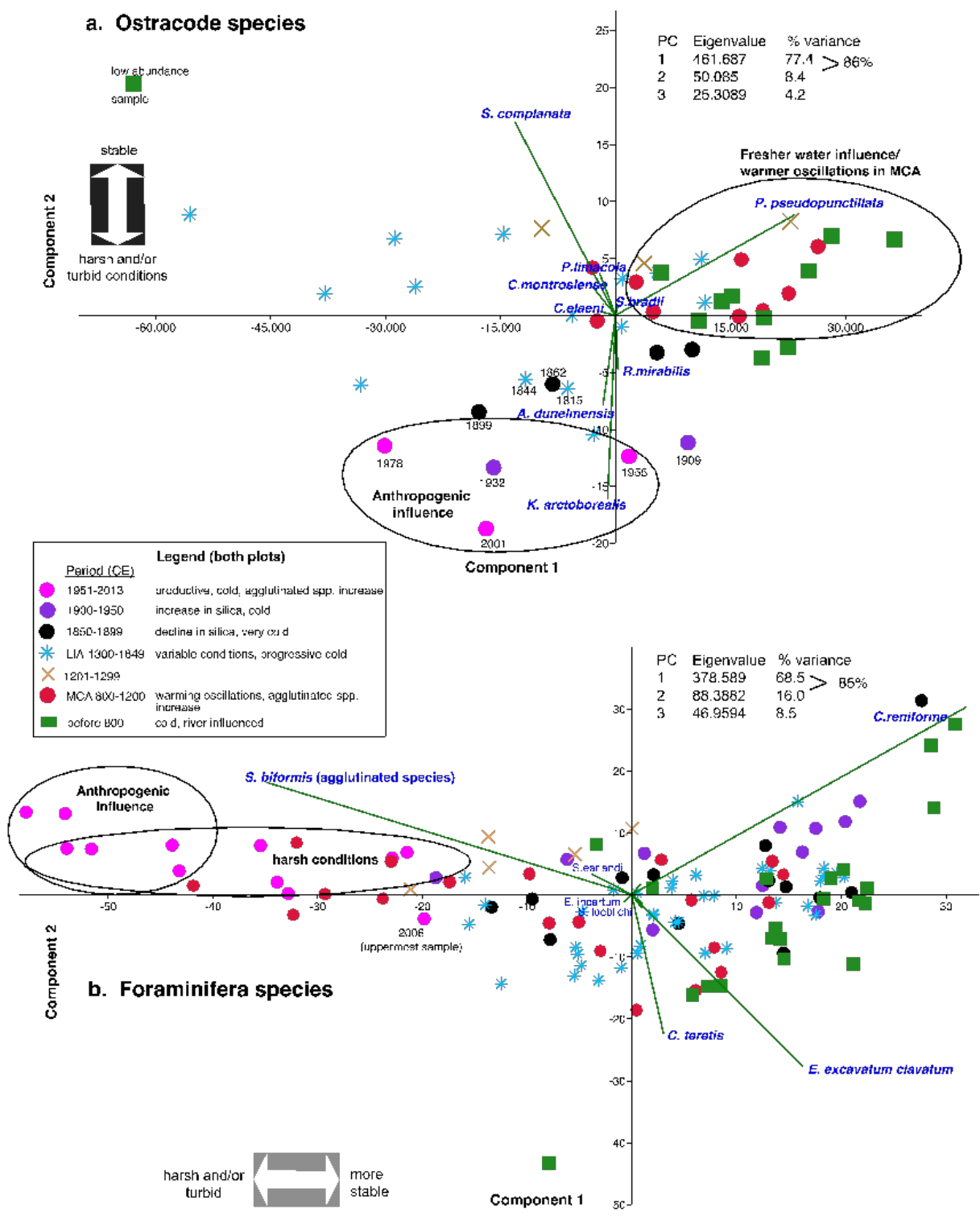


Figure 4.6. Stack plot of ostracode species that make up 98% of the assemblages by composite depth.

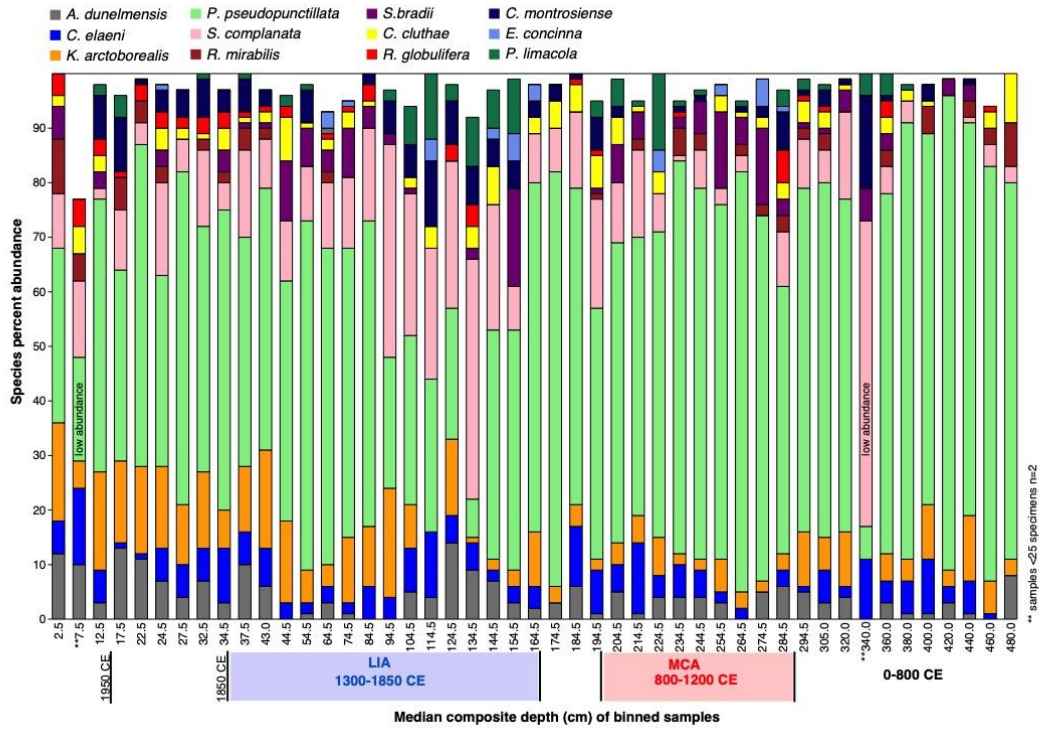


Figure 4.7. Stack plot of primary foraminifera species that make up ~95% of the assemblages by composite depth.

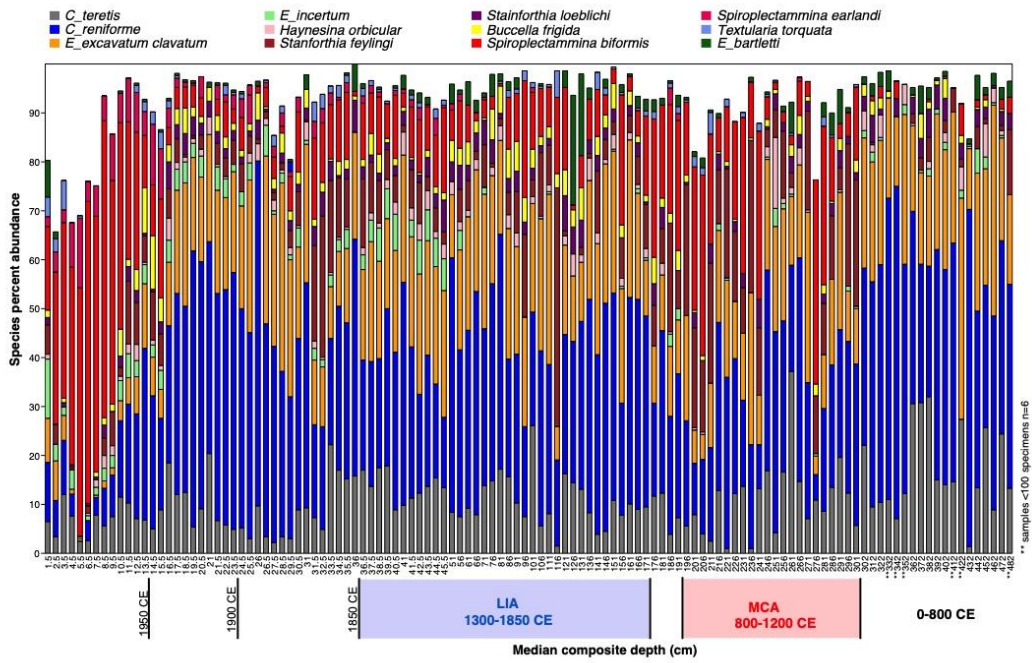


Figure 4.8a.) Number of ostracode specimens per binned sample; MC29 was binned every 5 cm, GGC30 every 10 cm and JPC32 every 20 cm. Two samples contained <25 specimens/binned sample, and these are indicated by yellow highlights. b.) Percent abundance of selected benthic ostracode and c.) foraminifera species (of total specimens/sample) against composite core depth. Selected foraminifera faunal data from Seidenstein et al (2018). Foraminifera species abundance in MC29 (black lines) are plotted separately from GGC30/JPC32. General periods of the LIA (1300-1850; ~36-160 cm composite depth) and MCA (800-1200; 195-294 cm), per our age model, are shown by blue and red shaded vertical bars, respectively. The beginning of each time zone is labeled 1, 2, 3, and 4. Confidence limits (95%) shown on the faunal plots were calculated using the algorithm for binomial probability (Raup, 1991).

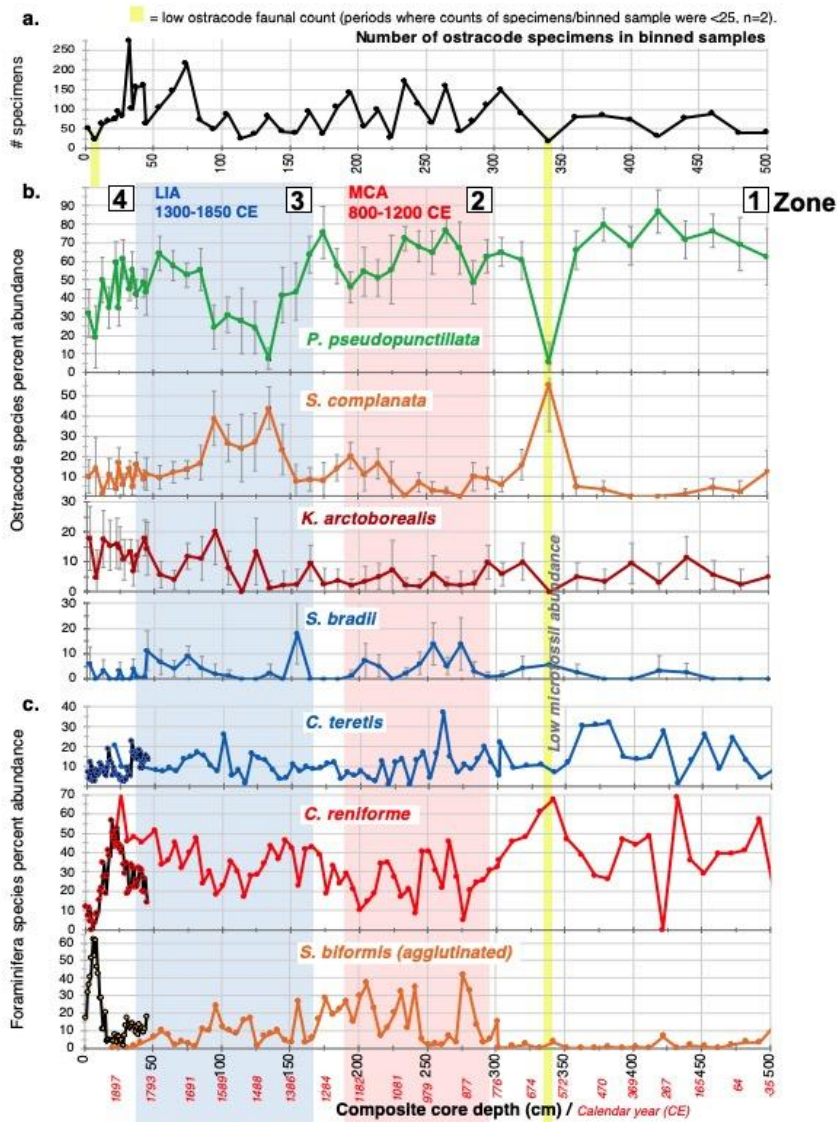
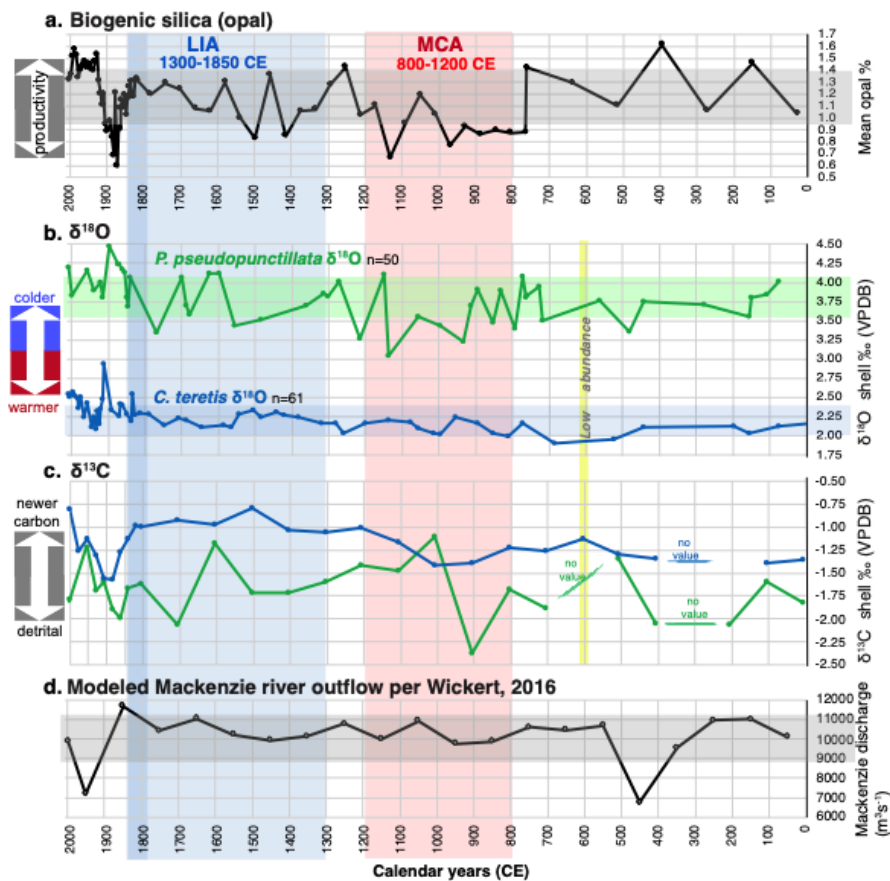


Figure 4.9a.) Percent of sediment biogenic silica against age (calendar years, CE); b.) Measurements of ostracode $\delta^{18}\text{O}$ (green) and foraminifera $\delta^{18}\text{O}$ (blue) against age; c.) Measurements of ostracode $\delta^{13}\text{C}$ (green) and foraminifera $\delta^{13}\text{C}$ (blue) against age. Carbon isotope values are binned (averaged) in 25-year intervals from 1800 to 2013 and binned by 100-year intervals from 0 to 1800 CE to smooth the large variability of measured values; d.) Modeled Mackenzie River outflow per Wickert (2016), and modern value representing 1990s from Carson et al. (1998). Shaded horizontal bars on plots indicate average standard deviation values.



Tables Chapter 4

Table 4.1. Dominant ostracode species used in the HLY1302 composite cores (multicore [MC29], gravity core [GGC30], and piston core [JPC32]) to infer water mass changes at the Mackenzie shelf site. SEM photos taken from Gemery et al., 2015.

Species	typical temperature	typical salinity	water mass	sediment substrate	food preference	representative climate zone	primary modern distribution*	mode of life	primary ecological reference(s)
<i>Paracyprideis pseudopunctillata</i>	cold ($\pm 1^{\circ}\text{C}$)	euryhaline, river proximal	winter water with fresher inputs	fine silty muds	phyto debris	arctic-subarctic / circum-Arctic	Nearshore waters off Greenland, Norwegian, Kara, Laptev, East Siberian, Beaufort, Chukchi Seas, and Norton Sound in Bering Sea	infaunal	Stepanova, 2006
<i>Sarsicytheridea bradii</i>	eurythermic but more common in $\pm 4.5^{\circ}\text{C}$	normal marine (31-33)	Pacific-Arctic waters	sands and silts	wide	arctic-subarctic / circum-Arctic	North Atlantic (north of Cape Cod and Georges Bank), Ungava Bay, Frobisher Bay, Hudson Bay, Gulf of Maine, straits of the Canadian Arctic Archipelago, Newfoundland, Labrador Sea, waters off Great Britain, Ireland, Norway, Greenland, Franz Josef Land, Spitsbergen, Novaya Zemlya, White, Baltic, North, Barents, Kara, Laptev, East Siberian, Chukchi nearshore waters off Aleutian Islands, Anadyr Bay, Bering, Norton Sound, nearshore waters off Alaska	infaunal	Stepanova, 2006; Freiwald and Mostafawi, 1998; Hazel, 1970
<i>Semicytherura complanata</i>	cold ($\pm 0-3^{\circ}\text{C}$)	normal marine, but high abundance in >33	winter water	sands and silts	unknown	arctic-subarctic / circum-Arctic	Areas where a polynya forms during wintertime; Greenland, White (southern inlet of the Barents Sea), Barents, Norwegian, Kara, Laptev, East Siberian, Chukchi, Bering, Beaufort Seas; Labrador Sea, Ungava, Frobisher, and Hudson bays, straits of the Canadian Arctic Archipelago, Ireland	infaunal	Stepanova, 2006; Brouwers et al., 2000; Cronin et al., 1994
<i>Kotoracythere arctoborealis</i>	cold ($\pm 0-3^{\circ}\text{C}$)	euryhaline/ lower salinity areas incl. $\sim 19-32$	winter water also with fresher inputs	sands and silts	unknown	arctic-subarctic / Western Arctic	Protected waters in Chaunskaya Bay (Eastern Siberian, Sea Shelf, Bering Sea around St. Lawrence Island, Chukchi Sea north of the Bering Strait, NE Chukchi	unknown	Gemery et al., 2021a; Cronin et al., 2021

Table 4.2 List of radiocarbon dates for the HLY1302 composite cores and calibrations using CALIB 8.2 software (Stuiver et al., 2021), the Marine20 calibration curve (Heaton et al., 2020) and a marine reservoir correction of $\Delta R = 477 \pm 60$ years (Pearce et al., 2017). Yellow highlight denotes seven new samples measured to improve the age model of Seidenstein et al (2018).

Accession #	Submitter Identification	Depth composite (cm)	Material	Uncalibrated age (yr BP)	Age error (yr)	ΔR	BP before present 1950 CE			
							Calibrated age range BP (2 σ confidence)		2 sigma % confidence	median age (BP)
							from	to		
OS-106827	HLY1302 MC-29A	30	mixed benthics	615	20	no	0	223	95.4	80
OS-154540	HLY1302_GGC30_15-17cm	36	mollusc	1,090	15	477 \pm 60	0	244	95.4	96
OS-154541	HLY1302_GGC30_45-47cm	66	mollusc	1,330	15	477 \pm 60	130	483	95.4	318
OS-130828	HLY1302_GGC30_154-156cm	175	mollusc	1,760	15	477 \pm 60	523	849	95.4	678
OS-154543	HLY1302_GGC30_172-174	195	mollusc	2,050	30	477 \pm 60	772	1161	95.4	964
OS-154650	HLY1302_GGC30_175-177	196	mollusc	2,010	55	477 \pm 60	709	1135	95.4	919
OS-154544	HLY1302_GGC30_235-237cm	256	mollusc	2,130	20	477 \pm 60	878	1244	95.4	1047
OS-106830	HLY1302 GGC-30, bot corecatcher	311	mixed benthics	2,340	20	477 \pm 60	1064	1426	95.4	1258
OS-130709	HLY13-02 JPC32, 70-72 cm	372	mollusc	2,530	20	477 \pm 60	1278	1642	95.4	1452
OS-130710	HLY13-02 JPC32, 250-252 cm	552	mollusc	2,890	20	477 \pm 60	1681	2095	95.4	1875
	Sediment reworked, not used:									
OS-131451	HLY13-02 JPC32, 260-262 cm	582	mixed benthics	3,180	20	477 \pm 60	2010	2445	95.4	2232
OS-154603	HLY1302_JPC32_340-342cm	642	mollusc	2,980	15	477 \pm 60	1765	2206	95.4	1986
OS-130711	HLY13-02 JPC32, 380-382 cm	689	mollusc	3,380	20	477 \pm 60	2308	2703	95.4	2497
OS-130825	HLY13-02 JPC32, 450-452 cm	752	mollusc	3,250	15	477 \pm 60	2104	2568	95.4	2327
OS-154604	HLY1302_JPC32_500-502cm	802	mollusc	3,110	20	477 \pm 60	1940	2339	95.4	2153
OS-130826	HLY13-02 JPC32, 620-622 cm	922	mollusc	3,570	15	477 \pm 60	2499	2917	95.4	2724
OS-130827	HLY13-02 JPC32, 710-712 cm	1012	mollusc	3,700	15	477 \pm 60	2697	3077	95.4	2869

Table 4.3 Summary of $\delta^{18}\text{O}$ and $\delta^{13}\text{C}$ isotopic data.

	$\delta^{18}\text{O}$ (‰ VPDB)		$\delta^{13}\text{C}$ (‰ VPDB)	
	<i>P.pseudo</i>	<i>C. teretis</i>	<i>P.pseudo</i>	<i>C. teretis</i>
Avg over 2ka record	3.8	2.3	-1.7	-1.2
stdev	0.31	0.18	0.48	0.32
n=	50	61	50	61
Avg last 100 yr	4.0	2.4	-1.6	-1.2
stdev	0.17	0.16	0.48	0.32
n=	6	16	6	16
Avg during end of LIA (1800-1900 CE)	4.1	2.3	-1.8	-1.2
n=	8	8	8	8
Avg during MCA	3.6	2.1	-1.8	-1.3
n=	9	10	9	10
‰ increase in $\delta^{18}\text{O}$ from MCA to LIA	0.5	0.2		
°C temperature decrease from MCA to LIA	~2	~1		
r^2 trend of increasing $\delta^{18}\text{O}$ from MCA to present (800- 2013 CE)	0.26	0.38		
r^2 trend of increasing $\delta^{13}\text{C}$ over 2ka record			0.02	0.27

Chapter 5: Overall Conclusions

5.1 Review of project goals and key findings

In this study, ostracodes are shown to be sensitive indicators of benthic environmental conditions, and can be used as a tool to assist in monitoring the progression of environmental changes, as well as detailing changes in the past.

Results from Chapter 2 (Gemery et al., 2021a) confirmed that ostracode abundance and distribution are controlled by bottom water temperature, salinity, organic carbon deposition, and sediment substrate, which are directly related to the transit of summer water masses. During the last decade, an incipient increase was found in two cold-temperate species, *Schizocythere ikeyai* and *Munseyella mananensis*, which primarily inhabit shallow North Pacific sediments off Asia. This finding suggests that these species are responding to recent increases in coastal and mid-shelf bottom water temperatures and/or carbon flux to the benthos. This chapter not only documented the biogeography of ostracodes in the Pacific-Arctic, it determined the controlling environmental factors that influence ostracode species in particular assemblages, which will ultimately improve the interpretation of fossil assemblages from sediment cores for paleoceanographic reconstructions.

In Chapter 3 (Gemery et al., 2021b) results confirmed that ostracode shell $\delta^{18}\text{O}$ is not secreted in equilibrium with ambient water $\delta^{18}\text{O}$, and vital-effect offsets for each species (relative to equilibrium inorganic calcite) are significant, ranging from +2.4 to +1.1‰. Regression analysis results supported that seasonal hydrography of warmer and less saline

Alaska Coastal Water and very cold, saline Bering Sea Water and Remnant Winter Water is reflected in stable isotope records of water $\delta^{18}\text{O}$ and in $\delta^{18}\text{O}$ values of two species, *N. leioderma* and *P. pseudopunctillata*. Notably, *S. bradii* was found to not be a good species to use for paleo $\delta^{18}\text{O}$ reconstructions due to large vital-effect offsets and lack of any correlation with temperature and seawater $\delta^{18}\text{O}$. Intra-sample variability of ostracode was found to be $\pm 0.2\%$, which supported that ostracode carbonate $\delta^{18}\text{O}$ primarily reflected mean summer water isotopic composition and temperature. Overall, this study provides calibration information for using ostracode $\delta^{18}\text{O}$ values to evaluate paleoceanographic bottom-water conditions and circulation patterns associated with specific water masses in the Bering and Chukchi Seas.

Chapter 4 (Gemery et al., 2022, submitted, *Micropaleontology*) presented a 2,000-year, multi-proxy paleoceanographic reconstruction that revealed short-term paleoenvironmental changes on the Mackenzie continental shelf. Specifically, microfossil carbonate $\delta^{18}\text{O}$ shifts were correlated to the Medieval Climate Anomaly (~800 to 1200 CE), Little Ice Age (~1500-1850 CE), and recent periods that indicate pronounced alterations in bottom water mass properties. During the Medieval Climate Anomaly, microfossil $\delta^{18}\text{O}$ suggested summer warming oscillations and periods of low productivity (as indicated by low silica and microfossil carbonate $\delta^{13}\text{C}$ values). Pronounced increases in agglutinated species suggested bottom waters were affected by increased water turbidity or anoxia, which was less conducive to calcareous faunas. During the Little Ice Age (~1500-1850 CE), progression to a colder, productive environment was indicated by high biogenic silica values and generally high ostracode $\delta^{18}\text{O}$. The coldest interval of the record occurred 1850-1900 CE, where high microfossil $\delta^{18}\text{O}$, low biogenic silica and low carbonate $\delta^{13}\text{C}$ values align, suggesting that enhanced summer sea ice suppressed productivity. Within the last ~60 years, changes in all investigated proxies are consistent with longer periods

of open water, high productivity, greater freshwater inputs and generally, greater variations in the bottom waters of Beaufort Sea shelf. Assessing effects of Arctic change from modern measurements is limited by the length of observational data sets. Because high-resolution sediment records on high-latitude continental shelves are rare, this record is important to understand past natural climate variability and contextualize benthic ecosystem change in the modern environment due to anthropogenic forcings.

Overall, the comprehensive results of this dissertation study pave the way for paleoceanographic questions to be answered using the faunal assemblages, ecology and chemical composition of microfossils in complex continental shelf ecosystems. The findings about specific species ecology and controls on species incorporation of stable oxygen isotopes into their carbonate shells illustrate the need for basic species-level ecological and geochemical studies. Lastly, these studies were only possible through, and further demonstrate the value of, long-term monitoring programs (like the Distributed Biological Observatory and predecessors) with comprehensive spatial coverage, physical and chemical oceanography as well as multi-trophic fauna studies.

5.2 Future work

Continued monitoring of temperature-sensitive ostracode species distributions in the Pacific-Arctic region is important to provide information on annual and decadal trends in species responses to climate and ecosystem change. Future efforts can be guided by utilizing the particular ostracode species defined as “biomonitors” of changing benthic environments (Chapter 2).

Ocean acidification (OA) is an important topic that may be interesting to explore further by utilizing ostracodes, particularly at DBO1 (St Lawrence Island, northern Bering Sea), DBO3 (southern Chukchi Sea), DBO4 (northeast Chukchi Sea), as these areas are known to be experiencing seasonal OA (Cross et al., 2014; 2018). In the recent decade, samples from the DBO1 ecoregion have been nearly barren of ostracodes, yet in prior decades, ostracodes had been abundant there. An area where progress might be made is to examine shells from living ostracodes from surface samples for evidence of OA based on mineralogical, elemental and structural carapace properties. This can be achieved by using a combination of methods, including scanning electron microscopy (SEM), energy dispersive X-ray spectroscopy (EDS) and Raman spectroscopy for elemental analysis, and X-ray microscope nano-computed tomography (XMCT). With these techniques, the elemental and structural composition, density, and thickness of ostracode valves can be measured over geographic regions and over time. Ostracode shell surface microstructures can also be characterized using SEM and XMCT. New surface sediments collected in the Bering and Chukchi Seas for ostracode analysis utilizing the DBO cross-shelf transects can be compared with archived ostracode collections at USGS from earlier years. Previous sampling sites could be matched up with the new sampling locations, strategically picked to assess known areas of seasonal OA.

Bibliography

- Aagaard, K.K., 1984. The Beaufort Undercurrent. In: Barnes, P.W., Schell, D.M., and Reimnitz, E., Eds. *The Alaskan Beaufort Sea: Ecosystems and environments*. New York: Academic Press, pp. 47–71.
- Addison, J. A., Finney, B. P., Jaeger, J. M., Stoner, J. S., Norris, R. D., and Hangsterfer, A., 2013. Integrating satellite observations and modern climate measurements with the recent sedimentary record: An example from Southeast Alaska. *Journal of Geophysical Research: Oceans*. 118: 3444–3461. doi:10.1002/jgrc.20243.
- Alley, R.B., Agustsdottir, A.M., Fawcett, P.J., 1999. Ice-core evidence of late-Holocene reduction in North Atlantic Ocean heat transport. *Geophysical Monograph*. 112: 301-312.
- Alve, E. 2010. Benthic foraminiferal responses to absence of fresh phytodetritus: A two-year experiment. *Marine Micropaleontology* 76:67–75. doi:10.1016/j.marmicro.2010.05.003
- Ammann, C. M., Joos, F., Schimel, D. S., Otto-Bliesner, B. L., Tomas, R. A., 2007. Solar influence on climate during the past millennium: results from transient simulations with the NCAR Climate System Model. *Proceedings of the National Academy of Sciences of the United States of America*. 104(10): 3713-8. doi: 10.1073/pnas.0605064103
- Anderson, R.K., Miller, G.H., Briner, J.P., Lifton, N.A., DeVogel, S.B., 2008. A millennial perspective on Arctic warming from ¹⁴C in quartz and plants emerging from beneath ice caps. *Geophysical Research Letters*. 35: L01502. doi:10.1029/2007GL032057
arcticdata.io [Internet]. NSF, Arctic Data Center. Available from [https://arcticdata.io/catalog/portals/DBO/]
- Arrigo, K. R., van Dijken, G. L., and Pabi, S., 2008. Impact of a shrinking Arctic ice cover on marine primary production. *Geophysical Research Letters*. 35(19): L19603.
<https://doi.org/10.1029/2008GL035028>
- Arrigo, K. R., and van Dijken, G. L., 2011. Secular trends in Arctic Ocean net primary production. *Journal of Geophysical Research*. 116: C09011.
- Arrigo, K.R., van Dijken, G.L., 2015. Continued increases in Arctic Ocean primary productions. *Progress in Oceanography*. 136: 60-70. doi:10.1016/j.pocean.2015.05.002
- Athersuch, J., Horne, D. J., and Whittaker, J. E., 1989. Marine and brackish water ostracods. *Synopses of the British Fauna (New Series) No. 43*. E. J. Brill, Leiden: 342 pp., 8 pls. doi: <https://doi.org/10.1017/S0025315400059178>
- Avery, S.V., 1996. Fate of caesium in the environment: Distribution between the abiotic and biotic components of aquatic and terrestrial ecosystems. *Journal of Environmental Radioactivity*. 30: 139-171.

Barnes, P.W., Reimnitz, E., Fox, D., 1982. Ice rafting of fine-grained sediment, a sorting and transport mechanism, Beaufort Sea, Alaska. *Journal of Sedimentary Petrology*. 52(2): 493-502.

Bauch, D. and Bauch, H.A., 2001. Last glacial benthic foraminiferal $\delta^{18}\text{O}$ anomalies in the polar North Atlantic: a modern analogue evaluation. *Journal of Geophysical Research*. 106(C5): 9135–9143.

Bauch, D., Erlenkeuser, H., Stanovoy, V., Simstich, J. R., Spielhagen, F., 2003. Freshwater distribution and brine waters in the southern Kara Sea in summer 1999 as depicted by $\delta^{18}\text{O}$ results. In: R. Stein, K. Fahl, D.K. Futterer, E.M. Galimov and O.V. Stepanets (Eds) *Siberian River run-off in the Kara Sea: characterization, quantification, variability and environmental significance*, Elsevier, Amsterdam, *Proceedings in Marine Science*. 6: 73-90.

Bauch, D., Hoelemann, J., Andersen, N., Dobrotina, E., Nikulina, A., Kassens, H., 2010. The Arctic shelf regions as a source of freshwater and brine-enriched waters as revealed from stable oxygen isotopes. *Polarforschung*. 80: 127-140.

Beer, J., 2000. Long-term indirect indices of solar variability. *Space Science Reviews*. 94(1): 53-66.

Bemis, B. E., Sepro, H. J., Bijma, J., and Lea, D. W., 1998. Reevaluation of the oxygen isotopic composition of planktonic foraminifera: Experimental results and revised paleotemperature equations. *Paleoceanography*. 13(2): 150-160.

Benson, R.H., 1961. Ecology of ostracode assemblages. In: Moore, R.C., Pitrat, C.W. (Eds.), *Treatise on Invertebrate Paleontology*. Geological Society of America. pp. Q56–Q63.

Benson, R.H., 1974. The role of ornamentation in the design and function of the ostracode carapace. *Geoscience and Man*. 6: 47–57.

Benson, R.H., 1984. Estimating greater paleodepths with ostracodes, especially in past thermospheric oceans. *Palaeogeography, Palaeoclimatology, Palaeoecology*. 48: 107–141.

Blanchard, A.L., Parris, C.L., Knowlton, A.L., Wade, N.R., 2013, Benthic ecology of the northeastern Chukchi Sea. Part I: Environmental characteristics and macrofaunal community structure, 2008-1010. *Continental Shelf Research*. 67: 52-66. doi:10.1016/j.csr.2013.04.021

Bluhm, B.A., Gebruk, A.V., Gradinger, R., Hopcroft, R.R., Huettmann, F., Kosobokova, K.N., Sirenko, B.I., and Weslawski, J.M., 2011. Arctic marine biodiversity: An update of species richness and examples of biodiversity change. *Oceanography*. 24(3): 232-248. <https://doi.org/10.5670/oceanog.2011.75>

Bluhm, B.A., Swadling, K.M., Gradinger, R., 2017. Sea ice as a habitat for macrograzers. In: Thomas DN (Ed.). *Sea Ice*. United Kingdom: John Wiley & Sons Ltd. 3: 394-414. doi:10.1002/9781118778371.ch16

Bornemann, A., Pirkenseer, C.M., De Deckker, P., Speijer, R.P., 2012. Oxygen and carbon isotope fractionation of marine ostracod calcite from the eastern Mediterranean Sea. *Chemical Geology*. 310–311: 114–125.

Boyer, T.P., Antonov, J.I., Baranova, O.K., Coleman, C., Garcia, H.E., Grodsky, A., et al. 2013. World Ocean Database, NOAA Atlas NESDIS 72. Levitus S (Ed.), Mishonov A (Technical Ed.), Silver Spring, MD. 209. doi:10.7289/V5NZ85MT. Available from [<https://www.nodc.noaa.gov/OC5/WOD13/>].

Boyer, T.P., Stephens, C., Antonov, J.I., Conkright, M.E., Locarnini, R.A., O'Brien, T.D., et al. 2002. World Ocean Atlas 2001, Volume 2: Salinity [CD-ROM]. Levitus S (Ed.), NOAA Atlas NESDIS 50, U.S. Government Printing Office, Washington D.C. 165.

Bradley, R.S., Briffa, K.R., Cole, J., Hughes, M.K., and Osborn, T.J., 2003a. The climate of the last millennium. In: Alverson, K.D., R.S. Bradley and T.F. Pedersen (eds.) *Paleoclimate, Global Change and the Future*. Springer Verlag, Berlin, 105-141. <http://www.geo.umass.edu/faculty/bradley/bradleypub.html>

Bradley, R.S., Hughes, M.K., Diaz, H.F., 2003b. Climate in Medieval time. *Science*. 302: 404-405. doi:10.1126/science.1090372

Bringué, M. and Rochon, A., 2012. Late Holocene paleoceanography and climate variability over the Mackenzie slope (Beaufort Sea, Canadian Arctic). *Marine Geology*. 291-294: 83-96.

Broecker, W.S., 2001. Was the Medieval warm period global? *Science*. 291(5508): 1497-1499. doi:10.1126/science.291.5508.1497

Brouwers, E. M., 1981. Tabulation of the ostracode assemblages and associated organisms from selected bottom grab samples taken in the northeast Gulf of Alaska, F.R.S. Townsend Cromwell Cruise EGAL-75-KC, 1975: U.S. Geological Survey Open-File Report. 81-1314: 134 p.

Brouwers, E. M., 1982a. Tabulation of the ostracode assemblages and associated fauna and flora from Van Veen samples taken in the northeast Gulf of Alaska, R/V Discoverer Cruise DC2-80-EG, June 1980: U.S. Geological Survey Open- File Report. 82-390.

Brouwers, E. M., 1982b. Tabulation of the ostracode assemblages and associated organisms from selected bottom grab samples taken in the northeast Gulf of Alaska, F.R.S. Townsend Cromwell Cruise EGAL-75-KC, 1975: Part II: U.S. Geological Survey Open-File Report. 82-949.

Brouwers, E. M., 1990. Systematic Paleontology of Quaternary Ostracode Assemblages from the Gulf of Alaska: Part 1. Families Cytherellidae, Bairdiidae, Cytheridae, Leptocytheridae, Limnocytheridae, Eucytheridae, Krithidae, Cushmaniidae. U.S. Geological Survey Professional Paper. 1510: 1–40.

- Brouwers, E.M., Jørgensen, N.O., and Cronin, T.M., 1991. Climatic significance of the ostracode fauna from the Pliocene Kap København Formation, north Greenland. *Micropaleontology*. 37: 245–267.
- Brouwers, E. M., 1992. Pliocene Paleoecologic Reconstructions based on Ostracode Assemblages from the Sagavanirktok and Gubik Formations, Alaskan North Slope. U.S. Geological Survey Professional Paper OFR. 92-321
- Brouwers, E. M., 1993. Systematic paleontology of Quaternary ostracode assemblages from the Gulf of Alaska: Part 2. Families Trachyleberididae, Hemicytheridae, Loxoconchidae, Paracytheridae. U.S. Geological Survey Professional Paper. 1531: 1–40.
- Brouwers, E. M., 1994. Systematic Paleontology of Quaternary Ostracode Assemblages from the Gulf of Alaska: Part 3. Family Cytheruridae. U.S. Geological Survey Professional Paper. 1544: 1–43.
- Brouwers, E.M., Cronin, T.M., Horne, D.J., Lord, A.R., 2000. Recent shallow marine ostracods from high latitudes: Implications for late Pliocene and Quaternary palaeoclimatology. *Boreas*. 29(2): 127-142.
- Brown, Z.W., van Dijken, G.L., Arrigo, K.R., 2011 A reassessment of primary production and environmental change in the Bering Sea. *Journal of Geophysical Research*. 116: C08014.
- Brown, Z.W., Arrigo, K.R., 2012. Contrasting trends in sea ice and primary production in the Bering Sea and Arctic Ocean. *ICES Journal of Marine Science*. 69: 7, 1180-1193.
doi:10.1093/icesjms/fss113
- Buzas, M.A., Culver, S.J., Jorissen, F.J., 1993. A statistical evaluation of the microhabitats of living (stained) infaunal benthic foraminifera. *Marine Micropaleontology*. 20: 311–320.
- Cage, A. G., Pieńkowski, A. J., Jennings, A., Knudsen, K. L., and Seidenkrantz, M.-S., 2021. Comparative analysis of six common foraminiferal species of the genera *Cassidulina*, *Paracassidulina*, and *Islandiella* from the Arctic–North Atlantic domain. *Journal of Micropalaeontology*. 40: 37–60. <https://doi.org/10.5194/jm-40-37-2021>
- Carmack, E. C., Macdonald, R. W., Papadakis, J. E., 1989. Water mass structure and boundaries in the Mackenzie shelf estuary. *Journal of Geophysical Research*. 94(C12): 18,043–18, 055. doi:10.1029/JC094iC12p18043
- Carmack, E. C. and Kulikov, E. A., 1998. Wind-forced upwelling and internal Kelvin wave generation in Mackenzie Canyon, Beaufort Sea. *Journal of Geophysical Research*. 103(C9): 18, 447–18, 458.
- Carmack, E.C. and Macdonald, R.W., 2002. Oceanography of the Canadian Shelf of the Beaufort Sea: A Setting for Marine Life. *Arctic*. 55(1): 29-45. doi: 10.14430/arctic733

- Carmack, E. C., Macdonald, R. W., Jasper, S., 2004. Phytoplankton productivity on the Canadian Shelf of the Beaufort Sea. *Marine Ecology Progress Series* 277: 37-50.
- Carson, M. A., Jasper, J. N., Conly, F.M., 1998. Magnitude and sources of sediment input to the Mackenzie Delta, Northwest Territories, 1974–94. *Arctic*. 51: 116–124.
- Chivas, A. R., De Deckker, P., Shelley, J. M. G., 1983. Magnesium, strontium and barium partitioning in non-marine ostracod shells and their use in paleoenvironmental reconstructions – a preliminary study. In Maddocks, R. F. (ed.), *Applications of Ostracoda, Proceedings of the Eight International Symposium on Ostracoda, University of Houston, Geoscience*, pp. 238–249.
- Chivas, A. R., De Deckker, P., Cali, J. A., Chapman, A., Kiss, E., Shelley, J. M. G., 1993. Coupled stable isotope and trace-element measurements of lacustrine carbonates as paleoclimatic indicators. In, P. K. Swart, K. C. Lohmann, J. McKenzie & S. Savin, (eds) *Climate change in continental isotopic records. American Geophysical Union, Geophysical Monograph Series*. 78: 113–121.
- Coachman, L.K., Aagaard, K., Tripp, R.B., 1975. *Bering Strait: The Regional Physical Oceanography*. University of Washington Press, Seattle.
- Cohen, A.C., and Morin, J.G., 1990. Patterns of reproduction in ostracodes; a review. *Journal of Crustacean Biology*. 10: 184–211.
- Coles, G. P., Whatley, R. C., and Moguevsky, A., 1994. The ostracod genus *Krithe* from the Tertiary and Quaternary of the North Atlantic. *Palaeontology*. 37: 71–120.
- Comiso, J. C., Meier, W. N., Gersten, R., 2017. Variability and trends in the Arctic Sea ice cover: results from different techniques. *Journal of Geophysical Research*. 122: 6883-6900.
- Cooper, L.W., Whitley, T.E., Grebmeier, J.M., and Weingartner, T., 1997. The nutrient, salinity, and stable oxygen isotope composition of Bering and Chukchi Seas waters in and near the Bering Strait, *Journal of Geophysical Research*. 102: 12563-12573.
- Cooper, L.W., Grebmeier, J.M., Larsen, I.L., Dolvin, S., Reed, A.J., 1998. Inventories and distribution of radiocaesium in arctic marine sediments: influence of biological and physical processes. *Chemistry and Ecology*. 15: 27-46.
- Cooper, L.W., Grebmeier, J.M., Larsen, I.L., Egorov, V.G., Theodorakis, C., Kelly, H.P., et al. 2002. Seasonal variation in sedimentation of organic materials in the St. Lawrence Island polynya region, Bering Sea. *Marine Ecology Progress Series*. 226: 13-26.
- Cooper, L. W., Benner, R., McClelland, J. W., Peterson, B. J., Holmes, R. M., Raymond, P. A., Hansell, D. A., Grebmeier, J. M., and Codispoti, L. A., 2005. Linkages among runoff, dissolved organic carbon, and the stable oxygen isotope composition of seawater and other

water mass indicators in the Arctic Ocean. *Journal of Geophysical Research*. 110: G02013. doi:10.1029/2005JG000031

Cooper L. W., McClelland, J. W., Holmes, R. M., Raymond, P. A., Gibson, J. J., Guay, C. K., Peterson, B. J., 2008. Flow-weighted values of runoff tracers ($\delta^{18}\text{O}$, DOC, Ba, alkalinity) from the six largest Arctic rivers. *Geophysical Research Letters*. doi: 10.1029/2008GL035007

Cooper, L.W., Savvichev, A.S., Grebmeier, J.M., 2015. Abundance and production rates of heterotrophic bacterioplankton in the context of sediment and water column processes in the Chukchi Sea. *Oceanography*. 28 (3): 84-99. doi:10.5670/oceanog.2015.59

Cooper, L.W., Grebmeier, J.M., 2018. Deposition patterns on the Chukchi shelf using radionuclide inventories in relation to surface sediment characteristics. *Deep Sea Research Part II: Topical Studies in Oceanography*. 152: 48-66. doi:10.1016/j.dsr2.2018.01.009

Coplen, T.P., 1994. Reporting of stable hydrogen, carbon, and oxygen isotopic abundance. *Pure and Applied Chemistry*. 66: 273–276. Triangle Park.

Craig, H., 1961. Standard for reporting concentrations of deuterium and oxygen-18 in natural waters. *Science*. 133: 1833–1834.

Craig, H., 1965. The measurement of oxygen isotope paleotemperature. In: *Stable Isotopes in Oceanographic Studies and Paleotemperatures* (E. Tongiorgi, Ed), Vol. 3, pp. 3-24. Spoleto: Conferences in Nuclear Geology.

Craig, H., and Gordon, L. I., 1965. Deuterium and oxygen-18 variations in the ocean and marine atmosphere. In: *Stable Isotopes in Oceanographic Studies and Paleotemperatures*, (E. Tongiorgi, Ed), Vol. 3, pp. 9–130. Spoleto: Conferences in Nuclear Geology.

Cronin, T.M., 1977. Late-Wisconsin Marine Environments of the Champlain Valley (New York, Quebec). *Quaternary Research*. 7: 238-253.

Cronin, T.M., 1977. Champlain Sea foraminifera and ostracoda: A systematic and paleoecological synthesis. *Géographie physique et Quaternaire*. 31: 107-122.

Cronin, T.M., 1977. Late-Wisconsin Marine Environments of Champlain Valley (New York, Quebec). *Quaternary Research*. 7: 238-253.

Cronin, T. M., 1981. Paleoclimatic implications of Late Pleistocene marine ostracodes from the St. Lawrence Lowlands. *Micropaleontology*. 27(4): 383-418.

Cronin, T. M., and Ikeya, N., 1987. The Omma-Manganji ostracod fauna (Plio-Pleistocene) of Japan and the zoogeography of circumpolar species. *Journal of Micropalaeontology*, 6(2): 65-88. <https://doi.org/10.1144/jm.6.2.65>

- Cronin, T. M., 1988. Paleozoogeography of postglacial ostracoda from northeastern North America. The Late Quaternary development of the Champlain Sea Basin. Geological Association of Canada Special Paper. 35: 125-144.
- Cronin, T. M., Briggs Jr, W. M., Brouwers, E. M., Whatley, R. C., Wood, A., and Cotton, M. A., 1991. Modern Arctic podocypid ostracode database. United States Geological Survey Open-File Report. 91-385: 1-51.
- Cronin, T.M., Whatley, R.W., Wood, A., Tsukagoshi, A., Ikeya, N., Brouwers, E.M., Briggs Jr., W.M., 1993. Microfaunal evidence for elevated Pliocene temperatures in the Arctic Ocean. *Paleoceanography*. 8(2): 161-173.
- Cronin, T.M., Holtz, T.R., Whatley, R.C., 1994. Quaternary paleoceanography of the deep Arctic Ocean based on quantitative analysis of Ostracoda. *Marine Geology*. 119: 305-332.
- Cronin, T. M., Gemery, L., Brouwers, E. M., Briggs, Jr., W. M., Wood, A., Stepanova, A., Schornikov E. I., Farmer, J., and Smith, K. E. S., 2010. Modern Arctic Ostracode Database. IGBP PAGES/WDCA Contribution Series Number: 2010-081.
- Cronin, T.M., Gemery, L., Briggs Jr., W.M., Jakobsson, M., Polyak, L., Brouwers, E.M., 2010. Quaternary sea-ice history in the Arctic Ocean based on a new ostracode sea-ice proxy. *Quaternary Science Reviews*. 29: 3415-3429.
- Cronin, T.M., Gemery, L., Brouwers, E.M., Briggs Jr., W.M., Wood, A., Stepanova, A., et al., 2010. Modern Arctic ostracode database. IGBP PAGES/WDCA. Contribution Series Number: 2010-08.
- Cronin, T.M., Gemery, L., Briggs Jr., W.M., Brouwers, E.M., Schornikov, E.I., Stepanova, A., Wood, A., Yasuhara, M., Siu, S., 2021. Arctic Ostracode Database 2020. NOAA's National Centers for Environmental Information (NCEI). Available from [<https://www.ncdc.noaa.gov/paleo/study/32312>]
- Cross, J. N., Mathis, J.T. Frey, K.E., Cosca, C. E., Danielson, S.L., Bates, N.R., Feely, R.A., Takahashi, T., Evans, W., 2014. Annual sea-air CO₂ fluxes in the Bering Sea: Insights from new autumn and winter observations of a seasonally ice-covered continental shelf. *Journal of Geophysical Research Oceans*. 119: 6693–6708. doi:10.1002/2013JC009579
- Cross, J.N., Mathis, J.T., Pickart, R.S., Bates, N.R., 2018. Formation and transport of corrosive water in the Pacific Arctic region. *Deep-Sea Research II*. 152: SOAR II, 67–81. doi: 10.1016/j.dsr2.2018.05.020
- Crowley, T.J., 2000. Causes of climate change over the past 1000 years. *Science*. 289: 270-277.
- Danielson, S.L, Eisner, L., Ladd, C., Mordy, C., Sousa, L., and Weingartner, T.J., 2017. A comparison between late summer 2012 and 2013 water masses, macro-nutrients, and

phytoplankton standing crops in the northern Bering and Chukchi Seas. *Deep-Sea Research II*. 135: 7–26. <https://doi.org/10.1016/j.dsr2.2016.05.024>

Danielson, S.L., Ahkinga, O., Ashjian, C., Basyuk, E., Cooper, L.W., Eisner, L., Farley, E., Iken, K.B., Grebmeier, J. M., Juranek, L., and others., 2020. Manifestation and consequences of warming and altered heat fluxes over the Bering and Chukchi Sea continental shelves. *Deep Sea Research Part II*. 177: 104781. <https://doi.org/10.1016/j.dsr2.2020.104781>

de Vernal, A., C. Hillaire-Marcel, D. Darby., 2005. Variability of sea ice cover in the Chukchi Sea (western Arctic Ocean) during the Holocene. *Paleoceanography*. 20: PA4018.

de Vernal, A., Hillaire-Marcel, C., Rochon, A., Fréchette, B., Henry, M., Solignac, S., & Bonnet, S., 2013. Dinocyst-based reconstructions of sea ice cover concentration during the Holocene in the Arctic Ocean, the northern North Atlantic Ocean and its adjacent seas. *Quaternary Science Reviews* 79: 111–121.

Decrouy, L., 2012. Biological and environmental controls on isotopes in ostracod shells. In: Horne, D.J., Holmes, J.A., Rodriguez-Lazaro, J., Viehberg, F., (Eds.), *Ostracoda as Proxies for Quaternary Climate Change*. *Developments in Quaternary Science*. 17: 165–181.

Decrouy, L., and Vennemann, T.W., 2013. Potential influence of the chemical composition of water on the stable oxygen isotope composition of continental ostracods. *Journal of Paleolimnology*. 50: 577-582. doi: 10.1007/s10933-013-9719-5

Devriendt, L. S., McGregor, H. V., Chivas, A.R., 2017. Ostracod calcite records the $^{18}\text{O}/^{16}\text{O}$ ratio of the bicarbonate and carbonate ions in water. *Geochimica et Cosmochimica Acta*. 214: 30-50.

Didié, C., and Bauch, H.A., 2002. Implications of upper Quaternary stable isotope records of marine ostracodes and benthic foraminifers for paleoecological and paleoceanographical investigations. In: Holmes, J.A. & Chivas, A.R. [Eds.]: *The Ostracoda: applications in Quaternary Research – Geophysical Monograph Series*. 131: 279–299.

Doxaran, D., Devred, E., and Babin, M., 2015. A 50% increase in the mass of terrestrial particles delivered by the Mackenzie River into the Beaufort Sea (Canadian Arctic Ocean) over the last 10 years. *Biogeosciences*. 12: 3551–3565. <https://doi.org/10.5194/bg-12-3551-2015>

Elofson, O., 1969. Zur Kenntnis der marinen Ostracoden Schwedens mit besonderer Berücksichtigung des Skageraks. *Zoologiska Bidrag fran Uppsala*. (Marine Ostracoda of Sweden with special consideration of the Skagerrak, Translation from German into English, Israel Program for Scientific Translations: 286 pp.). 1941; 19: 215-534, Figures 1-52.

Epstein, S., Buchsbaum, R., Lowenstam, H.A., Urey, H.C., 1951. Carbonate-water isotopic temperature scale. *Geological Society of America Bulletin*. 62: 417-426.

Epstein, S., Buchsbaum, R., Lowenstam, H.A., Urey, H.C., 1953. Revised carbonate-water isotopic temperature scale. *Geological Society of America Bulletin*. 64: 1315-1326.

Erlenkeuser, H., and von Grafenstein, U., 1999. Stable Oxygen Isotope Ratios in Benthic Carbonate Shells of Ostracoda, Foraminifera, and Bivalvia from Surface Sediments of the Laptev Sea, Summer 1993 and 1994.” In *Land–Ocean Systems in the Siberian Arctic: Dynamics and History*, Ed. by H. Kassens, H. A. Bauch, I. A. Dmitrenko, et al. (Springer-Verlag, Berlin, 1999), pp. 503– 514.

Farmer, J.R., Cronin, T.M., De Vernal, A., Dwyer, G. S., Keigwin, L.D., & Thunell, R.C., 2011. Western Arctic Ocean temperature variability during the last 8000 years. *Geophysical Research Letters*. 38(24).

Feder, H.M., Naidu, A.S., Jewett, S.C., Hameedi, J.M., Johnson, W.R., Whitley, T.E., 1994. The northeastern Chukchi Sea: benthos-environmental interactions. *Marine Ecology Progress Series*. 111 (1/2): 171-190.

Foukal, N. P., Pickart, R. S., Moore, G., & Lin, P. 2019. Shelfbreak downwelling in the Alaskan Beaufort Sea. *Journal of Geophysical Research: Oceans*. 124(10): 7201-7225.

Freiwald, A., and Mostafawi, N., 1998. Ostracods in a cold-temperate coastal environment, western Troms, northern Norway: Sedimentary aspects and assemblages. *Facies*. 38: 255–274.

Frenzel, P., Boomer, I., 2005. The use of ostracods from marginal marine, brackish waters as bioindicators of modern and quaternary environmental change. *Palaeogeography, Palaeoclimatology, Palaeoecology*. 225: 68-92

Frenzel, P., Keyser, D., and Veihberg, F.A., 2010. An illustrated key and (palaeo)ecological primer for Post- glacial to Recent Ostracoda (Crustacea) of the Baltic Sea. *Boreas*. 39: 567–575. 10.1111/j.1502-3885.2009.00135.x. ISSN 0300-9483.

Frey, K.E., Moore, G.W.K., Cooper, L.W., Grebmeier, J.M., 2015. Divergent patterns of recent sea ice cover across the Bering, Chukchi and Beaufort seas of the Pacific Arctic Region. *Progress in Oceanography*. 136: 32-49. doi: 10.1016/j.pocean.2015.05.009

Frey, K.E, Comiso, J.C., Cooper, L.W., Eisner, L.B., Gradinger, R.R., Grebmeier, J.M., and Tremblay, J.-É., 2017. Arctic Ocean primary productivity. In *Arctic Report Card 2017*. NOAA. <http://www.arctic.noaa.gov/Report-Card/Report-Card-2017/ArtMID/7798/ArticleID/701/Arctic-Ocean-Primary-Productivity>

Frey, K.E., Comiso, J.C., Cooper, L.W., Grebmeier, J.M., Stock, L.V., 2020. Arctic ocean primary productivity: The response of marine algae to climate warming and sea ice decline. In: *Arctic Report Card*, NOAA. Available from [<https://arctic.noaa.gov/Report-Card/Report-Card-2020/ArtMID/7975/ArticleID/900/Arctic-Ocean-Primary-Productivity-The-Response-of-Marine-Algae-to-Climate-Warming-and-Sea-Ice-Decline>]. doi:0.25923/vtdn-2198

Ganning, B., 1971. On the ecology of *Heterocypris salinus*, *H. incongruens*, and *Cypridopsis aculeata* (Crustacea, Ostracoda) from Baltic brackish water rockpools. *Marine Biology*. 8: 271-279.

Gemery, L., Cronin, T. M., Cooper, L. W., and Grebmeier, J. M., 2013. Temporal changes in benthic ostracode assemblages in the Northern Bering and Chukchi Seas from 1976 to 2010. *Deep-Sea Research II: Topical Studies in Oceanography*. 94: 68-79.

Gemery, L., Cronin, T.M., Briggs, W.M., Brouwers, E.M., Schornikov, E., Stepanova, A., Wood, A.M., Yasuhara, M., 2015. An Arctic and subarctic ostracode database: Biogeographic and paleoceanographic applications. *Hydrobiologia*. 786(1): 59-95.
<https://doi.org/10.1007/s10750-015-2587-4>

Gemery L., Cronin T.M., Poirier R.K., Pearce C., Barrientos N., O'Regan M., Johansson, C., Koshurnikov, A., and Jakobsson, M., 2017. Central Arctic Ocean paleoceanography from ~50 ka to present, on the basis of ostracode faunal assemblages from SWERUS 2014 expedition. *Climate of the Past*. <https://doi.org/10.5194/cp-2017-22>

Gemery, L., 2021. Data Release to Multi-proxy record of ocean-climate variability during the last 2 millennia on the Mackenzie Shelf, Beaufort Sea. U.S. Geological Survey data release. <https://doi.org/10.5066/P9SRRW6T>

Gemery, L., Cooper, L.W., Magen, C., Cronin, T.M., Grebmeier, J.M., 2021b. Stable oxygen isotopes in shallow marine ostracodes from the northern Bering and Chukchi Seas. *Marine Micropaleontology*. <https://doi.org/10.1016/j.marmicro.2021.102001>

Gemery, L., Cronin, T.M., Cooper, L.W., Roberts, L.R., Keigwin, L.D., Addison, J.A., Leng, M.J., Lin, P., Magen, C., Marot, M. E., Schwartz, V., 2022. Multi-proxy record of ocean-climate variability during the last two millennia on the Mackenzie Shelf, Beaufort Sea. *Micropaleontology*. Submitted.

GeoMapApp [Internet] Available from <http://www.geomapapp.org/index.htm>

Goethel, C.L., Grebmeier, J.M., and Cooper, L.W., 2019. Changes in abundance and biomass of the bivalve *Macoma calcarea* in the northern Bering Sea and the southeastern Chukchi Sea from 1998 to 2014, tracked through dynamic factor analysis models. *Deep Sea Research Part II*. 162:127–136. <https://doi.org/10.1016/j.dsr2.2018.10.007>

Gong, D., Pickart, R.S., 2015. Summertime circulation in the eastern Chukchi Sea. *Deep Sea Research Part II: Topical Studies in Oceanography*. 118 (Part A): 18-21.
[doi:10.1016/j.dsr2.2015.02.006](https://doi.org/10.1016/j.dsr2.2015.02.006)

Goosse, H., Renssen, H., Timmermann, A., Bradley, R.A., 2005. Internal and forced climate variability during the last millennium — a model-data comparison using ensemble simulations. *Quaternary Science Reviews* 24: 1345-1360.

Grebmeier, J., & McRoy, C.P., 1989. Pelagic-benthic coupling on the shelf of the northern Bering and Chukchi Seas. III Benthic food supply and carbon cycling. *Marine Ecology Progress Series*. 53: 79-91.

Grebmeier, J.M., Overland, J. E., Moore, S. E., Farley, E. V., Carmack, E. C., Cooper, L. W., Frey, K. E., Helle, J. H., McLaughlin, F.A., and McNutt, S. L., 2006. A Major Ecosystem Shift in the Northern Bering Sea. *Science*. 311(5766): 1461-1464.

Grebmeier, J.M., Moore, S.E., Overland, J.E., Frey, K.E., and Gradinger, R., 2010. Biological response to recent Pacific Arctic sea ice retreats. *Eos, Transactions of the American Geophysical Union*. 91(18): 161–162. <https://doi.org/10.1029/2010EO180001>

Grebmeier, J.M., 2012. Shifting patterns of life in the Pacific Arctic and sub-Arctic seas. *Annual Review of Marine Science*. 4: 63–78. <https://doi.org/10.1146/annurev-marine-120710-100926>.

Grebmeier, J.M., Cooper, L.W., 2014a. Bottom Water Temperature and Salinity (2000-2012). PacMARS. Version 1.0. Available from [PacMARS EOL data archive site <http://pacmars.eol.ucar.edu>]. doi:10.5065/D6VM49BM

Grebmeier, J., Cooper, L., 2014b. PacMARS sediment chlorophyll, a. Version 1.0., UCAR/NCAR. Earth Observing Laboratory. cited [2020 August 26]. doi:10.5065/D6W9576K

Grebmeier, J.M, Cooper, L.W., Ashjian, C.A., Bluhm, B.A., Campbell, R.B., Dunton, K.E., Moore, J., Okkonen, S., Sheffield, G., Trefry, J., and Pasternak, S.Y., 2015. Pacific Marine Arctic Regional Synthesis (PacMARS) Final Report, North Pacific Research Board. 259 pp.

Grebmeier, J. M., Bluhm, B. A., Cooper, L. W., Danielson, S., Arrigo, K. R., Blanchard, A. L., Clark, J. T., Day, R. H., Frey, K. E., Gradinger, R. R., Kedra, M., Konar, B., Kuletz, K. J., Lee, S. H., Lovvorn, J. R., Norcross, B. L., and Okkonen, S. R., 2015a. Ecosystem characteristics and processes facilitating persistent macrobenthic biomass hotspots and associated benthivory in the Pacific Arctic. *Progress In Oceanography*. 136: 92-114.

Grebmeier, J.M., Bluhm, B.A., Cooper, L.W., Denisenko, S.G., Iken, K., Kedra, M., and Serratos, C., 2015b. Time-series benthic community composition and biomass and associated environmental characteristics in the Chukchi Sea during the RUSALCA 2004-2012 Program. *Oceanography*. 28: 116-133. doi:10.5670/oceanog.2015.61

Grebmeier, J., Cooper, L., 2016. PacMARS Surface Sediment Parameters (1970-2012). Version 2.0., UCAR/NCAR - Earth Observing Laboratory. cited [2020 August 24]. doi:10.5065/D6416V3G. Data provided by NCAR/EOL under the sponsorship of the National Science Foundation. Available from [<https://data.eol.ucar.edu/>]

Grebmeier, J.M., Frey, K.E., Cooper, L.W., Kędra, M., 2018. Trends in benthic macrofaunal populations, seasonal sea ice persistence, and bottom water temperatures in the Bering Strait region. *Oceanography*. 31(2): 136–151. <https://doi.org/10.5670/oceanog.2018.224>

Hald, M., Steinsund, P. I., Dokken, T., Korsun, S., Polyak, L. & Aspeli, R., 1994. Recent and late Quaternary distribution of *E. excavatum forma clavata* in Arctic seas. Cushman Foundation Special Publication. 32: 141–153.

Hammer, Ø., Harper, D.A.T., Ryan, P.D., 2001. Past: Paleontological Statistics Software Package for Education and Data Analysis. *Palaeontologia Electronica*, 4(1): 9pp., 178kb. http://palaeo-electronica.org/2001_1/past/issue1_01.htm. *Palaeontologia Electronica*, <http://palaeo-electronica.org>; download at <https://www.nhm.uio.no/english/research/infrastructure/past/>

Hartmann, G., 1992. Zur Kenntnis der rezenten und subfossilen Ostracoden des Liefdefjords (Nordspitzbergen, Svalbard).i.teil. Mit einer tabelle subfossil nachgewiesener Foraminiferen. *Mitteilungen aus dem Hamburgischen Zoologischen Museum und Institut*. 89: 181-225.

Hayward, B.W., Grenfell, H.R., Savaa, A.T., and Daymond-King, R., 2007. Biogeography and ecological distribution of shallow-water benthic foraminifera from the Auckland and Campbell Islands, subantarctic southwest Pacific. *Journal of Micropaleontology*. 26: 127-143. <https://doi.org/10.1144/jm.26.2.127>

Hazel, J.E., Valentine, P.C., 1969. Three new ostracods from off northeast North America. *Journal of Paleontology*. 43: 741-752.

Hazel, J.E., 1970. Atlantic continental shelf and slope of the United States: Ostracode zoogeography in the southern Nova Scotian and northern Virginian faunal provinces. U.S. Geological Survey Professional Paper. 529-E: 1-21.

Hazel, J.E., 1970. Ostracode zoogeography, Nova Scotian and Virginian faunal provinces. Geological Survey Professional Paper. 529-E.

Heaton T.J., Köhler, P., Butzin, M., Bard, E., Reimer, R.W., Austin, W.E.N., Bronk Ramsey, C., Hughen, K.A., Kromer, B., Reimer, P.J., Adkins, J., Burke, A., Cook, M.S., Olsen, J., Skinner, L.C. 2020., Marine20 – the marine radiocarbon age calibration curve (0-55,000 cal BP). *Radiocarbon*. 62. doi: 10.1017/RDC.2020.68.

Higgins, R.P., and Thiel, H., 1988. Introduction to the study of meiofauna. Smithsonian Institution Press: Washington D.C. (ISBN 0-87474-488-1): 488 pp.

Hill, V., Ardyna, M., Lee, S.H., Varela, D.E., 2018. Decadal trends in phytoplankton production in the Pacific Arctic Region from 1950 to 2012. *Deep Sea Research Part II*. 152: 82-94. doi:10.1016/j.dsr2.2016.12.015

Holmes, J. A., and Chivas, A. R., 2002. Ostracod shell chemistry — Overview. – In: Holmes, J.A. & Chivas, A.R. [Eds.]: *The Ostracoda: applications in Quaternary Research – Geophysical Monograph Series*. 131: 185-204, AGU, Washington, D.C. <https://doi.org/10.1029/131GM10>

Holmes, J., Sayer, C.D., Liptrot, E., Hoare, D. J., 2010. Complex controls on ostracod palaeoecology in a shallow coastal brackish-water lake: implications for palaeosalinity reconstruction. *Freshwater Biology*. 55 (12): 2484e2498. [https://doi.org/ 10.1111/j.1365-2427.2010.02478.x](https://doi.org/10.1111/j.1365-2427.2010.02478.x)

Holmes, J. A., and DeDeckker, P., 2012. The Chemical Composition of Ostracod Shells: Applications in Quaternary Palaeoclimatology. *Developments in Quaternary Science*. 17: 131-143. <http://dx.doi.org/10.1016/B978-0-444-53636-5.00008-1>

Horne, D.J., 1983. Life-cycles of podocopid Ostracoda - a review (with particular reference to marine and brackish-water species). In: Maddocks, R. (Ed.), *Applications of Ostracoda. Proceedings of the Eighth International Symposium on Ostracoda*. University of Houston, Dept. of Geosciences, Houston, Texas, pp. 581–590.

Horne, D.J., Cohen, A., and Martens, K., 2002. Taxonomy, morphology and biology of Quaternary and living Ostracoda. In: Holmes, J.A. & Chivas, A.R. (Eds), *The Ostracoda: Applications in Quaternary Research*. AGU Geophysical Monograph. 131: 5–36.

Horne, D.J., Holmes, J.A., Rodriguez-Lazaro, J., Viehberg, F.A., 2012. Ostracoda as proxies for Quaternary climate change: Overview and future prospects, Editor(s): D.J. Horne, J.A. Holmes, J.Rodriguez-Lazaro, F.A. Viehberg, *Developments in Quaternary Sciences*, Elsevier. Volume 17: 305-315. <https://doi.org/10.1016/B978-0-444-53636-5.00018-4>

Hörner, T., Stein, R., Fahl, K., Birgel, D., 2016. Post-glacial variability of sea ice cover, river run-off and biological production in the western Laptev Sea (Arctic Ocean)—A high-resolution biomarker study. *Quaternary Science Reviews*. 143: 133–149.

Hunt, Jr., G.L., Blanchard, A.L., Boveng, P., Dalpadado, P., Drinkwater, K.F., Eisner, L., Hopcroft, R.R., Kovacs, K.M., Norcross, B.L., Renaud, P., Reigstad, M., Renner, M., Skjoldal, H.R., Whitehouse, A., Woodgate, R. A., 2013. The Barents and Chukchi Seas: comparison of two Arctic shelf ecosystems. *Journal of Marine Systems*. 109–110: 43–68.

Huntington, H.P., Danielson, S.L., Wiese, F.K., Baker, M., Boveng, P., Citta, J.J., De Robertis, A., Dickson, D.M.S., Farley, E., George, J.C., et al., 2020. Evidence suggests potential transformation of the Pacific Arctic ecosystem is underway. *Nature Climate Change*. 10(4): 342–348. <https://doi.org/10.1038/s41558-020-0695-2>.

Hut, G., 1987. Consultants' group meeting on stable isotope reference samples for geochemical and hydrological investigations, 16.-18.9.1985. Report to the Director General, International Atomic Energy Agency, Vienna.

Hutchins, L.W., 1947. The bases for temperature zonation in geographical distribution. *Ecological Monographs*. 17: 325-335.

- Iken, K., Bluhm, B.A., Søreide, J.E., 2013. Arctic Benthic Communities [in Arctic Report Card 2013]. <http://www.arctic.noaa.gov/reportcard>
- Ikeya, N., Cronin, T.M., 1993. Quantitative analysis of ostracoda and water masses around Japan: Application to Pliocene and Pleistocene paleoceanography. *Micropaleontology*. 39 (3): 263-281.
- Ikeya N., and Kato, M., 2000. The life history and culturing of *Xestoleberis hanaii* (Crustacea, Ostracoda). In: Horne D.J., Martens K. (eds) *Evolutionary Biology and Ecology of Ostracoda. Developments in Hydrobiology*, 419: 148. Springer, Dordrecht. <https://doi.org/10.1023/A:1003931901501>
- Ingram, C., 1998. Palaeoecology and geochemistry of shallow marine Ostracoda from the Sand Hole Formation, Inner Silver Pit, Southern North Sea. *Quaternary Science Reviews*. 17: 913-929.
- Intergovernmental Panel on Climate Change (IPCC)., 2021. *Climate Change 2021: The Physical Science Basis. Contribution of Working Group I to the Sixth Assessment Report of the Intergovernmental Panel on Climate Change* [Masson-Delmotte, V., P. Zhai, A. Pirani, S. L. Connors, C. Péan, S. Berger, N. Caud, Y. Chen, L. Goldfarb, M. I. Gomis, M. Huang, K. Leitzell, E. Lonnoy, J. B. R. Matthews, T. K. Maycock, T. Waterfield, O. Yelekçi, R. Yu and B. Zhou (eds.)]. Cambridge University Press. <https://www.ipcc.ch/report/ar6/wg1/#FullReport>
- Ishman, S.E., and Foley, K.M., 1996. Modern benthic foraminifer distribution in the Amerasian Basin, Arctic Ocean. *Micropaleontology*. 42(2): 206-220.
- Ito, E., and Forester, R.M., 2017. Holocene hydrologic and hydrochemical changes of the South Basin of Lake Manitoba, Canada, inferred from ostracode shell chemistry and autoecology. *Hydrobiologia*. 786(1): 97-124. <https://doi.org/10.1007/s10750-016-2668-z>
- Jackson, J. M., Melling, H., Lukovich, J. V., Fissel, D., and Barber, D. G., 2015. Formation of winter water on the Canadian Beaufort shelf: New insight from observations during 2009–2011. *Journal of Geophysical Research: Oceans*. 120: 4090–4107. doi:10.1002/2015JC010812.
- Jeffries, M. O., Overland, J. E., and Perovich, D. K., 2013. The Arctic shifts to a new normal. *Physics Today*. 66(10): 35-40.
- Jennings, A. E. and Helgadottir, G., 1994. Foraminiferal assemblages from the fjords and shelf of eastern Greenland. *Journal for Foraminiferal Research*. 24(2): 123-144.
- Jernas, P., Klitgaard-Kristensen, D., Husum, K., Ko, N., Tverberg, V., Loubere, P., Prins, M., Dijkstra, N., and Gluchowska, M., 2018. Annual changes in Arctic fjord environment and modern benthic foraminiferal fauna: Evidence from Kongsfjorden, Svalbard. *Global and Planetary Change* 163:119–40. doi:10.1016/j.gloplacha.2017.11.013.

- Ji, R., Jin, M., Varpe, Ø., 2013. Sea ice phenology and timing of primary production pulses in the Arctic Ocean. *Global Change Biology*. 19: 734-741. doi:10.1111/gcb.12074
- Joy, J. A. and Clark, D. L., 1977. The distribution, ecology and systematics of the benthic Ostracoda of the central Arctic Ocean. *Micropaleontology*. 23: 129-154.
- Kaufman, D.S., Schneider, D.P., McKay, N.P., Ammann, C.M., Bradley, R.S., Briffa, K.R., Miller, G.H., Otto-Bliesner, B.L., Overpeck, J.T., Vinther, B.M., Arctic Lakes 2 k Project Members., 2009. Recent warming reverses long-term Arctic cooling. *Science*. 235: 1236-1239. doi: 10.1126/science.1173983
- Keatings, K.W., Heaton, T.H.E., Holmes, J.A., 2002. Carbon and oxygen isotope fractionation in non-marine ostracods: Results from a natural culture environment. *Geochimica et Cosmochimica Acta*. 66 (10): 1701–1711; Amsterdam (Elsevier).
[https://doi.org/10.1016/S0016-7037\(01\)00894-8](https://doi.org/10.1016/S0016-7037(01)00894-8)
- Keyser D., and Walter R., 2004. Calcification in ostracodes. *Revista Española de Micropaleontología*. 36: 1-11.
- Kim, S.-T., O’Neal, J. R., 1997. Equilibrium and nonequilibrium oxygen isotope effects in synthetic carbonates. *Geochimica et Cosmochimica Acta*. 61(16): 3461–3475.
- Kipp, L.E., Charette, M.A., Moore, W.S., Henderson, P.B., Rigor, I.G., 2018. Increased fluxes of shelf-derived materials to the central Arctic Ocean. *Science Advances*. 4, eaao1302.
<https://doi.org/10.1126/sciadv.aao1302>
- Kornicker, L.S., 1959. Distribution of the ostracode suborder Cladocopa, and a new species from the Bahamas. *Micropaleontology*. 5 (1): 69-75.
- Kornicker, L.S., Wise, C.D., 1960. Some environmental boundaries of a marine ostracode. *Micropaleontology*. 6 (4): 393-398.
- Korsun, S. and Hald, M., 2000. Seasonal dynamics of benthic foraminifera in a glacially fed fjord of Svalbard, European Arctic. *Journal of Foraminiferal Research*. 30(4): 251-271.
- Kulikov, E., Carmack, E., Macdonald, R., 1998. Flow variability at the continental shelf break of the Mackenzie Shelf in the Beaufort Sea. *Journal of Geophysical Research: Oceans*. 103: 12725-12741.
- Lazar, K.B., Polyak, L., Dipre, G.R., 2016. Re-examination of the use of *Cassidulina neoteretis* as a Pleistocene biostratigraphic marker in the Arctic Ocean. *Journal of Foraminiferal Research*. 46 (2): 115–123. doi: <https://doi.org/10.2113/gsjfr.46.2.115>
- Ledu, D., Rochon, A., de Vernal, A., St-Onge, G., 2008. Palynological evidence of Holocene climate change in the eastern Arctic: a possible shift in the Arctic Oscillation at the millennial time scale. *Canadian Journal of Earth Sciences*. 45 (11): 1363–1375.

- Ledu, D., Rochon, A., de Vernal, A., St-Onge, G., 2010a. Holocene sea-ice history and climate variability along the main axis of the Northwest Passage. *Canadian Arctic. Paleoceanography*. 25: PA2213. <http://dx.doi.org/10.1029/2009PA001817>
- Ledu, D., Rochon, A., de Vernal, A., St-Onge, G., 2010b. Holocene paleoceanography of the northwest Passage, Canadian Arctic Archipelago. *Quaternary Science Reviews*. 29: 3468-3488.
- LeGrande, A. N., and Schmidt, G. A., 2006. Global gridded data set of the oxygen isotopic composition in seawater. *Geophysical Research Letters*. 33: L12604. doi:10.1029/2006GL026011
- Levings, C., 1975. Analyses of Temporal Variation in the Structure of a Shallow-water Benthic Community in Nova Scotia. *International Review of Hydrobiology*. 60(4): 449-470.
- Lewis, K.M., van Dijken, G.L., Arrigo, K.R., 2020. Changes in phytoplankton concentration now drive increased Arctic Ocean primary production. *Science*. 369 (6500): 198-202. doi:10.1126/science.aay8380
- Li, M., Pickart, R.S., Spall, M. A., Weingartner, T. J., Lin, P., Moore, G.W.K., Qi, Yi., 2019. Circulation of the Chukchi Sea shelfbreak and slope from moored timeseries. *Progress in Oceanography*. 172: 14-33. <https://doi.org/10.1016/j.pocean.2019.01.002>
- Lin, P., Pickart, R. S., Fissel, D. B., Borg, K., Melling, H., & Wiese, F. K., 2021. On the nature of wind-forced upwelling and downwelling in Mackenzie Canyon, Beaufort Sea. *Progress in Oceanography*. 198: 102674.
- Lin, P., Pickart, R.S., Fissel, D., Ross, E., Kasper, J., Bahr, F., Torres, D.J., O'Brien, J., Borg, K., Melling, H., 2020. Circulation in the vicinity of Mackenzie Canyon from a year-long mooring array. *Progress in Oceanography*. 187: 102396. doi: <https://doi.org/10.1016/j.pocean.2020.102>
- Lin, P., Pickart, R. S., McRaven, L. T., Arrigo, K. R., Bahr, F., Lowry, K. E., et al., 2019a. Water mass evolution and circulation of the northeastern Chukchi Sea in summer: Implications for nutrient distributions. *Journal of Geophysical Research: Oceans*. 127(7): 4416-4432.
- Lin, P., Pickart, R. S., Moore, G. W. K., Spall, M. A., & Hu, J., 2019b. Characteristics and dynamics of wind-driven upwelling in the Alaskan Beaufort Sea based on six years of mooring data. *Deep Sea Research Part II: Topical Studies in Oceanography*. 124(7): 4416-4432. <https://doi.org/10.1029/2019JC015185>
- Lisiecki, L.E., and Raymo, M. E., 2005. A Pliocene-Pleistocene stack of 57 globally distributed benthic $\delta^{18}\text{O}$ records. *Paleoceanography*. 20: PA1003. doi:10.1029/2004PA001071

- Macdonald, R.W., Wong C.S., Erickson, P.E., 1987. The distribution of nutrients in the southeastern Beaufort Sea: Implications for water circulation and primary production. *Journal of Geophysical Research*. 92: 2939–2952.
- Macdonald, R. W., Carmack, E. C., McLaughlin, F. A., Iseki, K., Macdonald, D. M., and O'Brien, M. C., 1989. Composition and modification of water masses in the Mackenzie Shelf Estuary. *Journal of Geophysical Research*. 94(C12): 18057–18070. <https://doi.org/10.1029/JC094iC12p18057>
- Mackensen, A. and Hald, M., 1988. *Cassidulina teretis* Tappan and *C. laevigata* d'Orbigny: Their modern and late Quaternary distribution in northern seas. *Journal for Foraminiferal Research*. 18: 16–24.
- Mackensen, A., Schumacher, S., Radke, J., and Schmidt, D.N., 2000. Microhabitat preferences and stable carbon isotopes of endobenthic foraminifera: clue to quantitative reconstruction of oceanic new production? *Marine Micropaleontology*. 40: 233–258.
- Mackiewicz, A., 2006. Recent benthic Ostracoda from Hornsund, south Spitsbergen, Svalbard Archipelago. *Polish Polar Research*. 27(1): 71-90.
- Majoran, S., and Agrenius, S., 1995. Preliminary observations on living *Krithe praetexta praetexta* (Sars, 1866), *Sarsicytheridea bradii* (Norman, 1865) and other marine ostracods in aquaria. *Journal of Micropalaeontology*. 14: 1–46; London (Geol. Soc.).
- Majoran, S., Agrenius, S., and Kucera, M., 2000. The effect of temperature on shell size and growth rate in *Krithe praetexta praetexta* (Sars). *Hydrobiologia*. 419(1): 141–148. <https://doi.org/10.1023/A:1003943617431>
- Mann, M.E., Zhang, A., Hughes, M.K., Bradley, R.S., Miller, S.K., Rutherford, S., Ni, F., 2008. Proxy-based reconstructions of hemispheric and global surface temperature variations over the past two millennia. *Proceedings of the National Academy of Sciences*. 105: 13252-13257.
- Martin, S., Drucker, R., 1997 The effect of possible Taylor columns on the summer ice retreat in the Chukchi Sea. *Journal of Geophysical Research: Oceans*. 102 (C5). [doi:10.1029/97JC00145](https://doi.org/10.1029/97JC00145)
- Mazzini, I., 2005. Taxonomy, biogeography and ecology of Quaternary benthic Ostracoda (Crustacea) from circumpolar deep water of the Emerald Basin (Southern Ocean) and the S Tasman Rise (Tasman Sea). *Senckenbergiana maritima*. 35(1): 1-119.
- McKay, N. and Kaufman, D., 2014. An extended Arctic proxy temperature database for the past 2,000 years. *Scientific Data*. 1: 140026. <https://doi.org/10.1038/sdata.2014.26>

Melling, H., and Riedel, D. A., 1996. Development of seasonal pack ice in the Beaufort Sea during the winter of 1991– 92: A view from below. *Journal of Geophysical Research*. 101: 11975-11992.

Melling, H., 2000. Exchanges of freshwater through the shallow straits of the North American Arctic. In Lewis, E. L., Jones, E. P., Lemke, P., Prowse, T. D. & Wadhams, P. (eds.): *The Freshwater Budget of the Arctic Ocean*, 479-502. Springer, Dordrecht.

Miller, G. H., Brigham-Grette, J., Alley, R. B., Anderson, L., Bauch, H. A., Douglas, M. S. V., Edwards, M. E., Elias, S. A., Finney, B. P., Fitzpatrick, J. J., Funder, S. V., Herbert, T. D., Hinzman, L. D., Kaufman, D. S., MacDonald, G. M., Polyak, L., Robock, A., Serreze, M. C., Smol, J. P., ... Wolff, E. W., 2010. Temperature and precipitation history of the Arctic. *Quaternary Science Review*. 29(15-16): 1679-1715.
<https://doi.org/10.1016/j.quascirev.2010.03.001>

Millero, F.J., 1993. What is PSU? *Oceanography*. 6 (3): 67.
<https://www.jstor.org/stable/43924646>

Moore, S.E. and Grebmeier, J.M., 2018. The Distributed Biological Observatory: Linking physics to biology in the Pacific Arctic region. *Arctic*. 71: 1–7.

Morin, J. G., and Cohen, A.C., 1991. Bioluminescent displays, courtship, and reproduction in ostracods, pp. 1-16. In, Bauer R. and Martin J. (eds.), *Crustacean Sexual Biology*. Columbia University Press, New York.

Mortlock, R. A., and Froehlich, P. N., 1989. A simple method for the rapid determination of biogenic opal in pelagic marine sediments. *Deep-Sea Research*. 36(9): 1415-1426.

Mueter, F. and Litzow, M., 2008. Sea Ice Retreat Alters the Biogeography of the Bering Sea Continental Shelf. *Ecological Applications*. 18(2): 309-320.

Mueter, F.J., Iken, K., Cooper, L.W., Grebmeier, J.M., Kuletz, K.J., Hopcroft, R.R., Danielson, S.L., Collins, R.E., and Cushing, D.A., 2021. Changes in diversity and species composition across multiple assemblages in the eastern Chukchi Sea during two contrasting years are consistent with borealization. *Oceanography*. 34(2): 38–51.
<https://doi.org/10.5670/oceanog.2021.213>.

Naidu, A.S., 1974. Sedimentation in the Beaufort Sea: A synthesis. *Marine Geology and Oceanography of the Arctic Seas*. 173-190.

Neale, J. W., and Howe, H. V., 1975. The marine Ostracoda of Russian Harbour, Novaya Zemlya and other high latitude faunas. In Swaine, F. H. (ed.): *Biology and Paleobiology of Ostracoda*, *Bulletin of American Paleontology*. 65: 282, 381-431.

Nelson, R.J., Ashjian, C., Bluhm, B., Conlan, K., Gradinger, R., Grebmeier, J., et al., 2014. Biodiversity and biogeography of the lower trophic taxa of the Pacific Arctic region:

sensitivities to climate change. In: Grebmeier JM, Maslowski W (Eds.). *The Pacific Arctic Region: Ecosystem Status and Trends in a Rapidly Changing Environment*. Dordrecht: Springer. 269-336.

Nikolopoulos, A., Pickart, R. S., Fratantoni, P. S., Shimada, K., Torres, D. J., Jones, E. P., 2009. The western Arctic boundary current at 152°W: Structure, variability, and transport. *Deep Sea Research Part II*. 56: 1164–1181. doi:10.1016/j.dsr2.2008.10.014

O'Neil, J.R., Clayton, R.N., Mayeda, T. K., 1969. Oxygen Isotope Fractionation in Divalent Metal Carbonates. *Journal of Chemical Physics*. 51 (12): 5547. <https://doi.org/10.1063/1.1671982>

Okazaki, Y., Takahashi, K., Asahi, H., Katsuki, K., Hori, J., Yasuda, H., Sagawa, Y., Tokuyama, H., 2005. Productivity changes in the Bering Sea during the late Quaternary. *Deep-sea Research Part II: Topical Studies in Oceanography*. 52: 2150-2162.

Okkonen, S., 2013. CTD Summary Data. Version 1.0. UCAR/NCAR - Earth Observing Laboratory. cited [2020 December 15]. doi:10.5065/D6DB7ZVJ. Data provided by NCAR/EOL under the sponsorship of the National Science Foundation. Available from [<https://data.eol.ucar.edu/>].

Overland, J. E., Wang, M., Walsh, J. E., and Stroeve, J. C., 2013. Future Arctic climate changes: Adaptation and mitigation time scales. *Earth's Future*. 2(2): 68-74.

Overland, J., Dunlea, E., Box, J.E., Corell, R., Forsius, M., Kattsov, V., Olsen, M., Pawlak, J., Reiersen, L.-O., Wang, M., 2018. The urgency of Arctic change, *Polar Science*. doi: <https://doi.org/10.1016/j.polar.2018.11.008>

Ozawa, H., 2003. Japan Sea ostracod assemblages in surface sediments: their distribution and relationships to water mass properties. *Paleontological Research*. 7 (3): 257-274.

Ozawa, H., 2004. Okhotsk Sea ostracods in surface sediments: Depth distribution on cryophilic species relative to oceanic environment. *Marine Micropaleontology*. 53: 245-260. doi:10.1016/j.marmicro.2004.06.002

pacmars.eol.ucar.edu [Internet]. Pacific Marine Arctic Regional Synthesis Data Archive; c2012. Available from [<http://pacmars.eol.ucar.edu/>].

PAGES 2k Consortium, Ahmed, M., Anchukaitis, K. et al., 2013. Continental-scale temperature variability during the past two millennia. *Nature Geoscience*. 6: 339–346. <https://doi.org/10.1038/ngeo1797>; <https://doi.org/10.1038/s41561-019-0400-0>

Pearce C., Varhelyi A., Wastegård S., Muschitiello F., Barrientos N., O'Regan M., Cronin T.M., Gemery L., Semiletov I., Backman J., Jakobsson M., 2017. The 3.6 ka Aniakchak tephra in the Arctic Ocean: a constraint on the Holocene radiocarbon reservoir age in the Chukchi Sea. *Climate of the Past*. 13:303.

Penney, D. N., 1989. Recent shallow marine Ostracoda of the Ikerssuak (Bredefjord) district, Southwest Greenland. *Journal of Micropaleontology*. 8(1): 55-75.

Perner, K., Moros, M., Kuijpers, A., Telford, R.J., Harff, J., 2011. Centennial scale benthic foraminiferal record of late Holocene oceanographic variability in Disko Bugt, West Greenland. *Quaternary Science Reviews*. 30: 2815-2826. 10.1016/j.quascirev.2011.06.018

Perner, K., Moros, M., Jennings, A., Lloyd, J.M., Knudsen, K.L., 2013. Holocene palaeoceanographic evolution of West Greenland. *The Holocene*. 23: 374–387.

Perner, K. Moros, M., Lloyd, J. M., Jansen, E. and Stein, R., 2015. Mid to late Holocene strengthening of the East Greenland Current linked to warm subsurface Atlantic water. *Quaternary Science Reviews*. 129: 296-307.

Peypouquet, J.P., Carbonel, P., Ducasse, O., Töulderer-Farmer, M., Lété, C., 1988. Environmentally Cued Polymorphism of Ostracods— A Theoretical and Practical Approach. A Contribution to Geology and to the Understanding of Ostracod Evolution. *Developments in Palaeontology and Stratigraphy*. 11:1003-1019. doi: 10.1016/S0920-5446(08)70235-8

Pickart, R.S., 2004. Shelfbreak circulation in the Alaskan Beaufort Sea: mean structure and variability. *Journal of Geophysical Research*. 109: C04024.
<https://doi.org/10.1029/2003JC001912>

Pickart, R.S., Weingartner, T.J., Pratt, L.J., Zimmermann, S., Torres, D.J., 2005. Flow of winter-transformed Pacific water into the Western Arctic. *Deep Sea Research Part II: Topical Studies in Oceanography*. 52 (24-26): 3175-3198. doi:10.1016/j.dsr2.2005.10.009

Pickart, R.S., Moore, G.W.K., Torres, D.J., Fratantoni, P.S., Goldsmith, R.A., Yang, J., 2009. Upwelling on the continental slope of the Alaskan Beaufort Sea: Storms, ice, and oceanographic response. *Journal of Geophysical Research*. 114: C00A13.
doi:10.1029/2008JC005009

Pickart, R.S., Spall, M.A., Moork, G.W., Weingartner, T.J., Woodgate, R.A., Aagaard, K., et al., 2011. Upwelling in the Alaskan Beaufort Sea: Atmospheric forcing and local versus non-local response. *Progress in Oceanography*. 88 (1-4): 78-100.

Pickart, R.S., Schulze, L.M., Moore, G.W.K., Charette, M.A., Arrigo, K.R., van Dijken, G., et al., 2013a. Long-term trends of upwelling and impacts on primary productivity in the Alaskan Beaufort Sea. *Deep-Sea Research I*. 79: 106-121.

Pickart, R.S., Spall, M.A., Mathis, J.T., 2013b. Dynamics of upwelling in the Alaskan Beaufort Sea and associated shelf-basin fluxes. *Deep-Sea Research*. 176: 35-51.

- Pickart, R.S., Moore, G.W.K., Mao, C., Bahr, F., Nobre, C., Weingartner, T.J., 2016. Circulation of winter water on the Chukchi shelf in early summer. *Deep-Sea Research II*. 130: 56–75.
- Pickart, R.S., Nobre, C., Lin, P., Arrigo, K.R., Ashjian, C.J., Berchok, C., et al., 2019. Seasonal to mesoscale variability of water masses and atmospheric conditions in Barrow Canyon, Chukchi Sea. *Deep-Sea Research Part II*. doi:10.1016/j.dsr2.2019.02.003
- Pieńkowski, A.J., Gill, N.K., Furze, M.F.A., Mugo, S.M., Marret, F. and Perreux, A., 2017. Arctic sea-ice proxies: Comparisons between biogeochemical and micropalaeontological reconstructions in a sediment archive from Arctic Canada. *The Holocene*. 27(5): 665- 682.
- Poirier, R.K., Cronin, T.M., Briggs Jr., W.M., Lockwood, R., 2012. Central Arctic paleoceanography for the last 50 kyr based on ostracode faunal assemblages. *Marine Micropaleontology*. 88–89: 65-76.
- Polyak, L., Korsun, S., Febo, L.A., Stanovoy, V., Khusid, T., Hald, M., Paulsen, B.E., Lubinski, D.J., 2002. Benthic foraminiferal assemblages from the southern Kara Sea, a river-influenced arctic marine environment. *Journal of Foraminiferal Research*. 32: 252–273.
- Polyak, L. Best, K.M., Crawford, K.A., Council, E.A., St-Onge, G., 2013. Quaternary history of sea ice in the western Arctic Ocean based on foraminifera. *Quaternary Science Reviews*. 79: 145-156. <https://doi.org/10.1016/j.quascirev.2012.12.018>.
- Polyak L., Belt S.T., Cabedo-Sanz, P., Yamamoto, M., Park, Y.H., 2016. Holocene sea-ice conditions and circulation at the Chukchi-Alaskan margin, Arctic Ocean, inferred from bio-marker proxies. *Holocene*. 26: 1810-1821.
- Post, E., Bhatt, U. S., Bitz, C. M., Brodie, J. F., Fulton, T. L., Hebblewhite, M., Kerby, J., Kutz, S. J., Stirling, I., and Walker, D. A., 2013. Ecological consequences of sea ice decline. *Science*. 341(6145): 519–524.
- Proshutinsky, A., Krishfield, R., Toole, J. M., Timmermans, M.-L., Williams, W., Zimmermann, S., Yamamoto-Kawai, et al., 2019. Analysis of the Beaufort Gyre freshwater content in 2003–2018. *Journal of Geophysical Research: Oceans*. 124: 9658-9689. <https://doi.org/10.1029/2019JC015281>
- Raup, D.M., 1991. The future of analytical paleobiology. *Short Courses in Paleontology*. 4: 207–216. doi:10.1017/S2475263000002208
- Ravelo, A.C. and Hillaire-Marcel, C., 2007. The Use of Oxygen and Carbon Isotopes of Foraminifera in Paleoceanography. *Developments in Marine Geology, Volume 1*. Elsevier B.V. doi:10.1016/S1572-5480(07)01023-8
- Rawlins, M. A., Steele, M., Holland, M. M., Adam, J. C., Cherry, J. E., Francis, J. A., Groisman, P. Y., Hinzman, L. D., Huntington, T. G., Kane, D. L., Kimball, J. S., Kwok, R.,

- Lammers, R. B., Lee, C. M., Lettenmaier, D. P., McDonald, K. C., Podest, E., Pundsack, J. W., Rudels, B., Serreze, M. C., Shiklomanov, A., Skagseth, Ø., Troy, T. J., Vörösmarty, C. J., Wensnahan, M., Wood, E. F., Woodgate, R., Yang, D., Zhang, K., Zhang, T., 2010. Analysis of the Arctic system for freshwater cycle intensification: Observations and expectations. *Journal of Climate*. 23: 5715–5737. doi: 10.1175/2010JCLI3421.1
- Roberts, L.R., Holmes, J.A., Horne, D.J., Leng, M.J., 2018. Effects of cleaning methods upon preservation of isotopes and trace elements in ostracods, *Quaternary Science Reviews*. 189: 197–209.
- Roberts, L.R., Holmes, J.A., Sloane, H.J., Arrowsmith, C., Leng, M.J., Horne, D.J., 2020. $\delta^{18}\text{O}$ and $\delta^{13}\text{C}$ of *Cyprideis torosa* from coastal lakes: Modern systematics and down-core interpretation. *Marine Micropaleontology*. 160: 101907. <https://doi.org/10.1016/j.marmicro.2020.101907>.
- Roca, J.R., and Wansard, G., 1997. Temperature influence on development and calcification of *Herpetocypris brevicaudata* Kaufmann, 1900 (Crustacea: Ostracoda) under experimental conditions. *Hydrobiologia*. 347, 91–95.
- Rohling, E. J., and Cooke, S., 1999. Stable oxygen and carbon isotopes in foraminiferal carbonate shells, in B. K. Sen Gupta (Ed) *Modern foraminifera* (pp. 239–258). Dordrecht, The Netherlands: Kluwer Academy.
- Rood, S. B., Kaluthota, S., Philipsen, L. J., Rood, N. J., and Zanewich, K. P., 2017. Increasing discharge from the Mackenzie River system to the Arctic Ocean. *Hydrological Processes*. 31: 150-160. doi: 10.1002/hyp.10986
- Rudels, B., Jones, E. P., Anderson, L. G., and Kattner, G., 1994. On the intermediate depth waters of the Arctic Ocean. In: O. M. Johannessen, R. D. Muench, and J. E. Overland (eds) *The Polar Oceans and Their Role in Shaping the Global Environment: The Nansen Centennial Volume*. Geophysical Monograph Series. 85: 33–46. AGU, Washington, D. C.
- Ryan, W.B.F., Carbotte, S.M., Coplan, J., O'Hara, S., Melkonian, A., Arko, R., Weissel, R.A., Ferrini, V., Goodwillie, A., Nitsche, F., Bonczkowski, J., Zensky, R., 2009. Global Multi-Resolution Topography (GMRT) synthesis data set. *Geochemistry, Geophysics, Geosystems*. 10, Q03014. doi:10.1029/2008GC002332
- Sars, G. O., 1866. Oversigt af Norges marine Ostracoder: Vidensk. -Selsk. Forhandl. Christiania. 17 (for 1865), 1-130.
- Sars, G. O., 1922-1928. *An account of the Crustacea of Norway Volume IX, Ostracoda*: Bergen Museum, Bergen, Norway.
- Schlitzer, R., 2018. Ocean Data View. <https://odv.awi.de>.

- Schornikov, E.I., 2001. Class ostracoda, orders Platycopida and Podocopida. In: Sirenko B.I. (Ed.). List of species of free-living invertebrates of Eurasian Arctic seas and adjacent deep waters: Explorations of the fauna of the seas. St. Peterburg, T. 51 (59): 99–103.
- Schornikov, E.I., 2006. Checklist of the ostracod (Crustacea) fauna of Peter the Great Bay, Sea of Japan. *Zootaxa*. 1294: 29-59. doi:10.5281/zenodo.173519
- Schornikov, E.I. and Zenina, M.A., 2006. Benthic ostracod fauna of the Kara, Laptev and East-Siberian seas (data from the expeditions carried out by the Pacific Oceanography Institute of the Eastern Branch of the Russian Academy of Sciences). *Proceedings of the Arctic regional center*. 4: 156-211. Izd. Dalnauka, Vladivostok (in Russian).
- Schröder-Adams, C.J., Cole, F.E., Medioli, P.J., Scott, D.B., Dobbin, L., 1990. Recent Arctic shelf Foraminifera—Seasonally ice covered vs. perennially ice-covered areas. *Journal of Foraminiferal Research*. 20: 8–36.
- Schröder-Adams, C. J. and van Rooyen, D., 2011. Response of Recent Benthic Foraminiferal Assemblages to Contrasting Environments in Baffin Bay and the Northern Labrador Sea, Northwest Atlantic. *Arctic*. 64: 317–341.
- Scott, D.B., Schell, T., Rochon, A., Blasco, S., 2008. Modern benthic foraminifera in the surface sediments of the Beaufort shelf, slope, and Mackenzie trough, Beaufort Sea, Canada: Taxonomy and summary of surficial distributions. *Journal of Foraminiferal Research*. 38: 228–250.
- Scott, D. B., Schell, T., St-Onge, G., Rochon, A., and Blasco, S., 2009. Foraminiferal assemblage changes over the last 15,000 years on the Mackenzie-Beaufort Sea Slope and Amundsen Gulf, Canada: Implications for past sea ice conditions. *Paleoceanography*. 24: PA2219. doi:10.1029/2007PA001575
- Seidenkrantz, M.-S., 1995. *Cassidulina teretis* Tappan and *Cassidulina neoteretis* new species (Foraminifera): stratigraphic markers for deep sea and outer shelf areas. *Journal of Micropaleontology*. 14: 145–157. <https://doi.org/10.1144/jm.14.2.145>
- Seidenstein, J.L., Cronin, T.M., Gemery, L., Keigwin, L.D., Pearce, C., Jakobsson, M., Coxall, H., Wei, E., Driscoll, N., 2018. Late Holocene paleoceanography in the Chukchi and Beaufort Seas, Arctic Ocean, based on benthic foraminifera and ostracodes. *Arktos*. <https://doi.org/10.1007/s41063-018-0058-7>
- Serreze, M. C., Crawford, A. D., Stroeve, J. C., Barrett, A. P., and Woodgate, R. A., 2016. Variability, trends, and predictability of seasonal sea ice retreat and advance in the Chukchi Sea, *Journal of Geophysical Research Oceans*. 121: 7308–7325. doi:10.1002/2016JC011977
- Shackleton, N., 1974. Attainment of isotopic equilibrium between ocean water and the benthonic foraminifera genus *Uvigerina*; isotopic changes in the ocean during the last glacial. *French National Centre for Scientific Research*, pp. 203–209.

Shannon, C.E. & Weaver, W., 1949. The mathematical theory of communication. The University of Illinois Press, Urbana, 117pp.

<http://eebweb.arizona.edu/courses/ecol206/shannon%20weaver-wiener.pdf>

Siddiqui, Q.A., Grigg, U.M., 1975. A preliminary survey of the ostracodes of Halifax Inlet. In: Swaine FH (Ed.). Biology and paleobiology of Ostracoda. Bulletin of American Paleontology. 65(282): 369-379.

Sigler, M.F., Mueter, F.J., Bluhm, B.A., Busby, M.S., Cokelet, E.D., Danielson, S., et al., 2017. Late summer zoogeography of the northern Bering and Chukchi seas. Deep-Sea Research Part II. 135: 168-189. doi:10.1016/j.dsr2.2016.03.005.

Simstich, J., Stanovoy, V., Bauch, D., Erlenkeuser, H., Spielhagen, R.F., 2004. Holocene Variability of Bottom Water Hydrography on the Kara Sea Shelf (Siberia) Depicted in Multiple Single-Valve Analyses of Stable Isotopes in Ostracods,” Marine Geology. 206(1–4): 147–164. <https://doi.org/10.1016/j.margeo.2004.01.008>

Smith, A.J. & Horne, D.J., 2002. Ecology of marine, marginal marine and nonmarine ostracodes. In: Holmes, J.A. & Chivas, A.R. (Eds), The Ostracoda: Applications in Quaternary Research, American Geophysical Union, Geophysical Monograph. 131: 37–64.

Stabeno, P.J., Duffy-Anderson, J.T., Eisner, L.B., Farley, E.V., Heintz, R.A., Mordy, C.W., 2017. Return of warm conditions in the southeastern Bering Sea: Physics to fluorescence. PLOS ONE. 12 (9): e0185464. doi:10.1371/journal.pone.0185464

Stabeno, P., Kachel, N., Ladd, C., and Woodgate, R., 2018. Flow patterns in the eastern Chukchi Sea: 2010–2015. Journal of Geophysical Research: Oceans. 123: 1177–1195. <https://doi.org/10.1002/2017JC013135>

Stabeno, P.J., Bell, S., Bond, N.A., Kimmel, D., Mordy, C., Sullivan, M.E., 2019. Distributed Biological Observatory Region 1: Physics, chemistry and plankton in the northern Bering Sea. Deep-sea Research Part II: Topical Studies in Oceanography. 162: 8-21. doi:10.1016/j.dsr2.2018.11.006

Stein, R., Fahl, K., Schade, I., Manerung, A., Wassmuth, S., Niessen, F., Nam, S.I., 2017. Holocene variability in sea ice cover, primary production, and Pacific-Water inflow and climate change in the Chukchi and East Siberian Seas (Arctic Ocean). Journal of Quaternary Science. 32: 362–379. <https://doi.org/10.1002/jqs.2929>

Stein, R., Fahl, K., 2000. Holocene accumulation of organic carbon at the Laptev Sea continental margin (Arctic Ocean): sources, pathways, and sinks. Geo-Marine Letters. 20: 27–36. <https://doi.org/10.1007/s003670000028>

Stepanova, A., Taldenkova, E., and Bauch, H.A., 2003. Recent Ostracoda of the Laptev Sea (Arctic Siberia): taxonomic composition and some environmental implications. *Marine Micropaleontology*. 48: 23-48.

Stepanova, A., Taldenkova, E., and Bauch, H. A., 2004. Ostracod species of the genus *Cytheropteron* from Late Pleistocene, Holocene and Recent sediments of the Laptev Sea (Arctic Siberia). *Revista Española de Micropaleontología*. 36(1): 83-108.

Stepanova A.Y., 2006. Late Pleistocene-Holocene and recent Ostracoda of the Laptev Sea. *Monograph. Suppl. Issue Russ. Paleontological Journal*. 40 (2): S91–S204.

Stepanova, A., Taldenkova, E., Simstich, J., and Bauch, H. A., 2007. Comparison study of the modern ostracod associations in the Kara and Laptev seas: Ecological aspects. *Marine Micropaleontology*. 63(3) 111-142.

Stepanova, A., Obrochta, S., Quintana, Krupinski, N.B., Hyttinen, O., Kotilainen, A., Andrés, T., 2019. Late Weichselian to Holocene history of the Baltic Sea as reflected in ostracod assemblages. *Boreas*. <https://doi.org/10.1111/bor.12375>. ISSN 0300-9483.

Stephens, C., Antonov, J.I., Boyer, T.P., Conkright, M.E., Locarnini, R.A., O'Brien, T.D., et al., 2002. *World Ocean Atlas 2001, Volume 1: Temperature* [CD-ROM]. Levitus S (Ed.), NOAA Atlas NESDIS 49, U.S. Government Printing Office, Washington D.C. 167.

Stevenson, D. E., Lauth, R.R., 2019. Bottom trawl surveys in the northern Bering Sea indicate recent shifts in the distribution of marine species. *Polar Biology*. 42: 407-421.

Stranne, C., Jakobsson, M., Björk, G., 2014. Arctic Ocean perennial sea ice breakdown during the Early Holocene Insolation Maximum. *Quaternary Science Reviews*. 92: 123-132. <http://dx.doi.org/10.1016/j.quascirev.2013.10.022>

Stroeve, J. C., M. Serreze, C., Holland, M. M., Kay, J., Maslanik, J., and Barrett, A. P., 2012. The Arctic's rapidly shrinking sea ice cover: A research synthesis. *Climatic Change*. 110(3-4): 1005–1027.

Stroeve, J. C., Markus, T., Boisvert, L., Miller, J., and Barrett, A., 2014. Changes in Arctic melt season and implications for sea ice loss. *Geophysical Research Letters*. 41(4): 1216–1225.

Stuiver, M., Reimer, P.J., and Reimer, R.W., 2021. CALIB 8.2 [WWW program] at <http://calib.org>. Accessed 2021-1-26.

Tanaka, G., 2009. Adaptive modifications of carapace outlines in the *Cytheroidea* (Ostracoda: Crustacea). *Biological Journal of the Linnean Society*. 97: 810–821.

Tappan, H., 1951. Northern Alaska index foraminifera. *Contributions from the Cushman Foundation for Foraminiferal Research*. 2:1–8.

- Teeter, J.W., 1973. Geographical distribution and dispersal of some Recent shallow-water marine Ostracoda. *Ohio Journal of Science*, Akron. 73(1): 46–54, 2 pls., 2 tabs.
- Theisen, B. F., 1966. The life history of seven species of ostracods from a Danish brackish-water locality. *Meddelelser fra Danmarks Fiskeri- og Havundersøgelser*. 4: 215–270.
- Timmermans, M.-L., Toole, J., Krishfield, R., 2018. Warming of the interior Arctic Ocean linked to sea ice losses at the basin margins. *Science Advances*. 4(8): eaat6773. doi: 10.1126/sciadv.aat6773
- Tsukagoshi, A., Briggs Jr, W.M., 1998. On *Schizocythere ikeyai* Tsukagoshi & Briggs sp. nov. *Stereo-Atlas of Ostracod Shells*. 25 (1-2): 43-52.
- Turpen, J.B., and Angell, R.W., 1971. Aspects of molting and calcification in the ostracod *Heterocypris*: *The Biological Bulletin* (The University of Chicago Press in association with the Marine Biological Laboratory), 140(2): 331-338. <https://www.jstor.org/stable/1540077>
- Urey, H.C., 1947. The thermodynamic properties of isotopic substances. *Journal of the Chemical Society (London)*, p. 562–581. doi:10.1039/jr9470000562
- van Dijk, I., Bernhard, J.M., de Nooijer, L.J., Nehrke, G., Wit, J.C. and Reichart, G.J., 2017. Combined impacts of ocean acidification and dysoxia on survival and growth of four agglutinated foraminifera. *Journal of Foraminiferal Research*. 47(3): 294-303. doi: 10.2113/gsjfr.47.3.294
- von Appen, W.-J., and Pickart, R.S., 2012. Two configurations of the western Arctic shelfbreak current in summer. *Journal of Physical Oceanography*. 42(3): 329-351.
- von Grafenstein, U., Erlernkeuser, H., and Trimborn, P., 1999. Oxygen and carbon isotopes in modern freshwater ostracod valves: assessing vital offsets and autecological effects of interest for palaeoclimate studies. *Palaeogeography, Palaeoclimatology, Palaeoecology*. 148: 133-152. [https://doi.org/10.1016/S0031-0182\(98\)00180-1](https://doi.org/10.1016/S0031-0182(98)00180-1)
- Walsh, J.J., McRoy, C.P., Coachman, L.K., Goering, J.J., Nihoul, J.J., Whitley, T.E., et al., 1989. Carbon and nitrogen cycling within the Bering Chukchi Seas – source regions for organic-matter effecting AOU demands of the Arctic Ocean. *Progress in Oceanography*. 22: 277-359. doi:10.1016/0079-6611(89)90006-2
- Wassmann, P., Duarte, C.M., Agusti, S., Sejr, M.K., 2011. Footprints of climate change in the Arctic marine ecosystem. *Biological Global Change*. 17(2): 1235-1249. doi:10.1007/s00300-010-0839-3
- Wefer, G. and Berger, W.H., 1991. Isotope paleontology: growth and composition of extant calcareous species. *Marine Geology*. 100: 207-248.

Weingartner, T.J., Cavalieri, D.J., Aagaard, K., Sasaki, Y., 1998. Circulation, dense water formation, and outflow on the northeast Chukchi shelf. *Journal of Geophysical Research*. 103: 7647-7661. doi:10.1029/98JC00374

Weingartner, T., Aagaard, K., Woodgate, R., Danielson, S., Sasaki, Y., and Cavalieri, D., 2005. Circulation on the north central Chukchi Sea shelf. *Deep Sea Research Part II*. 52(24-26): 3150–3174. doi:10.1016/j.dsr2.2005.10.01.

Weingartner, T., Dobbins, E., Danielson, S., Winsor, P., Potter, R., Statscewich, H., 2013. Hydrographic variability over the northeastern Chukchi Sea shelf in summer-fall 2008-2010. *Continental Shelf Research*. 67: 5-22. doi:10.1016/j.csr.2013.03.012

Weingartner, T.J., Potter, R.A., Stoudt, C.A., Dobbins, E.L., Statscewich, H., Winsor, P.R., Mudge, T.D., Borg, K., 2017a. Transport and thermohaline variability in Barrow Canyon on the northeastern Chukchi Sea shelf. *Journal of Geophysical Research*.
<http://dx.doi.org/10.1002/2016JC012636>.

Weingartner, T., Fang, Y-C., Winsor, P., Dobbins, E., Potter, R., Statscewich, H., et al. 2017b. The summer hydrographic structure of the Hanna Shoal region on the northeastern Chukchi Sea shelf: 2011–2013. *Deep Sea Research Part II: Topical Studies in Oceanography*. 144: 6-20. doi:10.1016/j.dsr2.2017.08.006

Whatley, R.C., 1982. Littoral and sublittoral Ostracoda from Sisimiut, West Greenland. In: Fox, A.D., and D.A. Stroud. Report of the 1979 Greenland White-Fronted Goose Study Expedition to Equalunqmiut Nunat. Western Greenland. University of Wales Press. pp. 269-284.

Whatley, R.C., and Coles, G., 1987. The late Miocene to Quaternary Ostracoda of Leg 94, Deep Sea Drilling Project. *Revista Española de Micropaleontología*. 19(1): 33-97.

Whatley, R., Eynon, M., Mognilevsky, A., 1998. The depth distribution of Ostracoda from the Greenland Sea. *Journal of Micropalaeontology*. 17: 15–32. <https://doi.org/10.1144/jm.17.1.15>

Wickert, A.D., 2016. Reconstruction of North American drainage basins and river discharge since the Last Glacial Maximum. *Earth Surface Dynamics*. 4: 831–869.
<https://doi.org/10.5194/esurf-4-831-2016>

Williams, W.J., Melling, H., Carmack, E.C., and Ingram, R.G., 2008. Kugmallit Valley as a conduit for cross-shelf exchange on the Mackenzie shelf in the Beaufort Sea. *Journal of Geophysical Research*. 113: C02007. doi:10.1020/2006JC003591

Williams, W.J., and Carmack, E.C., 2015. The ‘interior’ shelves of the Arctic Ocean: Physical oceanographic setting, climatology and effects of sea-ice retreat on cross-shelf exchange. *Progress in Oceanography*. 139: 24-41.

Wood, K.R., Bond, N.A., Danielson, S.L., Overland, J.E., Salo, S.A., Stabeno, P., et al., 2015a. A decade of environmental change in the Pacific Arctic region. *Progress in Oceanography*. 136: 12-31. doi:10.1016/j.pocean.2015.05.005

Wood, K., Wang, J., Salo, S., Stabeno, P., 2015b. The climate of the Pacific Arctic during the first RUSALCA decade 2004-2013. *Oceanography*. 28: 24-35. doi:10.5670/oceanog.2015.55

Woodgate, R.A., Aagaard, K., Weingartner, T.J., 2005a. Monthly temperature, salinity and transport variability of the Bering Strait throughflow. *Geophysical Research Letters*. 32: L04601. doi:10.1029/2004GL021880

Woodgate, R.A., Aagaard, K., and Weingartner, T.J., 2005b. A year in the physical oceanography of the Chukchi Sea: Moored measurements from autumn 1990-1991. *Deep Sea Research Part II*. 52 (24–26): 3116–3149. doi:10.1016/j.dsr2.2005.10.016

Woodgate, R. A., Weingartner, T., and Lindsay, R., 2012. Observed increases in Bering Strait oceanic fluxes from the Pacific to the Atlantic from 2001 to 2010 and their impacts on the Arctic Ocean water column. *Geophysical Research Letters*. 39: L24603. doi:10.1029/2012GL054092